Christian-Albrechts-Universität zu Kiel
Mathematisch-Naturwissenschaftliche Fakultät
Kieler Geographische Schriften
Band 121 | Kiel 2010

Natascha Oppelt

Monitoring of the Biophysical Status of Vegetation

Using Multi-angular, Hyperspectral Remote Sensing for the Optimization of a Physically-based SVAT Model

KIELER GEOGRAPHISCHE SCHRIFTEN

Herausgegeben vom Geographischen Institut der Universität Kiel
durch C. Corves, R. Duttmann, T. Freytag, R. Hassink,
W. Hoppe, H. Sterr, G. v. Rohr und R. Wehrhahn

Schriftleitung: P. Sinuraya

Band 121

NATASCHA OPPELT

Monitoring of the Biophysical Status of Vegetation Using Multi-angular, Hyperspectral Remote Sensing for the Optimization of a Physically-based SVAT Model

KIEL 2010

IM SELBSTVERLAG DES GEOGRAPHISCHEN INSTITUTS
DER UNIVERSITÄT KIEL
ISSN 0723 – 9874

ISBN 978-3-923887-63-7

Bibliographische Information Der DeutschenBibliothek
Die Deutsche Bibliothek verzeichnet diese Publikation in der Deutschen Nationalbibliografie; detaillierte bibliografische Daten sind im Internet über http://dnb.ddb.de abrufbar.

ISBN 978-3-923887-63-7

Die vorliegende Arbeit entspricht im Wesentlichen der von der Ludwig-Maximilians-Universität München im Jahre 2009 angenommenen gleichlautenden Habilitationsschrift.

Das Titelfoto zeigt das bayer. Alpenvorland
südlich von Gilching.

Foto: Natascha Oppelt

Foreword

My interest in the environment and in particular in plants is deeply rooted in my childhood in the Alps of Styria, which, as well as being my homeland, for me is still one of the most beautiful areas of unspoiled nature in the world. My academic studies and my scientific career to date at the Ludwig-Maximilians-Universität München have opened up to me many new perspectives, possibilities and methods for monitoring and investigating plants and their relationship to the environment.

A number of beneficial conditions contributed to the success of this paper. These are in particular a stimulating working atmosphere, the support of my mentor Prof. Dr. Wolfram Mauser, the availability of working materials and above all the excellent backing and support in my private surroundings.

First and foremost I would like to thank John Asquith, who found the strength and time to support me and encourage me in difficult phases. Besides this backing, which enabled me to concentrate on this work and which was an important foundation for its success, he also found the time to proofread the paper and to provide me with many notes and tips for improvement. Furthermore, as a native speaker, he put up with my linguistic outpourings with all the related problems that occur for a non-native speaker.

My thanks also go to my mentor Prof. Dr. Wolfram Mauser for his frequent support, discussions and critical suggestions and for allowing me the free space necessary for the completion of this paper. Prof. Mauser facilitated the contact to the European remote sensing community, which paved the way for my collaboration in international campaigns and projects. I also owe my introduction to modelling to him and the provision of the SVAT model PROMET for my work enabled the modelling spark to be ignited in me.

Tobias Hank also fuelled this modelling spark by providing me with an overview of the complex PROMET model. I would also like to thank Tobias Hank for his invaluable assistance with the photosynthesis models. With his support and the active help of student assistants, it was possible to successfully conduct both of the necessary field campaigns.

Another significant precondition for the success of this paper was the constant support of Dr. Roswitha Stolz, who besides being a helpful colleague also became a friend. Without her support and encouragement in the inevitable difficult phases, this paper would not have been a success. Our first joint interest is in New Zealand, after Austria the second most beautiful country in the world, which enabled interesting, educational and wonderful field trips to both countries. These would most certainly be described by the participating students as “strenuous”, which could be due to our second joint interest, sport. My

particular thanks are also due to her because she took the time, alongside her work, to critically review this paper and provide valuable suggestions for improvements.

Rainer Efinger was a constant help in processing the remote sensing data; the geometry of many data was in his hands. I would like to thank him for this work and for his services as the operator on the AVIS overflights. Thanks also to Dr. Heike Bach for the provision of the software for atmospheric correction. Furthermore, she enabled my scientific cooperation in the joint project *pre agro II*, which gave me invaluable insights into precision farming.

My thanks are due to Dr. Ingo Keding for always being willing to provide support in statistical matters, which were often dealt with during lunchtime discussions in the refectory. Not to be forgotten is the support of the farmers in the test area, Messrs. Stürzer, Zankl and Kiemer, who allowed access to their fields and patiently endured our weekly field visits. Mr. Stürzer also made his Schlagkartei records available and provided important information on matters of practical agricultural crop cultivation, for which I would like to offer my sincere thanks.

I would also like to thank the European Space Agency ESA for the provision of the CHRIS data within the scope of my function as Principal Investigator in the scientific mission of this sensor.

Many thanks also to Marcel Rangnow for his enduring patience in formatting the text, figures and tables.

My particular thanks go furthermore to two people from my private surroundings, whom I nevertheless do not wish to leave unmentioned: Ingold Lang, who in the last few years has been a teacher and a friend, and I very much hope that it will stay this way for many years to come, and Veronika Fussi, whom I will never forget.

To guard against too much sentimentality, I would like to end this foreword with a quote from Stephen Fry, which could not describe my situation more fittingly:

"I've counted up the words processed, a thing I do every hour, and, if technology can be trusted, it looks as if you're in for 94.536 of them. Good luck to you. You asked for it, you paid me for it, you've got to sit through it. As the man said, I've suffered for my art, now it's your turn."

Kiel 31.03.2010 Natascha Oppelt

Content

Foreword		I
Table of content		III
List of figures		XII
List of tables		XI
German summary (Zusammenfassung)		XIII
1	**Introduction**	1
2	**Photosynthesis and carbon assimilation**	7
2.1	**Chlorophyll and photosynthesis**	8
2.2	**Chlorophyll in the electromagnetic spectrum**	10
2.3	**Carbon assimilation**	11
2.3.1	The Calvin cycle	11
2.3.2	The C4 pathway	13
2.3.3	C3 versus C4 plants	14
2.4	**The C3 plant wheat** *(Triticum* spp*)*	14
2.5	**The C4 plant maize** *(Zea mays* L.*)*	15
3	**Test area and field measurements**	17
3.1	**Test area Gilching**	17
3.1.1	Geomorphology/Geology	18
3.1.2	Land cover	19
3.1.3	Climate	20
3.1.4	Test fields	23
3.2	**Field campaigns and acquired data**	24
3.2.1	Plant parameter	24
3.2.1.1	Phenological status	25
3.2.1.2	Plant height	26
3.2.1.3	Canopy density	26
3.2.1.4	Biomass	27
3.2.1.5	Chlorophyll content	28
3.2.1.6	Leaf area	29
3.3	**Field spectrometry**	30
3.4	**Photographic documentation**	32
3.5	**Sampling results**	32
3.5.1	Wheat	33
3.5.1.1	Sampling results – chlorophyll contents per mass	33
3.5.1.2	Sampling results – chlorophyll contents per area ground surface	35

3.5.2	Maize	37
3.5.2.1	Sampling results – chlorophyll contents per mass	37
3.5.2.2	Sampling results – chlorophyll contents per unit ground surface	39
3.6	**Evaluation of the results**	41
4	**Remote sensing data**	43
4.1	**Multi-angular remote sensing**	43
4.2	**CHRIS/PROBA-1**	45
4.2.1	Acquired data	47
4.2.2	Radiometric processing	48
4.2.3	Geometric processing	50
4.3	**AVIS**	51
4.3.1	Acquired data	53
4.3.2	Radiometric processing	54
4.3.3	Geometric processing	55
5	**Monitoring of canopy chlorophyll status**	57
5.1	**Reflectance anisotropy of vegetation canopies**	57
5.2	**Derivation of top-of-canopy chlorophyll**	60
5.2.1	Existing approaches	60
5.2.2	The chlorophyll absorption integral CAI	62
5.3	**Derivation of sun and shade chlorophyll using CHRIS data**	63
5.3.1	Wheat	64
5.3.2	Maize	67
5.3.3	Evaluation of the results	69
5.4	**Assessment of chlorophyll distribution maps**	70
5.5	**Transfer of results to AVIS data**	71
6	**Vegetation biophysics in the physically-based SVAT model PROMET**	75
6.1	**Modelling of the C3 pathway**	76
6.2	**Modelling of the C4 pathway**	78
6.3	**Input data**	79
6.4	**PROMET results**	80
6.4.1	Wheat 2004	80
6.4.2	Wheat 2005	82
6.4.3	Maize 2004	84
6.4.4	Maize 2005	86
6.5	**Concluding remarks**	87
7	**Assimilation of remotely sensed chlorophyll in PROMET**	89
7.1	**Chlorophyll and leaf absorptance**	89

7.2 Results using dynamised leaf absorptance 91
7.2.1 Wheat 2004 91
7.2.2 Wheat 2005 96
7.2.3 Maize 2004 100
7.2.4 Maize 2005 103

8 Synthesis 107
8.1 Distribution of chlorophyll within vegetation canopies 107
8.2 Monitoring of vertical chlorophyll distribution using hyperspectral, multi-angular remote sensing 108
8.3 Sensor dependency of the results 109
8.4 Chlorophyll and quantum yield 110
8.5 Assimilation of spatially distributed chlorophyll data in PROMET 110

9 References 113

Appendix

List of symbols, variables and constants 125
List of plant and soil parameters used in PROMET 127
Glossary 129

List of coloured figures

The following figures can be found as coloured versions in the middle part of the book:

Figure 7

Figure 16

Figure 28

Figure 32

Figure 36 - 41

Figure 44

Figure 46

Figure 48

Figure 50 - 54

List of figures

Fig. 1: Organisation chart of this thesis 5
Fig. 2: Simplified summary diagram of the light reaction of photosynthesis (modified after KAUFMAN et al. 1989) 8
Fig. 3: Energy absorption (~ ►) and excitation transfer (▭▹) between light harvesting pigments (left) and the chemical structure of chlorophyll a and b (right) (LAWLOR 2003) 9
Fig. 4: Absorption spectra of chlorophyll a and b in solution (left) and comparison of in vivo and in vitro chlorophyll absorption of soybean (right) (CHAPPELLE et al. 1992) 11
Fig. 5: Variation in photosynthetic mechanisms in higher plants: (a) C3 and (b) C4 photosynthetic carbon reduction (PCR) cycles (LAWLOR 2003) 12
Fig. 6: Location of the test area Gilching 18
Fig. 7: Digital maps of soil type and elevation in a Gauß Krüger (zone 4) coordinate system (the positions of the test fields are outlined and numbered in the soil map), the dimension of the test area is indicated by the solid line 18
Fig. 8: Percentage distribution of different land cover types in the test area Gilching 20
Fig. 9: Daily mean air temperature 2004 (top) and 2005 (bottom) as measured at "Gut Hüll" 21
Fig. 10: Precipitation 2004 (top) and 2005 (bottom) as measured at "Gut Hüll" 22
Fig. 11: Global radiation 2004 (top) and 2005 (2005) as measured at "Gut Hüll" 22
Fig. 12: Aerial photographs of the test fields and distribution of sampling points 23
Fig. 13: Differentiation between vegetation layers under direct and diffuse radiation regimes 25
Fig. 14: Relationship between chlorophyll a content per leaf area (chl_{LA} a) and per ground surface area (chl a) for wheat (left) and maize (right) as measured in 2005 30
Fig. 15: Setup of field spectrometer (left) and measurement pattern at each sampling point (right). The numbers indicate the order of measurements providing a mean spectrum of a sampling point 31
Fig. 16: Field spectrometer data as measured in 2005 for wheat (left) and maize (right) 32
Fig. 17: Statistics of chlorophyll content per mass [µg g^{-1}] as measured at the sampling points 34
Fig. 18: Chlorophyll content of wheat per mass [µg g^{-1}] as measured in 2004 and 2005; the upper bar graph indicates the sum of global irradiance as measured at the weather station "Gut Hüll" for the week prior to the

chlorophyll measurements 34
Fig. 19: Phenological development of wheat test fields 35
Fig. 20: Chlorophyll content per surface area [mg m^{-2}] wheat as measured in 2004 and 2005; the (blue) bar graph indicates the sum of global irradiance as measured at the weather station "Gut Hüll" for week prior to the chlorophyll measurements 36
Fig. 21: Statistics of wheat chlorophyll content per surface area [mg m^{-2}] as measured at the sampling points 36
Fig. 22: Chlorophyll content of maize per mass [µg g^{-1}] as measured in 2004 and 2005; the (blue) bar graph on the top indicates the sum of global irradiance as measured at the weather station "Gut Hüll" for the week prior to the chlorophyll measurements 38
Fig. 23: Statistics of the chlorophyll contents per mass [µg g^{-1}] as measured at the sampling points; std.error = standard error, std.dev = standard deviation 38
Fig. 24: Statistics of chlorophyll contents per surface area [mg m^{-2}] as measured at the sampling points; std.error = standard error, std.dev = standard deviation 39
Fig. 25: Chlorophyll content of maize per ground surface area [mg m^{-2}] as measured in 2004 and 2005; the blue bar graph indicates the sum of global irradiance as measured at the weather station "Gut Hüll" for the week prior to the chlorophyll measurements 40
Fig. 26: Phenological development of maize test fields in 2004 and 2005 40
Fig. 27: The platform PROBA-1 and CHRIS Fly-by Zenith Angles (FZA) and Minimum Zenith Angle (MZA) (SIRA 2004) 46
Fig. 28: Azimuth angles between the sensor and the sun (OPPELT & MAUSER 2007a) 48
Fig. 29: CHRIS and field spectrometer data (mean, minimum and maximum) gathered on June 2, 2005; the error bars indicate ±1.0 stdev of the CHRIS data 49
Fig. 30: CHRIS image stack (bgr = 437, 564, 669 nm) acquired on June 2 2005 (Gauß Krüger zone 4 coordinates); the test area is outlined 50
Fig. 31: Components of AVIS-2 (OPPELT & MAUSER 2007b) 51
Fig. 32. Sun-sensor azimuth angles for the multi-angular AVIS-2 acquisitions in 2004 54
Fig. 33. Brdf approximations of grass at 600 nm (left) and 675 nm (right), interpolated from measurements in the laboratory with a resolution of 5° and 16° in zenith and azimuth respectively; the illumination zenith angle is 35°, the illumination azimuth angle is 180° (SANDMEIER et al. 1998) 59

Fig. 34: a) Sample section of CHRIS data acquired on May 25, 2004 (bgr = 437, 564, 669 nm), b) proportion of shadows at the different viewing angles 60
Fig. 35: Continuum used to analyze the chlorophyll absorption feature in a reflectance spectrum (left) and continuum-removed absorption depth (right) (OPPELT 2002) 63
Fig. 36: Seasonal changes of ANIF derived from CHRIS bands in the Red and NIR for wheat 66
Fig. 37: Seasonal changes of the ANIF derived from CHRIS bands in the Red and NIR for maize 69
Fig. 38: Sun (left) and shade (right) chlorophyll a contents of wheat derived from CHRIS data acquired on May 25 2004, resampled to a grid size of 10 m 70
Fig. 39: Sun (left) and shade (right) chlorophyll a content of maize derived from CHRIS data acquired on July 21 2004, resampled to a 10 m grid size 71
Fig. 40: a) CAI images derived from AVIS (left) and CHRIS (right) nadir data acquired on May 25 2004; both images are resampled to a grid size of 10 m; b) CHRIS – AVIS CAI difference image, c) aerial photograph acquired in 2003 72
Fig. 41: Calculated AVIS chlorophyll contents for the sun (left) and shade (right) layers of wheat 74
Fig. 42: Diagram of the PROMET components (□) and their interfaces (⟶) (MAUSER & BACH 2008) 75
Fig. 43: Validation of PROMET results for wheat 2004 using the mean values of the field measurements at the five sampling points 81
Fig. 44: Measured yield (left), aggregated to a 10 x 10 m cell resolution and modelled yield (right) 81
Fig. 45: Validation of PROMET results for wheat 2005 using field measurements 83
Fig. 46: Measured (left) and modelled (right) yield for wheat 2005 83
Fig. 47: Validation of PROMET results for maize 2004 using field measurements 84
Fig. 48: Modelled leaf dry matter and total aboveground dry matter (silage yield) 85
Fig. 49: Validation of PROMET results for maize 2005 using field measurements 86
Fig. 50: Modelled leaf dry matter (left) and silage yield (right) for maize 2005 87
Fig. 51: Influence of CAI on the leaf absorptance (abs) for wheat (a) and maize (b) 91

Fig. 52: Modelled and measured fruit (left) and leaf (right) biomass for 2004 in comparison with field measurements at the different sampling points 93
Fig. 53: a) Modelled yield using CHRIS data acquired on May 25 (left) and AVIS data acquired on March 31 and May 25 2004 (right); b) resulting differences between modelled and measured yield (PROMET - measured) 94
Fig. 54: Difference image between measured and modelled yield (measured - PROMET abs_{const}) (left) and difference image between PROMET using CHRIS May 25 data and PROMET using abs_{const} (PROMET abs_{C0525} - PROMET abs_{const}) (right) 97
Fig. 55: Influence of abs on the relative total above-ground biomass modelled with PROMET; abs_{const} is marked red 97
Fig. 56: Development of leaf biomass using remotely sensed abs values combined with abs values adjusted to field management data ($PROMET_{precfarm}$, left) and difference between modelled and measured yield ($PROMET_{precfarm}$ - Measured) 98
Fig. 57: Modelled silage yield (left) and leaf biomass (right) using abs_{const} or abs_{RS} originating from different acquisition dates and sensors in comparison to field measurements at different sampling points 100
Fig. 58: Modelled silage yield using AVIS data acquired on May 25 2004 (left), CHRIS data acquired on July 21 2004 (centre) or a combination of AVIS and CHRIS data (right) 101
Fig. 59: Developmental of modelled total biomass throughout the vegetation period (left) and resulting silage yield using abs_{RS} which was recalibrated after three weeks (right) 102
Fig. 60: Modelled yield for maize 2005 using CHRIS data acquired on June 3 (left) and a combination of CHRIS data acquired on June 3 and AVIS/CHRIS data acquired on July 6 (right) 104
Fig. 61: Field measurements and corresponding trend lines at the different sampling points (the results of the sampling point in the low-productive zone is marked red) 105
Fig. 62: Influence of abs on the relative total silage yield (total above-ground biomass) modelled with PROMET; abs_{const} according to EVANS (1987) is marked red 106

List of tables

Tab. 1: Corner coordinates of the test area Gilching (Gauß-Krüger, Potsdam ellipsoid, Bessel date) 17
Tab. 2: Climate parameters as measured at "Gut Hüll" (the vegetation period was calculated from April 15 to October 15) 21
Tab. 3: Plant parameters measured during the field campaigns 2004 and 2005 25
Tab. 4: Principal BBCH growth stages (MEIER 2001) 26
Tab. 5: Results of the Shapiro-Wilk W test for wheat 33
Tab. 6: Results of the Shapiro-Wilk W test for maize 37
Tab. 7: Nominal central wavelengths and bandwidths for the CHRIS mode 5 data 46
Tab. 8: CHRIS data available for the vegetation periods 2004 and 2005 (w = wheat, m = maize) 47
Tab. 9: Parameter settings for the modelling of the CHRIS nadir atmosphere using MODTRAN-4 49
Tab. 10: Specification of AVIS-2 (modified, OPPELT & MAUSER 2007b) 52
Tab. 11: AVIS-2 centre wavelengths 53
Tab. 12: AVIS data acquired in 2004 and 2005, w = wheat, m = maize (letters in parenthesis indicate partly coverage of the test field) 53
Tab. 13: Parameter settings for the modelling of the AVIS nadir atmosphere using MODTRAN-4 55
Tab. 14: AVIS image acquisition settings in 2004 56
Tab. 15: CAI continuum start and end points 63
Tab. 16: Equations for wheat chlorophyll a estimation having the form $Chl = a \cdot e^{b \cdot CAI}$; fw = forward; bw = forward; N = Number of samples; r^2 = coefficient of determination between predicted and measured chlorophyll; n.s. = not significant; Est. err. = mean estimation error of Chl; a,b and est. err. are in mg m^{-2} 65
Tab. 17: Equations for wheat chlorophyll a estimation having the form $Chl = a + b \cdot CAI$; r^2 = coefficient of determination for the given equation 65
Tab. 18: Algorithms for maize chlorophyll a estimation having the form $Chl = a \cdot e^{b \cdot CAI}$; r^2 = coefficient of determination between predicted and measured chlorophyll 67
Tab. 19: Algortihms for maize chlorophyll a estimation having the form $Chl = a + b \cdot CAI$; r^2 = coefficient of determinationfor the given equation 68
Tab. 20: Statistics of CHRIS and AVIS CAI data of wheat acquired on May 25 2004 72
Tab. 21: Chlorophyll contents calculated for AVIS and CHRIS data of 25 May 2004 73
Tab. 22: Crop-specific parameters used 74

Tab. 23: Measured and modelled yield for wheat 2004 82
Tab. 24: Measured and modelled yield for wheat 2005 84
Tab. 25: Statistics of modelled leaf biomass and total above-ground biomass (silage yield) for maize 2004 85
Tab. 26: Statistics of modelled leaf biomass and total above ground biomass (silage yield) for maize 2005 87
Tab. 27: Comparison of yield measurements of wheat 2004 with modelled yield using PROMET with implemented CHRIS (C) and AVIS (A) abs_{RS} derived on different acquisition dates 92
Tab. 28: Coefficients of determination for modelled and measured fruit and leaf dry biomass at the different sampling points and mean difference at the sampling points [kg m^{-2}] between model and measurement (Field measurement – Promet) of the wheat field in 2004 95
Tab. 29: Comparison of yield measurements of wheat 2005 with modelled yield using CHRIS data on different acquisition dates 96
Tab. 30: Coefficients of determination for modelled and measured fruit and leaf dry biomass at the different sampling points and mean difference at the sampling points [kg m^{-2}] between model and measurement (Field measurement – Promet) of the wheat field in 2005 99
Tab. 31: Comparison of modelled yield for maize 2004 using CHRIS (C) and AVIS (A) data of different acquisition dates 101
Tab. 32: Coefficients of determination for modelled and measured total and leaf dry biomass at the different sampling points and mean difference at the sampling points [kg m^{-2}] between model and measurement (Field measurement – Promet) of the maize field in 2004 103
Tab. 33: Comparison of modelled yield for maize 2005 using CHRIS (C) and AVIS (A) data of different acquisition dates 105
Tab. 34: Coefficients of determination for modelled and measured total and leaf dry biomass at the different sampling points and mean difference at the sampling points [kg m^{-2}] between model and measurement (Field measurement – Promet) of the maize field in 2005 106

Zusammenfassung

Diese Arbeit ist das Ergebnis der letzten acht Jahre meines wissenschaftlichen Lebensweges und spiegelt die Schwerpunkte meiner Forschungsinteressen wider: Einen wesentlichen Schwerpunkt bildet das Thema Pflanzen, das nahezu unerschöpfliche Möglichkeiten der Forschung bietet. Der Großteil aller Austauschprozesse zwischen der Landoberfläche und der Atmosphäre werden durch Landpflanzen vermittelt (SCHURR et al. 2006). Dabei stellt die Photosynthese den primären Energiewandlungsprozess dar, der die Sonnenenergie in chemisch nutzbare Energie überführt, der Biomasseproduktion und Wachstum treibt. Photosynthese, Stoffproduktion und Pflanzenwachstum sind dynamische, in hohem Maße geregelte Prozesse, die von den verschiedensten Umweltfaktoren beeinflusst werden und zur Ausbildung vielfältiger räumlicher und zeitlicher Muster – von der Ebene der einzelnen Zelle bis zum Ökosystem – führen. Das Verstehen der komplexen Prozesse und ihrer Interaktionen führt dabei über die Analyse ihrer raumzeitlichen Dynamik auf verschiedenste Ebenen.

Die Zukunft vieler Themen der Menschheit ist eng mit dem Verständnis der raumzeitlichen Dynamik der Entwicklung und Funktion der Landpflanzen verbunden, wozu unter anderem die Sicherung der Ernährung und der Versorgung der Atmosphäre mit Sauerstoff gehört (OSMOND et al. 2004). Die Spannbreite der relevanten Muster reicht dabei von der subzellulären Ebene bis hin zu raum-zeitlichen Prozessen, die sogar aus dem Weltraum beobachtet werden können. Dies verdeutlicht die vielfältigen Möglichkeiten, welche Pflanzen für einen Wissenschaftler bieten und vielleicht erklärt sich damit mein Interesse an diesem Themenkomplex. Dabei liegt mir die Einbeziehung der Pflanzenphysiologie in die klassische Vegetationsgeographie besonders am Herzen.

Wer sich mit Vegetation beschäftigt, stößt bald auf Fragestellungen zum Pflanzenbau und zu modernen Methoden des Managements von Pflanzen im Rahmen derer ackerbaulichen Nutzung, die in den letzten Jahren aufgrund der geänderten Anforderungen des Landbaus an den Umweltschutz vermehrt auftauchten. Insbesondere im teilflächenspezifischen Anbau (precision farming) spielt die flächenhafte Untersuchung von Ackerkulturen eine wichtige Rolle, wobei hier eine besondere Rolle der Fernerkundung als Möglichkeit zur Beobachtung raumzeitlicher Prozesse zwischen und innerhalb von Pflanzenbeständen zukommt. Dabei stehen insbesondere hyperspektrale Instrumente im Zentrum des Interesses, da die Vielzahl der engbandigen Kanäle die Analyse von Pflanzeninhaltsstoffen, wie z. B. Chlorophyll, ermöglicht. Damit bietet sich eine Vielzahl von Möglichkeiten zur Beobachtung von pflanzenphysiologischen Vorgängen und deren raum-zeitlichen Mustern. Im Rahmen dieser Arbeit werden dabei C3 und C4 Pflanzen untersucht, welche die gängigsten Wege der Kohlenstoffassimilierung darstellen. Als Beispielpflanzen dienen Weizen (*Triticum aestivum* L.) und Mais (*Zea mays L.*), welche im Rahmen von Geländekampagnen in den Jahren 2004 und 2005 intensiv beprobt wurden und mit Hilfe von Fern-

erkundungssensoren im Laufe der Vegetationsperioden dieser beiden Jahre überflogen wurden, so oft es die örtlichen Wetterbedingungen erlaubten. Die Fernerkundungssensorik bestand aus dem satellitengestützten, Abbildenden Spektrometer CHRIS sowie dem flugzeuggetragenen Hyperspektralsensor AVIS. Die Analyse der Frage zur winkelabhängigen Beobachtung von Sonnen- und Schattenchlorophyll basiert auf regelmäßigen CHRIS Überflügen, welche die fernerkundliche Datengrundlage liefern. Räumlich hochaufgelöste, winkelabhängige Aufnahmen konnten im Jahr 2004 mit dem lehrstuhleigenen Sensor AVIS erhoben werden, dessen Daten als wertvolle Ergänzung dienen.

Neben der Analyse von Pflanzenbeständen hinsichtlich ihres Chlorophyllgehaltes und dessen raum-zeitlicher Dynamik stellt die modellhafte Abbildung dieser Dynamik einen weiteren Schwerpunkt dieser Arbeit dar. Pflanzen reagieren aufgrund ihrer sessilen Lebensweise auf globale Klimaveränderungen und auf regionale Umwelteinflüsse sehr sensibel. Dies verdeutlicht das seit Jahren wachsende Interesse an der Abbildung des pflanzlichen Stoffwechsels und der Photosynthese im Rahmen von Modellen (VON CAEMMERER 2000). Dafür ist ein vertieftes Verständnis des Metabolismus von Pflanzen erforderlich sowie eben die raum-zeitliche Dynamik, welche mit Hilfe von Fernerkundungsdaten abgebildet werden kann. Daher sollen die fernerkundlich abgeleiteten Chlorophyllgehalte von Sonnen- und Schattenbereichen in das physikalisch-basierte SVAT Modell PROMET implementiert werden. In PROMET wird die Photosynthese von Pflanzenbeständen bereits in einen Sonnen- und Schattenbereich unterteilt vorgenommen. Die obere Bestandesschicht unterliegt dabei einem Strahlungsregime, welches hauptsächlich von direkter Strahlung dominiert wird. Die untere, beschattete Bestandesschicht unterliegt einem Strahlungsregime, das von der diffusen Strahlungskomponente dominiert wird. Dabei wird die Absorption von Licht innerhalb der pflanzlichen Chloroplasten allerdings als konstant auf hohem Niveau angenommen. Die Einbindung von Fernerkundungsdaten soll Dynamisierung dieser Konstanten und damit eine Simulation der Photosyntheserate ermöglichen, die dadurch der Realität angenähert werden kann.

Die zentralen Zielsetzungen dieser Arbeit können folgendermaßen zusammengefasst werden:

1. Bestehen signifikante Unterschiede im Chlorophyllgehalt zwischen der oberen, besonnten Bestandesschicht und den beschatteten Bestandesbereichen von C3 und C4 Pflanzen?

2. Ermöglicht multi-angulare Fernerkundung die Ableitung der Unterschiede, welche im Gelände beobachtet werden?

3. Wie werden die Ergebnisse durch die Verwendung von unterschiedlichen Sensoren beeinflusst?

4. Welche Zusammenhänge bestehen zwischen dem Chlorophyllgehalt und der Abbildung der Photosynthese im Model PROMET?

5. Wie beeinflusst die Implementierung von Fernerkundungsdaten die Ergebnisse im Vergleich zu der konventionellen Verwendung der Modellkonstanten?

Diese zentralen Fragen, welche in der Arbeit ausführlich behandelt werden, werden im Folgenden zusammengefasst.

Verteilung des Chlorophyllgehaltes in Vegetationsbeständen

Aufgrund der fehlenden Datengrundlage war die Durchführung von Feldmessungen notwendig, welche im Rahmen von Feldkampagnen in den Jahren 2004 und 2005 in einem Testgebiet süd-westlich von München durchgeführt wurden. Im Rahmen dieser Geländekampagnen wurden Weizen- und Maisfelder in wöchentlichen Intervallen auf eine Reihe von Pflanzenparametern (feuchte und trockene Biomasse, Phänologie, Chlorophyllgehalt von Sonnen- und Schattenbereichen, LAI, usw.) hin untersucht. Diese Messungen fanden an jeweils fünf Probepunkten innerhalb des jeweiligen Feldes statt. Zusätzlich zu den regelmäßigen Probenahmen wurden an Überflugsterminen der Fernerkundungssensoren zusätzliche Feldbegehungen durchgeführt.

Die folgende Untersuchung beschränkt sich auf den Chlorophyllgehalt der Blätter, da diese Pflanzenorgane für die Photosynthese verantwortlich sind und damit den größten Anteil an Chlorophyll innerhalb der Pflanze beinhalten. Darüber hinaus sind die Blätter die Organe der Pflanzen, welche mit den Fernerkundungssensoren beobachtet werden (BLACKBURN 1989). Die wöchentlich durchgeführten Feldmessungen ergaben ein detailliertes Bild der untersuchten Pflanzenbestände, wobei signifikante Unterschiede zwischen der oberen Bestandesschicht und den darunter liegenden Bereichen beobachtet werden konnten. Neben dem deutlichen Unterschied, der sowohl im Chlorophyll a- und b-Gehalt zwischen den beiden Bestandesschichten bei Weizen und Mais beobachtet werden konnte, wurde ebenfalls eine erhebliche zeitliche Dynamik innerhalb einer Vegetationsperiode festgestellt. Die beobachtete zeitliche Dynamik wird insbesondere durch Düngemaßnahmen gesteuert: Jede Düngegabe führt zu einem deutlichen Anstieg v. a. der Chlorophyll a Gehalte (Sonne wie Schatten), wobei die Steigung des Anstieges von den meteorologischen Bedingungen um die Düngegaben bedingt wird. Höhere Temperaturen als Folge von hohem Strahlungseinfall im Frühjahr und ausreichende Niederschläge verstärken den Aufbau von Chlorophyll, welches in einem erhöhten Metabolismus und damit zu einem verstärkten Zuwachs an Biomasse führt. Niedrige Temperaturen, Spätfröste und geringer Strahlungsgenuss führen zu einer verzögernden Wirkung in der Zunahme des Chlorophyllgehaltes.

Die Ergebnisse der Feldmessungen zeigen, dass sowohl Weizen wie auch Maispflanzen den Chlorophyllgehalt ihrer Blätter dynamisch regulieren und in Anlehnung an sich (auch kurzfristig) ändernde Umweltbedingungen auf- bzw. abbauen. Die zu vermutende Abhängigkeit der Geschwindigkeit im Chlorophyllauf-, und -abbau von der Pflanzenart eröffnet ein weites Feld für weitere Untersuchungen. Die Ergebnisse verdeutlichen aber v. a. die Notwendigkeit, nicht nur die räumliche Dynamik im Chlorophyllgehalt der Bestandesoberschicht zu erfassen, was mit konventionellen Fernerkundungsmethoden möglich ist, sondern auch die Wichtigkeit, diese räumliche Dynamik auch in unteren, beschatteten Vegetationsschichten zu untersuchen, d. h. die vertikale Dynamik zu erfassen.

Die Feldmessungen wurden in zwei aufeinander folgenden Jahren durchgeführt. Ein Vergleich der phänologischen Entwicklung der Bestände mit der Entwicklung der Biomasse ergab, dass die Pflanzen trotz unterschiedlicher Wetterbedingungen eine annähernd parallele phänologische Entwicklung aufweisen, während die Entwicklung der Biomasse deutliche Unterschiede zeigt. Dadurch wird deutlich, dass die Entwicklung eines Pflanzenbestandes über deren Phänologie nicht unbedingt Rückschlüsse auf die bis dahin aufgebaute Biomasse zulässt.

Untersuchung der vertikalen Chlorophyllverteilung mit hyperspektraler, multi-angularer Fernerkundung

Die Annahme, dass hyperspektrale, multi-angulare Fernerkundung zur Ableitung des Sonnen- und Schattenchlorophylls von Vegetationsbeständen geeignet ist, beruht auf der Hypothese des sog. „Gap Effects“ (KIMES 1983). Diese theoretische Annahme wurde in dieser Arbeit am Beispiel des Chlorophyllgehaltes von den Ackerkulturen Weizen und Mais untersucht. Dies war bis dahin aufgrund der fehlenden Daten experimentell nicht nachweisbar. Die einzigartige Datengrundlage, welche innerhalb der Geländekampagnen erhoben werden konnte, ermöglicht eine erstmalige quantitative Überprüfung dieses Ansatzes für den Chlorophyllgehalt auf der Feldskala. Die Analyse beschränkte sich dabei auf den Chlorophyll a Gehalt der Blätter, da Chlorophyll a Moleküle als Reaktionszentren den Elektronentransport im Rahmen der Photosynthese regulieren und limitieren (HOPKINS 1995, BLACKBURN 2006).

Die Analyse der CHRIS Daten konnte die Annahme des Gap Effects für die Ableitung des Chlorophyllgehaltes von Weizen und Mais bestätigen und bestärkt die Annahme, dass biophysikalische Pflanzenparameter in besonnten und beschatteten Bestandesschichten mit Hilfe von hyperspektraler, multi-angularer Fernerkundung abgeleitet werden können. Der Sensor CHRIS eröffnet die Möglichkeit der Aufnahme der Erdoberfläche in fünf Beobachtungswinkeln (± 55°, ± 36°, ± Nadir) während eines Überfluges. Diese Konstellation führt im Testgebiet zu vorwärtsgerichteten Aufnahmen entgegen der Beleuch-

tungsrichtung, während die rückwärtsgerichteten Winkelaufnahmen annähernd parallel zur Beleuchtungsrichtung verlaufen.

Nach durchgeführter Atmosphärenkorrektur, Reflexionskalibrierung und geometrischer Korrektur der Daten bestätigte die nachfolgende Analyse in der Literatur beschriebene Ergebnisse, dass der Chlorophyllgehalt der besonnten Bestandesschicht mit Hilfe von Nadiraufnahmen abgeleitet werden kann (CHAPELLE et al. 1992, YODER & PETIGREW-CROSBY 1995, BLACKBURN 1998). Dabei erwies sich der Zusammenhang für Mais als deutlich stärker ausgeprägt ($r^2 = 0,84$) als für Weizen ($r^2 = 0,61$). Die Ergebnisse für Weizen konnten allerdings verbessert werden, wenn die „Nadir"-Aufnahmen des CHRIS getrennt in vorwärts- und rückwärtsblickende Aufnahmen analysiert wurden, wobei bei den vorwärtsblickenden Aufnahmen ein hoher statistischer Zusammenhang ermittelt werden konnte ($r^2 = 0,69$).

Die Ableitung des Schattenchlorophylls zeigt eine starke Abhängigkeit vom bidirektionalen Reflexionsverhalten der Bestände: Die Weizenfelder zeigten eine hohe Anisotropie im Bereich der rückwärtsblickenden Aufnahmewinkel, wobei der Hot Spot im Bereich der -36° Aufnahmen liegt. Die am niedrigsten ausgeprägte Bidirektionalität wurde bei den vorwärtsblickenden Aufnahmen beobachtet. Ein deutlicher Zusammenhang der Fernerkundungsdaten mit dem Schattenchlorophyll konnte in diesem Aufnahmebereich mit geringster Bidirektionalität nachgewiesen werden, d. h. den vorwärtsblickenden Nadirbildern und dem +36° Aufnahmen ($r^2 = 0,76$ bzw. 0,65).

Die Analyse der Maisfelder führte zu ähnlichen Ergebnissen, wobei der Hot Spot im Bereich der -55° Aufnahmen beobachtet wurde. Die Ableitung des Schattenchlorophylls zeigte ebenfalls die besten Ergebnisse bei den vorwärtsblickenden CHRIS Aufnahmen, wobei die Winkelbereiche bei +36° ($r^2 = 0,71$) und +55° ($r^2 = 0,70$) gleichermaßen gut abschneiden konnten. Die niedrigeren Aufnahmewinkel (36°) sind aber den höheren (55°) vorzuziehen, da mit zunehmendem Aufnahmewinkel die geometrische Auflösung der Daten abnimmt.

Aus früheren Studien sind Sättigungseffekte verschiedener Indices bei hohen Chlorophyllgehalten bekannt (OPPELT 2002, HABOUDANE et al. 2004, OPPELT & MAUSER 2004). OPPELT (2002) beschreibt die Sättigung des CAI bei Chlorophyll a Gehalten, welche 1 g m^{-2} überschreiten. Damit kann ein exponentieller Zusammenhang zugrunde gelegt werden, der in den obigen Ergebnissen beschrieben wurde. Allerdings werden im Rahmen dieser Arbeit Sättigungswerte nicht erreicht, wodurch die Annahme von linearen Zusammenhängen zu gleichen Ergebnissen führen würde.

Einfluss unterschiedlicher Sensoren

Die Verwendung verschiedener Sensoren beinhaltet immer auch die Frage der Vergleichbarkeit der Bilddaten, da je nach Sensor die geometrische Auflösung erheblich schwanken kann. Die in dieser Arbeit verwendeten Sensoren ergaben geometrische Auflösungen im Nadirbereich von 2 bzw. 4 m (AVIS) und 17 m (CHRIS). Um die vorgegebene Rastergröße für die Modellierung zu erfüllen, wurden beide Datensätze einem Resampling Verfahren (Nearest Neighbour) unterzogen und lagen damit in einer Pixelgröße von 10 m vor.

Neben der geometrischen Auflösung unterscheiden sich Reflexionsspektren unterschiedlicher Sensoren hinsichtlich der Kanalzahl, der Wellenlängenzuordnung der Kanäle und der Kanalbreite. Diese Unterschiede führen zu unterschiedlichen Reflexionsspektren und bei der Anwendung von Indizes zu oftmals nicht vergleichbaren Ergebnissen. Um diese Effekte zu minimieren, wird in dieser Arbeit eine Weiterentwicklung eines bestehenden Index, dem Chlorophyll Absorption Integral (CAI), vorgestellt. Mit Hilfe dieses Ansatzes, der auf der Methode der spektral Einhüllenden des Bereiches der Chlorophyllabsorption im roten Wellenlängenbereich basiert, gelingt es die oben genannten Effekte durch die Einführung einer künstlich einheitlichen Inkrementierung des Reflexionsspektrums in 0,1-nm-Schritten zu minimieren. Die Indexwerte von AVIS und CHRIS liegen bei Anwendung des CAIs im Wertebereich der 1.5-maligen Standardabweichung des jeweiligen anderen Sensors. Dabei liegen die CAI-Werte des AVIS tendenziell unter dem Wertebereich der CHRIS Daten.

Der direkte Vergleich von AVIS und CHRIS CAI Daten zeigte, dass beide Sensoren in der Lage sind, räumliche Heterogenitäten innerhalb der Felder mit der oben genannten Genauigkeit zu erfassen, wobei die höhere geometrische Auflösung von AVIS eine höhere Standardabweichung innerhalb eines Feldes bedingt. Die zusätzliche Verwendung von hochaufgelösten Daten begünstigt die Erfassung kleinräumiger Heterogenitäten, Windbruchbereiche oder Düngefenster, welche bei der ausschließlichen Analyse von CHRIS-Daten nicht aufgelöst werden können.

Chlorophyll und die Modellierung der Photosynthese in PROMET

Das flächenverteilt, physikalisch-basiert rechnende SVAT Model PROMET wurde im Rahmen dieser Arbeit verwendet. PROMET simuliert Wasser- und Energieflüsse und deren flächenhafte Verteilung in unterschiedlichen zeitlichen und räumlichen Skalen (MAUSER & BACH 2008). Der modulare Aufbau von PROMET ermöglicht dabei relativ leichten Zugang zu einzelnen Modulen, in diesem Fall dem Vegetationsmodul. Die Simulation der Photosynthese basiert hier bei C3 Pflanzen auf einem mechanistischen, biochemischen Ansatz zur vereinfachten Berechnung der im Calvin-Zyklus ablaufenden Pro-

zesse nach FARQUHAR et al. (1980). Bei C4 Pflanzen wird die Kohlenstoffassimilation des Calvin-Zyklus durch die Einführung eines zusätzlichen C4-Zyklus nach CHEN et al. (1994) berechnet. Beiden Ansätzen gemein ist die Annahme, dass der Elektronentransport eine Schlüsselrolle für die Verwertung der absorbierten photosynthetisch aktiven Strahlung (APAR) einnimmt und damit die Quantenausbeutung des Photosyntheseapparates bestimmt. In PROMET wird APAR durch eine konstante Zustandsgröße, den Blatt-Absorptionsgrad *abs*, reguliert (abs_{const} = 0,89).

Im Rahmen dieser Studie konnte der Zusammenhang zwischen *abs* und dem Chlorophyllgehalt hergestellt werden. Durch Einsetzen des mathematischen Zusammenhangs zwischen *abs* und Chlorophyll in die Regressionsgleichungen, welche im Rahmen der Ableitung des Chlorophyllgehaltes mit dem CAI ermittelt wurden, kann *abs* direkt aus den CAI Werten ermittelt werden. Mit Hilfe dieser Gleichungen wird eine Dynamisierung von *abs* für Sonnen- und Schattenchlorophyll möglich. Die daraus resultierenden *abs* Verteilungskarten können in PROMET assimiliert werden.

An dieser Stelle bestehen zahlreiche Anknüpfungspunkte für zukünftige Untersuchungen. Möglich sind dabei Untersuchungen, inwieweit artspezifische Beziehungen zwischen dem Chlorophyllgehalt und *abs* hergestellt werden können. Darüber hinaus stellt sich natürlich die Frage inwieweit eine Veränderung von *abs* über die Vegetationsperiode hin für unterschiedliche Pflanzenarten als konstanter Verlauf in PROMET eingehen kann.

Ergebnisse der Assimilierung von Fernerkundungsdaten in PROMET

Die Modellierung der C3 und C4 Photosynthese in PROMET ist das Ergebnis der Berechnung einer „potentiellen Photosyntheserate“ unter gegebenen Umweltbedingungen, die durch Parameter wie Strahlungsbedingungen, Temperatur, Wasserverfügbarkeit, Sauerstoff- und Kohlendioxydgehalt der Luft bestimmt werden. Dabei wird eine optimale Versorgung der Pflanzen mit Nährstoffen angenommen, was zu optimalen Wachstumsbedingungen im ganzen Pflanzenbestand führt. Defizite in der Nährstoffversorgung, mechanische Einwirkungen auf das Pflanzenwachstum, auftretende Krankheiten, Windwurf etc. können mit PROMET daher nicht nachgebildet werden. Dies führt zu sehr homogen entwickelten, modellierten Biomassen und Erträgen, welches in niedrigen Standardabweichungen in den Ergebnissen sichtbar wird.

Pflanzenbestände, die sich auch in der Realität sehr homogen entwickeln, können mit PROMET daher auch ohne die Einbindung von Fernerkundungsdaten gut nachgebildet werden, was für einen Maisbestand gezeigt werden konnte. Eine Validierung der Modellergebnisse mit Feldmessungen über die Vegetationsperiode ergab eine Unterschätzung der gemessenen Gesamt-Biomasse durch PROMET von nur 109 g m^{-2} (das entspricht 4,3 % der Gesamt-Biomasse). Generell zeigt PROMET bei der Abbildung von C4 Pflan-

zen hohe Genauigkeiten, wobei die Implementierung von flächenverteiltem *abs* zu einer weiteren Verbesserung der Modellergebnisse, wenn ein Bestand Zonen unterschiedlicher Pflanzenentwicklung aufweist. Hier liegt das Potential der Fernerkundungsdaten natürlich eindeutig in der flächenverteilten Abbildung realitätsnaher Bedingungen. Diese Genauigkeit bezieht sich sowohl auf mittlere Feldwerte als auch auf die punktförmige Validierung der Ergebnisse mit Hilfe der Geländemessungen. So konnte im oben beschriebenen Fall das Ergebnis mit dem Einsatz von Fernerkundungsdaten auf 59 g m^{-2} verbessert werden.

Im Falle von Weizen überschätzt PROMET im Allgemeinen sowohl die Pflanzenentwicklung wie auch den erzielten Ertrag um etwa 30 %, wenn keine Fernerkundungsdaten implementiert werden. Auch bei den Weizenbeständen wird die Entwicklung sehr homogen modelliert (niedrige Standardabweichung), wobei die Modellergebnisse zeigen, dass externe Faktoren wie reliefbedingte Beleuchtungsunterschiede oder Veränderungen im Bodentyp oder in der Bodenart abgebildet werden. Die Implementierung der dynamischen *abs* Werte zeigte bei Weizen sehr deutlich die Vorteile der Einbindung von Fernerkundungsdaten. Die Pflanzenentwicklung wird verbessert nachgebildet ebenso wie die Höhe und die Verteilung des Ertrages. Die flächenhafte Validierung des modellierten Ertrages mit GPS-gestützten Ertragsmessungen ergab, dass durch den Einsatz von Fernerkundungsdaten die Abweichungen des Modells von durchschnittlichen 30 % auf 8 % reduziert werden konnten.

Bei der Einbindung der Fernerkundungsdaten in PROMET bestehen unterschiedliche Möglichkeiten. Einige werden beispielhaft an verschiedenen Feldern vorgestellt: Die einfachste Art der Datenassimilation ist der Weg des sog. Updatings, d. h. ab dem Zeitpunkt, an dem dynamische *abs* Werte zur Verfügung stehen, wird die Modellkonstante (abs_{const}) durch die flächenhafte Verteilung (abs_{RS}) abgelöst, d. h. der Bestand wird mit dieser Verteilung weitergerechnet, bis eine neue abs_{RS} Verteilung zur Verfügung steht. Diese Methode liefert gute Ergebnisse, wenn im Laufe einer Vegetationsperiode regelmäßig abs_{RS} Daten zur Verfügung stehen. Das Updating führt sowohl bei C3 wie bei C4 Pflanzen zu einer Erhöhung der Dynamik innerhalb der Bestände und im Falle von Weizen zu einer deutlich realitätsnäheren Darstellung, d. h. Reduktion, des Ertrages. Die Genauigkeit der Modellergebnisse hängt ebenso von der geometrischen Auflösung des gewählten Sensors ab. So führt die Implementierung von AVIS Daten zu mehr Heterogenität im Bestand als beim Einsatz von CHRIS Daten. Die hohe räumliche Genauigkeit der AVIS Daten ermöglicht die modellgestützte Erfassung des Vorgewendes, der Traktorspuren sowie der Düngefenster, wodurch die höhere Dynamik im Bestand begründet liegt.

Darüber hinaus stellt sich der Zeitpunkt der Dynamisierung als wichtig heraus. So werden die Entwicklung der Biomasse sowie der Ertrag von PROMET deutlich unterschätzt, wenn abs_{RS} nur in frühen pflanzlichen Entwicklungsphasen verwendet werden, da damit der Absorptionsgrad der Blätter in darauf folgenden Phänologiestadien unterschätzt wird.

Um Fehleinschätzungen im Modell vorzubeugen, welche durch fehlende Fernerkundungsdaten bzw. große Lücken zwischen verfügbaren Datensätzen entstehen, wird die Methode der Rekalibrierung vorgestellt. Das bedeutet, dass abs_{RS} nach einem definierten Zeitintervall wieder zu abs_{const} zurückgesetzt wird. Die Validierung mit den punktuellen Feldmessungen ergibt, dass der Einsatz dieser Methode zu einer Erhöhung der Dynamik innerhalb des Feldes führt, aber die Rekalibrierung zu abs_{const} eine verbesserte Nachbildung späterer Entwicklungsstadien ermöglicht. Diese Methode kann auch bei großen zeitlichen Datenlücken angewendet werden, wobei eine Rekalibrierung mehrmals durchgeführt wird, was sowohl bei einem Weizen- als auch bei einem Maisbestand gezeigt werden konnte.

Eine Abwandlung der Rekalibrierung ist möglich, wenn Informationen über das Feldmanagement vorliegen. Diese Precision Farming Variante passt abs_{const} z. B. nach Düngung des Feldes an einen neuen abs_{const} Wert an, der zwar keine flächenverteilte Änderung beinhaltet, aber den Absorptionsgrad an die Veränderungen im Chlorophyllgehalt nach der Düngung anpasst. Ab dem Zeitpunkt an dem abs_{RS} Daten verfügbar sind, wird der angepasste Absorptionsgrad durch abs_{RS} ersetzt. Diese Vorgehensweise stellte sich als hocheffiziente Methode zur Ableitung des Ernteertrages von Weizen heraus, wobei die Abweichungen des Modells vom Ertrag nur noch 4,5 % betrugen. Damit ist das Potential der Anwendung von PROMET zur Ernteertragsschätzung im Bereich des Precision Farmings als hoch anzusehen. Dabei birgt die Beobachtung des Schattenbereiches die Möglichkeit, Pflanzenkrankheiten oder Stressfaktoren wie z. B. Schädlingsbefall im Frühstadium zu erkennen, da diese Probleme zuerst an chlorotischen Veränderungen an den Schattenblättern sichtbar werden. Dadurch können Düngemittel, aber auch Herbi- und Pestizide umweltschonend und kosteneffizient eingesetzt werden, da ein gezielter Einsatz auf den befallenen Teilflächen möglich ist.

Der Einfluss sich ändernder abs_{const} Werte in PROMET wurde gesondert für Weizen und Mais untersucht. Dabei wurde die Entwicklung der Biomasse eines Jahres unter Verwendung von abs_{const} simuliert. Der Vergleich der Ergebnisse für schrittweise höhere abs_{const} Werte zeigte für Weizen, dass der höchste Biomasseertrag bei der Verwendung von $abs_{const} = 0{,}83$ erzielt werden konnte. Dieser Punkt beschreibt den Umschlagpunkt von der Elektronentransport-limitierten Assimilationsrate hin zu einer Rubisco-limitierten Assimilationsrate. Bei weiter zunehmenden abs_{const} Werten erhöht sich im Laufe einer Vegetationsperiode die Wahrscheinlichkeit des wiederholten Auftretens dieser Bedingungen, die zu einer leichten Erniedrigung der gebildeten Biomasse führt. Dieses für C3 Pflanzen charakteristische Verhalten konnte bei Mais nicht beobachtet werden. Hier stieg der Biomasseertrag bis zu dem höchstmöglichen $abs_{const} = 1$ an. Diese Ergebnisse führen zu dem Vorschlag den momentan in PROMET festgesetzten $abs_{const} = 0{,}98$ (nach EVANS 1987) für Weizen in $abs_{const} = 0{,}83$ zu ändern, da dieser Wert den Annahmen der Nachbildung von Optimalbedingungen eher entspricht.

Die dargestellten Fakten eröffnen eine Vielzahl von neuen Ansätzen zur raum-zeitlichen Dynamisierung der Modellergebnisse mit Hilfe von hyperspektralen Fernerkundungsdaten. Die Anwendung multi-angularer Daten ermöglicht die dynamische Parametrisierung nicht nur in besonnten Bestandesschichten, sondern auch in unteren, beschatteten Bereichen. Die erzielten Ergebnisse können als Grundlage sowohl im Bereich des Precision Farmings auf Feldebene als auch für eine verbesserte Nachbildung der Rolle der Vegetation auf der Landschaftsebene (z. B. Simulation des Kohlenstoffkreislaufs) dienen.

1 Introduction

This thesis is the result of the last eight years of my life and reflects my main research interests, which stem from my strong personal relationship to vegetation matters, including my garden at home. A main interest is the integration of plant physiology into geographic research and remote sensing. Plants are the most important organisms on the Earth, and our existence is bound to the existence of green vegetation. Plants perform in a spatially and temporally heterogeneous environment. But even though we all know the basic principles of plant functionality such as photosynthesis, we also know that our understanding is only fragmentary (OSMOND et al. 2004). Recent years have been strongly influenced by the buzzword "global change", and with the growing interest in changing environmental conditions it has also become evident that our understanding of plant functions is far from systematic, quantitative or sufficient to predict plant performance in future climatic scenarios or to be exploited to attain a higher efficiency of resource use in crops (SCHURR et al. 2006). Nevertheless, complex interactions between a fluctuating environment and the dynamics of plant processes are crucial for the performance of plants in ecosystems. The enormously important role of their dynamic behaviour in natural and managed ecosystems demonstrates the need for research in this thematic field.

The basic idea for this thesis evolved from the research project ALADIN (coupled Analysis of chLorophyll and wAter status of vegetation using hyperspectral, bi-DIrectional remote seNsing), funded by the German Research Foundation (DFG). One of the topics of ALADIN is the investigation of multi-angular remote sensing data for a vertical profiling of biophysical vegetation parameters. The spatial and content proximity to the joint project GLOWA – Danube (Global change and the hydrological cycle), which is, among other topics, dealing with the further development of the soil-vegetation-atmosphere transfer (SVAT) model PROMET (Processes of RadiatiOn, Mass and Energy Transfer, MAUSER & BACH 2008), enabled the use of this model. The fusion of remote sensing data and ecosystem modelling is an important step towards a more realistic portrait of our environment and an improved understanding of biophysical processes (OSMOND et al. 2004). The cooperation with the joint project pre agro II, funded by the German federal ministry of education and research (bmb+f), was highly effective and led to an insight into the increasing importance of both remote sensing and modelling techniques also in the field of precision farming.

Thus, this study involves the fields of vegetation geography, precision agriculture, remote sensing and modelling and thus represents a modern approach to ecological research based on more than one of the classic scientific areas. The cooperation with researchers of various scientific backgrounds enabled its development to a self-contained unit, and furthermore gave plenty of opportunity to learn and pick up ideas for the present study as well as for future research.

One major topic for the understanding of plants is the functionality of plant pigments, which are of tremendous significance in the biosphere. Within leaf chloroplasts pigments absorb solar radiation and transfer the energy to initiate photosynthesis. The most important of these pigments are the chlorophylls (RICHARDSON et al. 2002). They have a dominant control upon the amount of solar radiation that a leaf absorbs, therefore foliar concentrations of chlorophylls control photosynthetic potential and, consequently, primary production (BLACKBURN 2006). Indeed, it has been argued that the chlorophylls are Earth's most important organic molecules as they are essential for photosynthesis (DAVIES 2004).

Given the importance of plant chlorophylls, information concerning their temporal dynamics and spatial variation can provide key contributions to a wide range of scientific investigations and environmental/agricultural management ventures. However, current capabilities for measuring foliar chlorophyll are limited. Traditional techniques involve extraction with a solvent and spectrophotometric analysis using standard procedures. However, these laboratory techniques are time and labour-intensive and provide only punctiform information. Thus, for whole canopies, pigments must be quantified by extrapolation from a limited number of samples. Faster, non-destructive measurements can be obtained using hand-held instruments, but the instrument readings need to be calibrated and there is still a requirement to extrapolate spatially from a restricted number of samples and measurements.

The different spectral absorption properties of pigments can be used to accurately measure individual pigment concentrations (LICHTENTHALER 1987, PORRA et al. 1989) and have enabled the analysis of chlorophyll samples in the laboratory since the 1970s. These properties, which are discussed in section 2, are also used to perform measurements of reflected radiation via remote sensing as a non-destructive method for quantifying pigments spatially.

Although multispectral remote sensing systems have been used for quantifying biophysical properties of vegetation such as the Leaf Area Index (LAI), the advent of airborne and, more recently, spaceborne hyperspectral instruments enables the acquisition of high resolution vegetation spectra and methods for imaging plant pigment concentrations (BLACKBURN 2006). In recent years, the availability of multiangular remote sensing data, where measurements of a given target are taken from several viewing angles, offers the possibility of exploiting directional information, which has been shown to be especially influenced by the geometric properties of the target (SANDMEIER et al. 1999, CHEN et al. 2003, CHOPPING et al. 2005). The combination of hyperspectral and multiangular sensors gave the idea of not only analyzing the top of a canopy, as is common using conventional nadir data, but also trying to gain an insight into vegetation canopies. The following up of this idea was funded by the DFG, which enabled the intensive field campaigns as well as the

operation of the airborne sensor AVIS (Airborne Visible/Infrared imaging Spectrometer), both of which were necessary due to the lack of data. However, the number of plants to be investigated was limited; therefore representatives have to be chosen. In this study representatives of the two main pathways of photosynthesis, namely C3 and C4 plants, were selected. The biochemical and biophysical differences of these two plant groups are described in section 2 together with the representatives chosen, i.e. wheat (*Triticum aestivum* L.) and maize (*Zea mays* L.). In addition to the AVIS data, multiangular CHRIS (Compact High Resolution Imaging Spectrometer) imagery forms the remotely sensed data basis. The CHRIS data were kindly provided by the European Space Agency (ESA), which operates the sensor in the scope of its Earth Observation Program and enabled access to the data within the scientific mission of this instrument. Both sensors, AVIS and CHRIS, as well as the processing of the data are described in section 4.

Besides the developments in hyperspectral data acquisition there has been an increasing intensity of research focused on developing techniques for analysing vegetation spectra in order to quantify pigment concentrations, especially of chlorophylls. To extract pigment information, a range of other factors that influence vegetation reflectance must be taken into account. The internal structure of leaves, with large numbers of refractive discontinuities between cell walls and intercellular air spaces, scatters incident radiation and allows a large proportion to pass back through the upper epidermis to be observed as reflected radiation. Water, pigments and other biochemicals absorb certain wavelengths of radiation, which reduces the reflectance in these regions. The leaf reflectance may also vary independently of pigment concentrations due to differences in internal structure, surface characteristics and moisture content. Furthermore, the reflectance spectrum of a whole canopy is influenced by factors such as the effects of leaf area, the orientation of leaves, ground coverage, and presence of non-leaf elements, areas of shadow and soil surface reflectance. These factors obscure the relationship between spectral reflectance and chlorophyll concentration (BLACKBURN 2006) and thus have to be considered. An overview of existing approaches for the derivation of vegetation chlorophyll is presented in sections 5.1 and 5.2. One approach, which has already proved to be a suitable chlorophyll estimator using conventional, nadir-looking data, is central to the discussion about the derivation of the vertical chlorophyll distribution. Its description and the enhancements performed are the focus of section 5.3.

Thus, the potential of airborne and spaceborne multi-angular data is analyzed for its capability to estimate not only the horizontal distribution of chlorophyll in wheat and maize canopies, but also its vertical distribution. This means that the canopy is differentiated into two canopy layers, a “sun” and a “shade” layer. The former is mainly influenced by direct radiation, while the latter is dominated by a diffuse radiation regime. Chlorophyll distribution maps (section 5.4) for sun and shade layers, for both wheat and maize canopies, result from the analysis of the remotely sensed data and form the link between

remote sensing data and the physically-based modelling of vegetation growth and development.

During the last few decades, the modelling of plant growth and development has become increasingly important (CHEN et al. 1999, WEISS et al. 2001, FARQUHAR et al. 2001, VERHOEF & BACH 2003, SCHURR et al. 2006). There is also an increasing recognition that there is a need for an accurate description of temporal and spatial variation of biophysical parameters, such as chlorophyll content, if processes such as photosynthesis are to be modelled successfully (BARRADAS et al. 1999, VON CAEMMERER 2000). In ecophysiological and productivity models the rates of photosynthesis are in general estimated on the basis of more or less simplified photosynthesis models, which need input information such as the irradiance, the chlorophyll a and b content or the content of the enzyme Rubisco. Remote sensing measurements can be used for an effective parameterization and validation of models (KEUR et al. 2001, KOETZ et al. 2005, VERHOEF & BACH 2007). To discuss the potential and benefits of the assimilation of remote sensing data and vegetation modelling, the remotely sensed chlorophyll maps are implemented in the SVAT model PROMET, whereby the fundamentals of the vegetation biophysics in PROMET are described in section 6. Section 7 is dedicated to the description of the assimilation of remote sensing data and the discussion of the results.

The scientific fields touched upon by this thesis were described in the previous paragraphs. An overview is also presented in Figure 1.

The main topics can be summarized as follows: The differences between the biophysical status of vegetation in the top-of-canopy layer and beneath are investigated via field measurements. The next step goes from the analysis of field measurements to their monitoring using remote sensing techniques. The top-of-canopy chlorophyll is known to be strongly related to nadir imagery. Here, a new idea is followed, which is based on the hypothesis that the chlorophyll content of the shade canopy layer can be derived using angular remote sensing and that the chlorophyll content of a vegetation canopy can thus be spatially derived for the two layers of interest. The hyperspectral sensors used for this study are satellite-based (CHRIS) and airborne (AVIS), resulting in data with different spatial resolutions on ground (decametre versus metre), different band settings and spectral resolutions. These differences in turn lead to different results when indices are applied. Last but not least, the remotely sensed chlorophyll data are assimilated into the physically-based SVAT model PROMET to dynamise the absorptance of the leaves, which has until now been implemented as a model state constant. The dynamised absorptance enables a more realistic, spatial-temporal simulation of photosynthesis and thus enables a more realistic, modelled behaviour of vegetation, which is a key for an accurate description of vegetation functioning in eco-physiological or agricultural management modelling approaches.

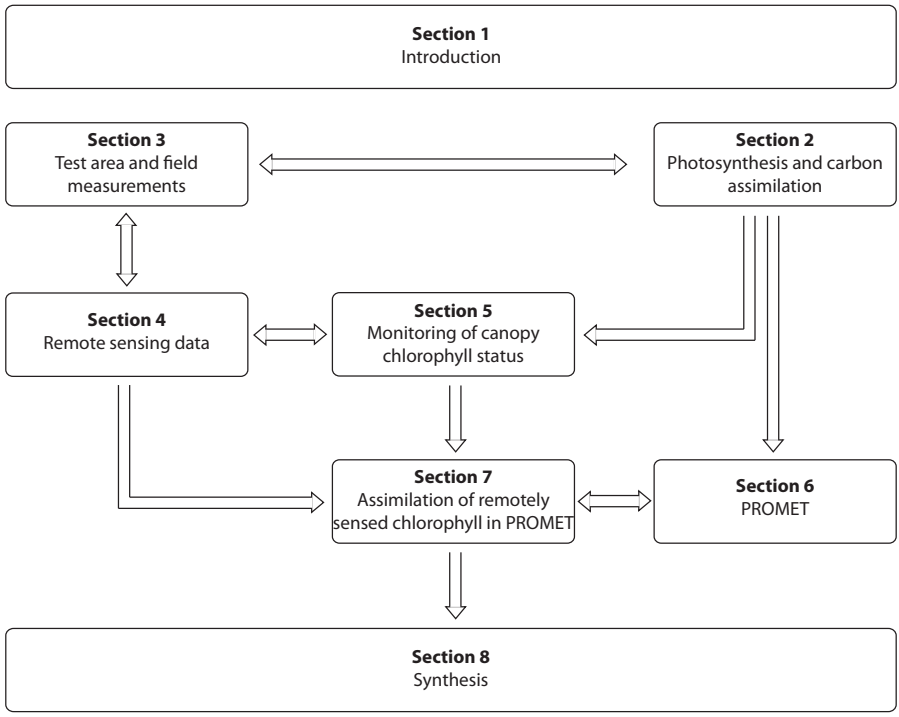

Fig. 1: Organisation chart of this thesis
Source: Own survey

2 Photosynthesis and carbon assimilation

Under natural conditions, photosynthesizing leaves are exposed to a variable stream of photons. The efficiency with which absorbed photons are finally used for photosynthetic electron transport and carbon fixation is highly regulated. Light reaction is commonly measured using the chlorophyll absorption features in the visible part of the electromagnetic spectrum (VIS), which correspond well with the fraction of absorbed photosynthetically active radiation (fAPAR) (SCHURR et al. 2006). In addition to being light driven, stomatal effects, leaf-internal CO_2 concentration and the amount and activity of ribulose 1,5-biphosphate carboxylase/oxygenase (Rubisco) also become important (LARCHER 2003). At the canopy level, the efficiency of carbon fixation is denoted "light use efficiency" (LUE). LUE refers to the projected ground surface rather than leaf area and describes the net canopy CO_2 fixation per unit of incoming photosynthetic radiation above the canopy. The spatial variability of LUE results in enormous variations of net photosynthetic productivity, which ranges from 30 to 1000 g C m^{-2} in different ecosystems (SCHURR et al. 2006).

Thus knowledge of the spatial distribution of LUE, fAPAR or chlorophyll content is essential for a realistic estimation of photosynthetic processes. Most of the existing studies of photosynthesis have been performed in the laboratory at constant or regulated light conditions. Natural light regimes, however, are far from being constant. Further processes also superimpose the physiological regulation of leaf photosynthesis at the canopy level: Physical processes and spatio-temporal fluctuations in vapour pressure, temperature, turbulent air movement or light intensity become important. Leaf structure and morphology adapt to the different environmental conditions in a canopy. Various tree species, for example, develop specially adapted sun and shade leaves (TERASHIMA & HIKOSAKA 1995).

The vegetation types investigated are wheat (*Triticum aestivum* L.) and maize (*Zea mays* L). Neither crop produces leaves adapted to shaded conditions, as every new leaf is exposed to direct radiation. This causes a reduced chlorophyll synthesis under shaded conditions (SMITH & WHITELAM 1997; LARCHER 2003). Due to the differences in radiation at the top of a canopy and beneath, the amount of chlorophyll differs between these two layers (OPPELT 2008).

Analyzing wheat and maize, two main functional types of photosynthesis and carbon fixation are highlighted, i.e. the C3 and the C4 CO_2 fixation pathway. The differences of wheat and maize canopies with respect to their assimilation processes will be introduced briefly in the following as far as this is necessary for the understanding of the topics described and discussed in sections 3 and 5 to 7. Detailed descriptions can be found in the

literature such as FURBANK & TAYLOR (1995), FURBANK (1997), KAUFMAN et al. (1989), HOPKINS (1995), LAWLOR (2001) and LARCHER (2003).

2.1 Chlorophyll and photosynthesis

The assimilation of carbon by leaves follows the general reaction of photosynthesis described in Equation 1 (KAUFMAN et al. 1989).

$$6\,CO_2 + 12\,H_2O \xrightarrow[\text{chloroplast}]{\text{photons}} C_6H_{12}O_6 + 6\,H_2O + 6\,O_2 \qquad \text{Equation 1}$$

Photosynthesis is the fundamental basis of green plants, and the principal organ of photosynthesis in higher plants is the leaf. The primary event in photosynthesis is the absorption of light by the photosynthetic pigments located in the thyalokoid membranes of the chloroplasts. These pigments are not distributed randomly, but are organized into two systems referred to as photosystem I (PSI) and photosystem II (PSII). These photosystems are organized as discrete units, which interact during the light reaction of photosynthesis.

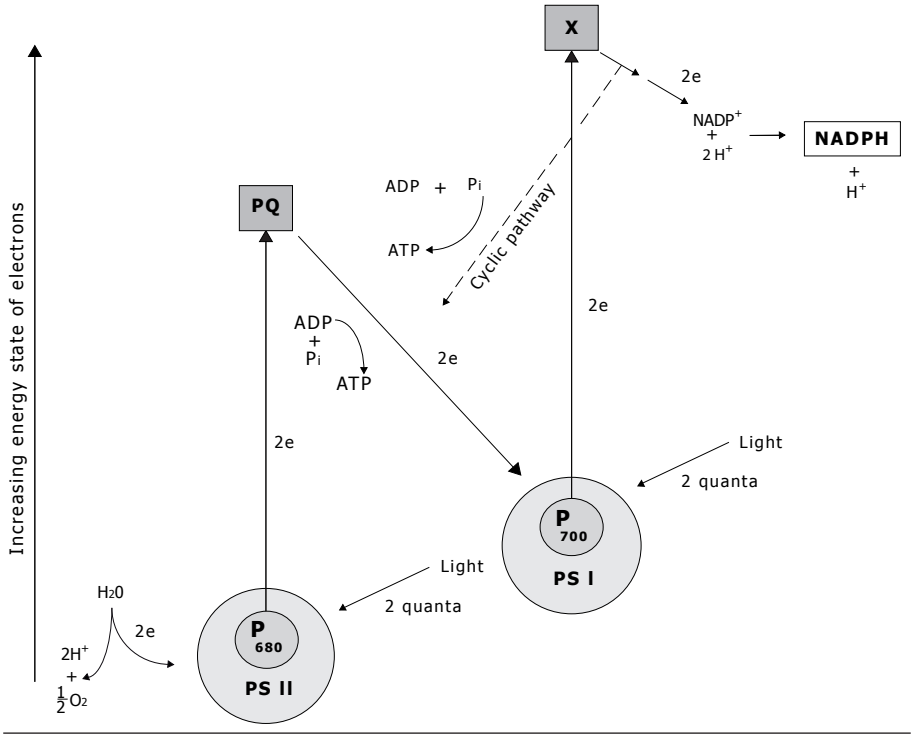

Fig. 2: Simplified summary diagram of the light reaction of photosynthesis
Source: Modified after KAUFMANN et al. 1989

The major events of the light reaction are outlined in Figure 2. The process is initiated when radiation is absorbed by the pigments of PSII and PSI, resulting in the excitation of electrons in the pigment molecules. The structure of chlorophyll and its arrangement within the photosystem is such that excitation energy gained is transferred from molecule to molecule towards the reaction centre (LAWLOR 2003), as illustrated in Figure 3. The chlorophyll a molecule itself consists of two parts, a porphyrin head and a long hydrocarbon tail. Chlorophyll b is similar except that a formyl group replaces the methyl group (Figure 3, right).

Each photosystem functions as a light-harvesting system and contains chlorophyll a and accessory pigments such as chlorophyll b and carotenoids. The key pigment molecule in PSII is chlorophyll a, denoted P_{680}. The index refers to the wavelength at which the absorption maximum of the particular molecule occurs. P_{680} is the reaction centre, which can accept energy from surrounding chlorophyll molecules of the PSII complex and transfers it to an acceptor molecule (PQ in Figure 2), resulting in the conversion of light to a form of chemical energy (KAUFMAN et al. 1989). The reaction centre of PSI is also a special molecule of chlorophyll a, in this case P_{700}. This is the one molecule in PSI capable of accepting energy from surrounding molecules and transferring it to an acceptor molecule (X in Figure 2).

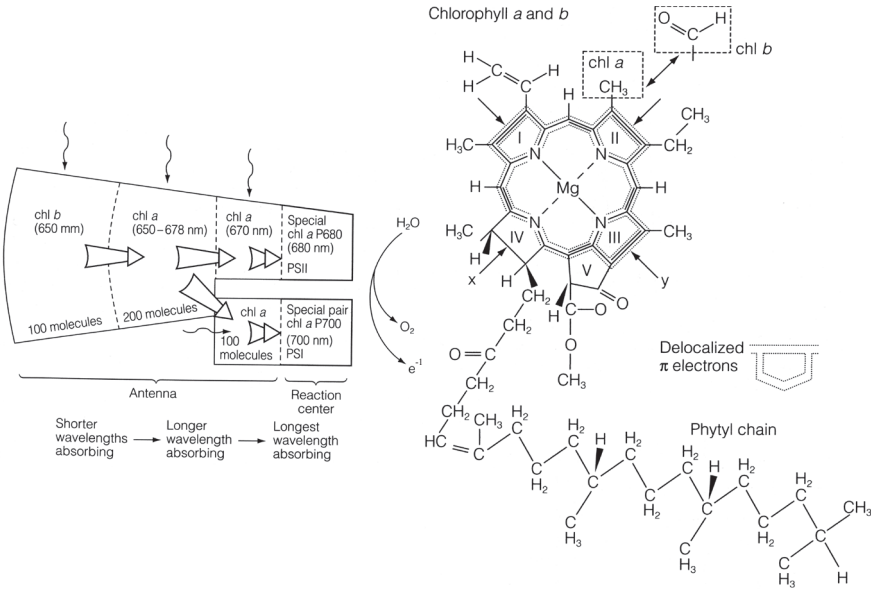

Fig. 3: Energy absorption (~►) and excitation transfer (▭▷) between light harvesting pigments (left) and the chemical structure of chlorophyll a and b (right)
Source: LAWLOR 2003

At this point an electron has been lost by a pigment molecule of both PSI and PSII. This leaves an imbalance in the distribution of electrons, with extra electrons on the acceptor molecules (PQ and X), but electrons missing from the pigment molecules in the two photosystems. This imbalance is resolved in the following way: The PSII electron is transferred to PSI via a series of electron carriers. Thus PSI returns to its original state. The PSI electron is transferred to $NADP^+$ while the missing electron of PSII is replaced by an electron from water (H_2O). This returns PSII to its original electron state (Figure 2) (KAUFMAN et al. 1989). Thus chlorophyll a is the limiting factor in the utilization of light for photosynthesis, because it receives electrons absorbed by the chlorophyll b and other auxiliary pigments and regulates the effective quantum yield.

2.2 Chlorophyll in the electromagnetic spectrum

As mentioned previously, the absorbance of light means that the energy of an absorbed photon is transferred to an electron of the chlorophyll molecule. The wavelength dependent maxima in light absorption correspond to the different energy levels in the molecule. Differences in absorption spectra enable chlorophyll a and b to be distinguished and measured spectrometrically in unpurified solutions. Measured in organic solvents after extraction from the plant, chlorophyll a absorbs most strongly at 430 nm and 660 nm and chlorophyll b at 460 nm and 640 nm (Figure 4, left). The chlorophyll analysis, which was carried out within the scope of the field campaigns, is based on such measurements in the laboratory (see section 3.2.6).

The conditions in the thylakoid membranes are different with the pigments bound in specific solutions to proteins. When aggregated in membranes, the chlorophyll a exhibits up to 10 absorption maxima, the main ones being at 660, 670, 678, 685 and 689 nm. Absorption peaks at 460 nm and 650 nm are caused by chlorophyll b (LAWLOR 2003). The close proximity of absorption bands of different constituents in an intact leaf results in considerable convolution of the absorption spectrum (Figure 4, right).

The photochemical properties of chlorophyll also present potential problems for plants. If the light energy absorbed by chlorophylls is not used in photosynthesis, the excess light energy must be dissipated in some way. This dissipation of excess energy can occur via a number of mechanisms, including fluorescence and reaction with other compounds. To limit the formation of free radicals, which can damage proteins and nucleic acids, plants have developed various mechanisms. One of these is the reduction or increase in the amount of chlorophyll by activating chlorophyll, the accumulation of chlorophyll biosynthetic intermediates as well as by chlorophyll degradation (DAVIES 2004). The first two are achieved via the accumulation of protochlorophyll a, which can be activated to chlorophyll a by the removal of an electron bond (HOPKINS 1995). Chlorophyll is degraded permanently in the plants; the half-life of chlorophyll within a plant leaf is estimated

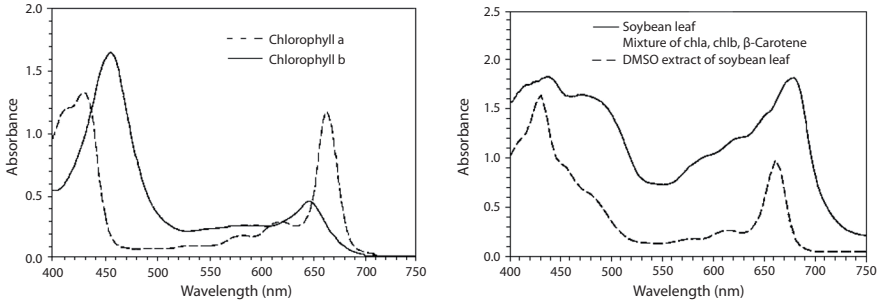

Fig. 4: Absorption spectra of chlorophyll a and b in solution (left) and comparison of in vivo and in vitro chlorophyll absorption of soybean (right)
Source: CHAPPELLE et al. 1992

to be between 6 and 50 hours. Chlorophyll is also degraded due to senescence or stress. The degradation of chlorophyll is a stepwise removal of phytol and magnesium, which are then transported out of the leaves to the remaining parts of the plant. Thus, the chlorophyll biosynthetic pathway is tightly regulated to keep the concentration of the intermediates below a phototoxic level (DAVIES 2004). The complete biosynthesis of chlorophyll will not be described here, but DAVIES (2004) provides a detailed discussion.

Thus, the chlorophyll content is highly dynamic and is regulated by the plants with respect to the environmental conditions such as irradiance, temperature, CO_2 and O_2 in air as well as on nutrient supply (LAWLOR 2001; LARCHER 2003). This can also be observed when looking at the results of the field measurements, which are described in section 3.

2.3 Carbon assimilation

The energy gained during the primary reactions of photosynthesis is used for the conversion of carbon dioxide to carbohydrates, which have a higher energetic value. Carbon assimilation also takes place in the chloroplasts and the basic mechanism and its regulation are very similar in all photosynthetic organisms (LAWLOR 2003), although differences are apparent in the way that different groups of plants produce assimilates in different environments. The most important methods of carbon assimilation – the Calvin cycle and the C4 metabolism – are within the scope of this study and will be described briefly in the following.

2.3.1 The Calvin cycle

Carbon dioxide assimilation is a cyclic, autocatalytic process, also called the Calvin cycle or the photosynthetic carbon reduction (PCR) cycle. The PCR cycle is a fundamental CO_2 assimilatory process in all photosynthetic organisms. The mechanism of CO_2 assimila-

tion by the PCR cycle is called C3 photosynthesis, as the first stable product is a 3-carbon compound (Figure 5 (a)); hence also the name C3 plants. C3 plants include more than 95% of the higher plants of the world. Additional processes for CO_2 accumulation have arisen, which do not replace the PCR cycle, but rather add to it. The most important of these mechanisms is the C4 syndrome, where a 4-carbon compound is the first product; hence the name C4 plants (KUTSCHERA 2002; LAWLOR 2003).

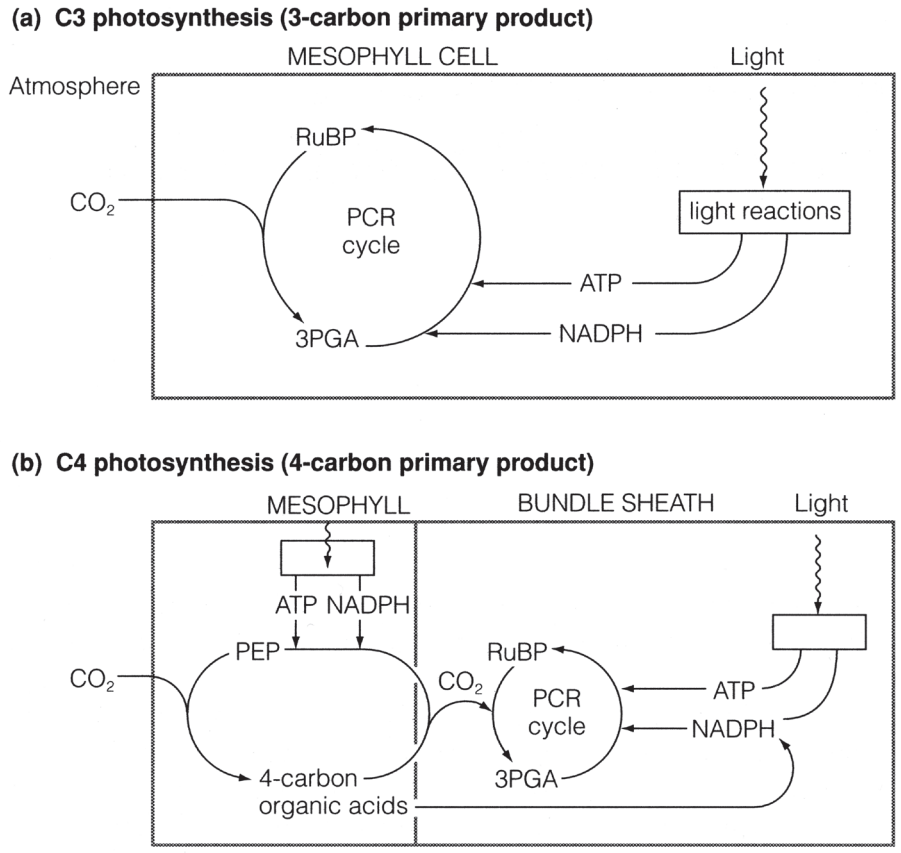

Fig. 5: Variation in photosynthetic mechanisms in higher plants: (a) C3 and (b) C4 photosynthetic carbon reduction (PCR) cycles
Source: LAWLOR 2003

After its arrival in the chloroplast, carbon dioxide is bound to an acceptor (Figure 5 (a)), the pentose phosphate ribulose-1,5-bisphosphate (RuBP), which then undergoes carboxylation catalyzed by the enzyme RuBP-carboxylase/oxydase (Rubisco). This enzyme is present in considerable amounts in the leaves. The carboxylation product, a 6-carbon

molecule, degrades immediately to produce two molecules of 3-phosphoglyceric acid (PGA). The PGA is reduced to glyceraldehyde-3-phosphate (GAP) over several steps involving the products of the light reaction of photosynthesis: adenosine triphosphate (ATP) and nicotinamide-adenine dinucleotide phosphate (NADPH). GAP flows into a pool of carbohydrates, from which various substances such as sugars, starch, amino acids etc. are synthesized. The acceptor is regenerated and can again bind CO_2 (LARCHER 2003).

Besides the fixation of CO_2, Rubisco also catalyzes the fixation of O_2 in a process known as photorespiration, which competes directly with the fixation of CO_2. At concentration levels of CO_2 typical for air, for every three CO_2 molecules fixed by Rubisco, approximately one O_2 molecule is fixed. This competition between O_2 and CO_2 and the energy costs associated with the recycling of GAP largely determine the efficiency of C3 photosynthesis in air (FURBANK & TAYLOR 1995; HATCH 1988).

2.3.2 The C4 pathway

The C4 pathway is a complex adaptation of the C3 pathway that overcomes the limitations of photorespiration. A conspicuous feature in C4 plants is the wreath-like arrangement of large chlorenchymatous cells around the bundle sheath of the leaves, the so-called Kranz-type anatomy. In these and other mesophyll cells, CO_2 is bound by the acceptor phosphoenylpyruvate (PEP) (see Figure 5 (b)) to form oxaloacetate, which is then reduced to malate. Instead of being processed in the mesophyll cells, the dicarboxylic acids are transported to the bundle sheath cells. In the chloroplasts of the bundle sheath, malate is broken down by enzymes into pyruvate and CO_2. The CO_2 thus released is captured by RuBP and processed via the PCR C3 pathway. The pyruvate is returned to the mesophyll cells and is used for the regeneration of PEP (LARCHER 2003; LAWLER 2003).

The enzyme PEP carboxylase (PEPcase) is extremely efficient and acts as a CO_2 pump. It also functions at very low concentrations of CO_2 and at elevated temperatures. However, the key feature of C4 photosynthesis is the compartmentalization of activities into two specialized cell and chloroplast types. Rubisco and the C3 PCR cycle are found in the inner ring of bundle sheath cells, which are separated from the mesophyll cells and from the intercellular air spaces by lamellae, which are highly resistant to the diffusion of CO_2 (FURBANK 1997). Thus, by virtue of this two stage CO_2 fixation pathway, the C4 cycle increases the concentration of CO_2 in the bundle sheath an estimated 10-fold over atmospheric concentrations. The net result is that the oxygenase activity of Rubisco is effectively suppressed and the PCR cycle operates more efficiently (HATCH 1988).

2.3.3 C3 versus C4 plants

In the C4 leaf, Rubisco is effectively separated from the atmosphere both physically and by an intermediate biochemical step. C4 Rubisco is located in the bundle sheath, with activity and content one-third of that in C3 leaves, but its specific activity is twice that of C3 plants (FURBANK 1997). Due to the absence of photorespiration in the mesophyll cells and because of their ability to continue photosynthesis even when the concentration of CO_2 inside the leaves is very low (e.g. when the stomata are almost closed), C4 plants are favoured over C3 plants at high temperatures and during moderate drought. Particularly under strong radiation, the high carboxylation efficiency is a considerable competitive advantage (FURBANK & TAYLOR 1995).

The small amount of Rubisco required for high rates of CO_2 assimilation increases the nitrogen (N) use efficiency. The decreased N content is a further advantage of C4 plants, because less N is required for C4 than C3 per unit of production. However, if some additional N is available, C3 plants dominate absolutely (LAWLOR 2003).

A major disadvantage is the sensitivity of many C4 plants to the cold. Low temperatures (below 5 - 7 °C) during the growing period have a negative effect on the development of the plants. Accordingly, the abundance of C4 species decreases along a regional climate gradient with increasing latitude and altitude (LARCHER 2003). Here, C3 plants have an advantage due to their low rate of photorespiration and because they need no energy for the fixation of CO_2 in the bundle sheath cells (FURBANK & TAYLOR 1995).

2.4 The C3 plant wheat (*Triticum* spp.)

Wheat (*Triticum* spp.), from the grass family *Poaceae*, was one of the first cultivated food crops. Today, wheat is grown on more land area than any other commercial crop and continues to be the most important food grain source for humans. It can be grown from regions near the Arctic Circles to lower latitudes near the equator. The crop is grown in a large variety of cultivars (cv) at altitudes ranging from sea level to more than 3000 m a.s.l. (CURTIS et al. 2002).

The optimum growth temperature is about 25 °C, with a minimum and maximum of 3 °C and 32 °C respectively. Wheat is adapted to a broad range of moisture conditions from xerophytic to littoral, and it can be grown in most locations where annual precipitation ranges from 250 to 1750 mm. Optimal production requires an adequate source of moisture availability during the growing season; however, too much precipitation can lead to yield losses from disease and root problems (HOPKINS 1995).

For winter wheat (*Triticum aestivum* L., cv Achat), which was investigated in this study, heading is delayed until the plant experiences a period of cold winter temperatures (0 to 5 °C). It is planted in the autumn to germinate and develop into young plants that remain in the vegetative phase during the winter and resume growth in early spring. This provides the advantage of using autumn moisture for germination and making effective use of early spring sunshine, higher temperatures and rainfall (CURTIS et al. 2002).

2.5 The C4 plant maize (*Zea mays* L.)

Maize (*Zea mays* L.) also belongs to the family of grasses *Poaceae* and was first cultivated in Mexico around 5000 B.C. (KAUFMAN et al. 1989). Today, a high proportion of maize is grown for ensiling. In the year 2007, only 21 % of the maize harvest in Germany was taken for the production of food, 79 % were used as silage (ZMP 2007).

Maize is an annual, non-tillering grass, which reaches heights of up to 3 m. Maize can be cultivated in regions where the daily mean temperatures are above 15 °C and no frosts occur during the growing season. The optimum temperature for germination is 18-20 °C, while the minimum lies at 10 °C. It can be cultivated in well drained soils and does not require much rainfall. Annual precipitation of 500 to 700 mm is sufficient for the development of the plants (LWG 2007).

According to the farmer, the maize fields investigated in this study were both grown with the cultivar Magister and were used for ensilage. In the test area the maize is normally sown at the end of May and harvested in autumn (end of September to beginning of October), when the water content of the plants reaches 65 to 70 % and the development stage of ripeness is reached, which ensures near maximum production of total digestible nutrients (LWG 2007).

3 Test area and field measurements

The general expectation of remote sensing is that it should ultimatively remove the need for information gathered on the ground. Indeed, if asked to justify the expenditure on remote sensing systems, many might be tempted to respond in terms of saving on ground based surveys. This view would be misguided. There is still a need for surface information to interpret remotely sensed data. The scope for environmental surveying and monitoring opened up by remote sensing may well increase the demand for surface information. In the last decade, the link between plant physiological status and the remote sensing signal was a major target of research (BLACKBURN 1998, BLACKBURN 2006, BROGE & MORTENSEN 2002, CHO & SKIDMORE 2006, DATT 1998, HABOUDANE et al. 2002, JAGO et al. 1999, OPPELT & MAUSER 2004, SIMS & GAMON 2002, YODER & PETTIGREW-CROSBY 1995). Nevertheless, no ground survey exists for the differentiation between sun and shade chlorophyll content of vegetation canopies. Therefore ground measurements are needed to form the basis for analysis, interpretation and validation of remote sensing data.

Intensive field campaigns were carried out in 2004 and 2005 to provide a foundation for chlorophyll analysis. An overview of the test area and a detailed description of the test fields, the acquired data, and the sampling results are addressed in the following sections.

3.1 Test area Gilching

The selection of the test area was determined by several factors such as the accessibility, the existence of feasible test fields and the probability of finding farmers that were willing to cooperate, since nearly all agricultural fields in Bavaria are private property.

Table 1: Corner coordinates of the test area Gilching (Gauß-Krüger, Potsdam ellipsoid, Bessel date)

	East (zone 4)	North
Upper left corner	445728	5 330425
Lower right corner	450583	5 322593

Source: Own survey

The test area chosen for the measurement campaigns is located near the town of Gilching, a medium-sized town belonging to the commuter belt of Munich, whose city centre lies 25 km to the south-west of the Bavarian capital. Gilching is part of the administrative district (“Landkreis”) Starnberg, a region that lies within the Alpine foothills, embedded

in the Ammersee in the west and the Starnberger See in the east. The corner coordinates are given in Table 1.

3.1.1 Geomorphology/Geology

The test area Gilching covers 27.1 km². The boundaries are mainly defined by the extent of two contiguous water protection areas that ensure the water supply of the district. The classification of the test area into natural entities leads to a differentiation into two units: The young moraine region of the Ammer-Loisach glacier (I, Figure 6) and the alluvial cover of the Munich plain (II) (MEYNEN & SCHMIDTHÜSEN 1953, GRAUL 1962).

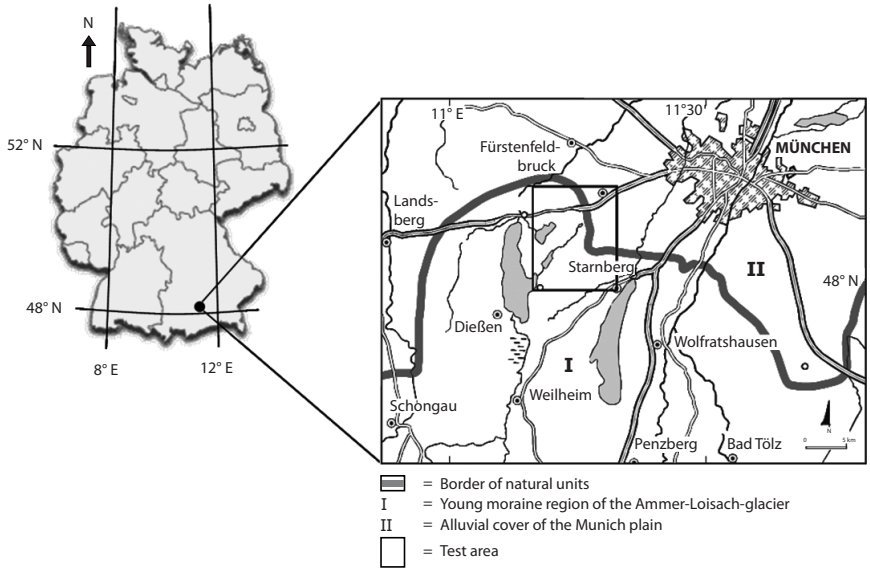

Fig. 6: Location of the area Gilching
Source: Own survey

Between the hilly region of the former Ammer-Loisach glacier and the Munich gravel plain there remains a strip of moraines of the Riß diluvium. Glacial waters cut their way through the moraines and formed the spillway of Gilching. This process can still be observed in the digital elevation map (DEM) of the area (Figure 7). The spillway covers most of the area. Its elevation rises softly from 550 m above sea level in the north to 640 m in the south. In the south-west and south-east the remaining moraines are visible as terraces. The south-western terrace is made up of older moraines originating from the Riß diluvium and is more evident with differences in elevation of up to 30 m towards the spillway. The south-eastern part originates from younger moraines of the Würm diluvium and shows differences in elevation of up to 10 m (GRAUL 1962, GROTTENTHALER 1980).

Also visible in the DEM is the motorway, which crosses the test area in west-east direction in the northern part of the test site.

The parent material is also visible in the existing soil textures. A sandy loam exists at the spillway while medium silt and silty loam dominate on the terraces. Braunerde and Para-Braunerde developed as dominant soil types, corresponding to cambisols in the FAO system (see Figure 7), which cover 90 % of the area. Pararendzina makes up 8 % of the area, namely on the south-west terraces. The remaining 2 % are Gleye which are observed in hollows spread over the test area (Bayerisches Geologisches Landesamt 1986).

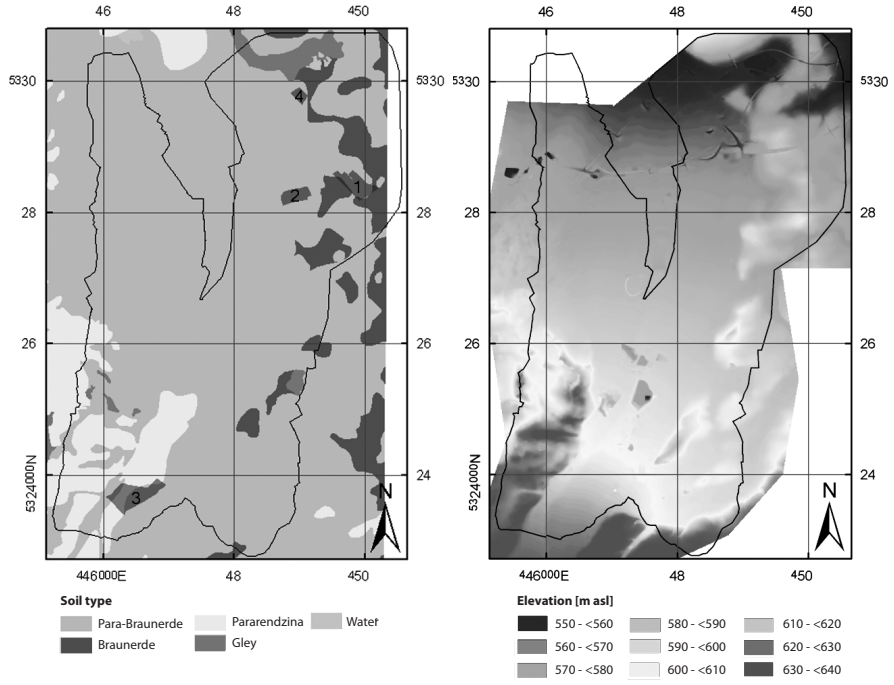

Fig. 7: Digital maps of soil type and elevation in a Gauß-Krüger (zone 4) coordinate system (the positions of the test fields are outlined and numbered in the soil map), the dimension of the test area is indicated by the solid line

Source: Own survey

3.1.2 Land cover

The land cover of Gilching is heterogeneous, as demonstrated in Figure 8. Land cover mappings in 2004 and 2005 showed that one-third of the test area is used as arable land, which is mainly located on the Braunerde and Para-Braunerde with their high agricultural potential (see also Figure 7). which is mainly located on the Braunerde and Para-Braunerde with their high agricultural potential (see also Figure 7).

The predominant crop types are wheat, maize and barley, but oat and rye can be found as well. A third of the area is occupied by forest, and 18.4 % are permanent grassland. The two crops of interest, maize and wheat, cover 3.55 % and 18 % of the area respectively. Since the underground is rich in glacial gravels several gravel pits exist, but there are almost no surface water bodies. Sealed areas make up 8.5 % of the test area.

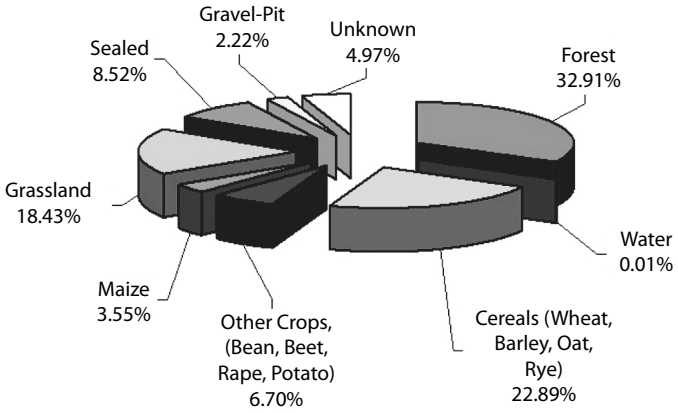

Fig. 8: Percentage distribution of different land cover types in the test area Gilching
Source: Own survey

3.1.3 Climate

A weather station of the Bavarian network of agro-meteorological stations in this region enables access to local weather monitoring. The station "Gut Hüll" provides information on precipitation, soil and air temperature, wind velocity, global radiation and air humidity since 1990 with an hourly resolution. This information is freely available on the homepage of the Bayerische Landesanstalt für Landwirtschaft (www.lfl.bayern.de/agm/start.php).

The temperature curves for 2004 and 2005 in Figure 9 exhibits the typical characteristics of a seasonal climate zone. A maximum in mid August and a minimum at the end of February are characteristic for a temperate continental climate.

The region is assigned following the KÖPPEN & GEIGER (1961) classification system as Cfb-climate, which indicates a cool, ever-moist and temperate climate. The summers are characterized by heavy rainfall due to predominant convective precipitation and the barrier effect of the Alps, whereas during wintertime less precipitation is recorded.

Although no water shortage occurs during the vegetation period of average years, the frequent and heavy rainfalls during July and August of 2005 (Figure 9) are exceptional

compared to the long-term records and caused many crops to moulder upon the field before there was a dry enough period for them to be harvested.

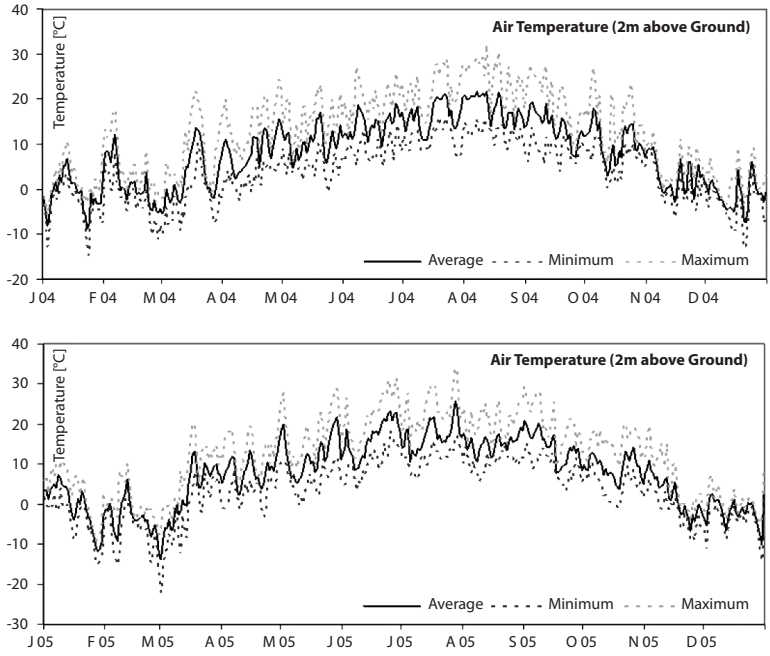

Fig. 9: Daily mean air temperature 2004 (top) and 2005 (bottom) as measured at "Gut Hüll" Source: Own survey

Comparing the climate parameters of 2004 and 2005 (Table 2) it becomes obvious that the mean temperatures in both years fall slightly below the 15-year average (1990-2005) of 8.34 °C

Table 2: Climate parameters as measured at "Gut Hüll" (the vegetation period was calculated from April 15 to October 15)

	15-year average	**2004**	**Vegetation period 2004**	**2005**	**Vegetation period 2005**
Mean Temperature [°C]	8.34	8.04	13.65	7.78	14.07
Sum of Precipitation [mm]	902	819.2	710	983	727.4
Sum of Global Radiation [Wh]	$10.32\ 10^5$	$10.93\ 10^5$	$8.08\ 10^5$	$11.03\ 10^5$	$7.99\ 10^5$

Source: Own survey

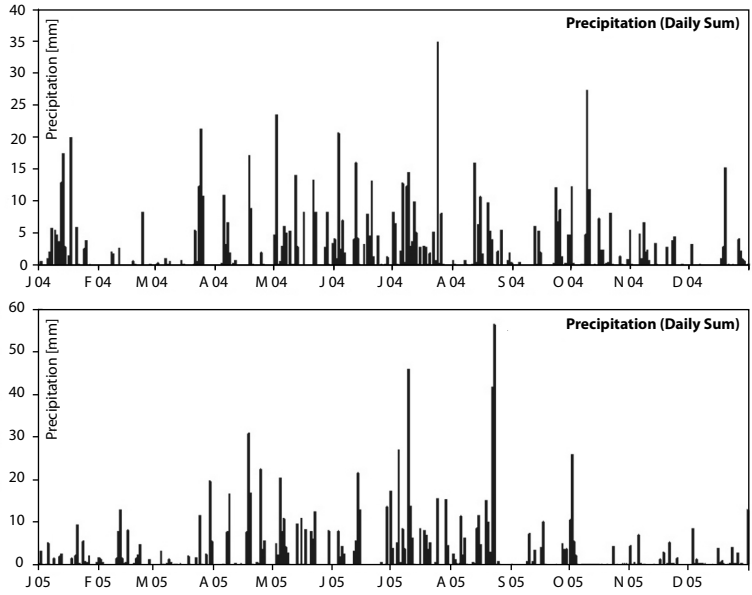

Fig. 10: Precipitation 2004 (top) and 2005 (bottom) as measured at "Gut Hüll"
Source: Own survey

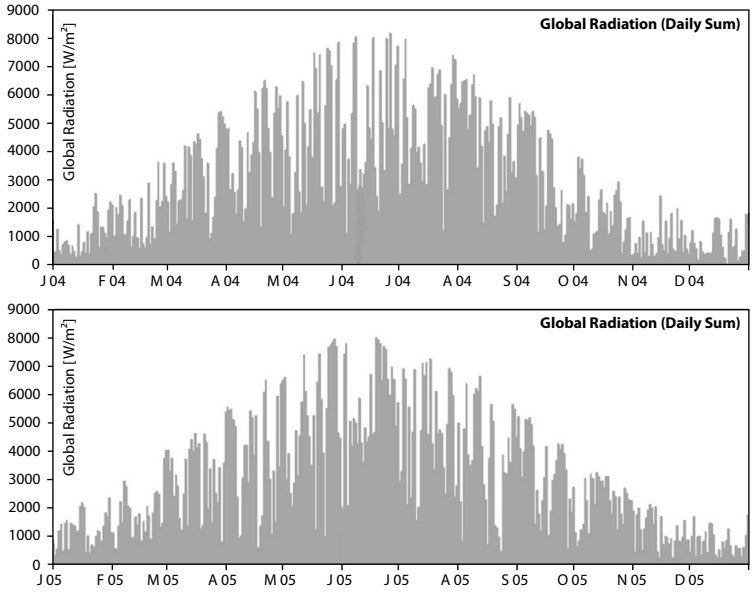

Fig. 11: Global radiation 2004 (top) and 2005 (2005) as measured at "Gut Hüll"
Source: Own survey

The precipitation during the measuring years varies strongly from the long-term average demonstrating that the area received 164 mm less precipitation in 2004 than in 2005. Therefore the campaigns included a relatively humid and a relatively dry year. However both measuring years recorded a slightly higher amount of global radiation than the long-term average (see also Table 2 and Figure 11).

3.1.4 Test fields

The selection of the test fields was determined by several factors including the environmental conditions and the contact to farmers who would be likely to cooperate. In terms of environmental conditions it was considered to be necessary to find fields with a C3 and a C4 crop for comparison of the two assimilation pathways large enough to be sampled by remote sensing systems. In addition the test fields should be relatively even level, so that more or less flat fields could be used for angular remote sensing techniques. Within the test area Gilching, four test sites were arranged. A wheat field and a maize field were chosen for each sampling year. The test fields were named after their owner. An overview of their location is given in Figure 7 (Stürzer wheat 2004 = 1, Stürzer wheat 2005 = 2, Kiemer maize 2004 = 4, and Zankl maize 2005 = 3). Mr. Stürzer enabled access to the file-system "Schlagkartei" where the data about field management and treatment are stored. These data are accessible for the wheat fields and were used as a valuable source of information. Moreover the weather station "Gut Hüll" is directly situated in the test field wheat 2004.

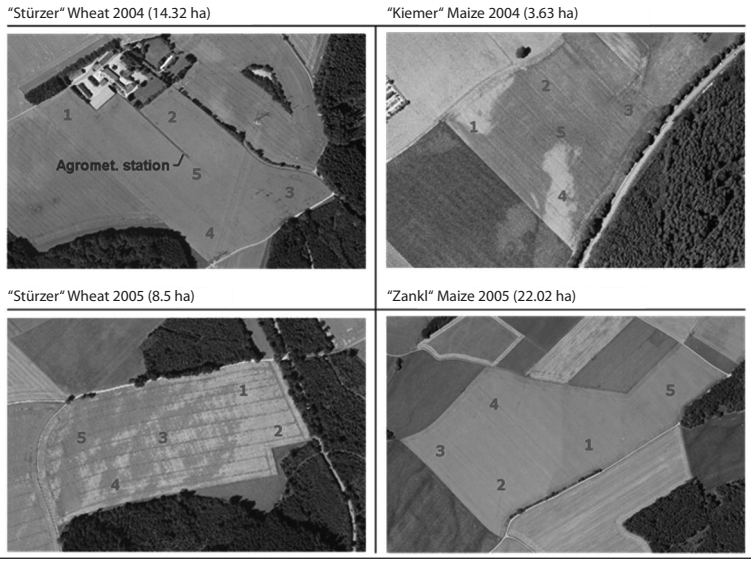

Fig. 12: Aerial photographs of the test fields and distribution of sampling points
Source: Own survey

For every field, five sampling points were selected and fixed via handheld GPS (GARMIN VISTA). The locations of the sampling points were selected in close cooperation with the farmers in order to gather ground truth data from areas in the field that exhibited differences in plant development and yield over recent years. The differences can be due to differences in soil types or texture within a field or slight variations of topography that lead to differences in water supply and/or drainage or the amount of incoming radiation. Different radiation regimes are also caused by shadowing near forests or groves. This selection procedure was necessary to minimize the effects of spatial autocorrelation between the sampling points, which would prevent both the statistical analysis of the ground survey and the relationship between ground data and the remote sensing signal. The aim of this study is the assessment of plant chlorophyll without consideration of soil type or growing conditions. Therefore it is necessary to monitor vegetation canopies with inner-field heterogeneities.

3.2 Field campaigns and acquired data

The gathering of the necessary ground truth data was accomplished by means of intensive field campaigns, which were carried out at regular weekly intervals throughout the vegetation periods of the years 2004 and 2005. An additional ground sampling was conducted on those remote sensing acquisition days that were two or more days away from a regular sampling day. In addition, field spectrometer measurements were conducted simultaneously to the remote sensing acquisitions to assist the processing of the hyperspectral imagery.

3.2.1 Plant parameter

The field measurements were carried out differentiating between two vegetation layers (Figure 13): The upper layer was defined as the part of the canopy where the predominant part of the radiation is received as direct sunlight, whereas the lower layer receives mostly diffuse radiation. The boundary between these two layers was set at the upper end of the first internodium, so that only the uppermost leaves are assigned to the upper layer. For the sake of convenience, the layers are named sun and shade layer in the following, although the name is somewhat misleading since the shade layer also receives some direct sunlight.

During the 2004 field campaign, samples were taken on 20 dates at the maize field and on 19 dates at the wheat field. In 2005 both fields were sampled on 18 days. All measurements were recorded in sampling reports, where additional information such as infections of plants, infestations with pests or physical damage caused by animals were also noted. The measured plant parameters of interest for this study are listed in Table 3 and will be described briefly in the following section.

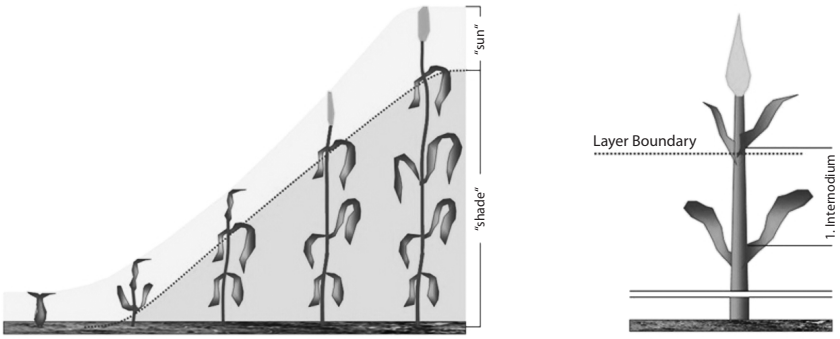

Fig. 13: Differentiation between vegetation layers under direct and diffuse radiation regimes
Source: OPPELT et al. 2006

In 2005, leaf area measurements were conducted to provide the conversion from chlorophyll contents per unit surface area and per unit leaf area respectively. Photographs were taken on every sampling date to provide a continuous visual documentation about the fields throughout the growing period.

Table 3: Plant parameters measured during the field campaigns 2004 and 2005

Parameter	Unit
Phenological status	[BBCH]
Height of leaf	[cm]
Height of shoot	[cm]
Stand density	[pl m^{-2}]
Dry biomass of leaf (sun and shade layer)	[g·m^{-2}]
Leaf chlorophyll a content (sun and shade layer)	[µg g^{-1}] and [mg m^{-2}], [µg cm^{-2}] only in 2005
Leaf chlorophyll b content (sun and shade layer)	[µg g^{-1}] and [mg m^{-2}], [µg cm^{-2}] only in 2005
Leaf area index (LAI, only 2005)	[dimensionless]

Source: Own survey

3.2.1.1 Phenological status

The phenological status of the plants was determined using the BBCH (Biologische Bundesanstalt für Land- und Forstwirtschaft, Bundessortenamt und CHemische Industrie) Code (MEIER 2001), where the developmental cycle of the plants is subdivided into ten clearly distinguishable phases (principal growth stages) from 0 (sowing) to 9 (ripeness). The principal growth stages may vary at a certain sampling date. If one or more proceed in parallel, they are indicated in the sampling reports if the description applies to at least 50 % of the plants at a sampling point. When average field parameters are presented the mode is used as the representative growth stage. If the plant development must be indicated more precisely, secondary growth stages can be used, which are defined as

short characteristic phases for each plant species. The combination of principal and secondary growth stages results in a two-digit integer code.

Table 4: Principal BBCH growth stages

Stage	Description
0	Germination, sprouting, bud development
1	Leaf development (main shoot)
2	Formation of side shoots, tillering
3	Stem elongation, shoot development (main shoot)
4	Development of harvestable vegetative parts or organs, booting (main shoot)
5	Inflorescence emergence (main shoot), heading
6	Flowering (main shoot)
7	Development of fruit
8	Ripening (maturity of fruit and seed)
9	Senescence, beginning of dormancy

Source: Meier 2001

3.2.1.2 Plant height

Plant height was determined using a folding rule. A set of ten measurements was averaged for the height of the flag leaf and for the shoot level.

At the beginning of the growing season the height of the leaves is higher than the height of the shoot. When the plant reaches the stage of booting (BBCH 40) the shoots begin to overtake the leaves in height. Assuming average growing conditions, the maximum plant height is reached just before flowering (BBCH 60). Both heights finally decrease slightly during ripening.

3.2.1.3 Canopy density

The density of a plant stand is described in plants per square meter [pl m^{-2}]. With arable crops this depends on the row spacing, the seed density along a row and the germination rate. The first two parameters are determined by the drilling machine while the latter is dependent on the seed. Not every seedling emerges in spring, but once the seedling has emerged the stand density remains constant. Therefore the canopy density was measured once in a season for each test field by counting the number of plants along one meter of a sowing row and along one meter perpendicularly to the rows. This process was repeated for every sampling point in a field. The resulting average stand density for maize was 9.5 pl·m^{-2} in 2004 and 11.5 pl·m^{-2} in 2005, for the wheat canopies 130 pl·m^{-2} in 2004 and 123 pl·m^{-2} in 2005 were counted. In the Schlagkartei the farmer reported a sowing rate for wheat of 250 grains·m^{-2}, thus germination rates of 52 % and 49.2 % respectively result.

The canopy density was used for the calculation of the biomass per square meter (see section 3.2.1.4) as well as for the calculation of the chlorophyll content per unit ground surface of maize by multiplying the extrapolated leaf biomass per square meter with the results of the chlorophyll analysis (section 3.2.1.5).

3.2.1.4 Biomass

For the derivation of plant biomass it is important to distinguish between maize and wheat. For the wheat canopies the plants along 0.25 m of a sowing row were cut directly above the ground at each sampling point. The plants were divided into sun and shade parts by clipping the stem at the upper end of the first internodium. After packing the two layer samples into waterproof plastic bags they were transported to the laboratory and divided manually into the stem, leaf and fruit fractions. These fractions were weighed, dried for 24 hours in a drying oven at 85 °C and weighed again to calculate the wet and dry biomass (BM_{wet} and BM_{dry} respectively [g m^{-2}]) per unit ground surface (Equation 2 and Equation 3).

$$BM_{wet} = \frac{4 \cdot SW_{wet}}{RD} \qquad \text{Equation 2}$$

$$BM_{dry} = \frac{4 \cdot SW_{dry}}{RD} \qquad \text{Equation 3}$$

where

SW_{wet}	sampling mass of wet biomass [g],
SW_{dry}	sampling mass of dry biomass [g], and
RD	row distance [m].

Because of the high amount of biomass to be sampled for maize, it was decided to harvest only three plants at each sampling point. The weighing and drying procedure in the laboratory was the same as for the wheat samplings leading to Equation 4 and Equation 5 for the calculation of the biomass per unit ground surface.

$$BM_{wet} = \frac{SW_{wet}}{3} \cdot \frac{PM}{RD} \qquad \text{Equation 4}$$

$$BM_{dry} = \frac{SW_{dry}}{3} \cdot \frac{PM}{RD} \qquad \text{Equation 5}$$

where

PM	maize plants along one meter of a sowing row.

The biomass measurements were used for the calculation of the chlorophyll content related to the leaf biomass per unit ground surface [mg·m^{-2}], which is described in the next section.

3.2.1.5 Chlorophyll content

The chlorophyll content of the leaves is, compared to the stem and fruit chlorophyll, most prominent in the photosynthetic processes and exhibits a dynamic behaviour (LARCHER 2003; LAWLOR 2003). Therefore the leaf chlorophyll content is the main topic for this investigation.

The chlorophyll content was not measured directly in the field, instead the samples were analyzed in the laboratory. On every sampling date, sun and shade leaves were collected at each sampling point and put into cryo tubes. To avoid chemical degradation of the chlorophyll, the samples were immediately frozen in liquid nitrogen before they were brought to the laboratory, where they were stacked in a freezer at -50 °C.

The analysis of the chlorophyll was performed according to the method described by PORRA et al. (1989). The samples were milled, weighed and the plant powder was dissolved in 80 % acetone before the supernatant was analyzed using a dual-beam photometer (PERKIN-ELMER Lambda 25). This spectroscopic measurement provided absorption coefficients for two specific wavelengths (663.6 nm for chlorophyll a and 646.6 nm for chlorophyll b) which were the basis for the calculation of the chlorophyll content per gram fresh biomass (Equation 6 and Equation 7).

$$\text{Chl a} = (12.5 \cdot A_a - 2.55 \cdot A_b) \cdot \frac{vol}{W_i} \qquad \text{Equation 6}$$

$$\text{Chl b} = (20.31 \cdot A_b - 4.91 \cdot A_a) \cdot \frac{vol}{W_i} \qquad \text{Equation 7}$$

where

Chl a	chlorophyll a content [µg g^{-1}],
Chl b	chlorophyll b content [µg g^{-1}],
A_a	absorption at 663.6 nm [%],
A_b	absorption at 646.6 nm [%],
vol	final volume of 80 % acetone in which the chlorophyll is dissolved [ml], and
w_i	initial mass of the dissolved plant powder [g] (PORRA et al. 1989).

Besides the chlorophyll content per mass, the chlorophyll content related to a unit ground surface was calculated because it is likely to be a more suitable parameter for a comparison with a spatial integral, i.e. remote sensing measurement (Equation 8). Information

on both contents per unit mass and content per unit surface area is valuable. The former indicates the physiological status or level of stress of plants while the latter can be used to evaluate the overall photosynthetic capacity or productivity of a canopy (BLACKBURN 1998).

$$\text{Chl a,b} = \text{Chl a,b } [\mu g \cdot g^{-1}] \cdot BM_{dry} \cdot 1000 \qquad \text{Equation 8}$$

where

Chl a,b Chlorophyll a (b) content per unit ground surface [mg·m^{-2}].

In 2005, the chlorophyll sampling was conducted using a clipping disk with an area of 1 cm². The resulting chlorophyll content is then related to both the chlorophyll content per mass and the chlorophyll content per leaf disk. The chlorophyll content per leaf disk is then multiplied with the measured LAI (see next section) to provide the chlorophyll content per leaf area on a unit ground surface (chl_{LA}).

Various literature can be found addressing chlorophyll contents related to leaf area [cm²]. This parameter will not be focused on for two reasons: firstly, the chlorophyll per leaf area [cm^{-2}] was measured only in 2005 leading to a data basis that is too small for a regression analysis with the remote sensing data. Secondly, in comparison with remote sensing measurements, the chlorophyll content per square centimetre seems to be, very likely as the content per gram, a measurement that is more related to a single plant than to a vegetation canopy. The chlorophyll content per leaf area can be transformed in a ground surface related parameter by multiplying it with the leaf area index (LAI). This can be done when the canopy is assumed to be a single layer, but conventional LAI measurements allow no vertical differentiation between sun and shaded canopy layers.

3.2.1.6 Leaf area

The Leaf Area measurements were carried out in 2005 using a LI-COR LAI 2000 instrument. The measurements themselves have to be conducted under diffuse light conditions. Therefore the measurements were conducted at dawn or dusk, while under clouded skies the measurements can also be done during the day.

The measuring technique combines a measurement of sky brightness above the canopy with measurements beneath the canopy while the sensor is viewing skywards. In practice, four below-canopy measurements are taken to achieve a suitable spatial average for the corresponding sampling point. To exclude the effect of the operator and the shadow he is casting during the measurements, the LAI-2000 was operated using the 180° azimuth view. Below and above canopy measurements were carried out at the same height with the same azimuth direction.

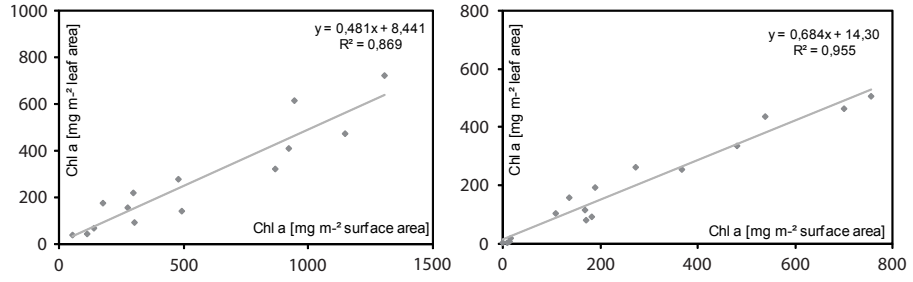

Fig. 14: Relationship between chlorophyll a content per leaf area (chl_{LA} a) and per ground surface area (chl a) for wheat (left) and maize (right) as measured in 2005
Source: Own survey

Chlorophyll contents per leaf area and per ground surface area are closely related, as presented in Figure 14. The results refer to the chlorophyll contents of both layers (sun and shade) because LAI measurements are available for the entire vertical canopy profile only. Nevertheless, these relationships are assumed to be constant for both observation years and therefore can be used to convert one unit into the other. Although the chlorophyll content per leaf area is used in most of the literature, the author proposes the use of the chlorophyll contents per leaf dry biomass. This is due to two reasons regarding plant physiology on the one hand and the conductance field measurements on the other: the amount of chlorophyll in a leaf depends on the leaf size, which is taken into account by the reference to the leaf area, but it also depends on the thickness of the leaves investigated, which is not directly taken into account. Using the leaf biomass as reference, both aspects are considered. However, the biomass measurements are destructive, but the experience of the author demonstrated that LAI measurements are highly error-prone due to the complex measurement setting. In addition, best measurements can be conducted just after sunrise or before dawn. This complicates the coordination with other field measurements, which are generally conducted around midday. Thus, the use of chlorophyll contents per surface area can be conducted whether the equipment for LAI measurements is available or not, and the plant samples can also be used for additional measurements in the laboratory such as carbon or nitrogen content.

3.3 Field spectrometry

Field spectrometer measurements were performed during AVIS or CHRIS overpasses to provide validation data for the atmospheric correction procedure of the remote sensing data (see section 4.1.2). The measurements were conducted using a combination of instruments (Ocean Optics SD2000 and SD2000 NIR), originally designed to be used in the laboratory, but adapted and optimized to in-field use by the author. The two detectors were combined to cover a spectral range from 440 nm to 980 nm with a sampling

rate of 0.3 nm. The instruments were connected to a tablet PC (Fujitsu Siemens Stylistic ST4100) mounted on a tripod. The radiation reflected by the target was gathered via a trifurcated reflection probe (Ocean Optics FCTR-3UV/IR), equipped with three different inner diameters to provide adjusted shares of energy as required by each detector. The reflection probe was steadied by an extendable arm which was also mounted on the tripod. A calibrated spectralon® target (SphereOptics SG-3120) was used as the reference panel. Using the trifurcated reflection probe it was possible to measure the surface and the reference panel simultaneously.

Each measurement was performed using the following procedure: First, the integration time was adjusted to the current radiation. Then the dark current measurement was performed by closing the apertures of the reflection probes. Finally, the measurements of the surface and the reference panel were performed. The result of each measurement is the mean of 50 individual spectra. To provide an insight into the spatial variability the extendable arm was moved in a semi-circle where eight additional measurements were conducted, leading to a measurement cycle of nine measurements (Figure 15). The final result of the sampling at one location was the mean of all the spectra taken during the transit through the semicircle and back, i.e. 450 spectra.

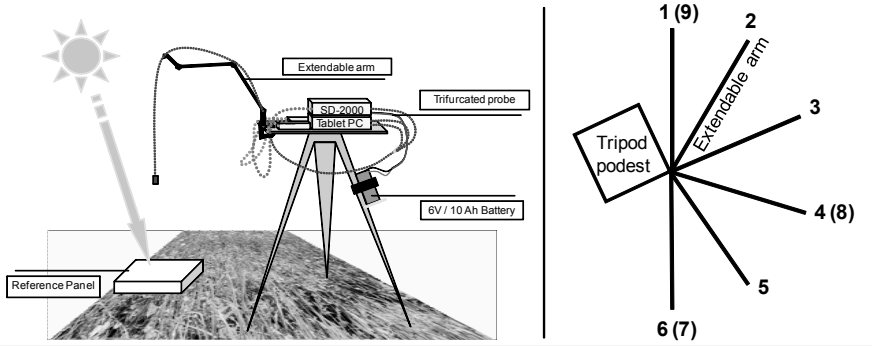

Fig. 15: Setup of field spectrometer (left) and measurement pattern at each sampling point (right). The numbers indicate the order of measurements providing a mean spectrum of a sampling point
Source: Own survey

The reflectance spectra were calculated according to Equation 9:

$$R = \frac{(DN - DC)}{(DN_{ref} - DC)} \qquad \text{Equation 9}$$

where

R	reflectance [%],
DN	grey value measured on the surface [digital number],

DN_{ref} grey value measured on the reference panel [digital number], and
DC dark current [digital number].

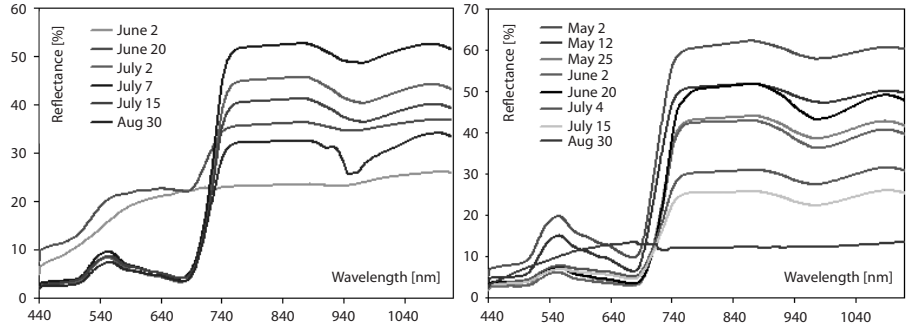

Fig. 16: Field spectrometer data as measured in 2005 for wheat (left) and maize (right)
Source: Own survey

Figure 16 summarizes the field spectrometer data gathered in 2005 for the wheat and maize fields. The phenological development can be reproduced well: increasing chlorophyll content and increasing biomass during the early growing stages result in decreasing reflectances in the visible (VIS) and increasing reflectances in the near infrared (NIR). The decrease in chlorophyll and vivid biomass during ripening leads to the inverse process with increasing VIS and decreasing NIR reflectances. The plant water absorption at 960 nm indicates the varying plant water status, which depends on the water availability and the phenological status.

3.4 Photographic documentation

The field measurements were accompanied by a series of digital photographs that document the development and enable a subsequent view of the test fields. At least three photographs of each test field were taken weekly: one side view to display the stratification and the height of the plants, an overhead picture to determine the ground coverage and an overview shot to gain an insight into the homogeneity of the fields.

3.5 Sampling results

In the following section only the results of the chlorophyll analysis are described, as they are the key variables in this study. A detailed discussion about the variability at every single point is not appropriate because the differences in chlorophyll sun and shade canopy layers are of interest. The discussion will be based on the mean field values, though the regression analysis was conducted with the measurements at each sampling point. Although the sampling points were selected under consideration of the spatial variability,

slope or yield characteristics to avoid spatial autocorrelation between the data, the aspect of temporal autocorrelation is still evident. It is important to note that the temporal pattern of the chlorophyll content was not investigated but rather the question of whether it is possible to assess vertical chlorophyll distribution with remote sensing techniques.

3.5.1 Wheat

The sampling results are presented separately for the contents per mass and for the contents per area ground surface. Before further analysis, the data were tested for outliers ($x > 2.5 \cdot stdev$), which were removed from the sample. Then the data were tested for normal distribution using the Shapiro-Wilk W test (SHAPIRO et al. 1968). The calculated probability p is the estimated probability of rejecting the null hypothesis. If the W statistics is significant, then the hypothesis that the respective distribution is normal should be rejected. W statistics shows that all results are not significant ($p > 0.05$) indicating that the null hypothesis has to be rejected and measured chlorophyll contents are distributed normally.

Table 5: Results of the Shapiro-Wilk W test for wheat

	Chl.a sun	**Chl.b sun**	**Chl.a+b sun**	**Chl.a shade**	**Chl.b shade**	**Chl.a+b shade**
p [µg g^{-1}]	0.41	0.17	0.21	0.13	0.08	0.13
p [mg m^{-2}]	0.99	0.99	0.98	0.18	0.16	0.18

Source: Own survey

3.5.1.1 Sampling results – chlorophyll contents per mass

The results of the weekly wheat sampling at the five sampling points are presented in Figure 17, while Figure 18 presents the temporal development of the mean field chlorophyll.

It is clearly visible that chlorophyll a for both sun and shade layer exhibits the most dynamic behaviour throughout the vegetation period. Differences also exist between chlorophyll a for the different layers, while chlorophyll b contents remain relatively stable at levels below 500 µg g^{-1}.

The main factors determining the chlorophyll a content are the fertilization and the amount of incoming radiation, which on its part is related to the air temperature (OPPELT 2002). The chlorophyll a content increases after the application of fertilizer or manure. The increase is delayed when the global radiance and/or air temperature are relatively low (e.g. application of fertilizer on May 17 2005). Assuming average growing conditions, the nitrogen in the fertilizer is metabolized within 30 days (DÖHLER 2007) resulting in

an increase of chlorophyll molecules in which this nitrogen is mainly stored during the vegetative growth phase, as shown in Figure 18.

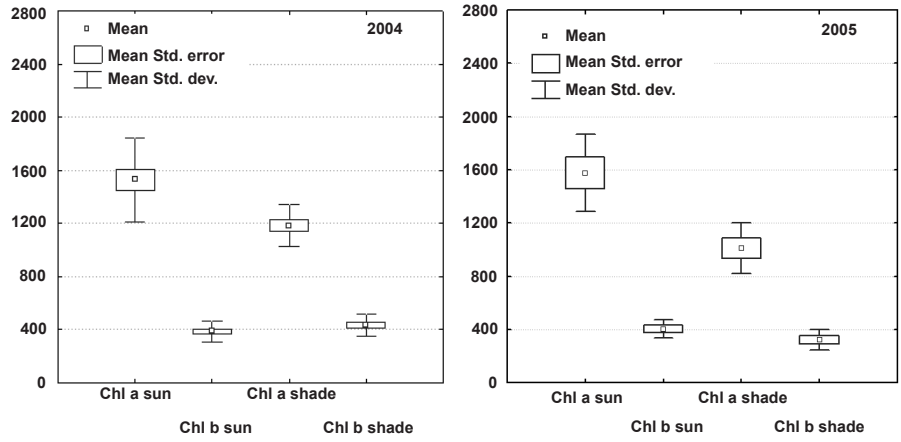

Fig. 17: Statistics of chlorophyll content per mass [µg g^{-1}] as measured at the sampling points
Source: Own survey

A remarkable decrease can be observed at the end of May 2005, which is caused by late frost events leading to a reduced metabolic activity. After the frost events in 2005 the wheat canopy exhibits a strong increase in chlorophyll a content, which is promoted by higher temperatures and a higher amount of incoming radiation.

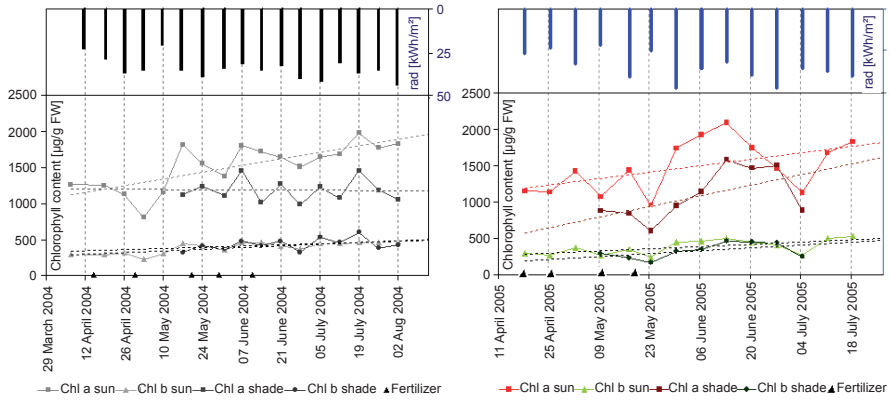

Fig. 18: Chlorophyll content of wheat per mass [µg g^{-1}] as measured in 2004 and 2005; the upper bar graph indicates the sum of global irradiance as measured at the weather station "Gut Hüll" for the week prior to the chlorophyll measurements
Source: Own survey

In general the mean plant development is very similar for both vegetation periods, as presented in Figure 19. This is certainly influenced by the fact that these fields were managed by the same farmer using precision farming techniques to optimize yield.

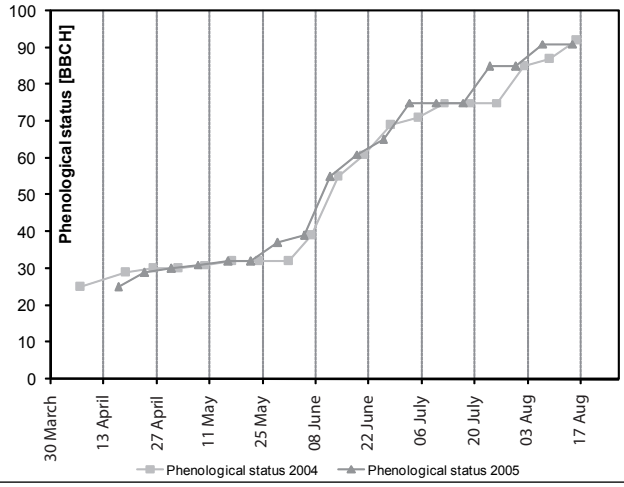

Fig. 19: Phenological development of wheat test fields
Source: Own survey

3.5.1.2 Sampling results – chlorophyll contents per ground surface area

When looking at the chlorophyll contents per unit ground surface area (Figure 20), the dynamic behaviour of chlorophyll a observed for the chlorophyll contents per mass is superimposed by the development of leaf biomass, which increases during spring and decreases after flowering. In both years, the chlorophyll contents of the shade layers became higher than the contents of the sun layers at the beginning of stem elongation. This is due to the fact that the sun layer of a canopy remains quite stable over the growth cycle, while the shade layer increases during the vegetative plant development. The shade layer for both chlorophyll a and b is therefore subject to a higher dynamic of the mean field values during the vegetation period compared to the sun layer, which is demonstrated in Figure 20, but is also evident for the chlorophyll measurements conducted at each sampling point (Figure 21). Nevertheless, the donation of fertilizer is the essential parameter for the main events of the generation of chlorophyll, which enables the development of biomass via photosynthesis. The slope of the increase depends, similarly to the chlorophyll contents per mass, on the meteorological situation. This is evident in May 2005, where the shade chlorophylls increase gently compared to 2004, and the impact of the fertilization is delayed by the low temperatures and the low level of incoming radiation.

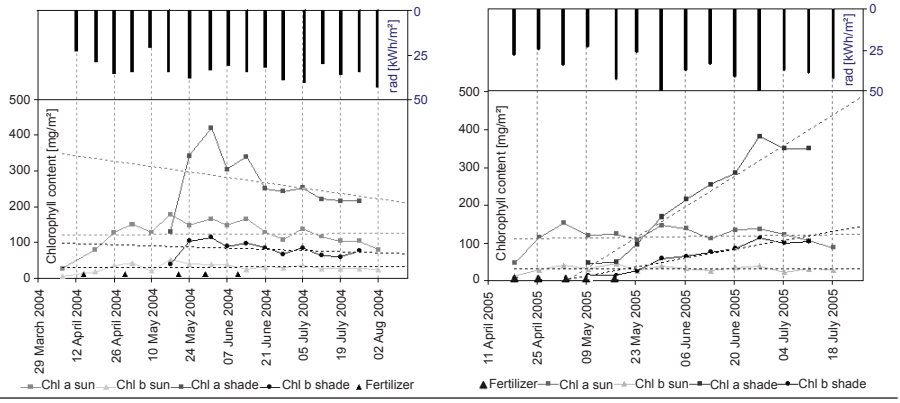

Fig. 20: Chlorophyll content per surface area [mg m^{-2}] for wheat as measured in 2004 and 2005; the upper bar graph indicates the sum of global irradiance as measured the weather station "Gut Hüll" for week prior to the chlorophyll measurements
Source: Own survey

It is important to note that the amounts of maximum chlorophyll incorporated in the canopies are similar, e.g. 420 mg m^{-2} chl a shade. However, the time at which the maximum is reached is quite different. For 2004, the maximum of the field mean was reached on June 1, while for 2005 the highest chlorophyll mean field values were monitored on June 27. This is again caused by the weather conditions during May 2005. Figure 21 demonstrates that the shade chlorophyll contents in 2005 are on a lower level than in 2004. This indicates a reduced development of leaf biomass in 2005, although a delay in the phenological development was not observed (Figure 19).

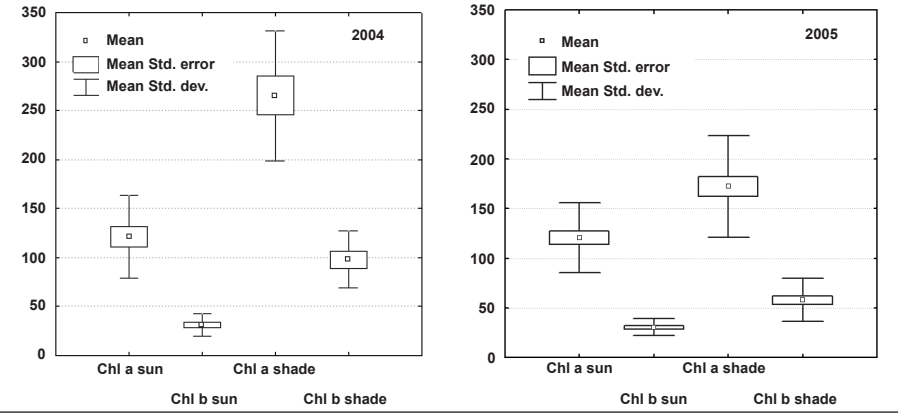

Fig. 21: Statistics of wheat chlorophyll content per surface area [mg m^{-2}] as measured at the sampling points
Source: Own survey

3.5.2 Maize

As for wheat, the sampling results for maize are presented separately for the chlorophyll contents per mass and for the contents per ground surface area. After removal of outliers, the data were tested for normal distribution using the Shapiro-Wilk W test. The W statistics shows that all results are not significant ($p > 0.05$), indicating that the measured chlorophyll contents are distributed normally.

Table 6: Results of the Shapiro-Wilk W test for maize

	Chl.a sun	Chl.b sun	Chl.a+b sun	Chl.a shade	Chl.b shade	Chl.a+b shade
p [µg g^{-1}]	0.92	0.52	0.86	0.51	0.38	0.54
p [mg m^{-2}]	0.19	0.14	0.17	0.33	0.30	0.34

Source: Own survey

3.5.2.1 Sampling results – chlorophyll contents per mass

Figure 22 presents the results of the chlorophyll measurements in 2004 and 2005 on a mean field basis. No management data are available for the maize fields, thus a discussion about the reaction to fertilization is not possible. Under normal conditions, the maize canopies in the test area are fertilized before or during sowing and perhaps also once during leaf development (BBCH 10), thus a direct effect of fertilization to chlorophyll content can not be observed in Figure 22.

Nevertheless, the influence of the weather situation, indicated by the global irradiance, is visible as well as the typical development of maize canopies throughout the vegetation period. During leaf development and tillering, the maize plantlets develop slowly until the beginning of July (see also phenological stages of the maize canopies in Figure 26).

Corresponding to the plant development, the chlorophyll contents increase slowly until the beginning of July, while during July they show a steep increase, again corresponding to the extreme growth of the maize plants until flowering. During fruit development and ripening, the chlorophyll contents decrease again. Although the phenological development is similar for both years, large differences can be observed in the amount of chlorophyll. The differences measured at the sampling points are presented in Figure 23 and show higher chlorophyll contents for 2005, especially of the shade chlorophyll.

These differences lead to the assumption that other cultivars than the previously mentioned cultivar Magister were sown. Differences in canopy height (270 cm in 2004 versus 320 cm in 2005) and sowing density (9.5 pl m^{-2} in 2004 and 11.5 pl m^{-2} in 2005) also

indicate different cultivars. The high global irradiance values especially during the early development in May and June 2005 had a stimulating effect on the chlorophyll contents. BAEUMER (1992) describes the close relationship between irradiance, chlorophyll content and yield. Under optimal growing conditions with a sufficient supply of water and nutrients, the photosynthetic rate is directly proportional to the irradiance. However, less global radiation during July and August 2005 reduced the chlorophyll contents temporarily, but the long-term level of content was not affected. For these reasons, different cultivars must be assumed.

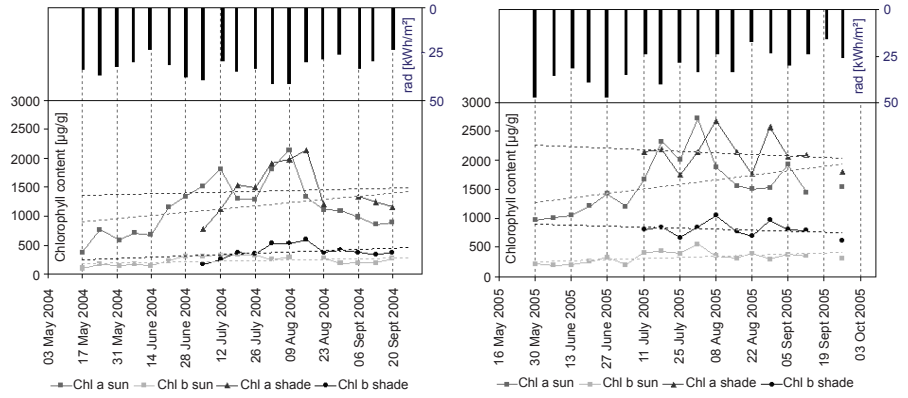

Fig. 22: Chlorophyll content of maize per mass [µg g^{-1}] as measured in 2004 and 2005; the upper bar graph on the top indicates the sum of global irradiance as measured at the weather station "Gut Hüll" for the week prior to the chlorophyll measurements

Source: Own survey

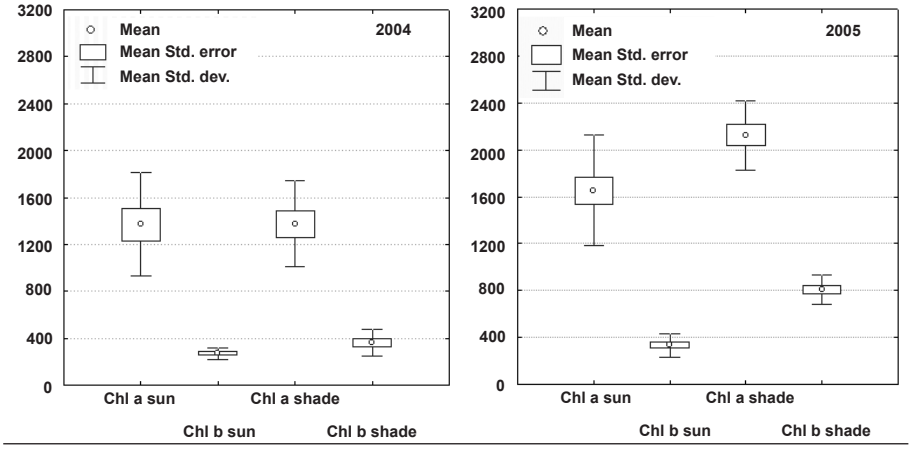

Fig. 23: Statistics of the chlorophyll contents per mass [µg g^{-1}] as measured at the sampling points; std.error = standard error, std.dev = standard deviation

Source: Own survey

3.5.2.2 Sampling results – chlorophyll contents per unit ground surface

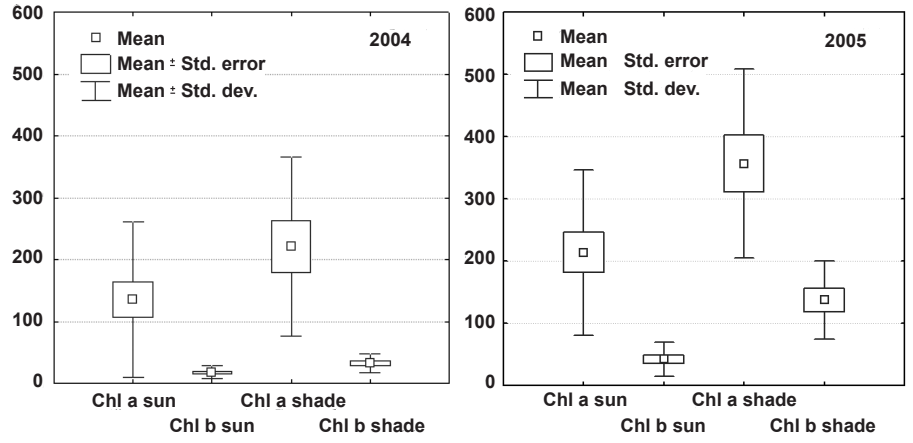

Fig. 24: Statistics of chlorophyll contents per surface area [mg m^{-2}] as measured at the sampling points; std.error = standard error, std.dev = standard deviation
Source: Own survey

The differences between the maize canopies are also apparent when analyzing the chlorophyll contents per unit ground surface area. The results of the field measurements are presented in Figure 24 and Figure 25. The chlorophyll contents display higher mean and maximum values in 2005 for both the sun and shade layer, while the phenological development is similar. Especially the shade chlorophyll is on a much higher level, which is caused by the higher chlorophyll contents per mass on the one side, but also by the larger dimension of the shade layer (larger plants) and the higher plant density in 2005 on the other.

Figure 25 presents the development of the maize canopies, which are typical for this plant species: steady growth during the first weeks results in low chlorophyll contents, which are caused by the low assimilation rate of nutrients. A heavy increase in chlorophyll content accompanies the fast development of the plants from the emergence of the flag leaf until flowering. During this period, the uptake of nutrients by the maize plants is enormously high and the daily nitrogen uptake may reach up to 5 kg ha^{-1} (Lüdtke Entrup & Oehmichen 2000).

A high nutrient uptake is accompanied by high chlorophyll contents both per mass (Figure 23) and per unit ground surface area (Figure 25). During the following grain filling period, the maize development is characterized by internal translocations. Much of the leaf nitrogen is shifted into the grains, whereby a large amount originates from storage proteins. But also nitrogen, which is incorporated into chlorophyll molecules, is trans-

located (LÜDTKE ENTRUP & OEHMICHEN 2000), resulting in reduced leaf chlorophyll contents.

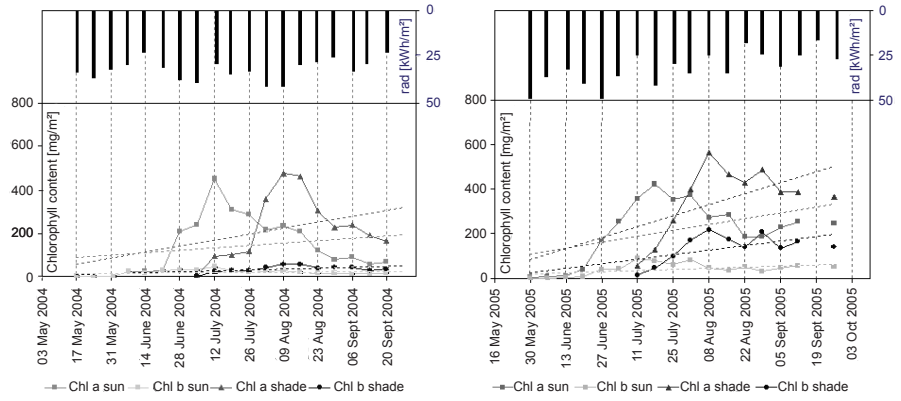

Fig. 25: Chlorophyll content of maize per ground surface area [mg m-²] as measured in 2004 and 2005; the upper bar graph indicates the sum of global irradiance as measured at the weather station "Gut Hüll" for the week prior to the chlorophyll measurements
Source: Own survey

As presented in Figure 26, the maize fields exhibited a comparable phenological development in 2004 and 2005, which was also observed with wheat. The single BBCH stages follow the same phenology, but the development of the biomass and of biophysical parameters such as the chlorophyll content show adaptations to the weather conditions.

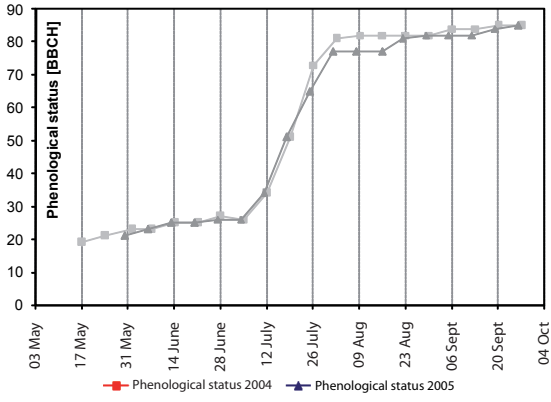

Fig. 26: Phenological development of maize test fields in 2004 and 2005
Source: Own survey

3.6 Evaluation of the results

The results of the field measurements indicate that the chlorophyll contents both per mass and per unit ground surface area vary during the vegetation period. A similar data basis with respect to chlorophyll is not known to the author, but results confirm statements in literature that chlorophyll is a highly variable and regulated pigment (Von Caemmerer 2000; Furbank & Taylor 1995; Furbank 1997; Oppelt & Mauser 2004; Schurr et al. 2006). Thus, there is a need for measurements repeated throughout the vegetation period to monitor the actual chlorophyll status of a canopy, which is the result of complex interactions between soil, temperature, irradiance, precipitation and field management, i.e. fertilization. Even for individual fields, it is very difficult to gather all information necessary to model vegetation growth and development, but this background information is included indirectly in the monitoring of the chlorophyll status using remote sensing techniques. Thus, remotely sensed derived chlorophyll provides a data source that indirectly includes this background information.

The results also illustrate the necessity of monitoring not only the spatial distribution of chlorophyll, but also the vertical distribution within a canopy, where differences were observed for both maize and wheat. This statement is embedded in a controversial discussion about chlorophyll contents of shade and sun leaves:

On the one side sun and shade leaves are described as being morphological adaptations to special environments and cannot be altered after leaf development. This is mainly proposed for different tree species (Pearcy 1990; Terashima & Hikosaka 1995; Schurr et al. 2006), but also for non-woody plants (Björkman 1881; Björkman & Demming 1987). Terashima & Hikosaka (1995) report the phenomenon that shade leaves contain much higher levels of chlorophyll per mass, but low chlorophyll content per leaf area. This is documented as a result of the fact that shade leaves have less mass per unit leaf area in comparison to sun leaves.

On the other side, there is literature where a much lower chlorophyll content of shade leaves compared to sun leaves is reported. Although these results are mostly based on herbaceous vegetation or crops (Evans 1993; Lawlor 2003), Laisk et al. (2005) describe decreased area-based chlorophyll content in a birch specie (*Betula pendula* L.), while it did not change in lime trees (*Tilia cordata* L.). The results of the field measurements 2004 and 2005 indicate that differences exist for both chlorophyll per mass and chlorophyll per unit ground surface area.

Thus, the chlorophyll content of sun and shade leaves seems to be highly species-dependent. However, even if there is a general morphological adaptation for a variety of species that cannot be altered after leaf development, biophysical and biochemical mechanisms

(described in section 2) exist that are able to regulate the chlorophyll content dynamically to changing environments. This leads to the conclusion that there is a need for further investigations to gather information about species-dependent differentiation between sun and shade canopy layers.

4 Remote sensing data

The processing and analysis of remotely sensed data are of particular importance for this study because these data form the basis for the assessment of the spatial distribution of chlorophyll in a canopy. Two sensors were used, the airborne imaging spectrometer AVIS and the spaceborne spectrometer CHRIS. The AVIS data were originally intended to provide the data for the analysis, but technical problems prohibited multi-angular AVIS acquisitions during 2005. Fortunately, the Gilching area is a test site within the scope of the scientific part of the CHRIS/PROBA mission, thus a series of multi-angular CHRIS acquisitions for 2004 and 2005 is available. Therefore the CHRIS data form the basis for the regression analysis. Regarding the relatively low geometric resolution of the CHRIS data for this task, it is appropriate to round up the results with the available airborne data.

First, some introductory remarks will be made about bi-directional, hyperspectral remote sensing. In the following, the spaceborne sensor CHRIS and the airborne system AVIS will be briefly introduced before the radiometric and geometric processing of the data is described. A large number of spectral indices exist in the literature, which can be applied to derive the chlorophyll content of vegetated areas. In this study, an enhancement of an existing index, the Chlorophyll Absorption Integral (CAI), is described and applied to the remote sensing data. Two kinds of maps are produced as an input for the SVAT model: Firstly, the conventional "top-of canopy" (sun chlorophyll) map which is used for the discussion about the profit of using conventional, nadir-looking remote sensing data as input data. Secondly, the shade chlorophyll maps, which enable the vertical differentiation into sun and shade canopy layers.

4.1 Multi-angular remote sensing

For many purposes, especially the remote sensing of canopy properties, the angular variation of the reflectance as the illuminating source and the detector move is of interest. A full characterization of the reflectance behaviour of a surface involves estimation of the bidirectional reflectance distribution function (brdf), which is the ratio of the radiance reflected into an infinitesimally small solid angle for any given angle at the reflecting surface to the incident irradiance from a given direction (NICODEMUS et al. 1977). When measuring radiation reflected from a surface, what is really measured is the spectral radiance (i.e. the radiant flux density emanating from a given surface per unit solid angle and per unit wavelength, expressed in $W\ m^{-2}\ sr^{-1}\ \mu m^{-1}$). Reflectance, a ratio of incoming to outgoing radiation, can be defined in a number of ways depending on the viewing and illumination conditions: these could be directional (restricted to a small angle) or hemispherical (integrating from the whole sky or surface). Usually, in the definition of reflectance, the degree of collimation of the source followed by that of the detector are

prefixed to the word reflectance (HAPKE 1993). This definition can be further specified as a spectral reflectance by considering a specific wavelength. In reality, no sensor has an infinitesimally small view angle, nor is the sun a point source. So, strictly, the term "conical" or "anisotropical" instead of "bi-directional" should be used with actual measurements (JONES et al. 2003; SCHAEPMAN-STRUB et al. 2006). However, the term bi-directional and anisotropical will be used in this thesis.

The use of multi-angular remote sensing offers the possibility of exploiting directional information, which has been shown to be especially influenced by the geometric properties of the target. Due to the availability of sensors, this has mainly been investigated using goniometer in the field and in the laboratory (WEISS et al. 2000; SANDMEIER et al. 1999; CASA & JONES 2005) or on the regional to global scale using MODIS (MODerate Imaging Spectrometer, 15 bands between 400 nm and 1000 nm, spatial resolution 250 - 1000 m), MISR (Multiangle Imaging SpectroRadiometer, four bands in the VIS and NIR, spatial resolution 250 m at nadir), POLDER-2 data (POLarization and Directionality of the Earth's Reflectances, operation in 2003, nine bands between 400 and 860 nm, spatial resolution 6 - 7 km) and SPOT VEGETATION (launched in 1998, four bands between 400 nm and 1750 nm, spatial resolution 1 km) (CHEN et al. 2003; WIDLOWSKI et al. 2004; DINER et al. 2005; SCHAEPMAN-STRUB et al. 2006; LIESENBERG et al. 2007). Besides the use of airborne data (BARNSLEY et al. 1997; CHOPPING et al. 2003; OPPELT & MAUSER 2006), the launch and operation of CHRIS/PROBA-1, the first spaceborne imaging spectrometer with a high spatial resolution, enabled the monitoring on a local to regional scale. Therefore investigations on these scales are published in recent years, but are mostly related to investigations about canopy structure and LAI retrieval (COMBAL et al. 2003; CASA & JONES 2004; KNEUBÜHLER et al. 2006; KOETZ et al. 2005; SCHAEPMAN et al. 2005). Few studies are directed towards the quantification of forest nitrogen (HUBER et al. 2008) or canopy chlorophyll (SCHOPFER et al. 2007; OPPELT & MAUSER 2007a).

This study proposes a variant on the multiangular approach based on the gap effect. The gap effect is the phenomenon that, in an erectophile canopy, the orientation of the leaves allows the lower, less illuminated canopy levels to be viewed (KIMES 1983). Therefore it is proposed that the chlorophyll content of lower leaves can be monitored with angular viewing. The precondition is, of course, that the chlorophyll content of the top-of-canopy leaves can also be derived using remote sensing data. Other phenomena that superimpose the gap effect occur, such as the anisotropic scattering of vegetation or effects caused by illumination direction and sun zenith angle. These phenomena have to be taken into account and are discussed in section 5 and 6.

4.2 CHRIS/PROBA-1

The sensor CHRIS was developed by Sira Technology Ltd to provide remote sensing data for land applications and aerosol measurements, but it is also used for coastal zone monitoring (BARNSLEY et al. 2004). CHRIS is one instrument payload on the ESA small satellite platform PROBA-1 (PRoject for On-Board Autonomy), which was launched in 2001. CHRIS was intended to demonstrate that compact imaging spectrometers can be low-cost but viable instruments when combined with agile small platforms (SIRA 2004). The exploitation of CHRIS data is organized by the ESA's Earth Science Division within the framework of the Earth Observation Preparatory Programme (ESA 1999), who kindly provided the data for this study.

In general, CHRIS provides a spectral coverage from 400 nm to 1050 nm, but it can be operated in five imaging modes that address the requirements of different applications and user groups. In this study, mode 5 data (land mode) are used providing 37 spectral bands with central wavelengths between 442 nm and 1019 nm. The spectral resolution varies between 6 nm at 716 nm (band no. 13) and 33 nm at 1019 nm (band no. 37). The central wavelengths may vary slightly with changes of sensor temperature. The nominal band allocation for mode 5 is given in Table 7. The nominal ground segment distance (GSD) is 17 m at nadir, but it can vary due to differences in the orbit altitude of PROBA-1 (between 550 and 680 km). With an image consisting of 748 x 374 pixels the resulting nominal image area is 12.7 x 6.36 km.

PROBA-1 can be manoeuvred in all three axes to view any target of interest. More significantly, by tilting the satellite in both the along-track and across-track directions during orbit, it is possible to acquire a set of up to five CHRIS images of a given target area, each at a different view zenith angle, in a single orbital overpass (BARNSLEY et al. 2004). Due to its narrow field of view (FOV = 1.3°), CHRIS is only occasionally able to image a target from directly overhead (i.e. nadir). More generally, PROBA-1 must be tilted at some angle in the across-track direction so that the target area falls within the sensor's FOV. Each target site therefore has an associated fly-by position on any given day, which is the point on the sub-satellite track closest to the target. CHRIS acquires images of the target when the zenith angle of the platform, with respect to the fly-by-position, is ±55°, ±36° and 0°. The zenith angles with respect to the target are typically larger than these values. This means that the angles at which images are acquired vary from site to site, depending on their positions with respect to the orbital track. The view zenith angle of the satellite at the fly-by position is known as the minimum zenith angle (MZA). The MZA and fly-by zenith angles (FZA) are illustrated in Figure 27 (SIRA 2002; SIRA 2004). A more detailed description of the CHRIS/PROBA-1 mission and the CHRIS instrument can be found in BARNSLEY et al. (2004).

Table 7: Nominal central wavelengths and bandwidths for the CHRIS mode 5 data

Band No.	Centre Wavelength [nm]	Bandwidth [nm]	Band No.	Centre Wavelength [nm]	Bandwidth [nm]
1	442	9	20	762	7
2	489	9	21	770	7
3	530	9	22	777	15
4	551	10	23	792	8
5	570	8	24	800	8
6	631	9	25	872	18
7	661	11	26	886	10
8	672	11	27	895	10
9	683	11	28	905	10
10	697	6	29	915	10
11	703	6	30	925	10
12	709	6	31	940	20
13	716	6	32	955	10
14	722	6	33	965	11
15	728	7	34	976	11
16	735	7	35	987	11
17	742	7	36	997	11
18	748	7	37	1019	33
19	755	7			

Source: Own survey

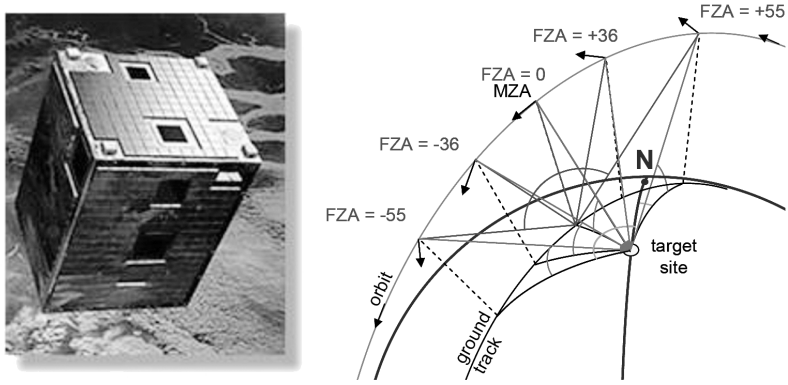

Fig. 27: The platform PROBA-1 and CHRIS Fly-by Zenith Angles (FZA) and Minimum Zenith Angle (MZA)
Source: SIRA 2004

The data, which are provided in Hierarchical Data Format (hdf), are corrected for dark current and smile effects (SIRA 2004). As described above, the orbital settings of CHRIS

are highly variable due to the fact that the platform's orbit is continually changing. Additionally, the nominal FZAs of the CHRIS data acquisitions rarely correspond to the actual viewing geometries. For this reason, all the parameters described above are provided in the header of every image of an acquisition sequence, which is a prerequisite for accurate processing of the data.

4.2.1 Acquired data

In total, nine CHRIS data sets were acquired in 2004 and 2005. Two acquisitions were carried out when the area was covered with snow (March 28 2004 and March 2 2005), therefore these data were not analysed. Three of the other data sets are available for 2004, while the remaining four data sets were acquired during the vegetation period of 2005 (Table 8).

Table 8: CHRIS data available for the vegetation periods 2004 and 2005 (w=wheat, m=maize)

Date	**-55°**		**-36°**		**0°**		**+36°**		**+55°**	
March 28 2004										
May 25 2004	w	m	w		w		w		w	m
July 21 2004					w	m	w	m	w	m
August 22 2004		m				m				m
March 2 2005										
May 25 2005	w		w	m	w	m	w	m	w	
June 2 2005	w	m	w	m	w	m		m	w	m
June 3 2005	w	m		m		m		m	w	m
July 6 2005	w				w		w	m		m

Source: Own survey

The angles in Table 8 correspond to the nominal FZAs (Figure 27). The real observation angles differ from the FZA with a mean value of 0.826°, a minimum of 0.2° (-55° FZA on 2 June 2005), and a maximum of 6.6° (+36° FZA on 2 June 2005).

CHRIS operates on a sun-synchronous orbit (inclination of 98°) with a descending path over the test area. For this reason, the forward-looking angles (+36°, +55°) are directed towards the sun and contain a large proportion of shadow, while the backward-looking angles (-36°, -55°) have a "sun-parallel" view direction hiding most of the shadows.

Stable acquisition times near noon (10:33 to 10:47 UTC) result in relatively constant sun zenith angles (27 - 30°). The relative azimuth angles between CHRIS and the sun are presented in Figure 28. Figure 28 also demonstrates that the forward and backward looking angles can be clearly differentiated. The backward-looking angles have small sensor-sun azimuths because they are viewing the target in the same direction as the sun. In contrast,

the forward-looking angles show sensor-sun azimuth angles around 180° indicating that they are pointing towards the sun. Both viewing geometries can be observed with the nadir data. As previously mentioned, this indicates that there are no "real" nadir data, but slightly forward or backward looking nadir-like acquisitions.

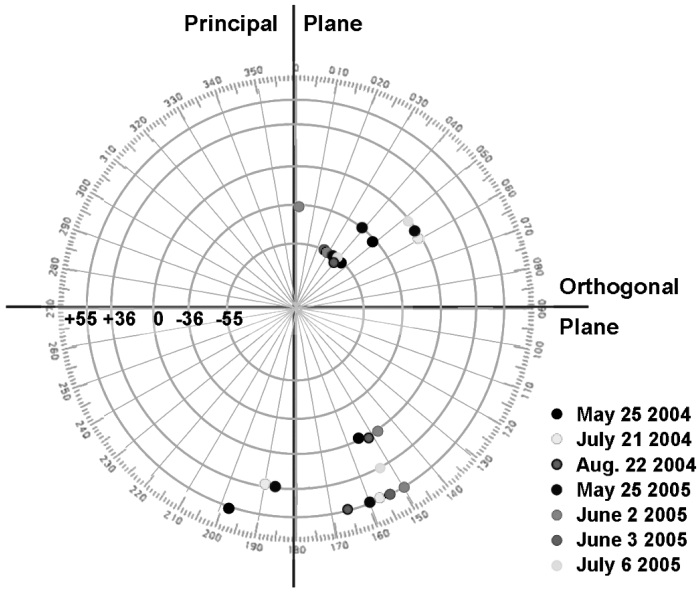

Fig. 28: Azimuth angles between the sensor and the sun
Source: Oppelt & Mauser 2007a

4.2.2 Radiometric processing

CHRIS data exhibited a non-systematic striping pattern, which resulted from temperature-varying calibration errors in the CHRIS imaging. This effect was corrected using an algorithm developed by Dr. Settle from Reading University (UK) for the CHRIS data. The processing re-adjusts the relative brightness of different columns to minimize the striping. The brightness of each column is assessed by measuring the average of pixel values that fall within the inter-quartile range i.e. the darkest 25% and the brightest 25% of pixels are rejected before averaging (Garcia & Moreno 2004).

After the destriping, the CHRIS data were atmospherically corrected and calibrated to reflectances. This procedure was carried out using an approach based on MODTRAN-4 (Berk et al. 2004; Bach 1995). The modelling of the atmosphere was conducted using standard atmospheric profiles modified with the Observation Zenith Angles (OZA) and Observation Azimuth Angles (OAA) given in the CHRIS header files. Table 9 shows the parameter settings used to model the atmospheric properties for the nadir acquisitions. The observation zenith and azimuth settings were changed for the angular data, resulting

in a separate atmospheric modelling for each image. The nominal FZAs are used in the following for simplification but represent ranges of actual angles around the nominal angles.

Table 9: Parameter settings for the modelling of the CHRIS nadir atmosphere using MODTRAN-4

Date	Atmosphere model	Water vapour factor	Visibility on ground [km]	Sun zenith angle [°]	OZA [°]	OAA [°]
May 25 2004	Temperate zone, summer	0.9	50	28	18.46	315.5
July 21 2004	Temperate zone, summer	1.2	25	29	14.58	225.0
August 22 2004	Temperate zone, summer	0.9	42	38	7.78	144.2
May 25 2005	Temperate zone, summer	1.1	50	28	10.08	224.9
June 2 2005	Temperate zone, summer	0.8	50	26	3.93	200.2
June 3 2005	Temperate zone, summer	1.0	70	26	21.5	315.2
July 6 2005	Temperate zone, summer	0.8	50	27	5.29	221.1

Source: Own survey

The validation of the radiometric correction was carried out using the field spectrometer measurements described previously. A comparison between CHRIS nadir reflectances and field spectrometer data is presented in Figure 29, where the mean value and the value range of all CHRIS pixels are compared with field spectrometer data gathered at the sampling points in the field. Figure 29 represents a typical status of the data and therefore is provided as an example. In general, the range of values is greater with the CHRIS data compared to the field spectrometer. In the VIS the reflectances match very well; the mean field values correspond almost exactly. Larger differences are observed for the NIR, which is due to the larger GSD, but also to directional effects occurring in the CHRIS data. In general, validation showed a good agreement between atmospherically corrected CHRIS data (FZA = 0°) and spectral ground measurements with deviations of the ground measurements ranging within ± 1.0 standard deviations of the CHRIS data.

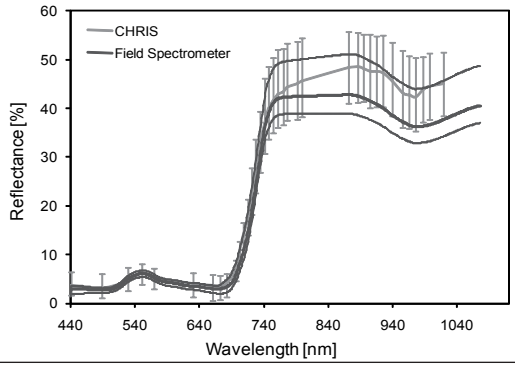

Fig. 29: CHRIS and field spectrometer data (mean, minimum and maximum) gathered on June 2, 2005; the error bars indicate ±1.0 stdev of the CHRIS data
Source: Own survey

4.2.3 Geometric processing

The geometric correction of the CHRIS data is important because pixel spacing differs for each of the angles: the greater the observation angle, the coarser is the geometric resolution.

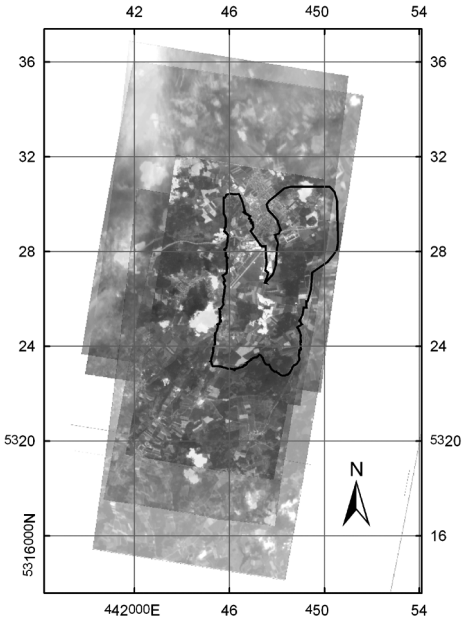

Fig. 30: CHRIS image stack (bgr = 437, 564, 669 nm) acquired on June 2 2005 (Gauß-Krüger zone 4 coordinates); the test area is outlined
Source: Own survey

The multiangular data were resampled to 17 m using bilinear interpolation and rectified with a 2nd order polynomial approach using aerial orthophotos of the area and ground control points. An example for a corrected set of CHRIS images is presented in Figure 30.

4.3 AVIS

The Airborne Visible and Infrared imaging Spectrometer (AVIS) is a pushbroom sensor that was designed and developed at the chair for Geography and Geographical Remote Sensing of the Ludwig-Maximilians-Universität München in 1998. The second generation of the system, AVIS-2, was operated in 2004 and 2005.

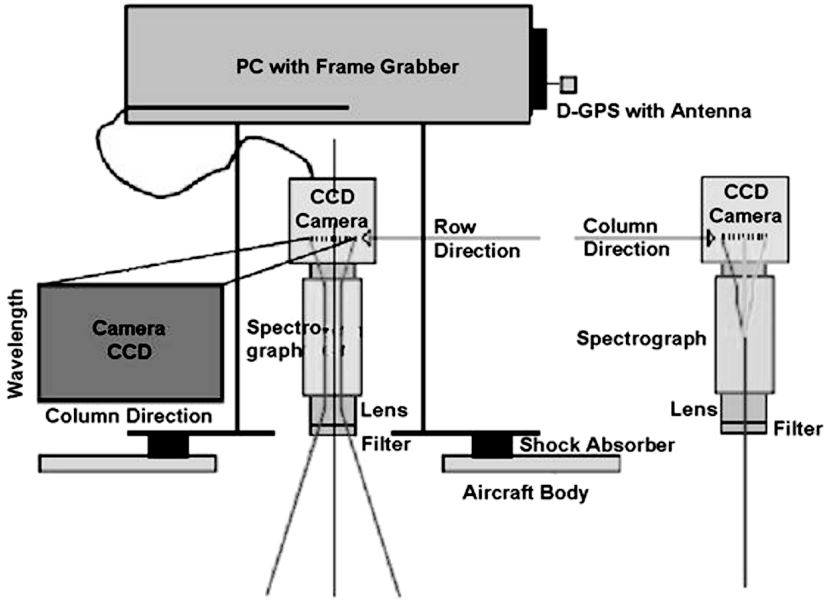

Fig. 31: Components of AVIS-2
Source: Oppelt & Mauser 2007b

AVIS-2 is a CCD-based system operating in the VIS and NIR (400 nm to 900 nm) spectral range with a spectral resolution of 9 nm. The components of AVIS-2 are presented in Figure 31. The system is based on a spectrograph (SPECIM Imspector $V9_{NIR}$), mounted to a black and white 2/3" CCD-video camera (Vosskühler 1300) and a filter-lens system. The radiation that passes the lens enters the spectrograph through a slit and is dispersed by a combination of gratings and prisms. The output of the spectrograph is a row of 300 pixels representing the wavelengths. The columns represent the spatial direction. The spectrograph is mounted to the video camera. When the system is moving above ground, a two-dimensional flight stripe is created. The digital signal is stored on the hard disk of

the connected PC together with additional data from an inertia navigation system (INS) and a global positioning system (GPS). These additional data are used for the geometric correction.

Table 10: Specification of AVIS-2

Specification	**AVIS-2**
Spectral range [nm]	400-870
Spectral resolution [nm]	9
Spectral sampling / resampling [nm]	3.7 / 7.4
Radiometric sampling [bits]	15
Number of bands (sampling / resampling)	128 / 64
Signal to Noise Ratio (SNR) [dB]	66 at 700 nm
Spatial resolution [pixels per line]	300
Spatial sampling [pixels per line]	640
Field of view (FOV) [rad]	1.16
Navigation system	INS + dGPS
Period of operation [years]	since 2001

Source: Oppelt & Mauser 2007b, modified

AVIS was conceived to be operated on different platforms, such as Dornier DO-27 or DO-228 and microlight aircrafts, where the sensor is mounted on vibration dampening mounts. In addition, AVIS-2 was designed to record along-track multi-angular images. The images are acquired during one pass over a flight strip by tilting the complete spectrometer at up to seven sensor angles relative to the sensor platform between +55° and –55°. The advantage of this procedure is that the illumination and atmospheric conditions do not change significantly during data acquisition (Oppelt & Mauser 2006).

Dedicated software for the processing of the data was developed by Prof. Wolfram Mauser. The system has been in commercial use since 2001 for environmental monitoring purposes in the fields of agriculture (Oppelt & Mauser 2003; Oppelt et al. 2007; Hank et al. 2007; Laudien et al. 2004), floristic mapping (Schmidtlein & Sassin 2004; Schmidtlein et al. 2007), inland water monitoring (Bach 2007) as well as for ESA studies (Scheiber & Oppelt 2005; Scheiber et al. 2006; Scheiber et al. 2007). A summary of AVIS-2 specifications and centre wavelengths are given in Table 10 and Table 11. A detailed description of AVIS-2 can be found in Oppelt & Mauser (2007b).

Table 11: AVIS-2 centre wavelengths

Band No.	Centre Wavelength [nm]	Band No.	Centre Wavelength [nm]	Band No.	Centre Wavelength [nm]	Band No.	Centre Wavelength [nm]
1	411.88	17	528.39	33	644.90	49	761.42
2	419.16	18	535.67	34	652.19	50	768.70
3	426.44	19	542.95	35	659.47	51	775.98
4	433.72	20	550.24	36	666.75	52	783.26
5	441.01	21	557.52	37	674.03	53	790.55
6	448.29	22	564.80	38	681.31	54	797.83
7	455.57	23	572.08	39	688.60	56	805.11
8	462.85	24	579.37	40	695.88	57	812.39
9	470.13	25	586.65	41	703.16	58	819.67
10	477.42	26	593.93	42	710.44	59	826.96
11	484.70	27	601.21	43	717.73	60	834.24
12	491.98	28	608.49	44	725.01	61	841.52
13	499.26	29	615.78	45	732.29	62	848.80
14	506.54	30	623.06	46	739.57	63	856.09
15	513.83	31	630.34	47	746.85	64	863.37
16	521.11	32	637.62	48	754.14		

Source: Own survey

4.3.1 Acquired data

When angular acquisitions are carried out with an airborne sensor at relatively low flight altitudes, accurate navigation is very important. The sensor has to be swivelled during flight, depending on the velocity and altitude of the aircraft.

Table 12: AVIS data acquired in 2004 and 2005, w = wheat, m = maize (letters in parenthesis indicate partly coverage of the test field)

Date	-55°		-45°		-25°		0°		25°		45°		55°	
March 31 2004	w		w		w		w		w		w		w	
May 25 2004	w				w			m	w	m	w			
June 8 2004							w	m						
July 22 2004		m		m			w	m		m		m		
August 10 2004								m						
Sept. 9 2004		m				m		m						
July 6 2005							w	m						

Source: Own survey

Technical problems prohibited angular monitoring in 2005, thus multiangular data are available only for 2004. One nadir acquisition was conducted in 2005 (see Table 12). In contrast to the CHRIS data with a relatively fixed, descending orbit, airborne acquisitions do not have a regular pointing pattern. Thus the sun-sensor geometry of the imagery depends on the heading of the aircraft. The relative sun-sensor azimuth angles of the AVIS-2 acquisitions are presented in Figure 32.

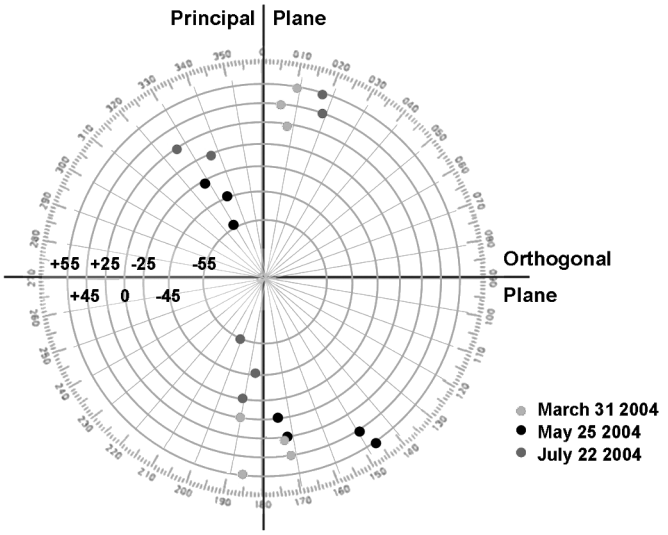

Fig. 32: Sun-sensor azimuth angles for the multi-angular AVIS-2 acquisitions in 2004
Source: Own survey

4.3.2 Radiometric processing

The radiometric processing of the data included radiometric pre-processing for sensor dark current, CCD homogeneity and smile effect. A detailed description of these pre-processing steps can be found in OPPELT & MAUSER (2007b).

After radiometric pre-processing, the atmospheric correction and calibration to reflectances was conducted (according to the processing of the CHRIS data) using MODTRAN-4 (BERK et al. 2000; BACH 1995). The modelling of the atmosphere was conducted using standard atmospheric profiles, which were modified using the OZAs and OAAs. Table 13 shows the parameter settings used to model the atmosphere for the AVIS nadir acquisitions. The observation zenith and azimuth settings were changed for the angular data resulting in a separate atmospheric modelling for each image.

Table 13: Parameter settings for the modelling of the AVIS nadir atmosphere using MODTRAN-4

Date	Atmosphere model	Water vapour factor	Visibility on ground [km]	Sun zenith angle [°]	OZA [°]	OAA [°]
March 31,2004	Temperate zone, summer	1.0	50	43.9	0.7	357.0
May 25, 2004	Temperate zone, summer	0.9	45	37.7	0.4	312.0
July 22, 2004	Temperate zone, summer	1.1	42	31.5	0.0	236.6

Source: Own survey

4.3.3 Geometric processing

The geometric processing of the AVIS data was carried out using the dGPS/INS data stored in the header of each image line. Data such as the aircraft location (latitude, longitude and altitude) and pointing information (roll, pitch and yaw) are used together with a digital elevation model to compensate for the motion of the aircraft and rectify the data. According to the processing of the CHRIS data, the AVIS data were also rectified to Gauß Krüger projection (Bessel ellipsoid, Potsdam date).

The pixel spacing or ground segment distance (GSD) of airborne data depends strongly on the aircraft altitude above ground h [m] and velocity v [m s^{-1}]. GSD of airborne images can also differ between an image line (across-track) and along the movement of the aircraft (along-track). The across-track GSD depends upon the number of pixels per line of the camera (Nc = 640) while the along-track GSD is determined by the frame rate i [s^{-1}] as described in Equation 10 and Equation 11 (OPPELT & MAUSER 2007b).

$$GSD_{across\ track} = \frac{h}{Nc} \qquad \text{Equation 10}$$

$$GSD_{along\ track} = \frac{v}{i} \qquad \text{Equation 11}$$

The acquisitions available for 2004 were carried out at different altitudes. According to Equation 11, this results in different GSDs, which are presented in Table 4-8. The AVIS data were resampled to a GSD of 4 m for the first two acquisitions and 2 m for the images acquired on July 22 using a nearest neighbour approach.

Table 14: AVIS image acquisition settings in 2004

Date	Altitude above sea level [m a.s.l.]	Altitude above ground [m a.g.]	Aircraft speed [m s^{-1}]	Frame rate [Hz]	$GSD_{acrosstrack}$ [m]	$GSD_{alongtrack}$ [m]
March 31, 2004	2700	2120	48	16	3.3	3.0
May 25, 2004	2700	2120	48	16	3.3	3.03
July 22, 2004	1350	770	40	16	1.2	2.5

Source: Own survey

5 Monitoring of canopy chlorophyll status

The spectral absorbance properties of chlorophyll, which are described in section 2, enable measurements of reflected radiation as a non-destructive method for its quantification. In particular, airborne hyperspectral sensors such as AVIRIS (Airborne Visible, InfraRed Imaging Spectrometer), HYMap (HYperspectral Mapping), ROSIS (Reflective Optics System Imaging Spectrometer) or AVIS (Airborne Visible and Infrared imaging Spectrometer) incited research focused on developing techniques for analyzing pigment contents of plants (CHAPPELLE et al. 1992; YODER & PETTIGREW-CROSBY 1995; BLACKBURN 1998; DATT 1998; JAGO et al. 1999; OPPELT & MAUSER 2001; BROGE & MORTENSEN 2002; HABOUDANE et al. 2002; OPPELT 2002; SIMS & GAMON 2004; OPPELT & MAUSER 2004). The launch of the imaging spectrometer CHRIS/PROBA in 2001 enabled the spaceborne monitoring of biophysical vegetation parameters on a regional to local scale (KNEUBÜHLER et al. 2006; SCHOPFER et al. 2007). The directional monitoring of both broad scale and local scale sensors is in general used for the assessment of canopy structure using the directional scattering behaviour of vegetation (CHEN et al. 2003; COMBAL et al. 2003; CASA & JONES 2004; CHOPPING et al. 2005; DINER et al. 2005; KOETZ et al. 2005; SCHAEPMAN et al. 2005). Only a few publications deal with the assessment of biophysical variables, such as chlorophyll, derived from the spectral reflectance of angular data (OPPELT et al. 2007; OPPELT & MAUSER 2007).

The assessment of the chlorophyll content of leaves in both the upper, sunlit canopy layer and the lower, less illuminated canopy levels is described in the following sections. A great variety of indices exists for chlorophyll estimation, but only one, the chlorophyll absorption integral CAI, is used in this study. This index enables a discussion about the sensitivity towards the reflectance anisotropy of vegetation; thus, this term is briefly described in the following.

5.1 Reflectance anisotropy of vegetation canopies

The anisotropic reflectance behaviour of vegetation is closely related to the "bidirectional reflectance distribution function" (brdf), which was defined by NICODEMUS et al. (1977) as the ratio of the radiance L reflected in one direction θ_r, φ_r to the incident irradiation E_i from direction θ_i, φ_i. It is thus a function (f_r) of two directions and of wavelength, and is an intrinsic property of the reflecting surface.

The brdf cannot be measured directly since an infinitesimally small sensor FOV would be required; it can only be approximated by measurements. In practise, brdf values are derived by dividing measured radiances L from small aperture solid angles by the incident hemispherical irradiance E_i (SANDMEIER et al. 1998), thus the term hemispherical reflectance would be more appropriate.

$$brdf = f_r(\theta_i, \varphi_i; \theta_r, \varphi_r; \lambda) \approx \frac{L(\theta_i, \varphi_i; \theta_r, \varphi_r; \lambda)}{E_i(\theta_i, \lambda)} \; [sr^{-1}]$$ Equation 12

where

L	sensor radiance [W m^{-2} sr^{-1} nm^{-1}],
E_i	incident radiation [W m^{-2} nm^{-1}],
λ	wavelength [nm],
θ_r	view zenith angle [°],
θ_i	sun zenith angle [°],
φ_r	view azimuth angle [°], and
φ_i	sun azimuth angle [°] (SANDMEIER et al. 1998).

A detailed description of the physical mechanisms underlying the relationship between vegetation anisotropy and canopy structure can be found in SANDMEIER et al. (1998). In short, multiple scattering effects determine the contrast between shadowed and illuminated components of a vegetation canopy and therefore strongly influence the brdf characteristics. Since multiple scattering effects depend on the canopy absorbance characteristics, brdf effects are spectrally variable. Figure 33 presents brdf approximations as measured in the laboratory, where the bidirectional reflectance factor (brf) is used. The brf is defined as the ratio of radiance reflected from a surface in a specific direction to the radiance reflected from a lossless Lambertian surface (Equation 13).

$$brf = (\theta_i, \varphi_i; \theta_r, \varphi_r; \lambda) = f_r(\theta_i, \varphi_i; \theta_r, \varphi_r; \lambda) \cdot \pi \quad [\text{dimensionless}]$$ Equation 13

The extent of spectral variability is related to the canopy architecture: in erectophile vegetation canopies the spectral brdf variability is high because of a strong anisotropy. In planophile canopies, however, the anisotropy effects are relatively small and the spectral anisotropy variability is limited (SANDMEIER & DEERING 1999). For this reason, the extent of spectral variability of anisotropy provides a measure of this structure parameter (CHEN et al. 2003, GOBRON et al. 2002, WIDLOWSKI et al. 2004, WEGSCHEIDER & OPPELT 2008).

Another method for deriving relative deviations in reflectance is the calculation of the aniso-tropy factor (ANIF). Instead of the comparison with a Lambertian surface as described for the brf, the ANIF describes the ratio of reflectance in a specific view direction in relation to the nadir reflectance. Thus, if a nadir image exists, it can easily be calculated for remote sensing data to analyze the spectral variability of the hemispherical reflectance. The ANIF [dimensionless] is defined as follows (SANDMEIER & ITTEN 1999):

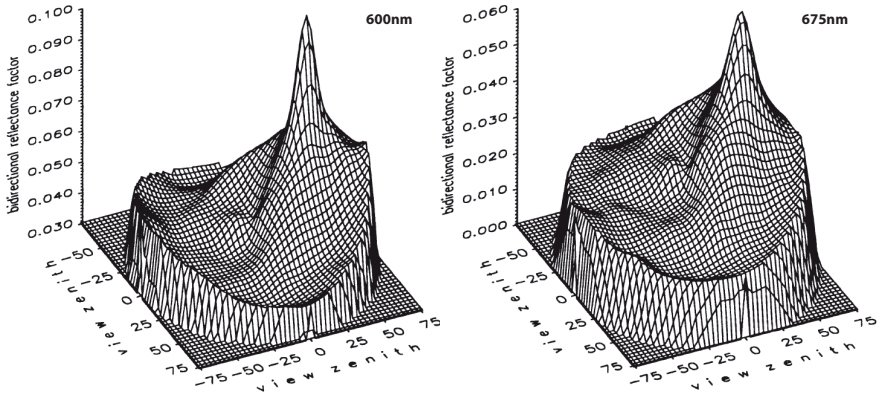

Fig. 33: Brdf approximations of grass at 600 nm (left) and 675 nm (right), interpolated from measurements in the laboratory with a resolution of 5° and 16° in zenith and azimuth respectively; the illumination zenith angle is 35°, the illumination azimuth angle is 180°

Source: SANDMEIER et al. 1998

In this study, a variant on the multiangular approach, which is based on the gap effect, is analyzed. The signal of radiation reflected or scattered to the sensor is superimposed by the effects of illumination and viewing geometry. The vegetation anisotropy is not analyzed explicitly, but knowledge of scattering and reflectance processes of vegetation canopies and the main influence parameters is important for the analysis of multiangular remote sensing data.

$$ANIF\ (\theta_i, \varphi_i, \theta_r, \varphi_r, \lambda) = \frac{R\ (\theta_i, \varphi_i, \theta_r, \varphi_r, \lambda)}{R\ (\theta_i, \varphi_i, \theta_r = 0, \varphi_r = 0\ , \lambda)} \qquad \text{Equation 14}$$

where

R spectral reflectance [%].

The effect of varying illumination conditions during one CHRIS overpass is demonstrated in Figure 34. Due to its orbit, CHRIS operates near the principal plane, where the azimuth between the sun and the sensor is near 0° and 180° respectively, leading to the so-called backshadow effect: The forward FZAs (+36°, +55°) are directed towards the sun and contain a large proportion of shadow, while the backward FZAs (-36°, -55°) have a "sun-parallel" view direction containing less shadow, a higher proportion of sunlit surfaces a higher incidence of sun glint (Figure 34 b). These effects lead to higher reflectances in the VIS for the backward FZAs. The point where the proportion of sunlit surfaces and sun glint is highest and thus the proportion of shadows lowest is the so-called hot spot. While brdf data provide an accurate measure of the hot spot, for the CHRIS data presented in Figure 34 the hot spot only can be assumed.

Although a multiple regression analysis can be assumed to be promising for chlorophyll assessment, the sample size of CHRIS images is too small to enable this kind of analysis. Thus, to enable a statistical relationship, effects on the reflectance spectra due to vegetation anisotropy must be negligible or constant. For the CHRIS imagery, the sun zenith angles vary between 27 and 30°. Thus, the influence due to the sun zenith angle can be assumed to be constant following results obtained by GALVAO et al. (2004), who reported negligible NDVI differences for pastures with sun zenith angle variations between 29° and 53°. Due to the near-polar orbit of CHRIS, the sun azimuth angles are also relatively constant. The CHRIS FZAs are divided into the forward and backward viewing angles. Due to the tilting of CHRIS, near-nadir observations should also be divided into backward and forward viewing angles as well to provide comparable sensor azimuth angles for further analysis (OPPELT & MAUSER 2007a).

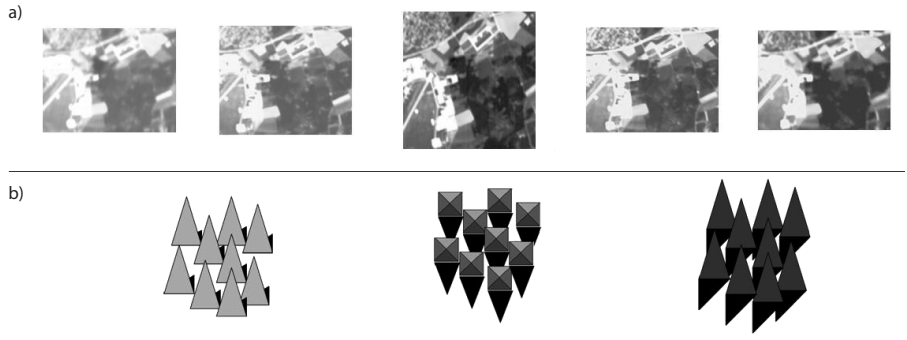

Fig. 34: a) Sample section of CHRIS data acquired on May 25, 2004 (bgr = 437, 564, 669 nm), b) proportion of shadows at the different viewing angles
Source: Own survey

5.2 Derivation of top-of-canopy chlorophyll

5.2.1 Existing approaches

Several groups of spectral variables have been identified to be of value in characterizing the way in which reflectance spectra vary with varying chlorophyll contents. Empirical relationships have been defined between the spectral variables and chlorophyll content. An alternative group of approaches for quantifying pigments from hyperspectral data is based on the numerical inversion of physically-based leaf and canopy radiative transfer models.

While there is little agreement in literature on the optimal wavelengths, there is good evidence from modelling studies that, at wavelengths where absorption coefficients of pigments are low, reflectance is more sensitive to high pigment concentrations. In con-

trast, spectral regions with high absorption are more sensitive to low pigment concentrations (JACQUEMOUD & BARET 1990; BLACKBURN 1998). This is confirmed by empirical evidence, which has demonstrated that reflectance at wavelengths corresponding to the lower and upper flanks of the major chlorophyll absorption feature in the Red is most sensitive to pigment concentrations over the normal range found in most leaves (LICHTENTHALER et al. 1996; CARTER & KNAPP 2001) and canopies (FILLELLA et al. 1995; YODER & PETTRIGREW-CROSBY 1995). In studies analyzing low concentrations of pigments in immature and senescent leaves and canopies, bands at the centre of absorption features are most sensitive to pigment contents (BLACKBURN 1998; SARI et al. 2005). OPPELT (2002) observed that most indices become saturated for chlorophyll contents higher than 1 g m^{-2}.

To deal with the difficulties in relating reflectance to individual bands, which are due to variations in the multiple controlling factors on reflectance especially at the canopy scale, many approaches use reflectance in multiple bands. Most of them have employed ratios of narrow bands within areas of the spectrum that are sensitive to pigments and those areas that are not sensitive. They were proposed as a means of solving the problems of overlapping absorptions of different pigments (CHAPPELLE et al. 1992) and the effects of leaf and canopy structure (PEÑUELAS et al. 1995). Many indices have been derived for chlorophyll quantification and are based on ratios of bands in the VIS and NIR (FILLELLA et al. 1995; SIMS & GAMON 2002), in the red (VOGELMAN et al. 1993), or in the NIR shoulder and red edge regions (GITELSON & MERZLYAK 1997). Most of the indices relate to total chlorophyll; only a few differentiate chlorophyll a and b, e.g. DATT (1998), OPPELT & MAUSER (2004) or ZARCO-TEJADA et al. (2005).

Thus, various indices exist to derive the chlorophyll content from hyperspectral remote sensing data, but they rarely deal with the directional information inherent to multi-angular data. There is also a need to investigate the behaviour of indices with regard to directional effects that may occur in remote sensing data, because their influence is highly dependent on the wavelength and thus on sensor band settings. This problem complicates the comparison of results published for different sensors and will be addressed in section 5.5.

A discussion of the results using different indices would go beyond the scope of this study. However, results using different indices can be found in VERRELST et al. (2006), OPPELT et al. (2007). In this study, only one approach – the chlorophyll absorption integral CAI – will be used for chlorophyll estimation. The results will be discussed and the implementation of remotely sensed chlorophyll maps into a physically-based model will be documented.

5.2.2 The chlorophyll absorption integral CAI

The CAI is an approach based on the measurement of absorption feature depth, which is obtained by fitting a continuum to vegetation reflectance. This method was first described by KOKALY & CLARK (1999) to assess nitrogen, lignin and cellulose for leaves of different tree and crop species. Linear segments are used to approximate the continuum. Once the continuum is established, the continuum-removed spectra are calculated by dividing the original reflectance values by the corresponding values of the continuum line. From the continuum-removed reflectance, the depth *D* [%] in the absorption feature is computed (Equation 15) with a uniform interval between bands of 0.1 nm.

$$D = 1 - R' \qquad \text{Equation 15}$$

where

R' continuum-removed reflectance [%].

The small interval for calculating the continuum removal was used to overcome difficulties with varying band settings of different sensors resulting in significantly different CAI values for the same target on the ground, which occurred for previous versions of the CAI where the interval was dependent on the band settings.

To minimize the influence of extraneous factors such as atmosphere, soil or topography, the absorption depths are normalized (KOKALY & CLARK 1999; CURRAN et al. 2001). This is calculated by dividing the absorption depth of each band by the absorption depth at the centre of the absorption D_c [%] according to Equation 16. The absorption depth centre is the minimum value of the continuum-removed absorption feature (see also Figure 35).

$$D_n = \frac{D}{D_c} \qquad \text{Equation 16}$$

where

D_n normalized absorption depths [dimensionless].

KOKALY & CLARK (1999) demonstrated a low sensitivity to background effects due to atmosphere, soil and topography. These results were confirmed at the leaf level by CURRAN et al. (2001) as well as by OPPELT (2002) for canopy chlorophyll content.

The end points of the continua depend on the sensor used and are defined in Table 15. The CAI start and end points were originally designed for the AVIS sensor with its high spectral resolution. The corresponding points for CHRIS had to be adapted to coincide with the CHRIS bands and were chosen as near as possible to the AVIS bands. The CAI

extends from the red wavelength region to the NIR, whereby the former includes the chlorophyll a absorptions and the latter is an area, which GITELSON & MERZLYAK (1997) found to be insensitive to chlorophyll. Another advantage of the CAI is that it includes both the lower and upper flanks of the chlorophyll absorption in the red as well as the central absorption. Thus it includes wavelengths sensitive to a wide range of chlorophyll contents, which was confirmed by OPPELT (2002).

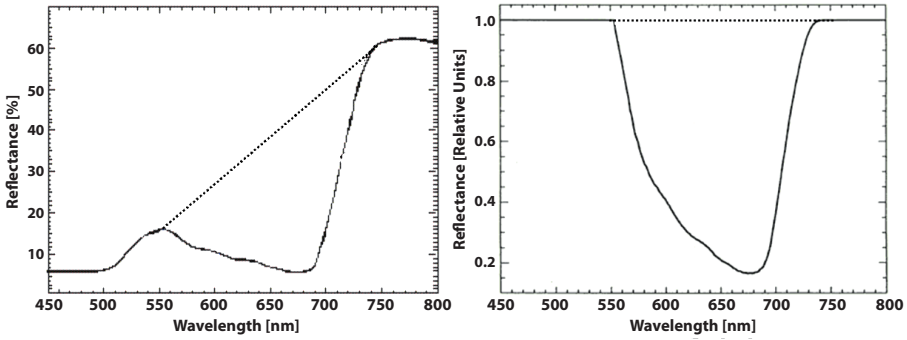

Fig. 35: Continuum used to analyze the chlorophyll absorption feature in a reflectance spectrum (left) and continuum-removed absorption depth (right)
Source: OPPELT 2002

Table 15: CAI continuum start and end points

	Continuum start point [nm]	**Continuum end point [nm]**
CHRIS centre wavelength	570	742
AVIS centre wavelength	600	740

Source: Own survey

5.3 Derivation of sun and shade chlorophyll using CHRIS data

Measurements of spectral reflectances are often determined at the top of the canopy, even for parameters within the plant canopy, by assuming a homogeneous distribution of this variable (JONES et al. 2003). However, for many purposes such as photosynthesis, the chlorophyll content within a canopy is important. In practice, measurements of the chlorophyll content inside a vegetation canopy are rare. There is no literature known to the author that differentiates field measurements of the leaf layers at the top of the canopy and beneath. Originally, the CHRIS data acquired in 2004 were intended to be used as the sample size for regression analysis, while the data acquired in 2005 were to be used to test the regression models derived in 2004. Unfortunately, the number of CHRIS images is too low to pursue this approach. To enable a statistical regression analysis, the data of both years had to be used.

The hypothesis on which the presented approach is based is that the angular monitoring of a canopy enables an insight into shaded canopy layers. The field measurements (section 3) demonstrated that there are significant differences between the chlorophyll content of leaves at the top of the canopy, which are mainly influenced by direct radiation, and the leaves in the shaded parts of a canopy, where they are influenced by a diffuse radiation regime. Thus, it is to be expected a differentiation between the chlorophyll content of sun and shade leaves using remote sensing will enhance the results of modelling approaches.

As described in section 2, chlorophyll a is the limiting factor in the utilization of light for photosynthesis, because it receives energy absorbed by chlorophyll b and other accessory pigments. For this reason, the following analysis and discussion are focused on chlorophyll a. The monitoring of the distribution of chlorophyll a via remote sensing provides a spatial integral measurement. Thus it seems to be appropriate to analyse the chlorophyll content on the basis of ground surface area. In the following, the term chlorophyll is used as a synonym for chlorophyll a. A detailed analysis of chlorophyll contents per mass can be read in OPPELT et al. (2007) and OPPELT & MAUSER (2007a). A discussion about wheat chlorophyll a and b assessment using CHRIS data can be found in OPPELT (2008).

Parts of the chloroophyll assessment of wheat (mg m^{-2}) using CHRIS data are already published in OPPELT (2009) and OPPELT (2010). Parts of the chlorophyll assessment of maize are published in OPPELT & HANK (2009).

5.3.1 Wheat

As mentioned previously, indices become saturated at high chlorophyll contents. The CAI is known to saturate at chlorophyll a contents higher than 1 g m^{-2}, which was derived for the chlorophyll a content of canopies where no differentiation was made between the sun and shade layers (OPPELT 2002). The effect of saturation indicates a non-linear relationship between CAI and chlorophyll, thus an exponential relationship is assumed in Table 16, where the results for the analysis of the CHRIS data for wheat are summarized. However, the chlorophyll contents monitored are below the saturation level and thus the results can be approximated assuming linear relationships (Table 17). The regression equations given both in Table 16 and Table 17 also indicate that they do not cross the ordinate at zero, but posses an offset, which is caused by the measured chlorophyll contents (see Figure 3-15). Hence, the valid range of the chlorophyll estimation using the equations given in Table 16 and Table 17 is, strictly speaking, limited for chlorophyll a contents in the sun layer between 90 and 220 mg m^{-2}, and in the shade layer between 140 and 400 mg m^{-2}.

At nadir, the top-of-canopy chlorophyll contents are reasonably highly correlated with the CAI. When grouping the nadir images into forward and backward data, the forward-

looking nadir data show high coefficients of determination for the chlorophyll contents of the sun and shade canopy layers, whereby the estimation error is higher for shade chlorophyll. The backward-looking nadir data are significantly, but moderately (-36°) or weakly (-55°) highly correlated with sun chlorophyll. Analyzing the ± 36° angles, Table 16 and Table 17 clearly show that significant correlations were derived for the forward FZA and shade chlorophyll, while the backward FZAs are moderately highly correlated with the sun chlorophyll. For high FZAs, the correlations become weaker (-55°) or insignificant (+55°).

Table 16: Equations for wheat chlorophyll a estimation having the form $Chl = a \cdot e^{b \cdot CAI}$; fw = forward; bw = backward; N = number of samples; r^2 = coefficient of determination between predicted and measured chlorophyll; n.s. = not significant; Est.err. = mean estimation error of Chl; a,b and est.err. are in mg m^{-2}

		Chl a sun					Chl a shade			
CAI	**N**	**r^2**	**a**	**b**	**Est.err.**		**r^2**	**a**	**b**	**Est.err.**
Nadir	24	0.61	19.1	3.26	51.6		n.s.	-	-	-
Nadir fw	12	0.69	19.2	3.43	100.1		0.76	8.59	5.29	183.4
Nadir bw	12	0.50	29.9	2.30	73.2		n.s.	-	-	-
+36°	18	n.s.	-	-	-		0.65	3.45	6.19	155.3
+55°	30	n.s.	-	-	-		n.s.	-	-	-
-36°	18	0.56	18.08	3.42	57.2		n.s.	-	-	-
-55°	24	0.33	10.41	3.97	79.8		n.s.	-	-	-

Source: Own survey

Table 17: Equations for wheat chlorophyll a estimation having the form $Chl = a + b \cdot CAI$; r^2 = coefficient of determination for the given equation

		Chl a sun					Chl a shade			
CAI	**N**	**r^2**	**a**	**b**	**Est.err.**		**r^2**	**a**	**b**	**Est.err.**
Nadir	24	0.61	-124.7	439.6	81.86		n.s.	-	-	-
Nadir fw	12	0.69	-165.9	528.5	98.67		0.75	-518.7	1223.1	190.7
Nadir bw	12	0.50	-32.86	256.4	72.15		n.s.	-	-	-
+36°	18	n.s.	-	-	-		0.65	-436.1	976.1	160.37
+55°	30	n.s.	-	-	-		n.s.	-	-	-
-36°	18	0.56	-69.92	353.3	69.19		n.s.	-	-	-
-55°	24	0.33	-129.2	419.2	75.04		n.s.	-	-	-

Source: Own survey

The results indicate a clear distinction between the degrees of correlation and the angles used:

(1) The top-of-canopy (sun) chlorophyll contents show the highest coefficients of determination with the near-nadir, forward FZA. The backward-nadir FZA shows significant correlation, but with a low coefficient of determination.
(2) The chlorophyll content of the shaded leaves in a canopy can be estimated using the forward-nadir FZA as well as the +36° FZA, whereby the forward-nadir angle shows a higher coefficient of determination.

These observations can be explained by the interrelationship of the following phenomena:

(1) The gap effect, and furthermore, the relative fractions of sunlit and shaded canopy components, which vary with varying viewing angles.
(2) The anisotropy of vegetation; to demonstrate the influence of the vegetation structure with seasonality and wavelength, Figure 36 shows ANIF values for CHRIS bands in the Red and NIR on different acquisition dates. The largest differences from the nadir response can be observed in the backward FZAs. The red band (left graph in Figure 36) exhibits a more anisotropic behaviour than the band in the NIR (right graph in Figure 36). This agrees with results published by SANDMEIER et al. (1999) and LIESENBERG et al. (2007). According to them, anisotropic effects are stronger in spectral regions of high absorbance such as the Red. On the other hand, anisotropy is less pronounced in the NIR due to the predominance of multiple scattering, which reduces the spectral contrast between shade and sun canopy components.
(3) In the VIS, backward FZAs contain a large proportion of sunlit leaves and an increasing proportion of sun glint towards the hot spot. This effect is also evident in Figure 36, which suggests that the hot spot is located near the -36° FZA.

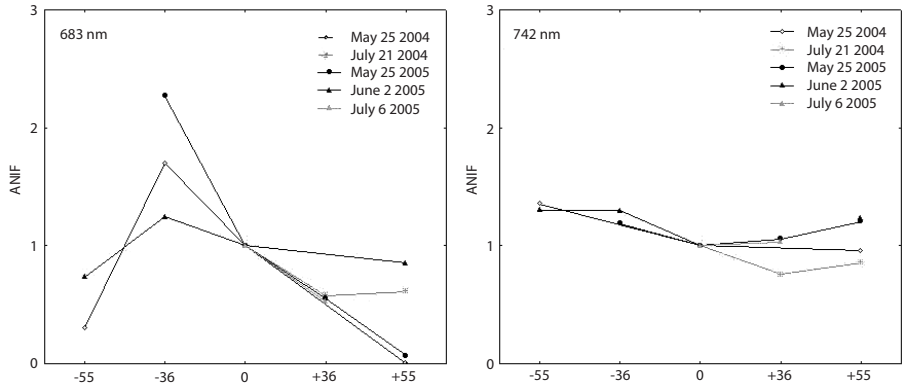

Fig. 36: Seasonal changes of ANIF derived from CHRIS bands in the Red and NIR for wheat
Source: Own survey

The high correlation for the shade chlorophyll contents with the forward FZAs (+ near-nadir and +36°) is caused by the combination of anisotropy and the gap effect. Small view angles near nadir are most likely to monitor the leaves of both the sun and the shade layer. With increasing viewing angle the fraction of shade leaves, which are monitored, increases. Based on the coefficients of determination in Table 17, the near-nadir to moderate forward-pointing view angles are the most suitable for vertical chlorophyll profiling. The view into the canopy becomes reduced with further increasing FZAs, resulting in insignificantly correlated data at the +55° FZA. Furthermore, very low reflectance values occurred in the forward 55° FZA, thus the amount of reflected radiation was too low for an analysis of the chlorophyll absorption feature.

For the backward FZAs, the view into less illuminated canopy levels, which can be proposed according to the gap effect, is more severely superimposed by the effects due to vegetation anisotropy and, especially, the high proportion of sunlit leaves and sun glint. These effects prohibit a significant correlation of the CAI with the chlorophyll content in shaded parts of the canopies. The top-of-canopy chlorophyll is not affected as much and shows moderate coefficients of determination in the backward FZAs. Again, the correlation becomes weaker with the -55° FZAs.

5.3.2 Maize

The results for maize are presented in Table 18 and Table 19, whereby the exponential functions are presented in the former and the linear relationships in the latter. In general, the relationship do not differ much between the exponential and the linear equations, although the estimation error is smaller when exponential functions are used, especially for the shade chlorophyll. Thus chlorophyll estimation in the range of values of the existing study can be approximated using linear regression equations.

Table 18: Algorithms for maize chlorophyll a estimation having the form $Chl = a \cdot e^{b \cdot CAI}$; r^2 = coefficient of determination between predicted and measured chlorophyll

		Chl a sun					Chl a shade				
CAI	**N**	**r^2**	**a**	**b**	**Est.err.**		**N**	**r^2**	**a**	**b**	**Est err.**
Nadir	18	0.84	3.53	4.67	7.32		6	n.s.	-	-	-
Nadir fw	12	0.71	2.02	57.03	46.58		0	-	-	-	-
Nadir bw	6	0.66	3.49	4.66	140.7		6	n.s.	-	-	-
+36°	18	0.53	3.56	4.93	37.80		8	0.74	0.93	6.30	71.3
+55°	29	0.74	1.16	7.61	39.22		10	0.66	0.32	8.60	101.5
-36°	12	n.s.	-	-	-		0	-	-	-	-
-55°	18	n.s.	-	-	-		0	-	-	-	-

Source: Own survey

The top-of-canopy chlorophyll of maize canopies can be estimated using all nadir images, whereby the results indicate that a differentiation into forward and backwards near-nadir FZAs is not necessary. On the contrary, the estimation error is least when all nadir data are used. These results confirm results previously obtained by OPPELT & MAUSER (2004) and GITELSON et al. (2005).

Table 19: Algorithms for maize chlorophyll a estimation having the form Chl = a + b × CAI; r² = coefficient of determination

		Chl a sun					Chl a shade				
CAI	**N**	**r²**	**a**	**b**	**Est.err.**		**N**	**r²**	**a**	**b**	**Est err.**
Nadir	18	0.82	2.5	135.2	7.6		6	n.s.	-	-	-
Nadir fw	12	0.71	1.65	253.5	51.1		0	-	-	-	-
Nadir bw	6	0.66.	-243.1	481.1	171.3		6	n.s.	-	-	-
+36°	18	0.58	5.77	184.1	40.87		8	0.71	-227.9	443.8	105.73
+55°	29	0.73	-22.31	346.6	39.06		10	0.70	990.2		110.99
-36°	12	n.s.	-	-	-		0	-	-	-	-
-55°	18	n.s.	-	-	-		0	-	-	-	-

Source: Own survey

These results also confirm the ability of the CAI to be sensitive over a wide range of chlorophyll contents, because the maize canopies were monitored over a large variety of chlorophyll contents (10.6 - 319.7 mg m^{-2}) and canopy closure (10 - 90 %). CAI also proved its low sensitivity to soil background and confirmed previous results described by OPPELT (2002).

The forward FZAs also provide good estimations of the sun leaf chlorophyll content, whereby the +55° FZA proved to be the most suitable viewing angle. The backward FZAs were unable to show significant results due to the high anisotropy in the sun-parallel view angles. Figure 37 presents the anisotropic reflectance behaviour of maize, which is more strongly developed in the backward FZAs and shows a maximum at -55°. Thus, the hot spot can be assumed to be near that viewing angle.

Examining the shade chlorophyll content, the limited sample size has to be taken into consideration. Shade chlorophyll could only be monitored after BBCH 30 (mid July in 2004 and 2005). This fact, as well as limited CHRIS coverage of the test fields, results in 6 nadir images, 8 and 10 forward 36° and 55° FZA images respectively. Shade chlorophyll can be assessed using the +36° FZA. The +55° FZA is also significantly and highly correlated with shade chlorophyll content, but with a higher estimation error than the +36° FZA. Comparable to the results for the wheat canopies, the estimation error is generally higher for shade chlorophyll than for sun chlorophyll.

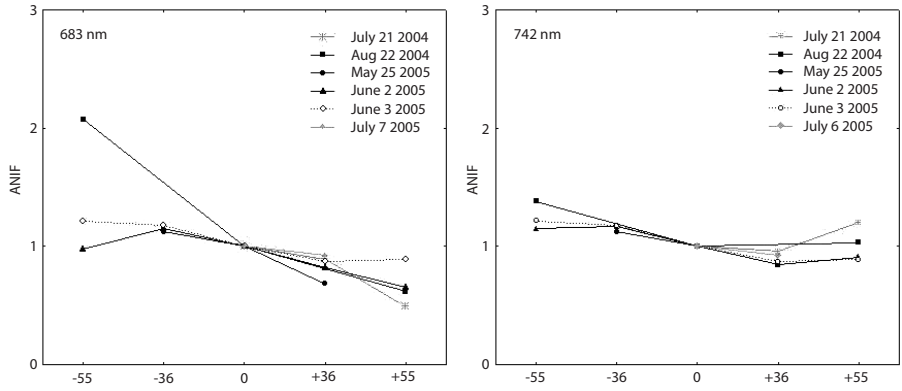

Fig. 37: Seasonal changes of ANIF derived from CHRIS bands in the Red and NIR for maize
Source: Own survey

5.3.3 Evaluation of the results

The previous sections demonstrated the capability to assess sun and shade chlorophyll content using angular remote sensing. In general, the forward FZAs are most suitable for the estimation of shade chlorophyll content, whereby the +36° FZA provided the best results for both wheat and maize. The results depend on the interrelationship between the varying proportion of shadows and the anisotropic reflectance behaviour of vegetation canopies. Both wheat and maize canopies are subject to these conditions: the FZA with the highest capability to assess chlorophyll is that with the least anisotropic behaviour in the chlorophyll absorption region, which in turn depends on the canopy structure. The backshadow effect also depends on the canopy structure, since the reflectance values become less for the forward FZAs. Figure 36 and Figure 37 indicate that the shadowing of the canopy in the forward direction is more pronounced in the wheat canopies, while the maize canopies are more translucent, which is mainly due to their lower canopy density. Very low reflectance values (especially in the Red) occurred for the +55° FZA, thus to some extent the amount of reflected radiation was too low for an analysis of the chlorophyll absorption feature.

Of course, the relatively large GSD of CHRIS may lead to criticism of the results of the above analysis. However, the validation of spatial measurements is always problematic. In general, measurements on the ground can only approximate the real conditions of a heterogeneous vegetation canopy, where even neighbouring leaves contain different chlorophyll concentrations. The author is aware of the fact that the validation of a spatial integral measurement with measurements at a limited number of sampling points is problematic, but there do not appear to be any realistic alternatives.

5.4 Assessment of chlorophyll distribution maps

The spatial distribution of the chlorophyll content of sunlit and shaded canopy layers can be calculated using regression equations presented in Table 17 and Table 18. Typical results for wheat and maize are presented in Figure 38 and Figure 39.

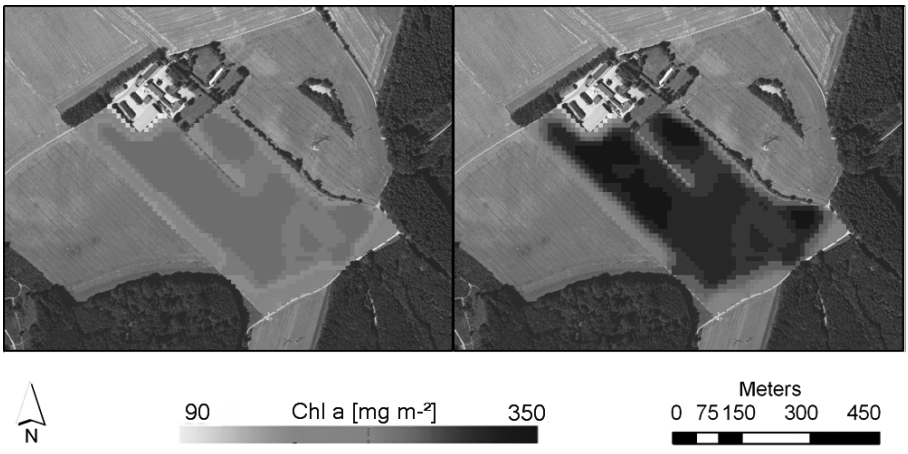

Fig. 38: Sun (left) and shade (right) chlorophyll a contents of wheat derived from CHRIS data acquired on May 25 2004, resampled to a grid size of 10 m
Source: Own survey

The chlorophyll distribution map presented in Figure 38 demonstrates both the spatial and vertical variability within a wheat canopy with CHRIS data acquired on May 25 2004. The nadir image was used for the calculation of sun chlorophyll a content, while the +36° image was used for the calculation of chlorophyll a content in the shade layer. The original CHRIS data were resampled to a cell size of 10 x 10 m to fit the model requirements. The chlorophyll a content of the sun layer varies between 90 and 187 mg m^{-2}, whereby the highest contents are apparent in the western and northern part of the field. A higher dynamic in the spatial distribution was monitored in the shade layer, where the calculated chlorophyll a content varies between 95 and 345 mg m^{-2}. In both canopy layers, the field margins are characterized by lower chlorophyll contents than in the centre of the field. This is caused by the superimposition of two effects: the occurrence of mixed pixels in the remote sensing data at the field margins as well as the lower vitality of plants due to increased soil compaction by the farming machinery in these areas, which also results in a reduced yield.

The distribution of chlorophyll in maize presented in Figure 39 represents a growth phase where the shade layer is not fully developed and, therefore, the sun layer contains more

chlorophyll than the shade layer (see also Figure 24). Both layers exhibit distinct spatial variations in chlorophyll content. Decreasing chlorophyll contents at the field margins are visible in the northwest and southeast. This can be explained by the location of the field, which is embedded between a street in the northwest and a country lane in the southeast, therefore the occurrence of mixed pixels on borders with a high contrast is likely. The south-western and north-eastern margins are not affected that much, due to adjacent fields grown with maize and wheat respectively.

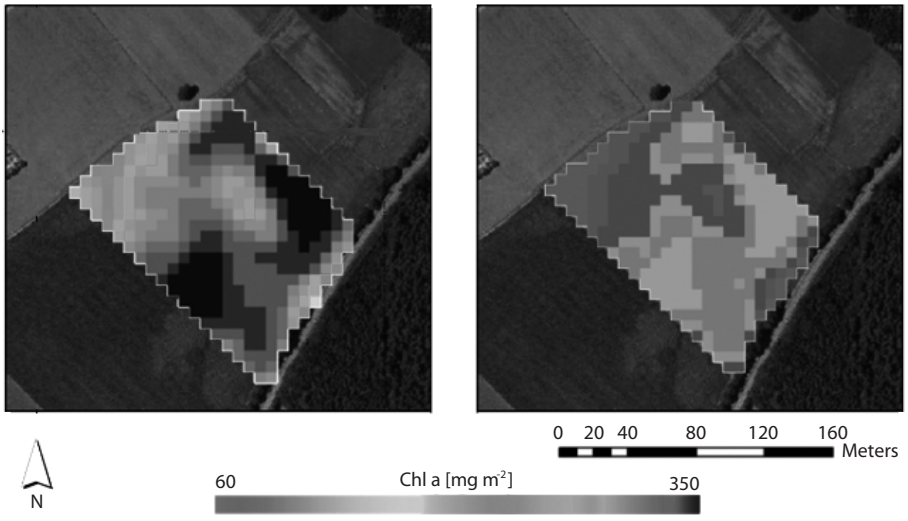

Fig. 39: Sun (left) and shade (right) chlorophyll a content of maize derived from CHRIS data acquired on July 21 2004, resampled to a 10 m grid size
Source: Own survey

5.5 Transfer of results to AVIS data

As previously stated, the portability of index results from one sensor to another can be problematic due to different band settings, spectral resolution and spectral response of the sensors used. This results in varying index values, because the shape of the reflectance curve is mapped differently. The capability of the CAI to reduce this effect due to its small sampling interval will be addressed.

The portability of the CAI results is discussed using the tandem overpass of AVIS and CHRIS on May 25 2004 as an example. The AVIS data were acquired between 10:00 and 10:30 UTC, i.e. nearly simultaneously to the CHRIS overpass, with a flight direction almost parallel to the principal plane. Thus the illumination conditions are comparable.

Table 20: Statistics of CHRIS and AVIS CAI data of wheat acquired on May 25 2004

	CHRIS	AVIS	Difference (CHRIS – AVIS)
Minimum	0.500	0.274	-0.084
Maximum	0.709	0.681	0.365
Mean	0.684	0.649	0.054
Stdev	0.028	0.030	0.034

Source: Own survey

Figure 40 presents CAI images of nadir AVIS and CHRIS data for wheat, Table 20 provides the statistics of both images.

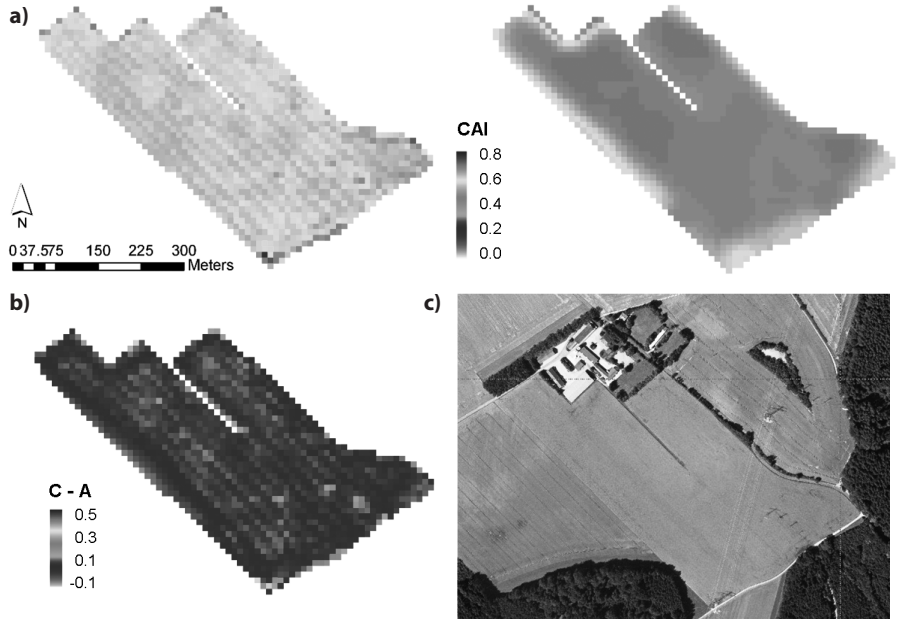

Fig. 40: a) CAI images derived from AVIS (left) and CHRIS (right) nadir data acquired on May 25 2004; both images are resampled to a grid size of 10 m; b) CHRIS – AVIS CAI difference image, c) aerial photograph acquired in 2003
Source: Own survey

Due to the lower geometric resolution, the CHRIS CAI presents a smooth image of the field, where "CAI areas" can be distinguished. Although resampled to a 10 x 10 m grid size, the AVIS CAI shows more details, e.g. the structure of the tractor lanes. Low CAI values can be observed in the northeastern part of the field and at the field margins, here especially in the south. The low CAI values in the eastern part of the field and at the southern margin are caused by transmission towers (also visible in the aerial photograph in Figure 40c). The high maximum difference is caused by one pixel, located at the south-

ern edge of the field, with an AVIS CAI value of only 0.27. However, the mean CAI values agree quite well, which is also demonstrated in Figure 40b, with difference CAI values (Table 20) fitting into 1.5 times the standard deviation.

Table 21 and Figure 41 present the results for the estimated sun and shade chlorophyll content, calculated using the equations given in Table 16 for nadir data and forward-nadir data respectively.

Of course, the same structural patterns are visible in the chlorophyll maps as in the CAI images, i.e. the dominant structure of the tractor lanes. However, specific areas with similar chlorophyll contents also become visible, especially when looking at the shade chlorophyll. Zones of high shade chlorophyll in the western part as well as in the very east of the field are apparent as well as the northern and southern margins characterized by low chlorophyll contents. The fertilization window is visible in both the sun and shade chlorophyll images.

Table 21: Chlorophyll contents calculated for AVIS and CHRIS data of 25 May 2004

Chl a sun [mg m^{-2}]	**Min**	**Max**	**Mean**	**Stdev**
AVIS	-3.37	175.50	152.91	12.67
CHRIS	95.00	187.39	176.06	12.44
Chl a shade [mg m^{-2}]				
AVIS	-183.08	314.60	229.42	53.16
CHRIS	92.5	349.39	242.41	75.64

Source: Own survey

The CAI values derived from the AVIS data are generally lower than those for the CHRIS data, leading to lower estimated chlorophyll contents. The negative chlorophyll value results from the pixel with very low CAI value described above and is marked red in Figure 41. Nevertheless, the mean values for the chlorophyll content estimated with AVIS data lie within the estimation error of the CHRIS data. Thus, the use of AVIS and CHRIS data lead to comparable results when applying the CAI for chlorophyll estimation.

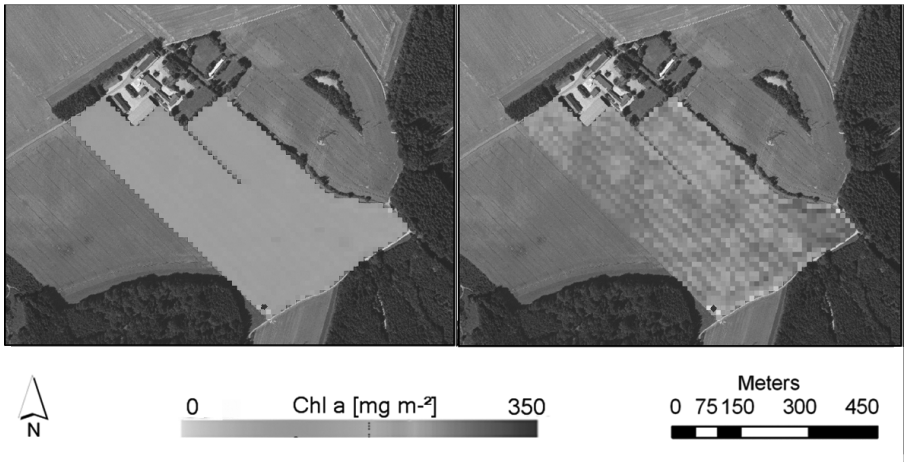

Fig. 41: Calculated AVIS chlorophyll contents for the sun (left) and shade (right) layers of wheat
Source: Own survey

Coloured figures

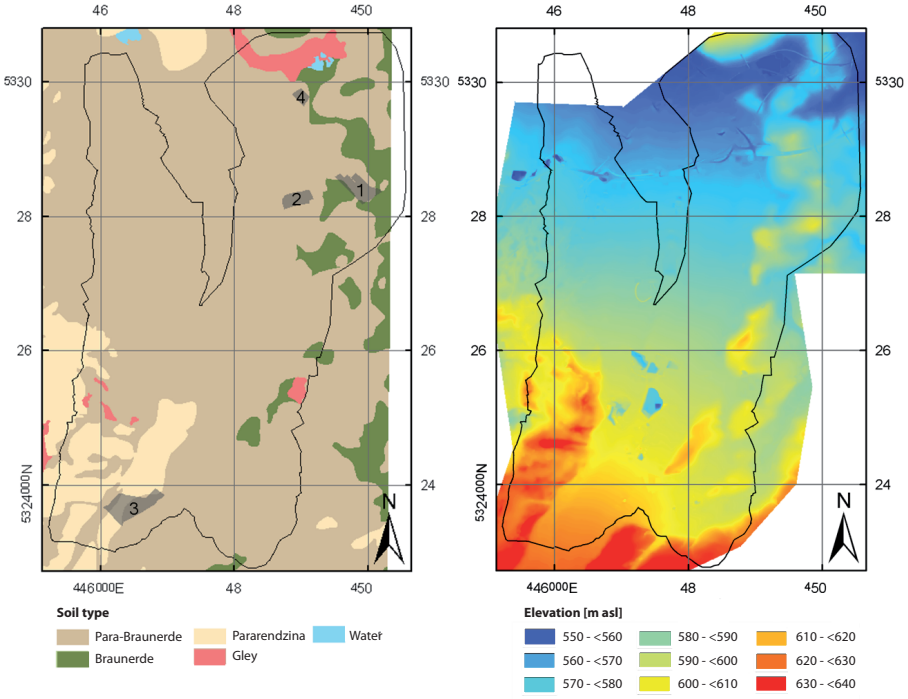

Fig. 7: Digital maps of soil type and elevation in a Gauß-Krüger (zone 4) coordinate system (the positions of the test fields are outlined and numbered in the soil map), the dimension of the test area is indicated by the solid line
Source: Own survey

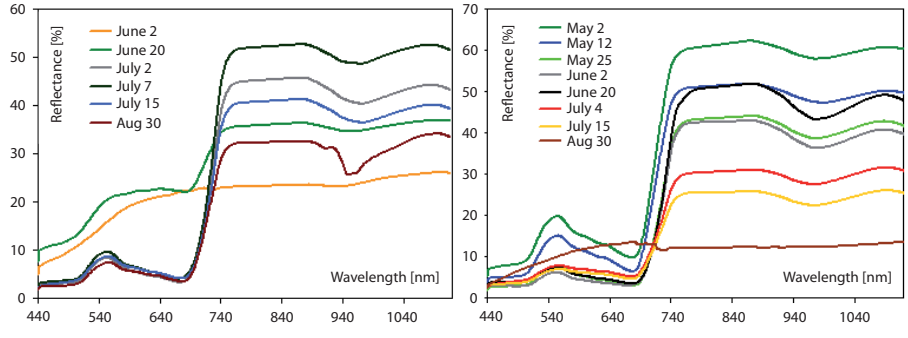

Fig. 16: Field spectrometer data as measured in 2005 for wheat (left) and maize (right)
Source: Own survey

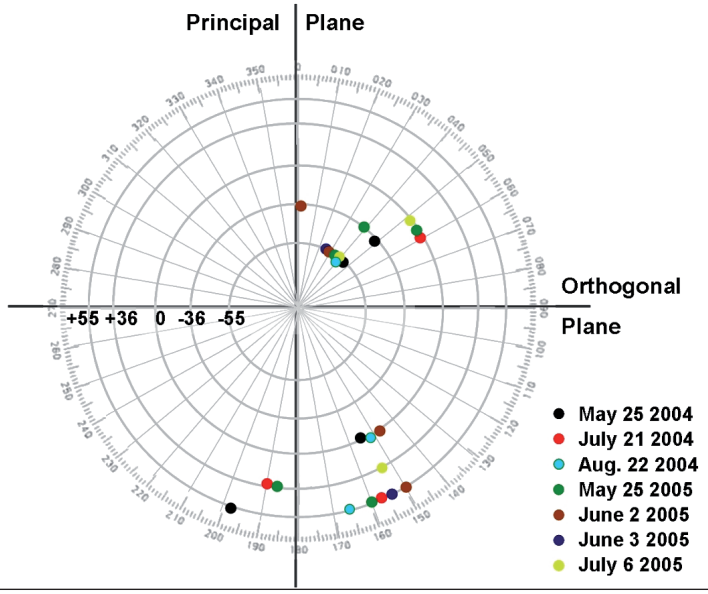

Fig. 28: Azimuth angles between the sensor and the sun
Source: OPPELT & MAUSER 2007a

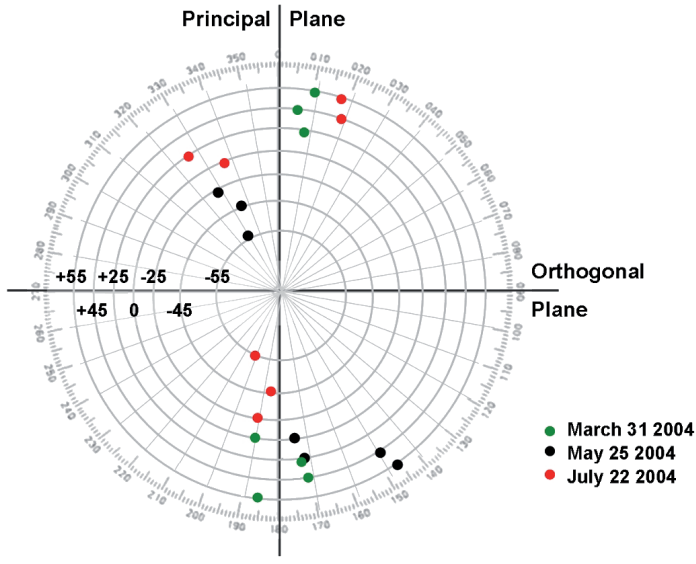

Fig. 32: Sun-sensor azimuth angles for the multi-angular AVIS-2 acquisitions in 2004
Source: Own survey

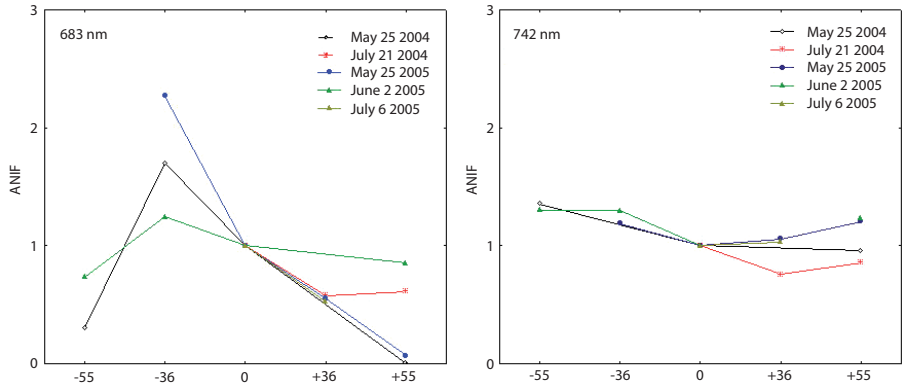

Fig. 36: Seasonal changes of ANIF derived from CHRIS bands in the Red and NIR for wheat
Source: Own survey

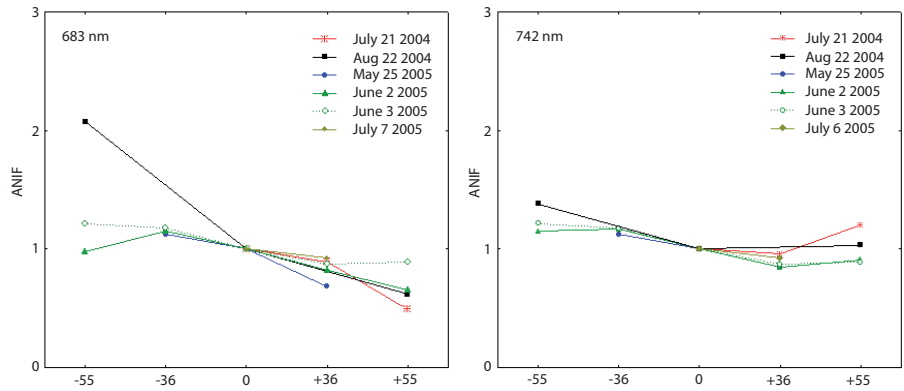

Fig. 37: Seasonal changes of ANIF derived from CHRIS bands in the Red and NIR for maize
Source: Own survey

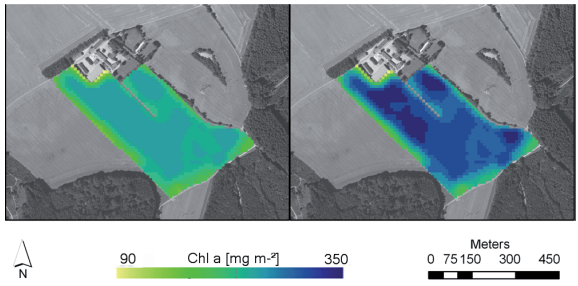

Fig. 38: Sun (left) and shade (right) chlorophyll a contents of wheat derived from CHRIS data acquired on May 25 2004, resampled to a grid size of 10 m
Source: Own survey

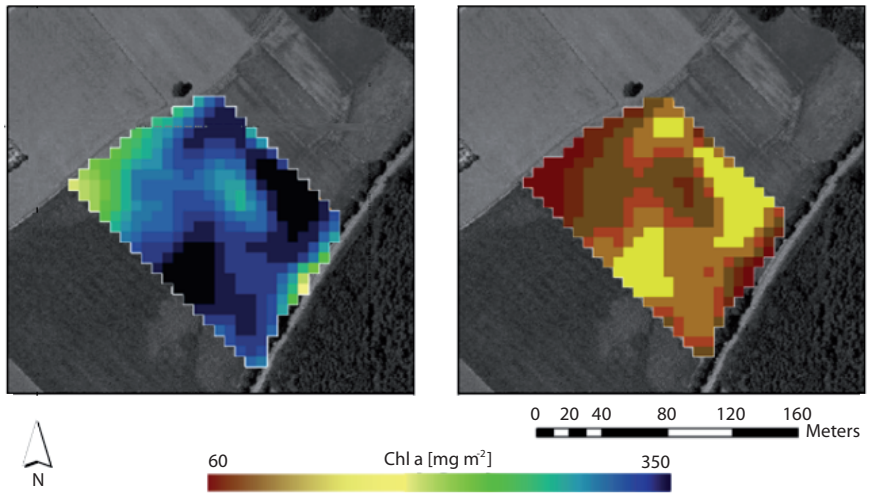

Fig. 39: Sun (left) and shade (right) chlorophyll a content of maize derived from CHRIS data acquired on July 21 2004, resampled to a 10 m grid size
Source: Own survey

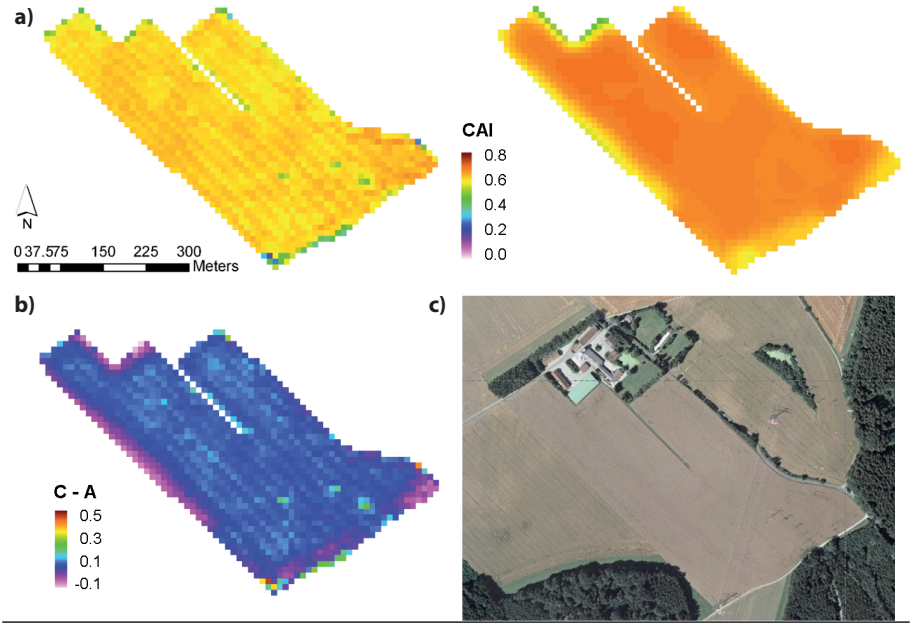

Fig. 40: a) CAI images derived from AVIS (left) and CHRIS (right) nadir data acquired on May 25 2004; both images are resampled to a grid size of 10 m; b) CHRIS – AVIS CAI difference image, c) aerial photograph acquired in 2003
Source: Own survey

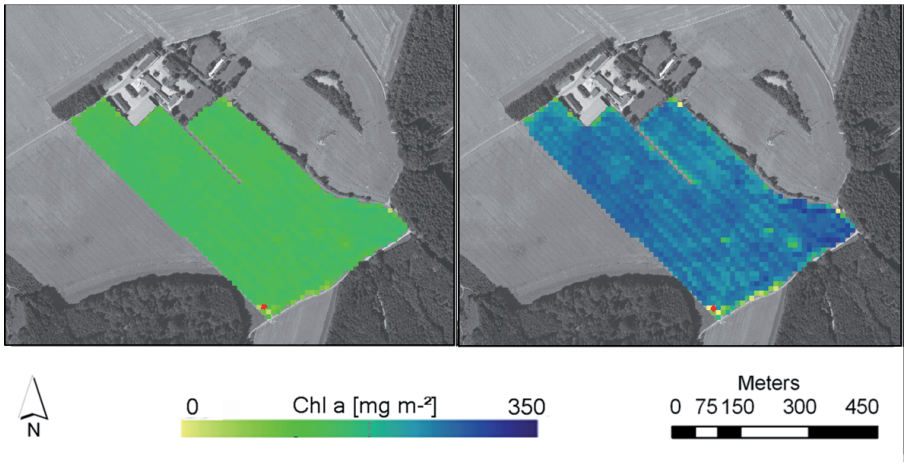

Fig. 41: Calculated AVIS chlorophyll contents for the sun (left) and shade (right) layers of wheat
Source: Own survey

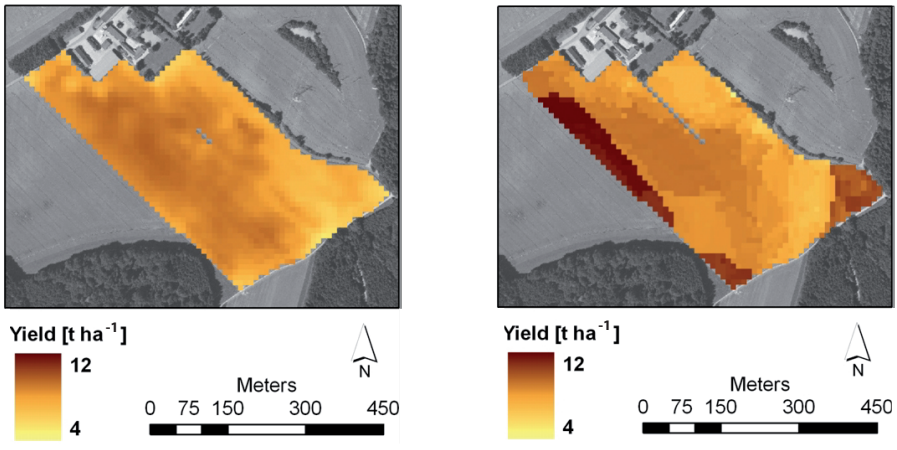

Fig. 44: Measured yield (left), aggregated to a 10 x 10 m cell resolution and modelled yield (right)
Source: Own survey

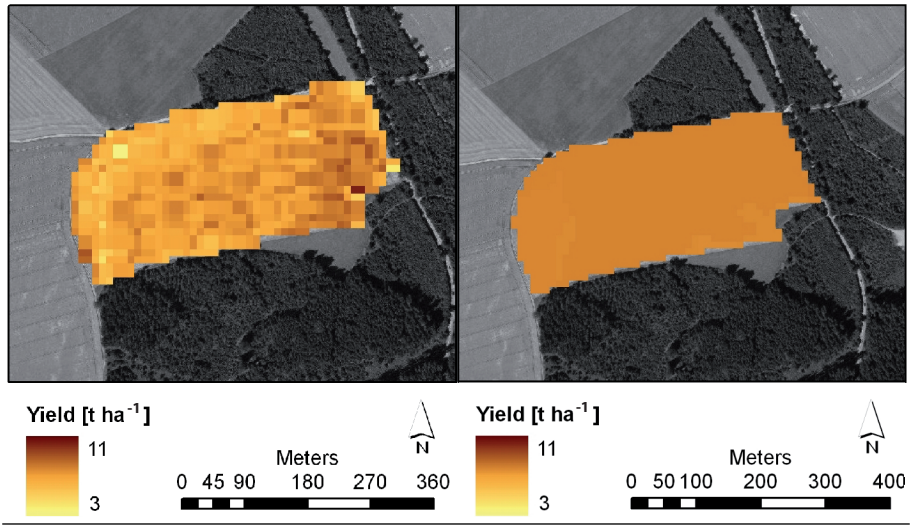

Fig. 46: Measured (left) and modelled (right) yield for wheat 2005
Source: Own survey

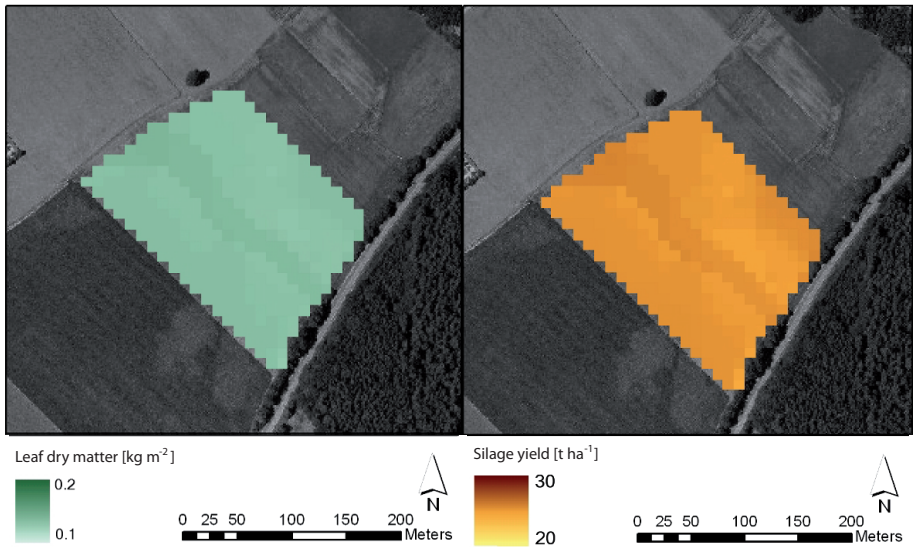

Fig. 48: Modelled leaf dry matter (left) and total aboveground dry matter (silage yield) (right)
Source: Own survey

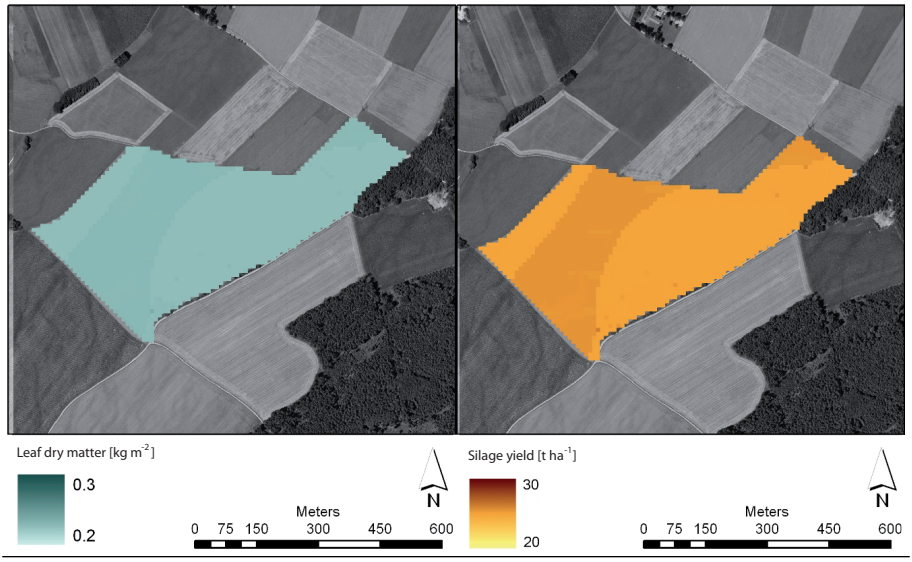

Fig. 50: Modelled leaf dry matter (left) and silage yield (right) for maize 2005
Source: Own survey

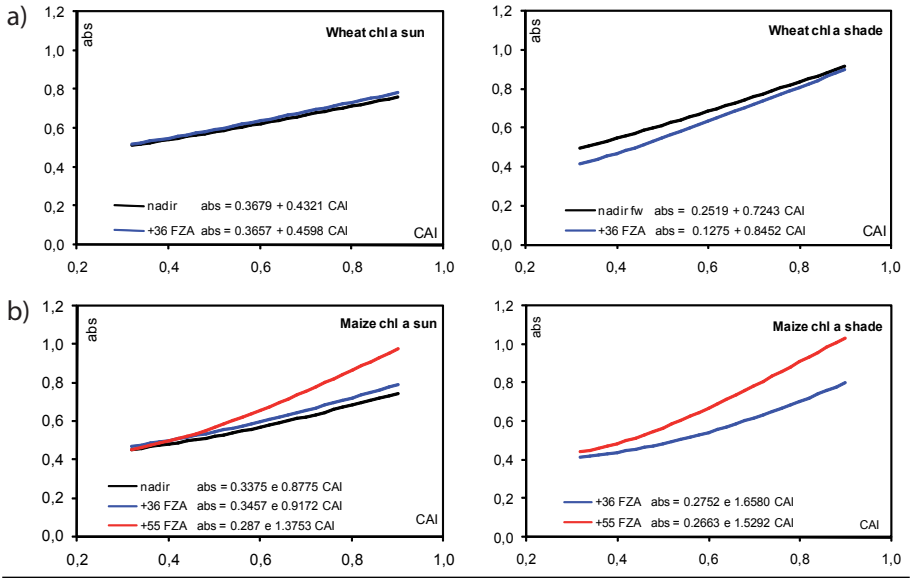

Fig. 51: Influence of CAI on the leaf absorptance (abs) for wheat (a) and maize (b)
Source: Own survey

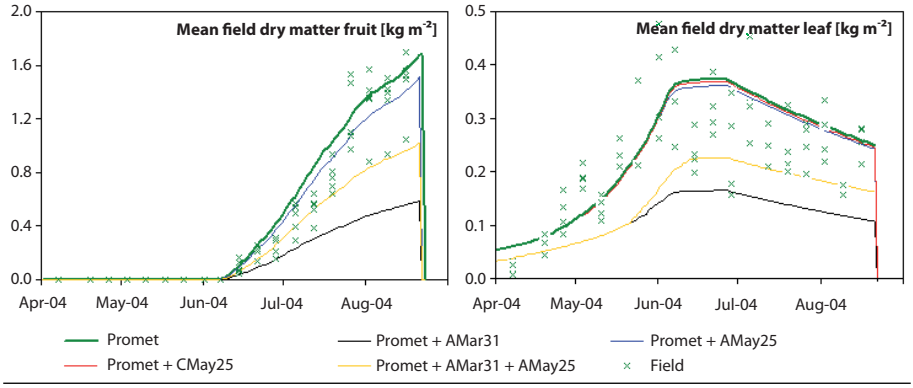

Fig. 52: Modelled and measured fruit (left) and leaf (right) biomass for 2004 in comparison with field measurements at the different sampling points

Source: Own survey

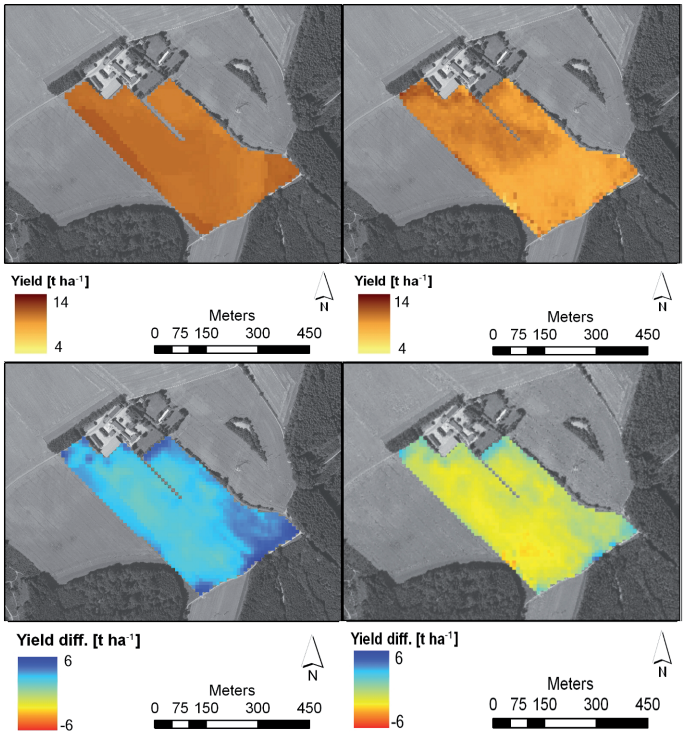

Fig. 53: a) Modelled yield using CHRIS data acquired on May 25 (left) and AVIS data acquired on March 31 and May 25 2004 (right); b) resulting differences between modelled and measured yield (PROMET – measured)

Source: Own survey

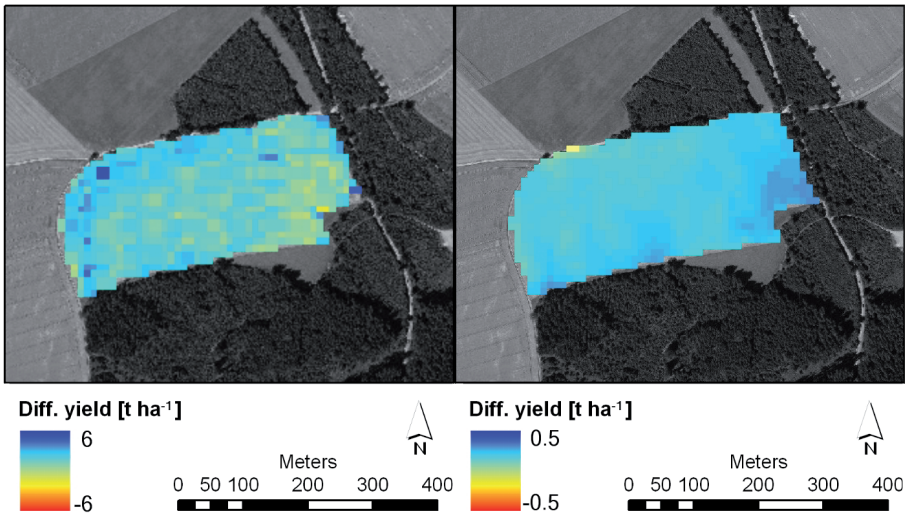

Fig. 54: Difference image between measured and modelled yield (measured - PROMET abs_{const}) (left) and difference image between PROMET using CHRIS May 25 data and PROMET using absconst (PROMET abs_{C0525} – PROMET abs_{const}) (right)

Source: Own survey

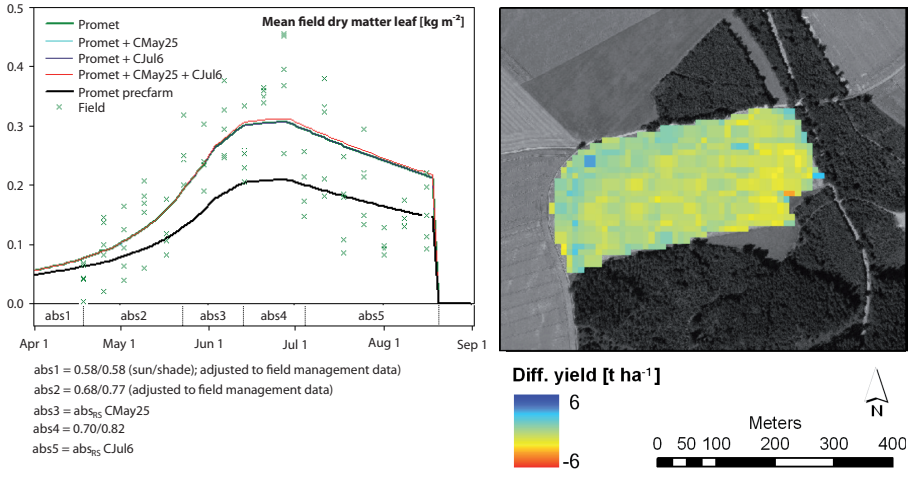

Fig. 56: Development of leaf biomass using remotely sensed abs values combined with abs values adjusted to field management data ($PROMET_{precfarm}$, left) and difference between modelled and measured yield ($PROMET_{precfarm}$ – measured)

Source: Own survey

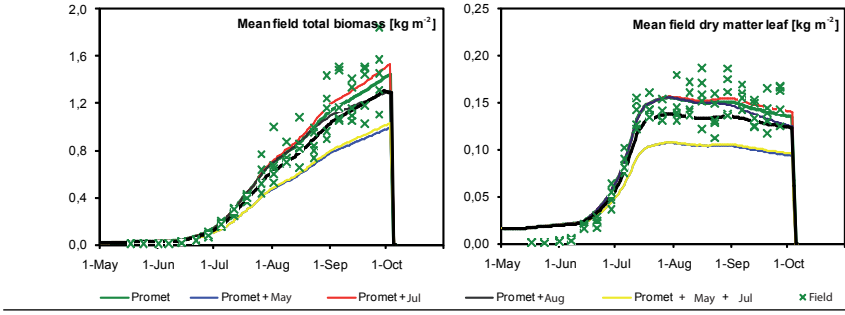

Fig. 57: Modelled silage yield (left) and leaf biomass (right) using absconst or abs_{RS} originating from different acquisition dates and sensors in comparison to field measurements at different sampling points

Source: Own survey

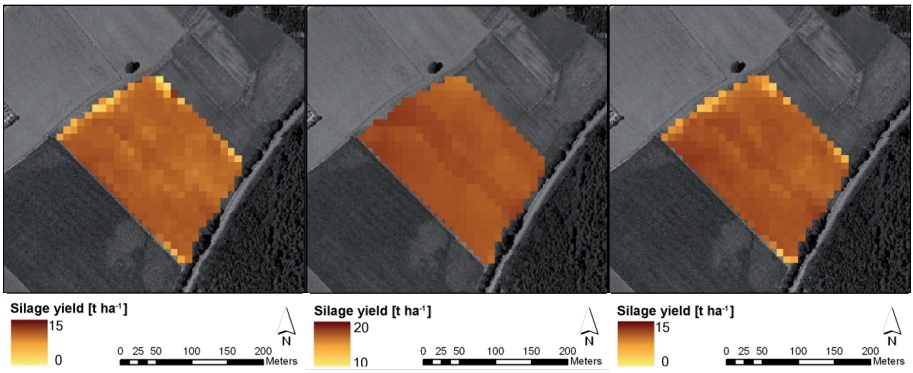

Fig. 58: Modelled silage yield using AVIS data acquired on May 25 2004 (left), CHRIS data acquired on July 21 2004 (centre) or a combination of AVIS and CHRIS data (right)

Source: Own survey

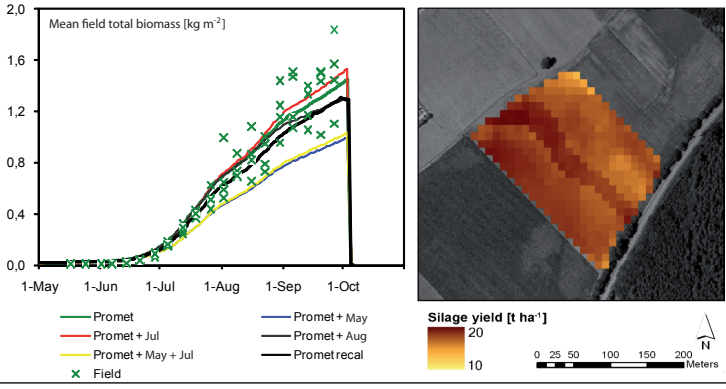

Fig. 59: Developmental of modelled total biomass throughout the vegetation period (left) and resulting silage yield using abs_{RS} that was reset to absconst after three weeks (right)

Source: Own survey

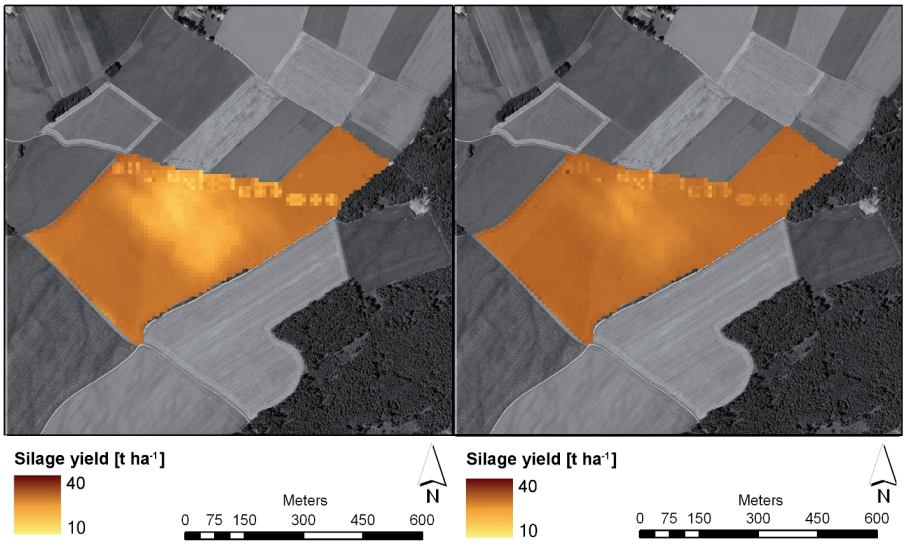

Fig. 60: Modelled yield for maize 2005 using CHRIS data acquired on June 3 (left) and a combination of CHRIS data acquired on June 3 and AVIS/CHRIS data acquired on July 6 (right)

Source: Own survey

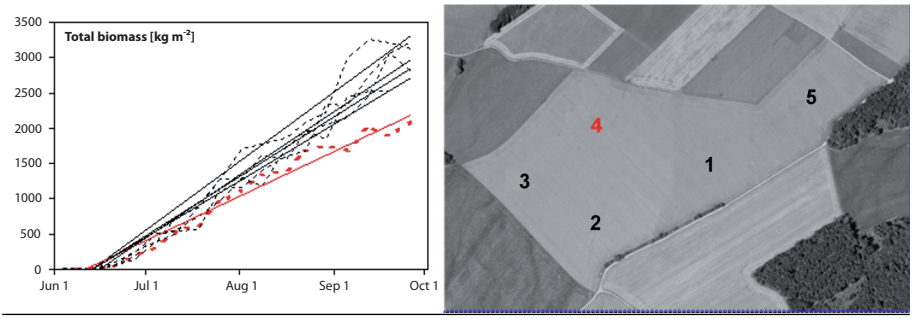

Fig. 61: Field measurements and corresponding trend lines at the different sampling points (the results of the sampling point in the low-productive zone are marked red)

Source: Own survey

6 Vegetation biophysics in the physically-based SVAT model PROMET

The physically-based SVAT model PROMET (PROcesses of radiation, Mass and Energy Transfer) was first developed at the chair for geography and Geographical Remote Sensing at the Ludwig-Maximilians-Universität München (MAUSER 1991; MAUSER & SCHÄDLICH 1998) and underwent major development within the GLOWA-Danube project as part of the decision support system DANUBIA, where it is used to simulate fields of land surface parameters on a 1 km grid size over the entire Upper Danube river basin (MAUSER et al. 2008). PROMET is a spatially distributed, raster-based model that calculates the evapotranspiration and water balance at different scales as a function of water availability, radiation balance and the physiological regulation mechanisms of heterogeneous plant canopies (LUDWIG & MAUSER 2000). The core model is based on eight components (meteorology; land surface energy and mass balance; vegetation; snow and ice; soil hydraulics and soil temperature; ground water; channel flow; man-made hydraulic structures) to simulate the water and energy fluxes for variable time steps. A spatial data modeller provides and organizes the spatial input data on the field-, micro- and macroscale (MAUSER et al. 2008).

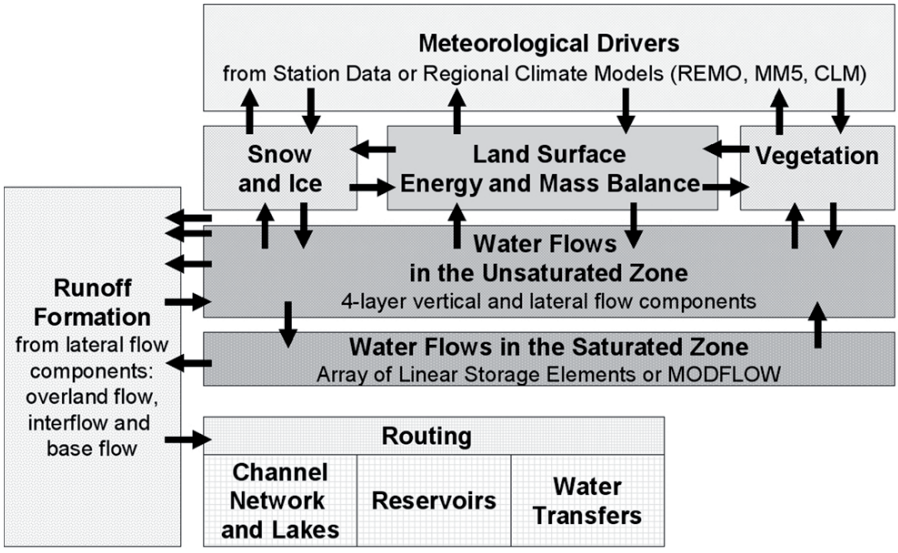

Fig. 42: Diagram of the PROMET components (□) *and their interfaces* (⟶)
Source: MAUSER et al. 2008

The model will not be described here, but a detailed description of PROMET and applications can be found in MAUSER et al. (2008). The vegetation component is subdivided into two sub-models which can be used alternatively: sub-model 1 is based on the Pen-

man-Monteith equation to calculate evapotranspiration. The vegetation is characterized only by its stomatal resistance, which controls the water transport in the plants. Environmental influence functions according to JARVIS & MORRISON (1981) and BALDOCCHI et al. (1987) are used as limiting factors for the opening of the stomata. Sub-model 1 is described in detail by MAUSER & SCHÄDLICH (1998).

Sub-model 2 is the subject of this study. Here, the energy balance of leaves is calculated using the incoming absorbed radiation and three variations of energy fluxes from and to the leaf: Besides convective and conductive heat transfer, the energy loss with the transport of latent heat due to transpiration processes is calculated as a major element of the leaf's energy balance. The simulation of transpiration is strongly connected to the gas exchange through the stomata and the cuticle of the leaf as described by FARQUHAR & WONG 1984. The gas exchange in turn is the result of photosynthetic activities within the chloroplasts of the leaf.

Photosynthesis is calculated according to a biochemical approach introduced by FARQUHAR et al. (1980) and FARQUHAR & VON CAEMMERER (1982), whereby net primary production is modelled on the basis of the temperature-dependent rate of RuBP reproduction and the availability of Rubisco, i.e. by simulating the Calvin cycle (see sections 2 and 6.1). The availability and transport of CO_2 is regulated by the stomatal resistance of the leaf (BALL et al. 1997, FALGE 1997). CHEN et al. (1994) extended FARQUHAR'S approach to C4 plants and forms the basis for the modelling of the C4 pathway, which is described in section 6.2.

Both approaches (FARQUHAR and CHEN) are based on the leaf level. To obtain canopy assimilation rates in PROMET, the processes in the leaf are scaled to the canopy via the relative leaf area in two canopy layers, i.e. the sunlit and shaded canopy components. A detailed description of the photosynthesis modelling in PROMET can be found in HANK (2008). The parameters and variables used are listed in Appendix 2.

6.1 Modelling of the C3 pathway

FARQUHAR et al. (1980) and FARQUHAR & VON CAEMMERER (1982) describe the steady-state CO_2 exchange of leaves measured by gas exchange to provide a mechanistic model for the response of photosynthesis to light, CO_2, O_2 and temperature. Those aspects of the stoichiometry of C3 photosynthesis that are relevant for the implementation of chlorophyll measurements in the model will be described briefly in the following.

The basis for this model is the calculation of the PCR cycle via the net CO_2 assimilation rate A [µMol m^{-2} s^{-1}] as given by Equation 17 (FARQUHAR et al. 1980):

$$A = \left[\frac{1 - (0.5\ O)}{C_i} \right] \min (V_c, V_j) + R_d \qquad \text{Equation 17}$$

where

O	internal concentration of O_2 in the intercellular air spaces [ml l^{-1}],
C_i	internal concentration of CO_2 in the intercellular air spaces [ppm],
V_c	carboxylation rate of Rubisco [µMol m^{-2} s^{-1}],
V_j	carboxylation rate of RuBP [µMol m^{-2} s^{-1}], and
R_d	day respiration [µMol m^{-2} s^{-1}].

The carboxylation rate V_c is limited by the amount, activation state and kinetic properties of Rubisco, while the carboxylation rate V_j is limited by the rate of RuBP regeneration via the rate of the electron transport.

Parameter V_c obeys the kinetics with respect to O_2 and CO_2:

$$V_c = \frac{V_{cmax}\ C_i}{(C_i + K_c\ (1 + \frac{O}{K_0}))} \qquad \text{Equation 18}$$

where

V_{cmax}	maximum rate of carboxylation [µmol m^{-2} s^{-1}],
K_c	Michaelis constant for Rubisco carboxylation [µl l^{-1} O_2], and
K_o	Michaelis constant for Rubisco oxygenation [ml l^{-1} CO_2].

The parameter V_j is regulated by the rate of electron transport J [µMol quanta^{-1} m^{-2} s^{-1}]:

$$V_j = \frac{J\ C_i}{(4\ (C_i + \frac{O}{\tau}))} \qquad \text{Equation 19}$$

The relationship between the electron transport and the "useful light absorbed by PSII" (VON CAEMMERER 2000) is defined as:

$$V_j = \frac{I_2 + J_{max} - \sqrt{(I_2 + J_{max})^2 - 4\theta\ I_2\ J_{max}}}{2\theta} \qquad \text{Equation 20}$$

where

I_2	PAR absorbed by PSII [µMol quanta^{-1} m^{-2} s^{-1}],
J_{max}	maximum electron transport [µMol quanta^{-1} m^{-2} s^{-1}], and
θ	empirical curvature factor [dimensionless].

Equations 17 to 20 demonstrate that FARQUHAR et al. (1980) simplified the description of the CO_2 assimilation to be limited either by the rate of electron transport and regeneration of RuBP or by the rate of RuBP carboxylation determined by Rubisco. Obviously, at low irradiance the rate of electron transport is the limiting factor and so the Rubisco activity depends on the rate of supply of RuBP. The rate of CO_2 assimilation varies as a function of CO_2 partial pressure due to the changing proportion of RuBP consumed by photorespiration. At high irradiances the potential rate of RuBP regeneration may exceed the rate of RuBP consumption by Rubisco if there is insufficient CO_2 available. There will therefore be a transition from an electron-transport-limited to a Rubisco-limited assimilation rate.

The input variables were mostly found empirically and are described in detail by EVANS et al (1993), ÖGREN & EVANS (1993) and VON CAEMMERER (2000).

6.2 Modelling of the C4 pathway

The C4 pathway is calculated according to CHEN et al. (1994) and is also based on the FARQUHAR model for the C3 pathway, but an additional PEPcase-dependent C4 cycle was added. The C4 cycle consists of the fixation of CO_2 by PEPcase, and the transport and decarboxylation of C4 acids (see section 2.3.2). The C3 cycle fixes CO_2 supplied by the C4 cycle using the C3 photosynthetic pathways located inside the bundle sheath cells.

According to CHEN et al. (1994), the C4 cycle of photosynthesis is assumed to be controlled solely by PEPcase. The dependence of the rate of the C4 cycle (V_4) upon CO_2 concentration is modelled by Michaelis-Menten kinetics:

$$V_4 = \frac{V_{4m} C_m}{C_m + k_p} \qquad \text{Equation 21}$$

where

C_m	CO_2 concentration in the mesophyll space [µMol m^{-2} s^{-1}],
k_p	Michaelis constant of PEPcase [µMol m^{-2} s^{-1}], and
V_{4m}	maximum assimilation rate at a given incident radiation [µMol m^{-2} s^{-1}].

V_{4m} is modelled according to

$$V_{4m} = \frac{\alpha_p I_2}{\sqrt{\left(1 + \frac{\alpha_p^2 I_2^2}{V_{pm}^2}\right)}} \qquad \text{Equation 22}$$

where

α_p	empirical parameter [µMol m^{-2} s^{-1}], and
V_{pm}	maximum carboxylation rate of PEPcase [µMol m-2 s-1].

6.3 Input data

For this study, PROMET was used on a field scale to model plant growth and development of the test fields. The input data required is pixel-based information on meteorology, soil, vegetation and relief, which have already been described in section 3. Parameter sets describing the soil properties and vegetation biophysics are also needed. The set of crop-specific parameters regulating the physiological development of the modelled vegetation is presented in Table , the soil parameters are listed in Appendix.

Table 22: Crop-specific parameters used

Plant Parameter	**Unit**
Leaf mass per leaf area	[kg m^{-2}]
Day of sowing	[DOY]
Day of harvest	[DOY]
Width of Leaf	[m]
Carboxylation capacity	[µMol m^{-2} s^{-1}]
Maximum rate of electron transport	[µMol quanta^{-1} m^{-2} s^{-1}]
Michaelis constant for O_2 at 25 °C	[µl l^{-1}]
Michaelis constant for C at 25 °C	[ml l^{-1}]
Respiration capacity at 25 °C	[g CO_2 m^{-2} s^{-1}]
Light use efficiency	[Mol CO_2 m^{-2}]
Coefficient of stomatal conductance	[dimensionless]
Leaf-internal concentration of O_2	[ml l^{-1}]
Cardinal temperatures	[°C]
Maximum root depth	[cm]

Source: Own survey

The soil and cultivar-specific parameters were adjusted in accordance with the literature and measurements from previous field campaigns. The spatial resolution of the raster-based data is determined by the resolution of the DEM used. In this case, the grid resolution was processed to meet the spatial resolution of the 10 x 10 m DEM provided by the Bavarian Land Surveying Office (Bayerisches Landesvermessungsamt).

Meteorological input data, such as temperature, precipitation, wind speed and radiation components, were provided by the German Weather Service (Deutscher Wetterdienst DWD) and spatially interpolated from 19 weather stations located within a radius of approximately 100 km around the test area. The results of the validation of the PROMET meteorology interpolated by the DWD data with variables measured at the agro-meteorological station "Gut Hüll" can be found in Hank et al. (2007), who report high coefficients of determination for precipitation ($r^2 = 0.84$) and temperature ($r^2 = 0.98$).

6.4 PROMET results

The modelling of both the C3 and C4 pathways as described in sections 6.1 and 6.2 results in the calculation of the potential photosynthesis under environmental conditions in terms of radiation, temperature, CO_2 and O_2 concentrations. The PROMET results for the test fields will be presented and discussed in the following subsections. The output variables of PROMET are manifold (MAUSER & SCHÄDLICH 1998; LUDWIG & MAUSER 2000; MAUSER et al. 2008), and each of them can be used as a validation source if field measurements are available. For this study the output variables plant height and biomass of stem, leaves and fruit will be discussed using the field measurements described in section 3. These variables were chosen, because they are pure derivates of the photosynthetic processes within plants. Since the plant height is modelled as a function of the relative LAI, the LAI shows an analogue trend and is hence not discussed separately. For the wheat canopies, GPS-based yield maps are available, therefore the modelled yield can be validated spatially using this data.

For all fields, the simulation run was started about four months prior to the sowing date of the crops to provide appropriate soil moisture conditions at the beginning of the plant growth.

Parts of the results for wheat are already published in OPPELT (2009) and OPPELT (2010). Parts of the results for the maize canopies are published in OPPELT & HANK (2009).

6.4.1 Wheat 2004

The simulation run for wheat 2004 was performed for the time frame June 1 2003 to August 31 2004 thus covering the growth cycle of a winter wheat crop. The wheat stand was sown on October 15 2003 and harvested on August 22 2004. The model results were extracted at exactly the five points that had also been sampled by the field campaign. The resulting time series were averaged and compared to the field data that had similarly been averaged for the five sample points. The results for the leaf, stem and fruit dry matter as well as the plant height are presented in Figure 43.

For the above-ground biomass (stem, leaf and fruit), the modelled values match the field data reasonably well in terms of their magnitude and also their course, resulting in high coefficients of determination between 0.78 for the leaves and 0.97 for the fruit (Figure 43). The development of the plant height is reproduced well by the model, although PROMET models canopy heights untimely (Figure 43).

Figure 43 demonstrates the high potential of PROMET in modelling the development of a wheat canopy. Nevertheless, validation using a spatial distribution of variables, if

available, is useful. Therefore, the modelled yield was validated using a digital yield map, which is presented in Figure 44.

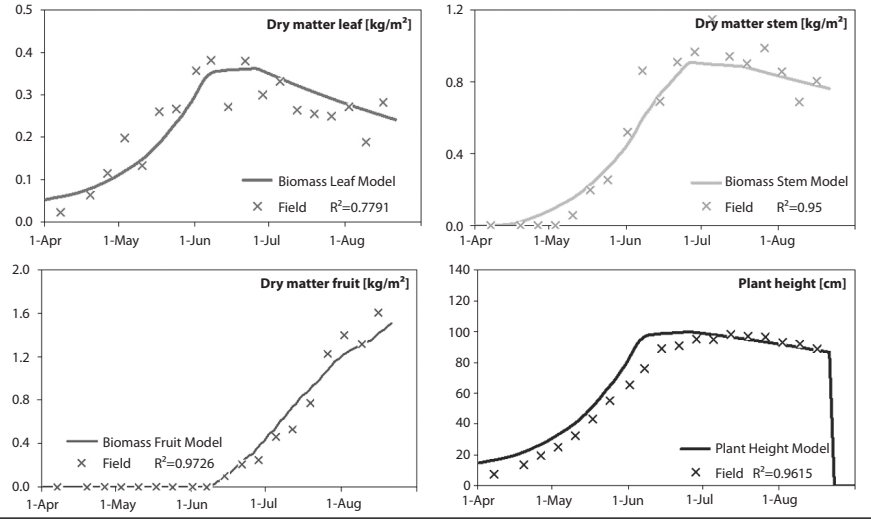

Fig. 43: Validation of PROMET results for wheat 2004 using the mean values of the field measurements at the five sampling points
Source: Own survey (figure partly published in OPPELT 2009 and OPPELT 2010)

For a comparison with the model results the original yield map was resampled to meet the model's resolution of 10 x 10 m. Apart from the marginal regions with lower yield and a distinct low-yield area in the eastern part of the field (5 – 6 t ha^{-1}), the measured variation in the stand mainly reaches from 7 to 12 t ha^{-1}, indicating that the crop has developed homogeneously.

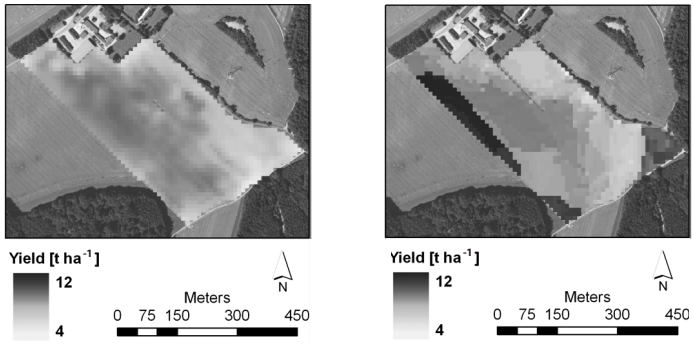

Fig. 44: Measured yield (left), aggregated to a 10 x 10 m cell resolution and modelled yield (right)
Source: Own survey (figure partly published in OPPELT 2009 and OPPELT 2010)

PROMET returned a modelled yield that ranges from approx. 10 to 12 t ha^{-1} with a mean value of 10.74 t ha^{-1} and a standard deviation of 0.58 t ha^{-1} (Table 23). The variability of the measured yield is higher, returning a standard deviation of 1.25 t ha^{-1}, while the mean yield value is 8.29 t ha^{-1}. The mean yield is therefore overestimated by 2.45 t ha^{-1} in the PROMET results. This is due to the fact that the model is not able to reproduce mechanically inflicted yield losses such as windfall or the lower plant densities in the field margins due to machine-induced stress. However, it reproduces patterns of productivity that can also be found in the yield map. This is influenced by variables that affect the radiation regime in the stand, such as the highly productive zone at the south-west exposed slope at the western margin of the field. The very eastern part of the field is also modelled as a high productive zone, which is due to a changing soil texture, but in the yield map this area is characterized as a low productive zone instead.

Table 23: Measured and modelled yield for wheat 2004

Yield	Min [t ha^{-1}]	Max [t ha^{-1}]	Mean [t ha^{-1}]	Stdev [t ha^{-1}]	Field sum [t]
Measured	4.96	11.70	8.29	1.25	120.49
PROMET	9.99	11.67	10.74	0.58	158.75

Source: Own survey

6.4.2 Wheat 2005

The simulation run for wheat 2005 was performed for the time frame from June 1 2004 to August 1 2005, covering the growth cycle of the wheat stand, which was sown on October 15 2004 and harvested on August 19 2005.

For the above-ground biomass of stem and fruit, the modelled values match the field data reasonably well with a slight overestimation of the model during ripening, resulting in coefficients of determination of 0.87 (Figure 45). In contrast to 2004, the stem mass is overestimated by PROMET during ripening. The modelled leaf biomass correlates moderately well with the measured values, resulting in a coefficient of determination of 0.5. The modelled leaf biomass agrees well with the measured leaf biomass during stem elongation. During booting, heading and flowering (see Figure 17 and Table 4), PROMET underestimates leaf biomass, whilst overestimating it during ripening. The results for the plant height are similar to those observed for 2004. The development of the plant height is reproduced well by the model, although the canopy height is modelled untimely.

PROMET results indicate a very homogeneously distributed yield with a mean yield of 8.37 t ha^{-1} and a standard deviation of only 0.024 t ha^{-1} (Figure 46 and Table 24). The homogeneity is due to the modelling of “potential” photosynthesis in a flat terrain without differences in soil texture.

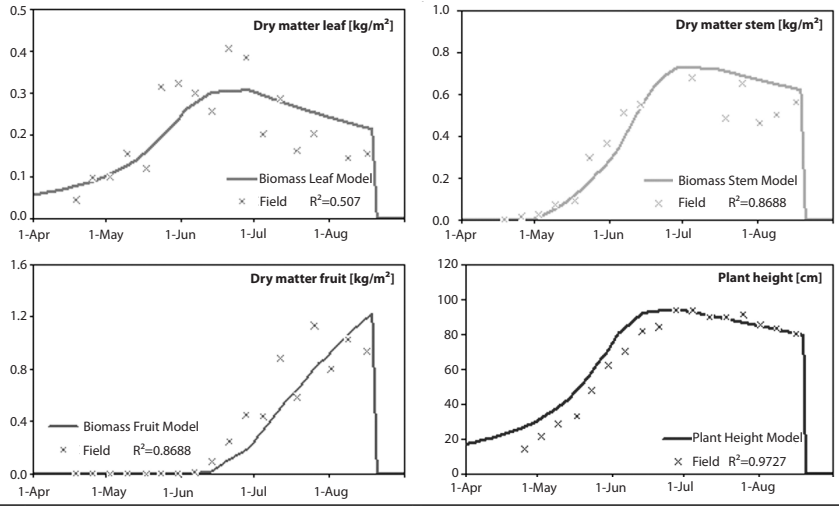

Fig. 45: Validation of PROMET results for wheat 2005 using field measurements
Source: Own survey (figure partly published in OPPELT 2009 and OPPELT 2010)

Therefore, the heterogeneity in the field, which can be observed in the digital yield map in Figure 46, could not be reproduced by the model. Also the fertilization window, which is visible in the yield map, does not appear in the PROMET yield. Compared with a measured yield ranging from 3.29 to 10.32 t ha^{-1} and a resulting mean of 7.04 t ha^{-1}, the modelled yield lies above the measured mean by 1.33 t ha^{-1}, i.e. 17% of the mean yield.

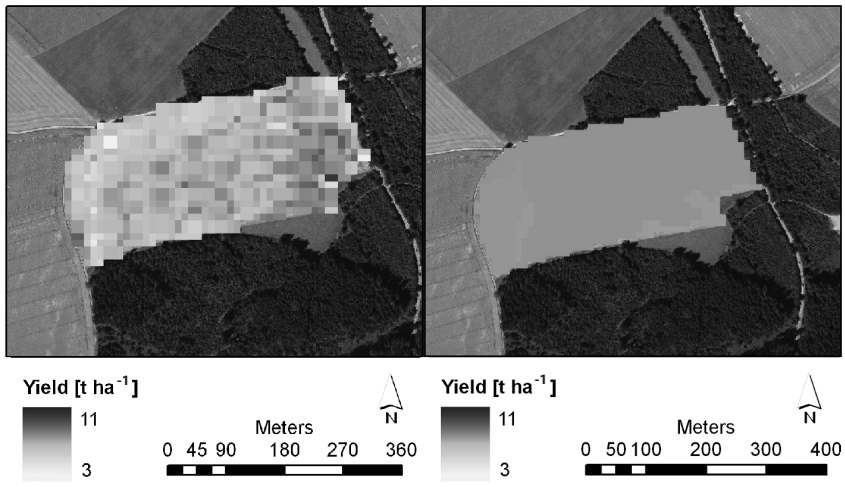

Fig. 46: Measured (left) and modelled (right) yield for wheat 2005
Source: Own survey (figure partly published in OPPELT 2009 and OPPELT 2010)

Table 24: Measured and modelled yield for wheat 2005

Yield	Min [t ha^{-1}]	Max [t ha^{-1}]	Mean [t ha^{-1}]	Stdev [t ha^{-1}]	Field sum [t]
Measured	3.29	10.32	7.04	0.848	59.21
PROMET	8.39	8.43	8.37	0.024	71.15

Source: Own survey

6.4.3 Maize 2004

The sowing date is not known for the maize canopy, the harvest was on October 5. The sowing period for silage maize for this region is recommended for the last week of April (LFL 2008); therefore the simulation run for maize in 2004 was performed from January 1 to October 30. Yield mappings were not recorded for the maize canopies; therefore a validation using the spatial distribution of the yield is not possible. The validation of the modelling results with the field measurements are presented in Figure 47.

According to Figure 47, the model results fit best for the development of the grain biomass with both the development and values. The biomass of the leaves also exhibits a high coefficient of determination, but leaf development is overestimated during the development of the main shoot and tillering, while during ripening the leaf biomass is slightly underestimated by the model (see also Table 4 and Figure 24).

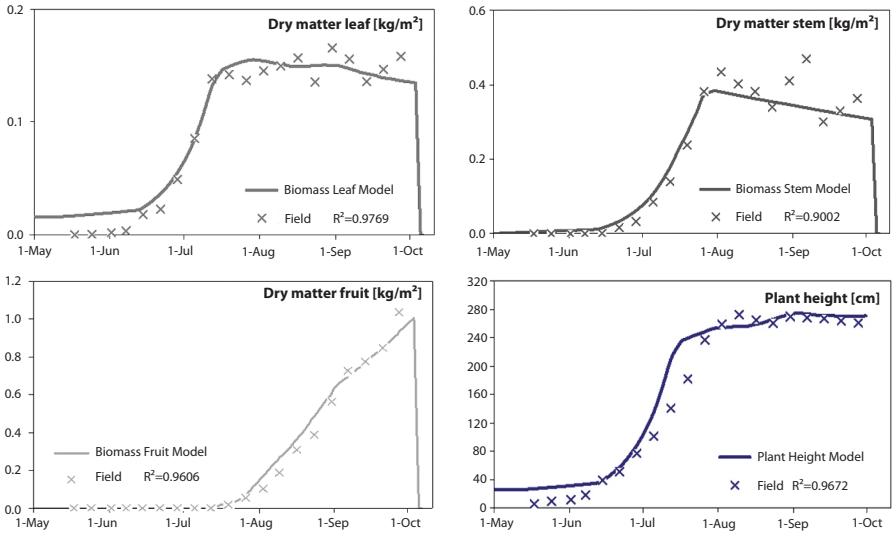

Fig. 47: Validation of PROMET results for maize 2004 using field measurements
Source: Own survey

An underestimation by the model can also be observed for the stem biomass during ripening, while prior to this PROMET is able to replicate the development well. The leaf biomass is overestimated during most of the growing period, but fits well during ripening.

Table 25: Statistics of modelled leaf biomass and total above-ground biomass (silage yield) for maize 2004

	Min	Max	Mean	Stdev	Field sum
Leaf biomass [kg m-²]	0.127	0.139	0.133	0.002	4.83 t
Silage yield [t ha^{-1}]	14.6	15.9	15.5	0.21	56.3 t

Source: Own survey

Figure 48 presents the spatial distribution of the leaf biomass and total biomass as derived with PROMET. Both parameters are distributed very homogeneously, since the field is located on a slight slope, but with a constant exposition towards south-west. Also the soil texture does not vary within the field, thus resulting in a homogeneous image for leaf and total biomass (Table 25).

Grain yield of silage maize is normally not recorded, because the total biomass removed from the field is used for silaging. Therefore, the modelled total dry biomass (i.e. aboveground biomass) can be used to estimate the silage yield, which is published to range between 45 and 55 t ha^{-1} fresh biomass (LFL 2008). Assuming a standard dry matter content of approximately 35% (KTBL 2005), the regional mean of silage dry matter content lies between 15 and 20 t ha^{-1}. With a mean value of 15.5 t ha^{-1} the modelled yield thus lies within the yield range in this area.

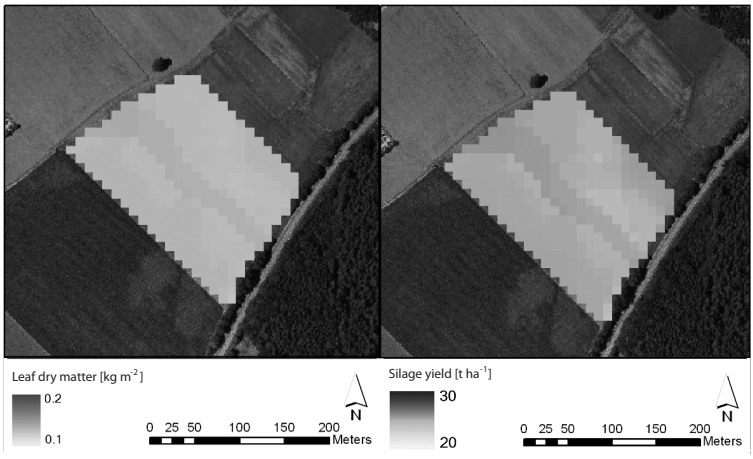

Fig. 48: Modelled leaf dry matter (left) and total aboveground dry matter (silage yield) (right)
Source: Own survey

6.4.4 Maize 2005

The sowing date is not known for the maize canopy in 2005 either, while the harvest was on September 29. Thus the sowing date was again assumed to be on April 20 resulting in a simulation run ranging from January 1 to October 30. Yield mappings were not recorded for the maize canopies; therefore a validation using the spatial distribution of the yield is not possible. The validation results using the field measurements are presented in Figure 49.

The measured and modelled leaf biomass is generally on a higher level than in 2004, which is caused by the higher plant density (section 3.2.4). This could not be traced by the model, thus the differences between the modelled and measured parameters are large. Nevertheless, PROMET is able to trace the general development of the leaf biomass, which results in a high coefficient of determination. Similarly to the results for 2004, leaf biomass is overestimated during tillering and stem elongation; but in contrast to 2004, where it was also possible to trace this parameter well during ripening, the measured and modelled leaf biomass differs greatly in 2005. A similar situation can be observed for the stem biomass. The fruit dry matter is, comparable to 2004, overestimated by PROMET during the development of the fruit, but during the ripening this parameter is slightly underestimated. The plant height is overestimated over the whole growing season.

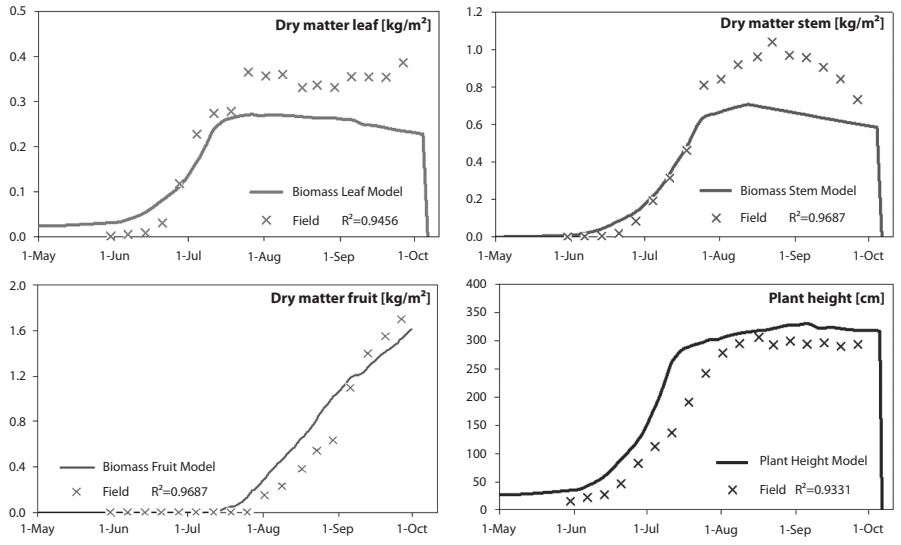

Fig. 49: Validation of PROMET results for maize 2005 using field measurements
Source: Own survey (figure partly published in Oppelt 2009 and Oppelt 2010)

The flat topography as well as a homogeneous soil texture lead to a very low spatial heterogeneity in the field, which is demonstrated in Figure 50 and Table 26. The strip of slightly increased values that crosses the field in south-southwest to north-northeast direction, is due to a different soil type. In this area of "higher" biomass values, a Rendzina developed on the same soil texture (sandy loam) as opposed to Para-Braunerde (corresponding to FAO cambisols) in the surrounding area. However, the resulting differences between these two soil types in leaf and total biomass are in the range of 0.003 kg m^{-2} and 0.3 t ha^{-1} respectively.

Table 26: Statistics of modelled leaf biomass and total above ground biomass (silage yield) for maize 2005

	Min	Max	Mean	Stdev	Field sum
Leaf biomass [kg m-²]	0.225	0.235	0.227	0.001	50.0 t
Silage yield [t ha^{-1}]	24.8	26.3	25.1	0.24	553.2 t

Source: Own survey

6.5 Concluding remarks

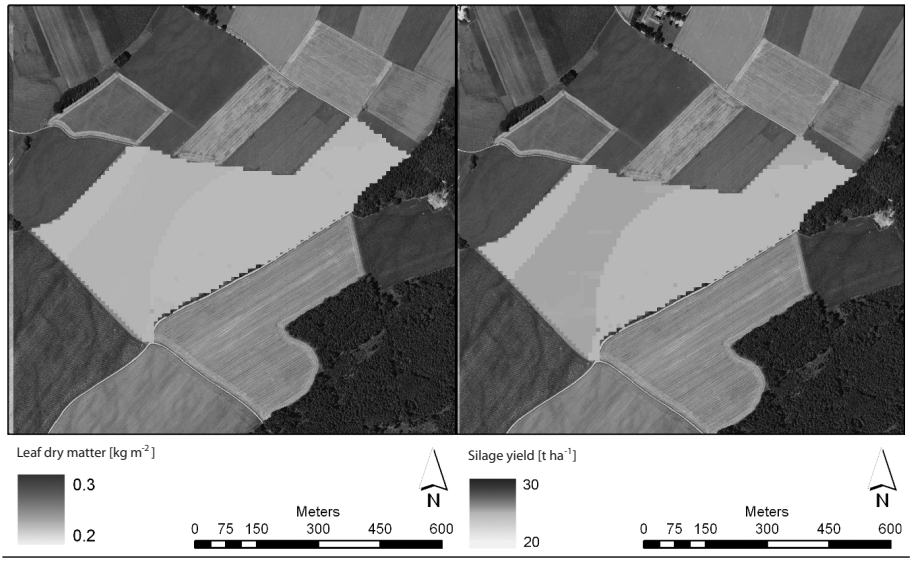

Fig. 50: Modelled leaf dry matter (left) and silage yield (right) for maize 2005
Source: Own survey

The results show that, although PROMET was developed in the sense of a landscape model whose main application is the simulation of water cycle components on the mesoscale, it is able to reproduce biological variables in realistic dimensions. The results demonstrate that PROMET is able to reproduce effects on plant development that are

caused by a varying radiation regime. The radiation regime on its part depends, along with the macro-meteorological situation, on factors, such as relief (exposition), which influences the amount of incoming radiation within the field and thus results in a different plant development. However, the effects due to differences in the soil type or texture can also be modelled well.

Keeping in mind that PROMET calculates an optimum photosynthesis under given environmental conditions, the results are very promising. However, the results also demonstrate that, under real conditions, differences result between the model and measured reality, e.g. on a deficit in nutrient supply, mechanical inflictions or plant diseases. To overcome these limitations, the implementation of "real conditions" will be introduced and discussed in the next section.

7 Assimilation of remotely sensed chlorophyll in PROMET

7.1 Chlorophyll and leaf absorptance

The previous section dealt with the CO_2 fixation during C3 and C4 photosynthesis. Equations 20 and 22 demonstrate the relationship between the assimilation rate and the absorbed PAR by PSII. The calculation of I_2 is described by FARQUHAR & VON CAEMMERER (1982) as follows:

$$I_2 = I_p \cdot abs \left(\frac{(1-f)}{2} \right) \qquad \text{Equation 23}$$

where

f	correction factor [dimensionless], and
abs	absorptance of the leaf [dimensionless].

According to the modelling approach of FARQUHAR et al. (1980) and CHEN et al. (1994), many of the parameters are assigned *a priori*. Equation 23 also includes the model state constants *f* and *abs*: the leaf absorptance refers to mean relative quantum yield in the range of the photosynthetic active radiation (PAR), i.e. 400 – 700 nm. The quantum yield is the CO_2 assimilation in the absence of photorespiration and represents the maximum efficiency with which light can be converted to chemical energy by photosynthesis (FARQUHAR & VON CAEMMERER 1982). The quantum yield is wavelength-dependent and exhibits a maximum at 600 nm, thus in Equation 23 it is calculated by normalizing the quantum yields at various wavelengths in the PAR with the maximum quantum efficiency measured at 600 nm. EVANS (1987) reports that *abs* is independent of species (also for C4 plants) and proposes a constant value of $abs_{const} = 0.89$. The factor *f* corrects for the fact that quantum yields obtained in the laboratory under different illumination conditions vary with different illumination sources. According to VON CAEMMERER (2000), for field measurements the correction factor *f* is assumed to be 0.15.

Although the parameters in Equation 23 are commonly assumed to be constants, some studies can be found that deal with a more dynamic and spatially distributed parameterization of I_2: GENTY et al. (1989) demonstrated that chlorophyll a fluorescence enables the calculation of the electron flux through PSII for various C3 species using Equation 24:

$$J = \beta \, abs \, I_p \left(1 - \frac{F_s}{F_{m'}}\right) \qquad \text{Equation 24}$$

where

β	fraction of absorbed irradiance that reaches PSII [dimensionless],
F_s	fluorescence during a brief saturating light pulse [dimensionless], and
$F_{m'}$	fluorescence during steady-state photosynthesis [dimensionless].

KRALL & EDWARDS (1992) described the use of fluorescence for the estimation of the C4 photosynthetic rate. In recent years, remotely sensed fluorescence data has been the subject of photosynthesis applications based on sun-induced fluorescence (e.g. HOGE et al. 2003, HU et al. 2005). Also a variety of airborne and tractor-mounted instruments have been used to investigate photosynthetic activity via the sun (e.g. GAMON et al. 1990, ZARCO-TEJADA et al. 2000) or laser-induced fluorescence (e.g. LICHTENTHALER et al. 1990, RICHARDS et al. 2003).

FIELD & MOONEY (1986) proposed a species and growth-independent relationship between the leaf nitrogen content and the photosynthetic rate, because all intrinsic biochemical and photo-biological processes require nitrogenous compounds. EVANS (1983) reported a strong linear relationship between RuBP carboxylase and leaf nitrogen of various species. He also reported a logarithmic relationship between chlorophyll content with the RuBP carboxylase activity for wheat leaves, thus a link between CO_2 assimilation and chlorophyll content is evident. BJÖRKMAN & DEMMIG (1987) analyzed 44 different C3 and C4 species for their variation in *abs* and found leaf absorptance ranging from 0.65 to 0.94, but they propose the use of a mean value which lies at 0.838. However, the results described by BJÖRKMAN & DEMMIG (1987) and THAYER & BJÖRKMAN (1990) indicate an existing large variability in *abs*, which is currently not taken into account in PROMET. They described the effect of an increased *abs* with increasing chlorophyll content calculated per leaf area chl_{LA} [mg m^{-2}] for *Hedera canariensis*, having the form described in Equation 25:

$$abs = -0.0735 + 0.3484 \cdot \log chl_{LA} \qquad \text{Equation 25}$$

They report a chlorophyll a/b ratio of 2.7, thus for chlorophyll a (*chl a*) Equation 25 can be rewritten as:

$$abs = -0.0217 + 0.3460 \cdot \log chl\ a_{LA} \qquad \text{Equation 26}$$

The chlorophyll a content per leaf area is then converted into chlorophyll a content per unit ground surface (*chl a* [mg m^{-2}]) using the regression equations given in Figure 15.

$$abs = -0.0217 + 0.346 \cdot \log(8.4413 + 0.4817\ chl\ a) \qquad \text{Equation 27}$$

Assuming Equation 27 to be valid for other species, *chl a* can be substituted by the equations given in Tables 16 and 18, and can then be estimated directly using the CAI. The resulting relationship between the CAI and the absorptance are presented in Figure 51, thus enabling a dynamic parameterization of *abs*.

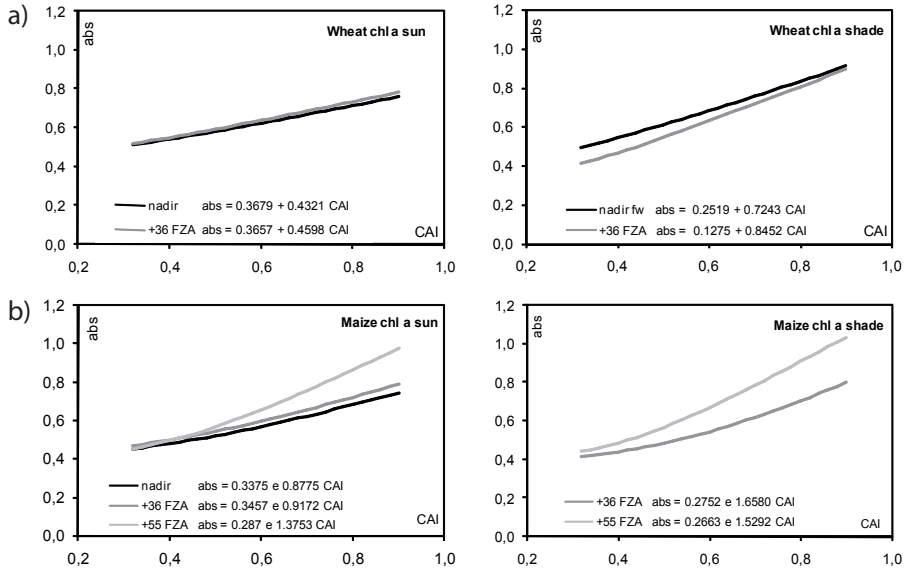

Fig. 51: Influence of CAI on the leaf absorptance (abs) for wheat (a) and maize (b)
Source: Own survey

The equations for wheat can be well approximated using linear functions. For maize, the relationship between *abs* and CAI can best be expressed using exponential functions. For both plants species, the anisotropy is reflected in the slope of the function. The higher the FZA, the steeper the slope is.

7.2 Results using dynamised leaf absorptance

The equations given in Figure 51 are used to calculate a spatial distribution of *abs*, which is then implemented in PROMET. Here, I_2 is modelled using the constant value proposed by EVANS (1987) ($abs_{const} = 0.89$) until a remotely sensed *abs* (abs_{RS}) map is available. Then on, the abs_{RS} is used to calculate I_2. The abs_{RS} in turn is used until the end of the vegetation period, but is replaced again if an additional abs_{RS} map is available for a later day. The results achieved for the test fields are discussed in the next sections.

Parts of the results are already published in OPPELT (2009) and OPPELT (2010).

7.2.1 Wheat 2004

For the wheat field in 2004, CHRIS data acquired on May 25 and AVIS data acquired on March 31 and May 25 were implemented in PROMET. The results are summarized in Table 27, Table 28, Figure 52 and Figure 53. They demonstrate that the use of an abs_{RS}

enables a more realistic modelling of the yield, i.e. in this case the yield is lowered, but the results depend strongly – as could have been expected – on the time (or developmental stage of the plants) when abs_{const} was changed into abs_{RS} as well as on the sensor used.

The time when a remotely sensed *abs* distribution is available is crucial for two reasons: firstly, if spatially distributed *abs* is available at the beginning of the vegetation period, this period can be modelled more realistically, because in the early growth stages the abs_{RS} values turned out to be much lower than abs_{const} (see Figure 52 right). With progressive plant development the chlorophyll content and therefore also the absorptance increase, resulting in a low modelled yield. This effect can be observed when only remote sensing data that were acquired in early developmental stages (March 31, during tillering) was implemented in PROMET, where the measured yield was underestimated by 40 %. This is presented in Figure 52 with the modelled course of the fruit and leaf biomass. The other variables such as stem biomass and plant height react in the same way and therefore are not presented separately. Figure 52 also demonstrates the large variability of the field measurements indicating that, even in an agricultural stand managed using precision farming techniques, heterogeneity occurs that complicates the comparison between modelled variables and measurements.

Table 27: Comparison of yield measurements of wheat 2004 with modelled yield using PROMET with implemented CHRIS (C) and AVIS (A) abs_{RS} derived on different acquisition dates

Yield [t ha^{-1}]	Min	Max	Mean	Stdev	Field sum [t]
Measured	4.96	9.70	8.29	1.25	120.49
PROMET	9.99	11.67	10.74	0.27	153.75
PROMET + C May 25	9.33	13.79	10.25	0.26	146.78
PROMET + A May 25	8.17	11.07	10.12	0.28	144.92
PROMET + A Mar 31	4.12	9.69	5.19	0.81	74.32
PROMET + A Mar 31 + A May 25	5.24	11.04	7.67	0.69	109.83

Source: Own survey

PROMET still overestimates yield when remote sensing data from the end of stem elongation (May 25) are used, although the yield is lower than without the use of abs_{RS}. In this case, the plants were able to develop under best conditions during stem elongation, which is the growth period with the highest increase in leaf biomass (see also Figure 19). Thus, best results could be achieved using a combination of abs_{RS} from an early developmental stage and an enhanced growth stage (see also Figure 53a right), whereby May 25 is quite a late acquisition date.

Besides the implementation date of abs_{RS}, the sensor affects the results as well, which is demonstrated in Figure 53. The smaller GSD of AVIS results in a more dynamic behav-

iour of the CAI and hence *abs*, which in turn results in a higher dynamic in the modelled yield. Chlorophyll and CAI values derived with AVIS were generally on a lower level than those derived with CHRIS, which again results in a lower modelled yield using AVIS data.

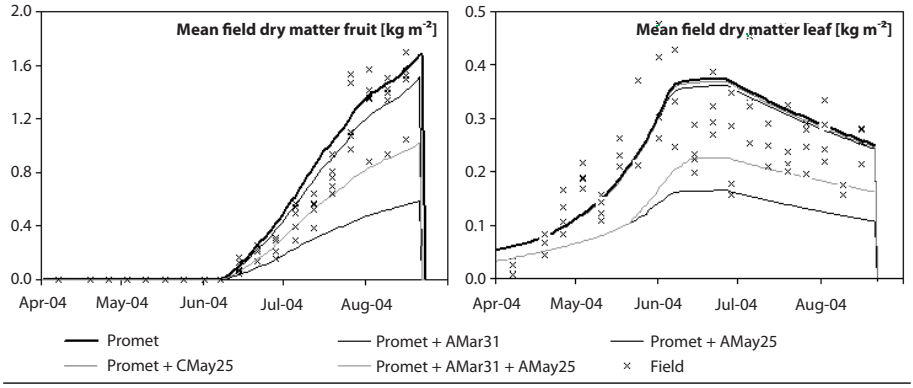

Fig. 52: Modelled and measured fruit (left) and leaf (right) biomass for 2004 in comparison with field measurements at the different sampling points
Source: Own survey

Figure 53 also presents the spatial distribution of the yield as modelled with PROMET when CHRIS or AVIS data are implemented. When using CHRIS data the modelled yield is not as patchy as without the assimilation of remote sensing data, but attenuates the basic structure given by the model using abs_{const} (see Figure 44). Due to the late acquisition date the yield is still overestimated for all pixels, resulting in a difference image characterized by positive values (bluish colours in Table 31b left) with a mean overestimation of 1.9 t ha^{-1} (the value range is between 0.6 and 5.4 t ha^{-1}, in comparison to a mean of 2.7 t ha^{-1} and a range of 1.3 to 6.1 t ha^{-1} when abs_{const} is used). The attenuating effect increases when AVIS data are implemented. Especially when both the March and May AVIS acquisitions are used, the highly productive zone at the western margin is attenuated as well as the highly productive zone at the very east, which is now modelled as a moderately productive zone. The resulting differences between modelled and measured yield, which are presented in Figure 53b (right), now range between -1.3 and +3.2 t ha^{-1}. Thus, while the yield is overestimated for all pixels when only the May 25 data are used (Table 27), an underestimation occurs for some pixels when the March 31 AVIS data are implemented as well.

Both difference images also demonstrate that the field headlands are problematic areas where yield is overestimated when either CHRIS or AVIS data are used, although the effect is less pronounced with airborne acquired data. The problem of mixed pixels is inherent to remote sensing data, and at agricultural fields this problem is superimposed

by the existing reduced plant vitality at the field margins. However, leaving the headlands aside, the difference image in Figure 53 presents very good results, especially for abs_{RS} based on AVIS data.

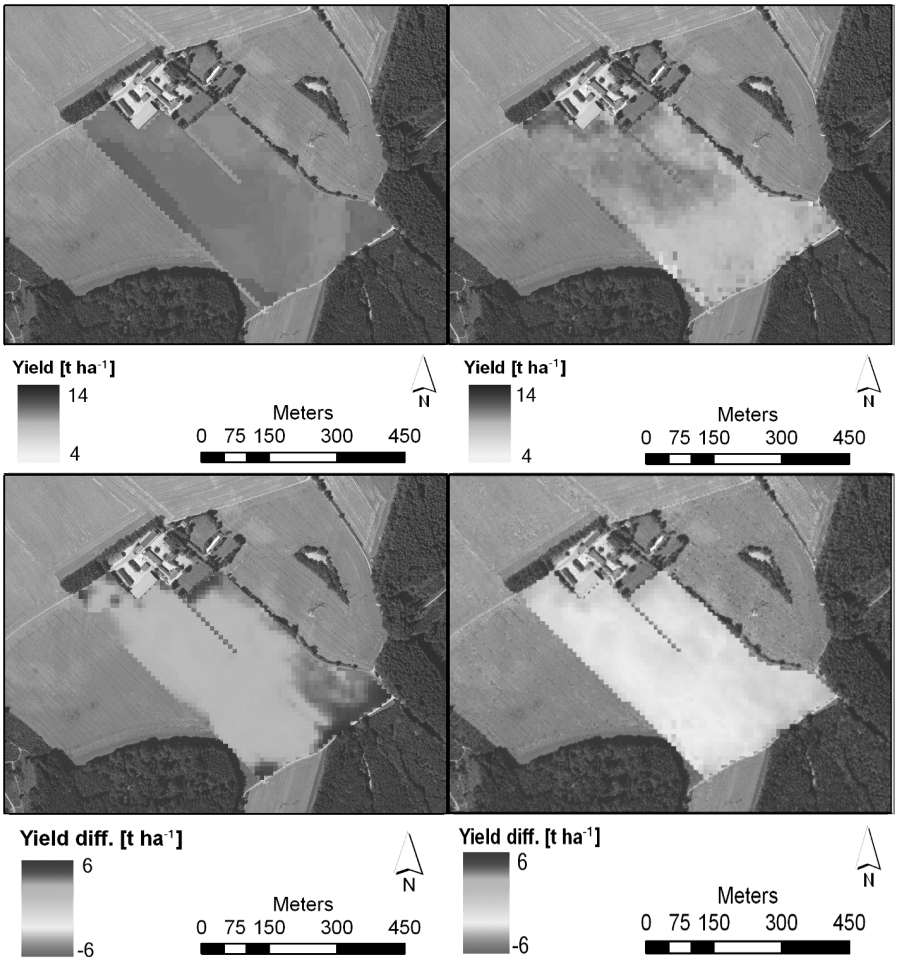

Fig. 53: a) Modelled yield using CHRIS data acquired on May 25 (left) and AVIS data acquired on March 31 and May 25 2004 (right); b) resulting differences between modelled and measured yield (PROMET–measured)
Source: Own survey (figure partly published in Oppelt *2010)*

Table 28 presents the validation of PROMET modelled fruit and leaf dry biomass with the field measurements at the different sampling points throughout the year. This validation confirms the previously discussed results, i.e. that the best results can be achieved when the high resolution AVIS data acquired in March and May are assimilated. Table 28

also demonstrates that the fruit development is modelled in a high quality without using remote sensing data, but even the high coefficients of determination can be enhanced with the implementation of remote sensing data. Both sensors lead to a better simulation at the sampling points, except for P3, which shows a slightly higher coefficient of determination without the use of abs_{RS}. The mean difference between the field measurements at the sampling points and the modelled fruit biomass at the corresponding pixels (Mean diff in Table 28) confirm these results. The best results for the simulation of both the fruit and leaf biomass could be achieved when the combined March and May AVIS acquisitions were implemented.

Table 28: Coefficients of determination for modelled and measured fruit and leaf dry biomass at the different sampling points and mean difference [kg m^{-2}] between model and measurement (Field measurement – PROMET) of the wheat field in 2004

Fruit dry biomass	**P1**	**P2**	**P3**	**P4**	**P5**	**Mean**	**Mean diff**
PROMET	0.880	0.963	0.921	0.845	0.964	0.869	-0.007
PROMET + C May 25	0.961	0.963	0.914	0.945	0.964	0.970	-0.014
PROMET + A Mar 31	0.955	0.964	0.917	0.939	0.955	0.966	0.063
PROMET + A May 25	0.961	0.963	0.915	0.945	0.964	0.971	-0.014
PROMET + A Mar 31 + A May 25	0.967	0.963	0.916	0.941	0.959	0.967	0.003

Leaf dry biomass	**P1**	**P2**	**P3**	**P4**	**P5**	**Mean**	**Mean diff**
PROMET	0.420	0.733	0.654	0.528	0.463	0.507	-0.006
PROMET + C May 25	0.418	0.729	0.649	0.529	0.657	0.770	-0.013
PROMET + A Mar 31	0.550	0.745	0.677	0.533	0.498	0.790	0.113
PROMET + A May 25	0.418	0.758	0.649	0.566	0.659	0.767	-0.012
PROMET + A Mar 31 + A May 25	0.571	0.763	0.681	0.561	0.646	0.777	0.009

Source: Own survey

The potential of implementing remote sensing data becomes clearer when looking at the results for the leaf biomass. Here, the within-field variations can be reproduced more realistically when abs_{RS} is used instead of abs_{const}. The implementation of both CHRIS and AVIS data result in higher coefficients of determination at the different sampling points, whereby again the higher resolution of AVIS increases the quality of the modelled results. The importance of the phenological stage at which abs_{RS} is introduced can be observed at P1 and P3, where the remote sensing data of both CHRIS and AVIS lead to a lower agreement between model and measurement when *abs* is updated at the end of stem elongation on May 25. In contrast, the model results are greatly enhanced when the AVIS March data are implemented. P1 especially is an area where the yield is overestimated by PROMET, and the development of the leaf biomass is modelled more accurately by implementing

the remote sensing data, whereby the enhancement is better the earlier the remote sensing data are acquired.

7.2.2 Wheat 2005

For 2005, only CHRIS data that were acquired on May 25 and July 6 are available for the assimilation of absRS in PROMET. The results for the mean field values, which are given in Table 29, show that PROMET is again unable to reproduce the variability within the field and overestimates the measured yield by approx. 20 %. However, the modelled mean yield is even higher if absRS is used, both for May 25 and for July 6.

Table 29: Comparison of yield measurements of wheat 2005 with modelled yield using CHRIS data from different acquisition dates

Yield [t ha^{-1}]	Min	Max	Mean	Stdev	Field sum [t]
Measured	3.29	10.32	7.04	0.848	59.21
PROMET	8.29	8.43	8.37	0.024	71.15
PROMET + C May 25	8.54	8.84	8.78	0.045	75.39
PROMET + C Jul 6	8.38	8.72	8.57	0.044	71.77
PROMET + C May 25 + C Jul 6	8.54	8.87	8.76	0.046	74.32

Source: Own survey

While PROMET using abs_{const} still overestimates the mean yield, Figure 54 (left) demonstrates that the yield is also underestimated for some pixels. The range of deviations lies between -2.1 and 5.8 t ha^{-1}, whereby the highest positive deviations occur within the fertilization window and the highest negative deviations occur especially in the south-eastern part of the field. The differences between PROMET using abs_{C0525} and using abs_{const}, which are presented in Figure 54 (right), show that the use of abs_{C0525} leads to an increase of modelled yield over the entire field, except at two pixels on the north-western field margin.

This indicates that abs_{RS} values exceed abs_{const} values for nearly all pixels on both acquisition dates. However, analysis of the abs_{RS} data exhibits a range of values between 0.72 and 0.79, thus the modelled abs_{RS}-dependent yield should be more under than overestimated. To analyse the influence of *abs* on the plant development and thus the yield, the total biomass was modelled as a reference using incrementally increasing values for abs_{const}. The results, which are presented in Figure 55, show an increase of total biomass until $abs_{const} = 0.83$ and decreasing biomass with further increasing *abs* values.

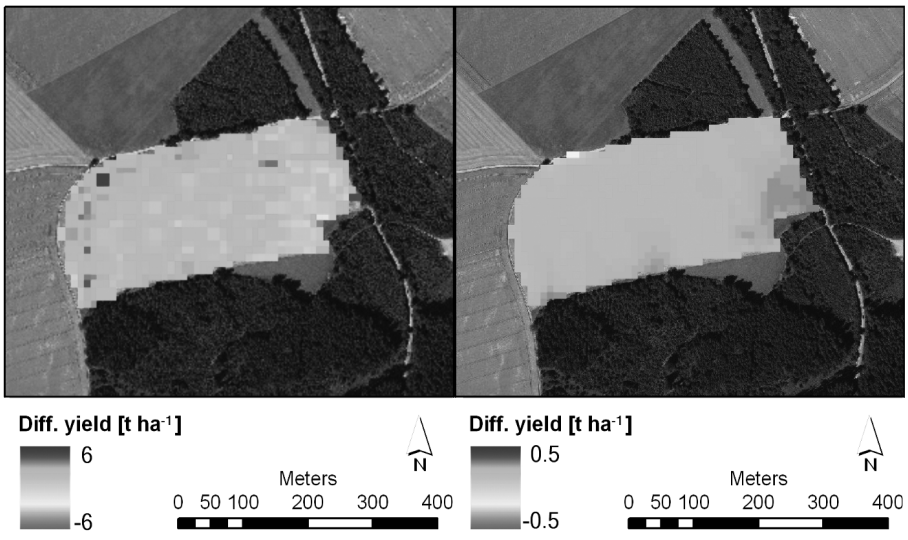

Fig. 54: Difference image between measured and modelled yield (measured - PROMET abs_{const}) (left) and difference image between PROMET using CHRIS May 25 data and PROMET using absconst (PROMET abs_{C0525} – xPROMET abs_{const}) (right)
Source: Own survey (figure partly published in OPPELT 2010)

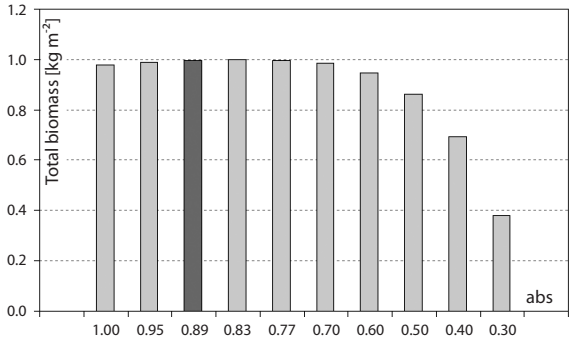

Fig. 55: Influence of abs on the relative total above-ground biomass modelled with PROMET; abs_{const} according to EVANS (1987) is marked red
Source: Own survey (figure partly published in OPPELT 2010)

These results indicate that the optimal plant development and therefore potential photosynthesis in PROMET is reached when abs = 0.83. Thus, for the wheat field in 2005, the modelled biomass as well as the yield increase if abs_{RS} ranges between 0.77 and 0.88. The lowered modelled biomass indicate that the maximum electron transport rate is reached when *abs* = 0.83. Therefore, a further increase in absorbed radiation is unable to enhance CO_2 assimilation. Obviously, this is the situation where the electron-transport-dependent

CO_2 assimilation rate is changing to a Rubisco-limited assimilation rate and characterizes the occurrence of light-saturated conditions. The slight decrease of total biomass when *abs* is higher than 0.89 is due to the fact that the probability of light-saturation conditions occurring throughout the vegetation period is higher for higher *abs*. Thus, repeatedly occurring sub-optimal photosynthetic rates due to repeatedly occurring excess light conditions progressively lower the development of biomass.

Bearing in mind that the irradiance at which light saturation of CO_2 assimilation occurs also depends on other environmental factors such as air CO_2 concentrations and temperature (VON CAEMMERER 2000), it can be proposed that for the modelling of potential photosynthesis under average field conditions abs_{const} should be changed to 0.83, because the value proposed by EVANS (1987) is beyond the optimum. This modification will, of course, result in higher assimilation rates, biomass production and yield than those modelled with $abs_{const} = 0.89$, but with unambiguous results.

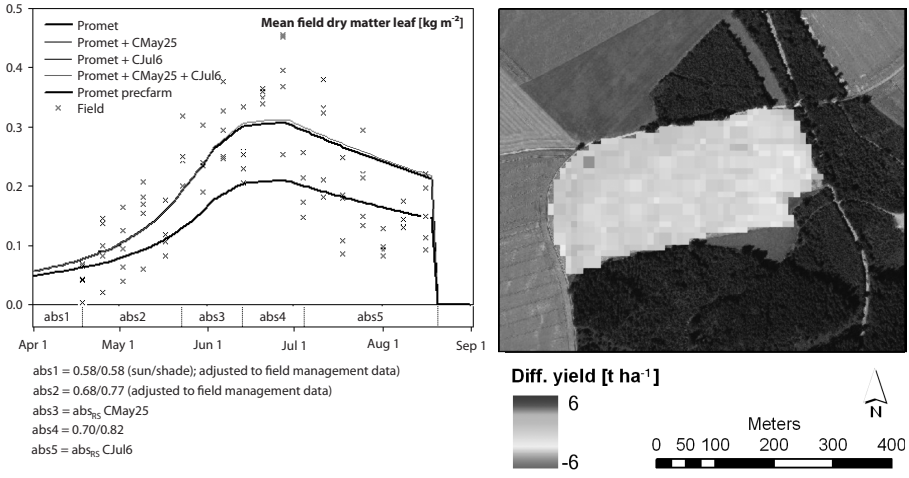

Fig. 56: Development of leaf biomass using remotely sensed abs values combined with abs values adjusted to field management data ($PROMET_{precfarm}$, left) and difference between modelled and measured yield ($PROMET_{precfarm}$ – measured)
Source: OPPELT 2009

Lack of remote sensing data or large time gaps between two acquisition dates lead to abs values being inadequate for the specific growing period. These problems can be avoided if the abs_{RS} values are traced back to abs_{const} after a certain period of time. This possibility is discussed in section 7.1.3 for maize as an example. Another approach is to adjust the model conditions to best fit additional information such as field management data. For this field, management data are available, and these can be used to optimize the *abs* values used in the model. Figure 56 presents the development of the leaf biomass as well as the spatial distribution of the yield if *abs* is adjusted according to the chlorophyll informa-

tion from the Schlagkartei, the fertilization dates and abs_{RS} are used for a time period of three weeks after the acquisition date. The total yield is then underestimated by PROMET by only 2.53 t ha^{-1}, the differences between modelled and measured yield range between -3.1 and 3.4 t ha^{-1} (Figure 56 right), whereby the CHRIS GSD turned out to be too large to resolve the fertilization window where the maximum difference of 3.4 t ha^{-1} occurred. The mean difference lies at -0.31 t ha^{-1}, indicating that this procedure can be used to estimate the yield within the scope of precision farming applications.

Table 30: Coefficients of determination for modelled and measured fruit and leaf dry biomass at the different sampling points and mean difference [kg m^{-2}] between model and measurement (Field measurement – PROMET) of the wheat field in 2005

Fruit dry biomass	**P1**	**P2**	**P3**	**P4**	**P5**	**Mean**	**Mean diff**
Promet	0.609	0.785	0.832	0.676	0.944	0.868	0.068
PROMET + C May 25	0.609	0.788	0.834	0.678	0.944	0.873	0.029
PROMET + C Jul 6	0.605	0.782	0.829	0.676	0.943	0.866	0.053
PROMET + C May 25 + C Jul 6	0.611	0.789	0.834	0.677	0.944	0.871	0.031
$PROMET_{precfarm}$	0.651	0.796	0.838	0.694	0.945	0.879	0.019

Leaf dry biomass	**P1**	**P2**	**P3**	**P4**	**P5**	**Mean**	**Mean diff**
PROMET	0.640	0.513	0.332	0.239	0.509	0.507	-0.012
PROMET + C May 25	0.630	0.529	0.358	0.238	0.505	0.584	-0.015
PROMET + C Jul 6	0.640	0.513	0.332	0.239	0.509	0.507	-0.012
PROMET + C May 25 + C Jul 6	0.623	0.509	0.326	0.239	0.505	0.498	-0.014
$PROMET_{precfarm}$	0.667	0.618	0.538	0.426	0.516	0.599	0.015

Source: Own survey

Table 30 presents the validation of PROMET results with the corresponding field measurements at the different sampling points and demonstrates the importance of the point in time at which the remote sensing data is acquired. PROMET is able to trace the fruit development well, resulting in high coefficients of determination with use of either abs_{const} or abs_{RS}. Comparable to the wheat field in 2004, the development of the leaf biomass is not modelled as accurately as the development of the fruit, but in contrast to 2004 the implementation of abs_{RS} is not able to enhance the modelled results. This is due to the late CHRIS acquisition dates, which modify the optimal plant development as late as at the end of stem elongation. The best results were achieved using the management-adjusted ($PROMET_{precfarm}$) *abs* values, whereby the spatial variability within the field is not captured with this procedure. The mean difference between the modelled and measured fruit and leaf biomasses also confirm the potential of remote sensing data to enhance the model results.

7.2.3 Maize 2004

The validation of the model results for maize is more difficult than for wheat, because no spatial distribution of any of the variables is available. Therefore the validation has to be performed using the mean field results and the measurements at the different sampling points.
For 2004, one AVIS (May 25) and two CHRIS (July 21 and August 22) acquisitions are available, whereby the former represents an early developmental stage (tillering) and the latter the beginning of flowering stage and ripening. The modelled results for the silage yield and the leaf biomass are given in Figure 57, Figure 58 and Table 31.
For the maize field in 2004, the PROMET yield is again highest when using the constant abs according to EVANS (1987), and the low standard deviation (stdev = 0.21 t ha^{-1}, see section 6.4.3) indicates that almost no heterogeneity exists within the field. This is in contrast to the field measurements, which are presented in Figure 57 and show variations of up to 0.5 t ha^{-1} measured at the different sampling points.

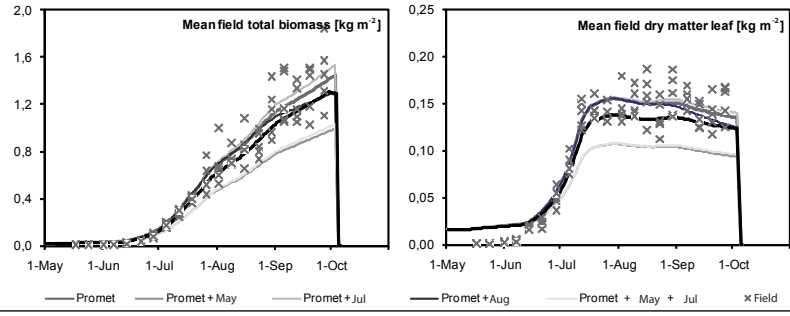

Fig. 57: Modelled silage yield (left) and leaf biomass (right) using absconst or abs$_{RS}$ originating from different acquisition dates and sensors in comparison to field measurements at different sampling points

Source: Own survey

Figure 58 and Table 31 demonstrate that the use of remote sensing data enhances the monitoring of the deviations from the mean field conditions. The earlier a spatially distributed *abs* is introduced, the more heterogeneously developed is the simulated stand at the end of the growing period. The advantage of implementing additional remote sensing data lies in the adjustment of the canopy absorptance properties, which would generally result in an increase of biomass and yield in the model. The CHRIS acquisition dates can be assumed to be too late for a proper characterization of the maize stand, because the whole stem elongation phase was modelled using an *abs* characterization derived during tillering. Thus, the resulting yield is also underestimated by PROMET when the combination of AVIS and CHRIS acquisition dates is used as the *abs* input (see Figure 57).

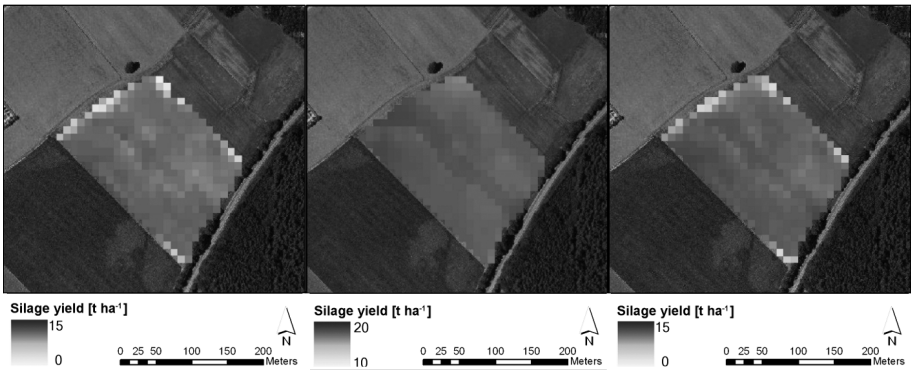

Fig. 58: Modelled silage yield using AVIS data acquired on May 25 2004 (left), CHRIS data acquired on July 21 2004 (centre) or a combination of AVIS and CHRIS data (right)
Source: Own survey

Table 31: Comparison of modelled yield for maize 2004 using CHRIS (C) and AVIS (A) data of different acquisition dates

Yield [t ha^{-1}]	**Min**	**Max**	**Mean**	**Stdev**	**Field sum [t]**
PROMET	14.6	15.9	15.5	0.21	56.30
PROMET + C Jul 21	14.4	17.7	15.4	0.49	55.90
PROMET + A May 25	2.90	12.9	10.4	1.35	37.75
PROMET + A May 25 + C Jul 21	3.80	12.7	11.9	1.26	43.20
PROMET + C Aug 22	14.5	15.5	15.3	0.20	55.60

Leaf Biomass [kg m^{-2}]					**Field sum [t]**
PROMET	0.127	0.139	0.133	0.002	4.83
PROMET + C Jul 21	0.126	0.149	0.139	0.004	4.94
PROMET + A May 25	0.031	0.176	0.091	0.023	3.30
PROMET + A May 25 + C Jul 21	0.034	0.106	0.096	0.010	3.48
PROMET + C Aug 22	0.120	0.138	0.134	0.002	4.76

Source: Own survey

If there is just one remote sensing acquisition available or there is a large time gap between acquisition dates, the problem can be avoided by recalibrating abs_{RS} back to abs_{const} after a defined period of time. Of course, this possibility is not restricted to maize canopies, but will be addressed here exemplarily. Figure 59 presents the modelled development of leaf biomass if the absorptance is reset to abs_{const} three weeks after the remote sensing acquisition together with the resulting spatial distribution of the silage yield. Although the mean modelled yield (50.8 t ha^{-1}) does not vary significantly from those presented in Table 31, the temporal development of the biomass differs and the spatial heterogeneity can be

observed in the resulting yield with a relatively high spatial dynamic (12.8 to 15.1 t ha^{-1}) and a high standard deviation (1.3 t ha^{-1}).

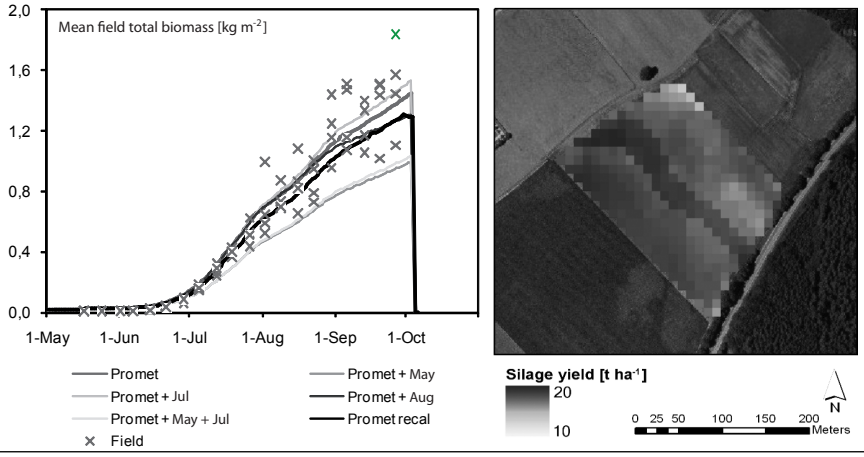

Fig. 59: Developmental of modelled total biomass throughout the vegetation period (left) and resulting silage yield using abs_{RS} that was reset to absconst after three weeks (right)
Source: Own survey

Thus the recalibration of *abs* is a rational way to adjust the absorptance of the plants to abs_{const} if large gaps in the remote sensing data occur, because *abs* changes according to the chlorophyll content, which in turn changes continuously (see section 2). This recalibration should be applied very carefully, because *abs* influences the amount of radiation absorbed by the plants and the subsequent CO_2 assimilation and development of biomass in the model.

Table 32 demonstrates the very good results for the punctiform validation of the model results. Even without the use of remote sensing data PROMET is able to trace the development of both leaf and total biomass very well. The implementation of the remote sensing data is able to enhance the already good results for some of the sampling points, i.e. P1, P3 and P5, whereby the results of the "recalibrated" PROMET are most promising. The mean differences (mean diff) in Table 32 between the field measurements at the sampling points and the mean values of the model results at the corresponding pixels demonstrate that PROMET is not only able to trace the developmental course of the maize canopy, but also to model the silage yield as well as the leaf biomass that are overestimated by PROMET by a mean of 9 g m^{-2}, which is an enormously good result. Only the recalibrated PROMET, which underestimates the yield by 8 g m^{-2}, is able to achieve a slightly better result. These results indicate that this canopy has developed homogeneously enough that remote sensing data are not really necessary to enhance the results for the mean field values, as far as it can be validated with a limited number of sampling points. However,

Figure 57 and Figure 58 also demonstrate that the modelled yield is lowered at the field margins if remote sensing data are implemented. This is most likely to occur in reality, but cannot be validated with the available field measurements.

Table 32: Coefficients of determination for modelled and measured total and leaf dry biomass at the different sampling points and mean difference [kg m^{-2}] between measurement and model (Field measurement – PROMET) of the maize field in 2004

Total dry biomass	**P1**	**P2**	**P3**	**P4**	**P5**	**Mean**	**Mean diff**
PROMET	0.886	0.897	0.817	0.902	0.907	0.900	-0.009
PROMET + C Jul 21	0.887	0.899	0.817	0.905	0.970	0.962	-0.032
PROMET + A May 25	0.888	0.897	0.817	0.904	0.909	0.962	0.168
PROMET + A May 25 + C Jul 21	0.888	0.897	0.829	0.904	0.971	0.963	0.159
PROMET + C Aug 22	0.886	0.897	0.817	0.902	0.907	0.900	-0.009
$PROMET_{recal}$	0.903	0.910	0.867	0.905	0.971	0.962	0.008

Leaf dry biomass	**P1**	**P2**	**P3**	**P4**	**P5**	**Mean**	**Mean diff**
PROMET	0.945	0.847	0.935	0.866	0.960	0.902	-0.004
PROMET + C Jul 6	0.945	0.947	0.932	0.968	0.960	0.977	-0.005
PROMET + A May 25	0.946	0.946	0.915	0.965	0.963	0.980	0.026
PROMET + A May 25 + C Jul 21	0.946	0.942	0.939	0.967	0.963	0.979	0.024
PROMET + C Aug 22	0.944	0.847	0.936	0.866	0.950	0.902	-0.004
$PROMET_{recal}$	0.957	0.959	0.940	0.973	0.963	0.979	0.002

Source: Own survey

7.2.4 Maize 2005

For the analysis of the largest test field, the maize field 2005, one AVIS and two CHRIS acquisitions are available to implement remote sensing data. CHRIS data are available for June 3 and July 6, which correspond to the developmental stages of early tillering and the end of tillering respectively. A nadir AVIS acquisition is also available for July 6, which was used to calculate the sun chlorophyll and abs respectively, while the CHRIS +36 FZA was used to calculate the shade chlorophyll and abs respectively.

Figure 60 and Table 33 demonstrate that the use of remote sensing data enables the monitoring of heterogeneities occurring within the field throughout the vegetation period. Areas with a reduced development of biomass become apparent, such as the zone with lower productivity in the centre of the field or the linear structure that crosses the field in west-east direction. The latter cannot feasibly be an effect of striping in the CHRIS data, as this feature is visible in both CHRIS acquisitions as well as in the AVIS data. Also, the slightly lowered yield indicates a former field lane, which is now ploughed and used as an agricultural area. The still highly compacted subsoil leads to a slightly reduced plant

development in such areas, which in turn affects the yield. This zone of lower productivity is most prominent if CHRIS data acquired during early tillering are used. This area is still visible when remote sensing data from the end of tillering are used, but is reduced in both size and magnitude (Figure 60). The field measurements, which are presented in Figure 61, confirm that the sampling point located in the low-productive zone is characterized by reduced biomass development throughout the whole vegetation period.

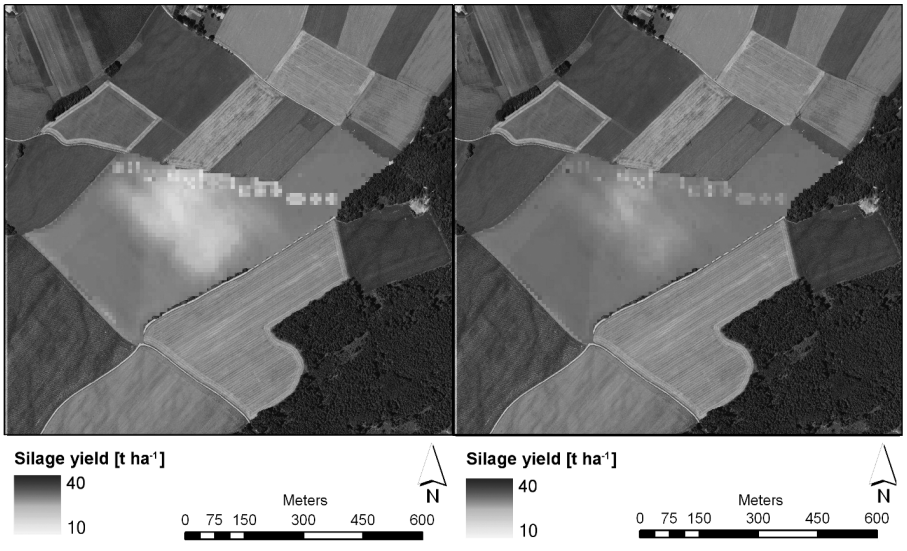

Fig. 60: Modelled yield for maize 2005 using CHRIS data acquired on June 3 (left) and a combination of CHRIS data acquired on June 3 and AVIS/CHRIS data acquired on July 6 (right)

Source: Own survey (figure partly published in OPPELT & HANK 2009)

Table 33 demonstrates that abs_{RS} is also able to model CO_2 assimilation and hence biomass production and yield more accurately, in this case when the remote sensing data acquired on July 6 are implemented. To analyze whether the maize field behaves in the same way as wheat, the total above-ground biomass was also modelled using various values of *abs* as the model state constant. The results, which are presented in Figure 62, demonstrate that the maize canopies do not show light saturation effects, but increasing CO_2 assimilation and biomass production until the maximum *abs* value (*abs* = 1.0) is reached. Therefore, even *abs* values higher than abs_{const} = 0.89 result in higher assimilation rates and a higher yield at the end of the growing season. This behaviour is characteristic for C4 plants, which are adapted to high irradiance, where the CO_2 assimilation is limited by the maximum carboxylation rate of PEPcase and not by the maximum electron transport rate (see section 6.2). Thus PROMET is able to reproduce this behaviour well.

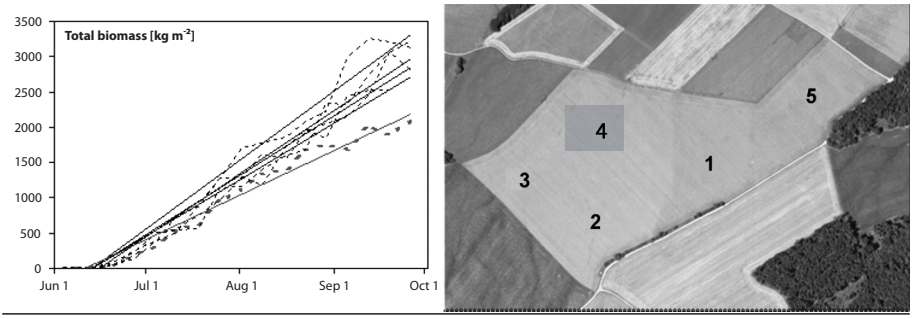

Fig. 61: Field measurements and corresponding trend lines at the different sampling points (this figure can be found as coloured version)
Source: OPPELT and HANK 2009

Table 33: Comparison of modelled yield for maize 2005 using CHRIS (C) and AVIS (A) data of different acquisition dates

Yield [t ha^{-1}]	**Min**	**Max**	**Mean**	**Stdev**	**Field sum [t]**
PROMET	24.8	26.3	25.1	0.24	553.2
PROMET + C Jun 3	7.9	29.8	23.8	4.12	524.1
PROMET + AC Jul 6	18.6	32.6	26.6	1.65	586.3
PROMET + C Jun 3 + AC Jul 6	8.6	37.2	23.9	4.11	526.8

Leaf Biomass [kg m^{-2}]					**Field sum [t]**
PROMET	0.225	0.235	0.227	0.001	50.0
PROMET + C Jun 3	0.076	0.279	0.204	0.034	44.92
PROMET + AC Jul 6	0.176	0.269	0.232	0.011	51.08
PROMET + C Jun 3 + AC Jul 6	0.076	0.279	0.203	0.033	44.70

Source: Own survey

Table 34 demonstrates the very good model results, which were achieved for 2005, when the development of a PROMET pixel is validated using the field measurements at the corresponding sampling point. Again, the model results can be enhanced using the remote sensing data, which becomes apparent at P4, which is located in the low-productive zone. At this sampling point, the high potential of assimilating remote sensing data is manifested. Although the developmental course can be traced very well by the model, which is indicated by the high coefficients of determination, the differences between the modelled and measured yield and leaf dry biomass are higher compared to 2004. Both parameters are underestimated by PROMET, independent of whether abs_{const} or abs_{RS} is used, but the mean difference at the sampling points is reduced when abs_{RS} is implemented. The best results were obtained with the use of the combined AVIS/CHRIS acquisition in July, where PROMET underestimates the yield by 59 g m^{-2} and the leaf biomass by 25 g m^{-2}.

Although these results are not as good as for 2004, the achieved accuracy is still very high.

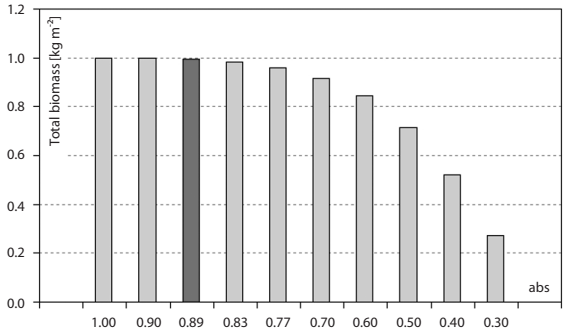

Fig. 62: Influence of abs on the relative total silage yield (total above-ground biomass) modelled with PROMET; absconst according to EVANS (1987) is marked darker

Source: Own survey

Table 34: Coefficients of determination for modelled and measured total and leaf dry biomass at the different sampling points and mean difference [kg m^{-2}] between model and measurement (Field measurement – PROMET) of the maize field in 2005

Total dry biomass	**P1**	**P2**	**P3**	**P4**	**P5**	**Mean**	**Mean diff**
PROMET	0.802	0.883	0.925	0.829	0.924	0.945	0.108
PROMET + C Jun 3	0.928	0.963	0.959	0.921	0.920	0.953	0.095
PROMET + AC Jul 6	0.928	0.961	0.959	0.930	0.929	0.971	0.059
PROMET + C Jun 3 + AC Jul 6	0.928	0.962	0.960	0.932	0.939	0.952	0.095

Leaf dry biomass	**P1**	**P2**	**P3**	**P4**	**P5**	**Mean**	**Mean diff**
PROMET	0.902	0.906	0.916	0.724	0.907	0.946	0.049
PROMET + C Jun 3	0.914	0.915	0.928	0.834	0.907	0.953	0.057
PROMET + AC Jul 6	0.914	0.915	0.926	0.828	0.908	0.951	0.025
PROMET + C Jun 3 + AC Jul 6	0.914	0.915	0.928	0.836	0.908	0.872	0.057

Source: Own survey

8 Synthesis

The aim of the research described in this thesis was to investigate ways in which remote sensing data can provide a spatial distribution of plant chlorophyll, but also a vertical profile through vegetation canopies. The hyperspectral sensors used for this study are the spaceborne CHRIS/Proba and the airborne AVIS, which both offer an angular monitoring of the land surface at various viewing angles. The derived chlorophyll content was assimilated into the raster-based SVAT model PROMET to enable a spatially distributed and dynamic adjustment of model state constants to variables in different canopy layers. The main research issues can be summarized as follows:

1. Do significant differences occur in the biochemical composition at the top of a vegetation canopy and beneath and are there differences between C3 and C4 plants?

2. Does multi-angular hyperspectral remote sensing allow an insight into vegetation canopies to derive the differences of biochemical parameter distribution observed in the field?

3. How do different sensors affect the results?

4. How does the chlorophyll affect photosynthesis in the SVAT model PROMET?

5. What are the advantages of assimilating remotely sensed chlorophyll distributions into PROMET instead of using model state constants and what problems occur?

The previous seven sections have served to delineate and discuss the issues and problems that occurred. Solutions have been suggested to improve understanding of the distribution of biophysical variables in our environment and how it is possible to use this information in the modelling of plant growth and development. In this section, each of the issues mentioned above is summarized, presenting the main results and offering suggestions for further studies.

8.1 Distribution of chlorophyll within vegetation canopies

Field measurements (section 3) were conducted regularly in 2004 and 2005 for wheat (*Triticum aestivum* L.) and maize (*Zea mays* L.) canopies, whereby the former represents the C3 and the latter the C4 photosynthetic pathway. The analysis was performed for the chlorophyll content of the leaves, because the leaves are the organs responsible for photosynthesis and thus contain the highest proportion of chlorophyll within the plant. The field measurements demonstrate that significant differences occur between the chlorophyll content at the top of a canopy and in lower levels of a plant stand. These differences

are due to the illumination conditions within the canopy, which result in a differentiation into two canopy levels, i.e. the sun and shade layer. The former is mainly influenced by direct radiation, whereas the latter is dominated by diffuse radiation, which is scattered, transmitted or reflected by other organs of that particular plant and/or other plants. The chlorophyll content exhibits distinct variations within the growing period, whereby the main increases are due to fertilization. The gradient of the increase and the reaction time of the plants to fertilization in turn depend on environmental factors such as irradiance, precipitation and temperature. These results are embedded in a controversial discussion about chlorophyll contents of sun and shade leaves as being morphological adaptations or effects of metabolic regulations by the plant. However, the results found in the scope of this study confirm the point that plants are able to regulate the chlorophyll content within days in reaction to environmental variations. Thus, mechanisms of chlorophyll regulation or morphological adaptations appear to be highly species-dependent and offer a wide range for future investigation. The results also illustrate the necessity of monitoring not only the spatial distribution of chlorophyll, but also the vertical distribution within a vegetation canopy.

The field measurements, which were conducted in two successive years, also demonstrate that the phenological development of the agricultural plants investigated is stable, even though the weather conditions varied within the two years. Late frosts, which occurred in May 2005, led to a reduced development of biomass, but the phenological development was not affected. This indicates that crops are cultivated in such a manner that they have similar phenological development, and the build-up of biomass is not directly linked to the phenological stages, but is adapted by the plants according to the meteorological situation. These results indicate that the development of a plant canopy via its phenological stage does not necessarily enable an estimation of biomass production at a particular phenological stage.

8.2 Monitoring of vertical chlorophyll distribution using hyperspectral, multi-angular remote sensing

The main hypothesis for this question was that, according to the gap effect, the angular monitoring of erectophile vegetation enables the viewing of lower, less illuminated canopy levels. Due to the lack of data, this hypothesis could previously not be validated. The unique data set gathered during the field campaigns enabled a quantitative validation of the gap effect for the chlorophyll content on the field scale.

The results show that this hypothesis can be confirmed for wheat and maize and multi-angular imagery can be used to derive sun and shade chlorophyll. It is important to note that the results depend strongly on the vegetation anisotropy. As vegetation anisotropy in turn depends on the sensor-sun geometry, the sun-synchronously orbiting CHRIS/PRO-

BA was able to provide a data basis with near-constant sensor and illumination conditions, whereby CHRIS monitors the surface at five different viewing angles (± 55°, ± 36°, ± nadir).

The analysis of the nadir data confirmed previously published results that the top-of-canopy chlorophyll can be estimated using nadir data (OPPELT 2002, OPPELT & MAUSER 2004, OPPELT et al. 2007), whereby the degree of correlation for maize was higher ($r^2 = 0.84$) than for wheat ($r^2 = 0.61$). The results for wheat were improved ($r^2 = 0.69$) when forward-looking nadir data were used for the analysis.

The derivation of shade chlorophyll depends on the degree of anisotropy: the wheat canopies exhibit high anisotropy in the backward-looking FZAs with a hot spot around the -36° view angle. The least anisotropy was observed at the forward FZAs. The analysis of the CHRIS data demonstrates that significant and high correlations for shade chlorophyll exist for the view angles where the anisotropy is low, i.e. forward nadir and +36° FZA. The maize canopies behave similarly, but with a hot spot around the -55° FZA and best results for shade chlorophyll derivation using the +36° and +55° viewing angles. However, if available the +36° FZAs were preferred, because the higher the view angles the lower the spatial resolution.

Unfortunately, the CHRIS data basis is not sufficient to enable a multiple regression approach. The author assumes this approach to be interesting for obtaining higher estimation accuracies using "best-subsets" for the chlorophyll derivation, especially for the maize canopies, which show reasonably high correlations for all forward-viewing FZAs.

8.3 Sensor-dependency of the results

In general, results from hyperspectral indices are influenced by the wavelengths used, but also by the band settings as well as the spectral resolution of the sensor, which often hinders a comparison of results derived with different sensors. In this study an enhancement of an existing index, the Chlorophyll Absorption Integral CAI, was used to minimize sensor influences due to band settings or bandwidth. A direct comparison between results derived with CHRIS and AVIS demonstrated that the different spatial resolutions of the sensors affect the potential to monitor in-field heterogeneities, but the mean field values correspond well (AVIS data range within 1.5 times the standard deviation of CHRIS data). Nevertheless, the higher the spatial resolution the higher is the variance in a field, and the additional use of an airborne sensor with high spatial resolution improves the monitoring of heterogeneities such as low- or high-productive zones and fertilization windows.

The saturation of indices at high chlorophyll contents is known from the literature (OPPELT 2002, HABOUDANE et al. 2002, OPPELT & MAUSER 2004). OPPELT (2002) described

the CAI to become insensitive at chlorophyll a contents higher than 1 g m^{-2}. Saturation effects generally result in an exponential function describing the relationship between the CAI and the chlorophyll content, which form the basis for the results described in the previous sections. However, these saturation limits were not reached during this study.

8.4 Chlorophyll and quantum yield

The model used in this study was the physically-based SVAT model PROMET. PROMET calculates the spatial distribution of water and energy fluxes for variable time steps and spatial scales. The modular assembly of PROMET facilitates the modification of individual components, in this study the vegetation component. The modelling of photosynthesis is based on a biochemical approach that simulates net CO_2 assimilation for C3 plants by a simplified calculation of the Calvin cycle according to the mechanistic model of FARQUHAR et al. (1980). Net assimilation rates of C4 plants are calculated by using the C3 pathway but with an additional C4 cycle in accordance with CHEN et al. (1994), which simulates the fixation of CO_2 by PEPcase. However, both pathways are based on the assumption that electron transport is the key for the utilisation of absorbed photosynthetic active radiation (PAR), which in turn defines quantum yield. The absorbed PAR is calculated using the incoming PAR and an empirically derived model state constant, the leaf absorptance *abs*. Due to the relationship between *abs* and the chlorophyll content, and the regression equations derived between chlorophyll and CAI for the different view angles, the *abs* can be directly related to the CAI values. These direct relationships enable the establishment of spatially distributed CAI, chlorophyll or *abs* maps for both sun and shade canopy layers, whereby the *abs* maps are assimilated in PROMET.

There are many connecting points for future research related to this topic. For example, the relationship between quantum yield and chlorophyll content is, as is the case for most of the state constants, based on laboratory measurements of some specific plant species, which are assumed to be valid for other species. Therefore, a large field for investigation is on the one hand whether these dependencies can be verified for other species or if others would be more appropriate. On the other hand, the underlying relationships are generally derived in the laboratory. The transfer of results derived in the laboratory to field conditions is a difficult task and should therefore not completely dismissed.

8.5. Assimilation of spatially distributed chlorophyll data in PROMET

The approaches for the simulation of CO_2 assimilation used in PROMET are based on the leaf level. The upscaling to canopy photosynthesis is conducted by using the relative leaf area in two canopy layers, i.e. sun and shade layer. Thus, PROMET already uses a two-layer approach to derive canopy photosynthesis, whereby the absorbed PAR is calculated using the leaf absorptance *abs* as a model state constant. The modelling of the C3 and C4

pathways in PROMET results in the calculation of the potential photosynthesis under environmental conditions in terms of radiation, temperature, water availability, O_2 and CO_2 concentrations and sufficient nutrient supply. Therefore, given optimal photosynthetic activity of the plants, the optimum development of biomass and yield is modelled. In general, PROMET was able to trace the development of maize with a high level of accuracy at the mean field scale as well as when the model results are validated using the results of the field measurements (mean field deviation of modelled to measured biomass < 10 %). For wheat canopies, PROMET generally overestimates biomass development and yield by approximately 30 %, because a lack of nutrients, plant infections and mechanical stress cannot be traced. External factors such as varying illumination conditions due to relief, or changes in soil texture or type are traced by the model, but if these external factors vary little within a stand, the field is modelled too homogeneously.

The assimilation of remotely sensed, dynamic *abs* values in PROMET enables the implementation of the "real conditions" at specific dates and thus results in a more realistic modelling of plant development and yield. Different approaches exist to assimilate the remote sensing derivatives in PROMET. The simplest approach is that the remotely sensed data are directly inserted in PROMET, and the model state constant *abs* is made variable. This updating works well if regular remote sensing observations are available throughout the growth cycle. The results for both C3 and C4 plant canopies demonstrate that the replacement of abs_{const} with remotely sensed variable abs_{RS} increases the modelled spatial dynamic in the fields and more accurately models the yield. In this context it is important to note that the quality of the results depend strongly upon the spatial resolution of the sensor as well as upon the dates for which remote sensing acquisitions are available. The former affects the potential to monitor spatial differences and details while the latter affects the amount of biomass modelled in a growing period. When remote sensing data acquired during early developmental stages of the plants are assimilated in PROMET and the remaining growth is simulated using the associated *abs* distribution maps, the resulting modelled biomass and hence yield is underestimated. Analysis at a wheat canopy resulted in an underestimation of the measured yield by the model of 40 %.

To alleviate this problem, which occurs when there is a lack of remote sensing data or a large gap between two acquisitions, abs_{RS} can be reset to abs_{const} after a defined time period. This approach is able to further minimize the error between the model and field measurements and was demonstrated for a maize canopy. If field management data are available, the abs_{const} can be adjusted accordingly. This procedure enables a highly effective and realistic tool for yield prediction, which was demonstrated for a wheat canopy. Using this approach, the best results were derived with a mean deviation of 0.31 t ha^{-1}, which corresponds to an error of 4.5 %.

Moreover, the assimilation of remote sensing data enables the monitoring of heterogeneities within the fields. Areas with reduced plant development, which can be a sign of insufficient nutrient supply, plant infections or stress, can be identified and assigned to the model. In particular, deficiencies in plant vitality, which primarily occur in the shade canopy layer, are useful to detect plant infections, which primarily are visible in this part of a canopy due to the appearance of chlorotic leaves in this canopy layer. If the spatial resolution of the sensor is sufficiently high, windfall areas or fertilization windows can be monitored which also enhances the accuracy of yield forecasts. This result is very promising and leaves plenty of room for future research in the field of precision farming.

The influence of changing abs_{const} values on the model was analyzed by simulating the development of biomass for a growing period using incrementally increasing abs_{const} values. The results demonstrate that for wheat canopies the production of biomass increases continuously with increasing *abs* values until $abs = 0.83$. Further increasing *abs* values result in a decrease in modelled biomass, which indicates that $abs > 0.83$ represents the increasing occurrence of light-saturated conditions. This is the point at which the electron transport-dependent CO_2 assimilation rate changes into a Rubisco-limited assimilation rate. The decrease of biomass development when $abs > 0.83$ is due to the increased probability of light-saturated conditions occurring throughout the vegetation period. This is characteristic behaviour for C3 plants and was not observed for C4, where an increase of abs_{const} results in a continuously higher modelled biomass. The model state constant ($abs_{const} = 0.89$) in PROMET is defined according to results published by EVANS (1987), but the results of this study lead to the proposition that for the modelling of optimum photosynthesis under field conditions, for C3 plants abs_{const} should be modified to 0.83.

The results demonstrate the high potential value of PROMET not only within the scope of precision farming applications; the opportunities to dynamise *abs* are also important for the simulation of landscapes or ecosystems. Thus, the end of this study opens up many new areas for research!

9 References

BACH, H. (1995): Die Bestimmung hydrologischer und landwirtschaftlicher Oberflächenparameter aus hyperspektralen Fernerkundungsdaten. München (Münchner Geographische Abhandlungen 21).

BACH, H. (2007): Macrophytenklassifikation auf Grundlage von Satellitenbildern am Beispiel des Steinhuder Meeres. München. URL: http://www.vista-geo.de/vista/dokumente/Gewaessermonitoring.pdf (Retrieved on: 28.08.2007).

BAEUMER, K. (1992): Allgemeiner Pflanzenbau. Stuttgart.

BALDOCCHI, D. D., B. B. HICKS & P. A. CAMERA (1987): Canopy Stomata Resistance Model for Gaseous Depositions to Vegetated Surfaces. In: Atmospheric Environment 21 (1), pp. 91-101.

BALL, J., I. WOODROW & J. BERRY (1987): A Model Predicting Stomatal Conductance and its Contribution to the Control of Photosynthesis under Different Environmental Conditions. In: Progress in Photosynthesis Research (4), pp. 221-224.

BARRADAS, V. L., H. G. JONES & J. A. CLARK (1999): Leaf Orientation and Distribution in a Phaseolus vulgaris L. Crop and their Relation to Light Microclimate. In: International Journal of Biometeorology 43 (2), pp. 64-70.

BARNSLEY, M., D. ALLISON & P. LEWIS (1997): On the Information Content of Multiple View Angle (MVA) Images. In: International Journal of Remote Sensing 18 (9), pp. 1937-1960.

BARNSLEY, M., J. SETTLE, M. CUTTER, D. LOBB & F. TESTON (2004): The PROBA/CHRIS Mission: A Low-cost Smallsat for Hyperspectral Multiangle Observations of the Earth Surface and Atmosphere. In: IEEE Transactions on Geoscience and Remote Sensing 42 (7), pp. 1512-1520.

Bayerisches Geologisches Landesamt (Ed.) (1986): Standortkundliche Bodenkarte von Bayern 1:500 000, L7932 Fürstenfeldbruck. München.

BERK, A., G. ANDERSON, P. ACHARYA, L. S. BERNSTEIN, J. H. CHETWYND, M. L. HOKE, M. W. MATTHEW, E. P. SHETTLE & S. M. ADLER-GOLDEN (2000): MODTRAN 4 Version 2 User Manual. Air Force Research Laboratory, Space Vehicles Directorate. Massachusetts.

BJÖRKMAN, O. (1981): Responses of Different Quantum Flux Densities. In: Lange, O. L., P. S. Nobel & C. B. Osmond (Eds): Enzyclopedia of Plant Physiology 12. pp. 57-107.

BJÖRKMAN, O. & B. DEMMIG (1987): Photon Yield of O_2 Evolution and Chlorophyll Fluorescence Characteristics at 77 K among Vascular Plants of diverse Origins. In: Planta 170 (4), pp. 489-504.

BLACKBURN, G. A. (1998): Quantifying Chlorophylls and Carotenoids at Leaf and Canopy Scales: An Evaluation of Some Hyperspectral Approaches. In: Remote Sensing of Environment 66 (3), pp. 273-285.

BLACKBURN, G. A. (2006): Hyperspectral Remote Sensing of Plant Pigments. In: Journal of Experimental Botany 58 (4), pp. 1-13.

BROGE, N. H. & J. V. MORTENSEN (2002): Deriving Green Crop Area Index and Canopy Chlorophyll Density of Winter Wheat from Spectral Reflectance Data. In: Remote Sensing of Environment 81 (1), pp. 45-57.

CARTER, G. A. & A. K. KNAPP (2001): Leaf Optical Properties in Higher Plants: Linking Spectral Characteristics to Stress and Chlorophyll Concentrations. In: American Journal of Botany 88 (4), pp. 677-684.

CASA, R. & H. G. JONES (2004): Retrieval of Crop Canopy Properties: A Comparison Between Model Inversion from Hyperspectral Data and Image Classification. In: International Journal of Remote Sensing 25 (6), pp. 1119-1130.

CHAPPELLE, E. W., M. S. KIM & J. E. MCMURTREY (1992): Ratio Analysis of Reflectance Spectra (RARS): An Algorithm for the Remote Estimation of the Concentration of Chlorophyll a, Chlorophyll b and the Carotenoids in Soybean Leaves. In: Remote Sensing of Environment 39 (6), pp. 239-247.

CHEN, D. X., M. B. COUGHENOUR, A. K. KNAPP & C. E. OWENSBY (1994): Mathematical Simulation of C_4 Grass Photosynthesis in Ambient and Elevated CO_2. In: Ecological Modelling 73 (1-2), pp. 63-80.

CHEN, J., JLS. LIU, R. LACAZE & J. ROUJEAN (1999): Daily Canopy Photosynthesis Model Through Temporal and Spatial Scaling for Remote Sensing Applications. In: Remote Sensing of Environment 84 (2-3), pp. 516-525.

CHEN, JM., J. LUI, S. G. LEBLANCE, R. LACAZE & J. ROUJEAN (2003): Multi-angular Optical Remote Sensing for Assessing Vegetation Structure and Carbon Absorption. In: Remote Sensing of Environment 84 (4), pp. 516-525.

CHO, M. & A. SKIDMORE (2006): A New Technique for Extracting the Red Edge Position from Hyperspectral Data: The Linear Extrapolation Method. In: Remote Sensing of Environment 101 (2), pp. 181-193.

CHOPPING, M. J., A. RANGO & K. M. HAVSTAD (2003): Canopy Attributes of Desert Grassland and Transition Communities Derived from Multiangular Airborne Imagery. In: Remote Sensing of Environment 85 (3), pp. 339-354.

COMBAL, B., F. BARET & M. WEISS (2003): Retrieval of Canopy Biophysical Variables from Bidirectional Reflectance – Using Prior Information to Solve the Ill-posed inverse problem. In: Remote Sensing of Environment 84 (1), pp. 1-15.

CURRAN, P. J., J. L. DUNGAN & D. L. PETERSON (2001): Estimating the Foliar Biochemical Concentration of Leaves with Reflectance Spectrometry. In: Remote Sensing of Environment 76 (3), pp. 349-359.

CURTIS, B. C., S. RAJARAM & H. G. MACPHERSON (2002): Bread Wheat – Improvement and Production. Rome (FAO Plant Production and Protection Series 30).

DATT, B. (1998): Remote Sensing of Chlorophyll a, Chlorophyll b, Chlorophyll a+b, and Total Caro-tenoid Content in Eucalyptus Leaves. In: Remote Sensing of Environment 66 (29), pp. 111-121.

DAVIES, KM. (2004): Plant Pigments and their manipulation. Annual Plant Reviews, Volume 14. Oxford.

DEERING, D., E. MIDDLETON & J. IRONS (2005): Prairie Grassland Bidirectional Reflectances Measured by Different Instruments at the FIFE Site. In: Journal of Geophysical Research 97 (D17), pp. 18, 887-18, 903.

DINER, D. J., B. H. BRASWELL & R. DAVIES (2005): The Value of Multiangle Measurements for Retrieving Structurally and Radiatively Consistent Properties of Clouds, Aerosols, and Surfaces. In: Remote Sensing of Environment 97 (4), pp. 495-518.

DÖHLER, H. (2007): Energiepflanzen. Darmstadt.

European Space Agency (1999): Exploitation of CHRIS Data from the Proba Mission for Science and Applications. Experimenters Handbook, Issue 4: Baseline Programme.

EVANS, J. R. (1983): Nitrogen and Photosynthesis in the Flag Leaf of Wheat (Triticum aestivum L.). In: Plant Physiology 72 (2), pp. 297-302.

EVANS, J. R. (1987): The Dependence of Quantum Yield on Wavelength and Growth Irradiance. In: Australian Journal of Plant Physiology 14 (1), pp. 69-79.

EVANS, J. R. (1989): Photosynthesis and Nitrogen Relationships in Leaves of C3 Plants. In: Oecologica 78 (1), pp. 9-19.

EVANS, J. R., I. JAKOBSEN & E. ÖGREN (1993): Photosynthetic Light Response Curves, 2. Gradients of Light Absorption and Photosynthetic Capacity. In: Planta 189 (2), pp. 191-200.

FALGE, E. (1997): Die Modellierung der Kronendachtranspiration von Fichtenbeständen (Picea abies (L.) Karst.) mit unterschiedlichen Modellierungsansätzen. Bayreuth (Bayreuther Forum Ökologie 48).

FARQUHAR, G. D., S. VON CAEMMERER & J. A. BERRY (1980): A Biochemical Model of Photosynthetic CO_2 Assimilation in Leaves of C3 Species. In: Planta 149 (1), pp. 78-90.

FARQUHAR G. D. & S. VON CAEMMERER (1982): Modelling of Photosynthetic Responses to Environmental Conditions. In: LANG O. K., P. S. NOBEL & C. B. OSMOND (Eds.): Encyclopedia of Plant Physiology, New Series, 12B. Berlin, pp. 550-587.

FARQUHAR, G. D. & C. S. WONG (1984): An Empirical Model of Stomatal Conductance. In: Australian Journal of Plant Physiology 11 (3), pp. 191–210.

FARQUHAR, G. D., S. VON CAEMMERER & J. A. BERRY (2001): Models of Photosynthesis. In: Plant Physiology 125 (1), pp. 42-45.

FIELD C. & H. A. MOONEY (1986): The Photosynthesis-nitrogen Relationship in Wild Plants. In: GIVINISH, T. J. (Eds.): On the Economy of Plant Form and Function. Cambridge, pp. 25-55.

FILELLA, I., L. SERRANO, J. SERRA & J. PEÑUELAS (1995): Evaluating Wheat Nitrogen Status with Canopy Reflectance Indices and Discriminant Analysis. In: Crop Science 35 (5) pp. 1400-1405.

FURBANK, R. T. & W. C. TAYLOR (1995): Regulation of Photosynthesis in C3 and C4 Plants: A Molecular Approach. In: The Plant Cell 7 (7), pp. 797-807.

FURBANK, R. T. (1997): C4 pathway. In: Raghavendra, A. S. (Eds.): Photosynthesis. Cambridge, pp. 123-135.

GALVAO, L., F. PONZONI, J. EPIPHANIO, B. RUDORFF & A. FORMAGGIO (2004): Sun and View Angle Effects on NDVI Determination of Land Cover Types in the Brazilian Amazon Region with Hyperspectral Data. In: International Journal of Remote Sensing 25 (10), pp. 1861-1879.

GAMON, J. A., C. B. FIELD, W. BILGER, O. B. BJÖRKMAN, A. L. FREDEEN & J. PEÑUELAS (1990): Remote Sensing of the Xanthophyll Cycle and Chlorophyll Fluorescence in Sunflower Leaves and Canopies. In: Oecologica 85 (1), pp. 1-7.

GARCIA, J. C. & J. MORENO (2004): Removal of Noises in CHRIS/PROBA Images: Application to the SPARC Campaign Data. Proc. of the 2nd CHRIS/PROBA workshop. ESA/ESRIN, Frascati (I), April 28 - 30 2004 (ESA SP-578).

GENTY, B., J. M. BRIANTAIS & N. BAKER (1989): The Relationship Between the Quantum Yield of Photosynthetic Electron Transport and Quenching of Chlorophyll Fluorescence. In: Biochimica Biophysica Acta (990), pp. 87-92.

GITELSON, A. A. & M. N. MERZLYAK (1997): Remote Estimation of Chlorophyll Content in Higher Plant Leaves. In: International Journal of Remote Sensing 18 (12), pp. 2691-2697.

GITELSON, A. A., A. VINA, V. CIGANDA, D. C. RUNDQUIST & T. J. ARKEBAUER (2005): Remote Estimation of Canopy Chlorophyll Content in Crops. In: Geophysical Research Letters 32 (5), pp. 1-4.

GOBRON N., B. PINTY, M. W. VERSTAETE, J. L. WIDLOWSKI & D. D. DINER (2002): Uniqueness of Multiangular Measurements – Part II: Joint Retrieval of Vegetation Structure and Photosynthetic Activity from MISR. In: IEEE Transactions on Geoscience and Remote Sensing 40 (7), pp. 1574-1592.

GRAUL, H. (1962): Naturräumliche Gliederung Deutschlands – die naturräumlichen Einheiten auf Blatt 180 Augsburg. Bundesanstalt für Länderkunde und Raumforschung, Bad Godesberg.

GROTTENTHALER, W. (1980): Geologische Karte von Bayern 1:25 000 – Erläuterungen zu, Blatt Nr. 7833 Fürstenfeldbruck. Bayerisches Geologisches Landesamt, München.

HANK T., N. OPPELT & W. MAUSER (2007): Physically Based Modeling of Photosynthetic Processes. In: STAFFORD, J. V. (Eds.). Precision Agriculture '07. Wageningen, pp. 165-172.

HANK T. (2008): Physically-based Modelling of Photosynthetic Processes and the Impact of Changing Climate to Vegetation. PhD, Ludwig-Maximilians-Universität München (Germany).

HAPKE, B. (1993): The Theory of Reflectance and Emittance Spectroscopy. Cambridge.

HABOUDANE, D., J. MILLER, N. TREMBLAY, P. ZARCO-TEJADA & L. DEXTRACE (2002): Integrated Narrow-band Vegetation Indices for Prediction of Crop Chlorophyll Content for Application to Precision Agriculture. In: Remote Sensing of Environment 81 (2-3), pp. 416-426.

HATCH, M. D. (1988): C4 Photosynthesis: A Unique Blend of Modified Biochemistry, Anatomy and Ultrastructure. In: Biochemical Biophysical Acta (895), pp. 81-106.

HOGE, F. E., P. E. LYON, R. N. SWIFT, J. K. YUNGEL & M. R. ABBOTT (2003): Validation of Terra-MODIS Phytoplankton Chlorophyll Fluorescence Line Height. In: Applied Optics 42 (15), pp. 2767-2771.

HOPKINS, W. G. (1995): Introduction to Plant Physiology. New York.

HU, C. M., F. E. MULLER-KARGER, C. TAYLOR, K. L. CARDER, C. KEBLE, E. JOHNS & C. A. HEIL (2005): Red Tide Detection and Tracing Using MODIS Fluorescence Data. A Regional Example in SW Florida Coastal Water. In: Remote Sensing of Environment 97 (3), pp. 311-321.

HUBER, S., M. KNEUBÜHLER, B. KOETZ, J. SCHOPFER, N. ZIMMERMANN & K. ITTEN (2008): Contribution of Directional CHRIS/Proba Data for Estimating Canopy Biochemistry in Forest. In: Journal of Applied Remote Sensing (In Review).

JACQUEMOUD, S. & F. BARET (1990): PROSPECT: A Model of Leaf Optical Properties Spectra. In: Remote Sensing of Environment (34), pp. 75-91.

JAGO, R., M. CUTLER & P. CURRAN (1999): Estimating Canopy Chlorophyll Concentration from Field and Airborne Spectra. In: Remote Sensing of Environment 68 (3), pp. 217-224.

JARVIS P. G. & J. I. MORISSON (1981): The Control of Transpiration and Photosynthesis by Stomata. In: JARVIS, P. G. & T. A. MANSFIELD (Eds.): Stomatal Physiology. Cambridge, pp. 248-279.

JONES, H. G., N. ARCHER, E. ROTENBERG & R. CASA (2003): Radiation Measurement for Plant Ecophysiology. In: Journal of Experimental Botany 54 (384), pp. 879-889.

KAUFMAN, P. B., T. F. CARLSON, P. DAYANANDAN & M. L. EVANS (1989): Plants – Their biology and importance. New York.

KEUR, P., S. HANSEN, K. SCHELDE, A. THOMSEN (2001): Modification of DAISY SVAT Model for Potential Use of Remotely Sensed Data. In: Agricultural and Forest Meteorology 106 (3), pp. 215-231.

KIM M. S., C. S. T. DAUGHTRY, E. W. CHAPPELLE, J. E. MCMURTREY & C. L. WALTHALL (1994): The Use of High Spectral Resolution Bands for Estimating Absorbed Photosynthetically Active Radiation. Proc. of ISPRS 6th Int. Symposium on Physical Measurements and Signatures in Remote Sensing, Val d'Isère (F), pp. 299-306.

KIMES, D. (1983): Dynamics of Directional Reflectance Factor Distributions for Vegetation Canopies. In: Applied Optics 22 (9), pp. 1364-1372.

KNEUBÜHLER, M., B. KOETZ, S. HUBER, J. SCHOPFER, R. RICHTER &K. ITTEN (2006): Monitoring Vegetation Growth using Multi-angular CHRIS/Proba data. Proc. of the IEEE IGARSS 2006, Denver (USA), pp. 2677-2680.

KOETZ, B., M. KNEUBÜHLER, J. L. WIDLOWSKI, F. MORSDORF, M. SCHAEPMAN & K. ITTEN (2005): Assessment of canopy structure and heterogeneity from multi-angular CHRIS-PROBA data. Proc. 9th Int. Symposium on Physical Measurements and Signatures in Remote Sensing (ISPMSRS), Beijing (China), pp. 73-78.

KOETZ, B., F. BARET, H. POILVE & J. HILL (2005): Use of Coupled Canopy Structure Dynamic and Radiative Transfer Models to Estimate Biophysical Canopy Characteristics. In: Remote Sensing of Environment 95 (1), pp. 115-124.

KÖPPEN, W. P. & R. GEIGER (1961): Klima der Erde. Darmstadt.

KOKALY, R. F. & R. N. CLARK (1999): Spectroscopic Determination of Leaf Biochemistry Using Band-depth Analysis of Absorption Features and Stepwise Multiple Linear Regression. In: Remote Sensing of Environment 67 (3), pp. 276-287.

KRALL, J. P. & G. E. EDWARDS (1992): Relationship Between Photosystem II Activity and CO2 Fixation in Leaves. In: Plant Physiology 86 (1), pp. 180-187.

KTBL (Kuratorium für Technik und Bauwesen in der Landwirtschaft Ed) (2005): Faustzahlen für die Landwirtschaft. Darmstadt.

KUTSCHERA, U. (2002): Prinzipien der Pflanzenphysiologie. Heidelberg.

LAISK, A. & F. LORETTO (1996): Determining Photosynthetic Parameters from Leaf CO_2 Exchange and Chlorophyll Fluorescence. In: Plant Physiology 110 (3), pp. 903-912.

LAISK, A., H. EICHELMANN, V. OJA, B. RASULOV, E. PADU, I. BICHELE, H. PETTAI & U. KULL (2005): Adjustment of Leaf Photosynthesis to Shade in a Natural Canopy: Rate Parameters. In: Plant, Cell and Environment 28 (3), pp. 375-388.

LARCHER, W. (2003): Physiological Plant Ecology. Berlin.

LAUDIEN R., G. BARETH & G. DOLUSCHITZ (2003): Comparison of remote sensing based analysis of crop diseases by using high resolution multispectral and hyperspectral data – case study: Rhizoctonia solani in sugar beet. Proc. of the 12th Int. Conference on Geoinformatics – Geospatial Information Research: Bridging the Pacific and Atlantic, Gävle (Sweden), pp. 670-676.

LAWLOR, D. W. (2001): Photosynthesis. Oxford.

LFL (Bayerische Landesanstalt für Landwirtschaft und Pflanzenbau) (2008): Sortenberatung Silomais. URL: http://www.lfl.bayern.de/ipz/mais/16422/index.php (Retrieved on: 23.01.2008).

JONES, H., N. ARCHER, E. ROTENBERG & R. CASA (2003): Radiation Measurement for Plant Ecophysiology. In: Journal of Experimental Botany 54 (384), pp. 879-889.

LANDSBERG J. J., S. D. PRINCE, P. C. JARVIS, R. E. MCMURTRIE, R. J. LUXMOORE & B. E. MEDLYN (1996): Energy Conversation and Use in Forests: An Analysis of Forest Production in Terms of Radiation Utilization Efficiency (ε). In: GHOLZ H. L., K. NAKANE & H. SHIMODA (Eds.): The Use of Remote Sensing in the Modelling of Forest Productivity. Dordrecht, pp. 273-298.

LICHTENTHALER, H. K. (1987): Chlorophylls and Carotenoids – Pigments of Photosynthetic Biomembranes. In: Methods in Enzymology (148), pp. 350-382.

LICHTENTHALER, H. K., R. HÁK & U. RINDERLE (1990): The Chlorophyll Fluorescence Ratio F690/F730 in Leaves of Different Chlorophyll Content. In: Photosynthetic Research 25 (3), pp. 295-298.

LICHTENTHALER, H. K., A. A. GITELSON & M. LANG (1996): Non-destructive Determination of Chlorophyll Contents of Leaves of a Green and an Aurea Mutant of Tobacco by Reflectance Measurements. In: Journal of Plant Physiology 148 (3-4), pp. 483-493.

LIESENBERG, V., L. GALVAO & F. PONZONI (2007): Variations in Reflectance with Seasonality and Viewing Geometry: Implications for Classification of Brazilian Savanna Physiognomies with MISR/Terra Data. In: Remote Sensing of Environment 107 (1-2), pp. 276-286.

LUDWIG, R. & W. MAUSER (2000): Modelling Catchment Hydrology within a GIS Based SVAT-Model Framework. In: Hydrology and Earth System Sciences 4 (2), pp. 239-249.

LÜTKE ENTRUP, N. & J. OEHMICHEN (2000): Kulturpflanzen. Gelsenkirchen.

MEIER, U. (Ed.). (2001): Growth Stages of Mono- and Dicotyledonous Plants – BBCH Monograph. Berlin.

MEYNEN, E. & J. SCHMIDHÜSEN (1953): Handbuch der naturräumlichen Gliederung Deutschlands. Bundesanstalt für Landeskunde und Raumforschung. Bad Godesberg.

MAUSER, W. (1991): Modeling the Spatial Variability of Soil Moisture and Evapotranspiration with Remote Sensing Data. Proc. of the International Symposium on Remote Sensing and Water Research, Enschede (NL), pp. 174-182.

MAUSER, W. & S. SCHÄDLICH (1998): Modeling the Spatial Distribution of Evapotranspiration on Different Scales using Remote Sensing Data. In: Journal of Hydrology 212-213 (1-4), pp. 250-267.

MAUSER, W. & H. BACH (2008): PROMET – A Physical Hydrological Model to Study the Impact of Climate Change on the Water Flows of Medium Sized, Complex Watersheds. In: Journal of Hydrology (In review).

MORAN, J. A., A. K. MITCHELL, G. GOODMANSON & K. A. STOCKBURGER (2000): Differentiation Among Effects of Nitrogen Fertilization Treatments in Conifer Seedlings by Foliar Reflectance: A Comparison of Methods. In: Tree Physiology 20 (16), pp. 1113-1120.

NICODEMUS, F., J. RICHMOND, J. HSIA, I. GINSBERG & T. LIMPERIS (1977): Geometrical Considerations and Nomenclature for Reflectance. National Bureau of Standards Monograph. US Government Printing Office.

ÖGREN, E. & J. R. EVANS (1993): Photosynthetic Light Response Curves, 1. The Influence of CO_2 Partial Pressure and Leaf Inversion. In: Planta 189 (2), pp. 182-190.

OPPELT, N. & W. MAUSER (2001): The Chlorophyll Content of Maize (Zea Mays) derived with the Airborne Imaging Spectrometer AVIS. Proc. of ISPRS 8th International Symposium "Physical Measurements and Signatures in Remote Sensing, Aussoir (F), pp. 407-412.

OPPELT, N. (2002): Monitoring of Plant Chlorophyll and Nitrogen Status Using the Airborne Imaging Spectrometer AVIS. Ludwig-Maximilians-Universität München, Faculty for Earth and Environmental Sciences, Munich, 2002.

OPPELT, N. & W. MAUSER (2003): Hyperspectral Remote Sensing – vA Tool for the Derivation of Plant Nitrogen and its Spatial Variability within Maize and Wheat Canopies. In: STAFFORD, J. V. & A. WERNER (Eds.): Precision Agriculture '03. Wageningen, pp. 493-498.

OPPELT, N. & W. MAUSER (2004): Hyperspectral Monitoring of Physiological Parameters of Wheat During a Vegetation Period Using AVIS Data. In: International Journal of Remote Sensing 25 (1), pp. 145-160.

OPPELT, N., T. HANK & W. MAUSER (2006): Coupled Analysis of Vegetation Chlorophyll and Water Content Using Hyperspectral, Bidirectional Remote Sensing. Project report for the German Research Foundation (DFG) (OP 92/1-1), 2006.

OPPELT, N. & W. MAUSER (2006): Three Generations of the Hyperspectral Imaging Spectrometer AVIS – Expectations, Applications, Results. Proc. of SPIE conference "Europhotonics Europe", Strasbourg (France), 02.04.-07.04.2006, Vol. 6189, SPIE, Bellingham, Wash. ISBN 97-80819462459.

OPPELT, N. & W. MAUSER (2007a): Characterization of Sun and Shade Chlorophyll in Wheat Using Angular CHRIS/Proba Data. ESA Envisat Symposium, Montreux 23-27 April, 2007a. ESA publication SP-636 (CD-ROM).

OPPELT, N. & W. MAUSER (2007b): The Airborne Imaging Spectrometer AVIS: Design, Characterization and Calibration. In: Sensors 7 (9), pp. 1934-1953.

OPPELT, N., T. HANK & W. MAUSER (2007): Assessment of Vertical Variation of Chlorophyll Using Hyperspectral, Multi-angular Imagery. In: Stafford, J. V. (Ed.). Precision Agriculture '07. Wageningen, pp. 181-188

OPPELT, N. (2008): Vertical Profiling of Vegetation Canopies Using Multi-angular Remote Sensing Data. In: Canadian Journal of Remote Sensing 34 (2), pp. 314-325.

OPPELT, N. & T. HANK, (2009): Improved Modelling of Maize Growth by Combining a Biophysical Model of Photosynthesis with Hyperspectral Remote Sensing. In: HENTEN, E. J., D. GOENSE & C. LOKHORST (Eds.): Precision Agriculture 09, Wageningen Academic Publishers, pp. 133-140.

OPPELT, N. (2009): Wheat Growth Modelling by a Combination of a Biophysical Model Approach and Hyperspectral Remote Sensing Data. Proc. SPIE Eur. Remote Sens., 31.08.-3.09.2009, Berlin (Germany) 7472 (doi:10.1117/12.830322).

OPPELT, N. (2010): The use of remote sensing data to assist crop modelling under climate change conditions. In: Journal of Applied Remote Sensing (In review).

OSMOND, C. B., G. ANANYEV, J. BERRY, P. FALKOWSKI, C. LANGDON, G. LIN & R. MONSON (2004): Changing the Way we think about Global Change Research: Scaling Up in Experimental Ecosystem Science. In: Global Change Biology 10 (4), pp. 393-407.

PEARCY, R. W. (1990): Sunflecks and Photosynthesis in Plant Canopies. In: Annual Review of Plant Physiology and Plant Molecular Biology 41, pp. 421-453.

PEÑUELAS, J., F. BARET & I. FILELLA (1995): Semi-empirical Indices to Assess Carotenoids/Chlorophyll a Ratio from Leaf Spectral Reflectance. In: Photosynthetica 31 (2), pp. 221-230.

PORRA, R. J., P. E. KRIEDMAN & W. A. THOMSON (1989): Determination of Accurate Extinction Coefficients and Simultaneous Equations for Assaying Chlorophyll a and b Extracted with Four Different Solvents: Verification of the Concentration of Chlorophyll Standards by Atomic Absorption Spectroscopy. In: Biochimica et Biophysica Acta 975, pp. 384–394.

RICHARDS, J. T., A. C. SCHURGER, G. CHAPPELLE & J. A. GUIKEMA (2003): Laser-Induced Fluorescence Spectroscopy of Dark and Light Adapted Bean (Phaseolus vulgaris L.) and Wheat (Triticum aestivum L.) Plants Grown Under Three Irradiance Levels and Subjected to Fluctuating Conditions. In: Remote Sensing of Environment 84 (3), pp. 323-341.

RICHARDSON, A. D., S. P. DUIGAN & G. P. BERLYN (2002): An Evaluation of Non-invasive Methods to Estimate Foliar Chlorophyll Content. In: New Phytologist 153 (1), pp. 185-194.

SANDMEIER, S., C. MÜLLER, B. HOSGOOD & G. ANDREOLI (1998): Sensitivity Analysis and Quality Assessment of Laboratory BRDF Data. In: Remote Sensing of Environment 64 (2), pp. 176-191.

SANDMEIER, S., E. MIDDLERTON, D. DEERING & W. QIN (1999): The Potential of Hyperspectral Bidirectional Reflectance Distribution Function Data for Grass Canopy Characteristics. In: Journal of Geophysical Research 104 (D8), pp. 9547-9560.

SANDMEIER, S. R. & K. I. ITTEN (1999): A field Goniometer System (FIGOS) for Acquisition of Hyperspectral BRDF Data. In: IEEE Transactions on Geoscience and Remote Sensing 37 (2), pp. 978-986.

SARI, M., N. K. SOMNEZ & A. KURKLU (2005): Determination of Seasonal Variations in Solar Energy Utilization by the Leaves of Washington Navel Orange Trees (Citrus sinensis L. Osbeck). In: International Journal of Remote Sensing 26 (15), pp. 3295-3307.

SCHAEPMAN, M., B. KOETZ, G. SCHAEPMAN-STRUB & K. ITTEN (2005): Spectrodirectional Remote Sensing for the Improved Estimation of Biophysical and Chemical Variables: Two Case Studies. In: Journal of Applied Earth Observation and Geoinformation 9, pp. 204-223.

SCHAEPMAN-STRUB, G., M. SCHAEPMAN, T. PAINTER, S. DANGEL & J. MARTONCHIK (2006): Reflectance Quantities in Optical Remote Sensing – Definitions and Case Studies. In: Remote Sensing of Environment 103 (1), pp. 27-42.

SCHEIBER, R., N. OPPELT & W. MAUSER (2005): AquiferEx Optical and Radar Campaign – Experiment Plan. European Space Agency, ESRIN.

SCHEIBER, R., N. OPPELT, R. HORN, I. HAJNSEK, K. BEN KHADRA, M. KELLER, S. WEGSCHEIDER, W. MAUSER & R. BIANCHI (2006): AquiferEx Optical and Radar Campaign: Objectives and First Results. Proc. 6th European Conference on Synthetic Aperture Radar, Dresden May 16-18. CD-ROM publication ISBN 3-8007-2960-1.

SCHEIBER, R., I. HAJNSEK, R. HORN, N. OPPELT, W. MAUSER, B. BEN BACCAR & R. BIANCHI (2007): AquiferEx: Results of the Optical and Radar Campaign in Tunisia. Proc. of the POLinSar Workshop, Frascati (Italy) January 22-24. ESA publication SP-644 (CD-ROM).

SCHLÄPFER, D., J. NIEKE & K. I. ITTEN (2007): Spatial PSF Nonuniformity Effects in Airborne Pushbroom Imaging Spectrometry Data. In: IEEE Transactions on Geoscience and Remote Sensing 45 (2), pp. 458-468.

SCHMIDTLEIN, S. & J. SASSIN (2004): Mapping of Continuous Floristic Gradients in Graslands Using Hyperspectral Imagery. In: Remote Sensing of Environment 92 (1), pp. 126-138.

SCHMIDTLEIN, S., P. ZIMMERMANN, R. SCHÜPFERLING & C. WEISS (2007): Mapping of Floristic Continuum. Ordination Space Position Estimated from Imaging Spectroscopy. In: Journal of Vegetation Science 18 (1), pp. 131-140.

SCHOPFER, J., N. OPPELT, T. SCHNEIDER, W. DORIGO, M. KNEUBUEHLER & K. ITTEN (2007): Towards a Comparison of Spaceborne and Ground-based Spectro-directional Reflectance Data. ESA Envisat Symposium, Montreux 23-27 April. ESA publication SP-636 (CD-ROM). ISBN 92-9291-200-1.

SCHURR, U., A. WALTER & U. RASCHER (2006): Functional Dynamics of Plant Growth and Photosynthesis – From Steady State to Dynamics – From Homogeneity to Heterogeneity. In: Plant, Cell and Environment 29 (3), pp. 340-352.

SHAPIRO, S., M. WILK & H. CHEN (1968): A Comparative Study of Various Tests of Normality. In: Journal of the American Statistical Association 63 (324), pp. 1343-1372.

SIMS, D. & J. GAMON (2002): Relationships Between Leaf Pigment Content and Spectral Reflectances Across a Wide Range of Species, Leaf Structures and Developmental Stages. In: Remote Sensing of Environment 81 (2), pp. 337-354.

SIRA Technology Ltd. (2002): CHRIS data format. Issue 1.

SIRA Technology Ltd. (2004): CHRIS data format. Issue 4.1.

SMITH, H. & G. C. WHITELAM (1997): The Shade Avoidance Syndrome: Multiple Responses Mediated by Multiple Phytochromes. In: Plant Cell Environment 20 (6), pp. 840–844.

TERASHIMA, I. & K. HIOSAKA (1995): Comparative Ecophysiology of Leaf and Canopy Photosynthesis. In: Plant, Cell and Environment 18 (10), pp. 1111-1128.

THAYER, S. S. & O. BJÖRKMAN (1990): Leaf Xanthophylls Content and Composition in Sun and Shade Determined by HPLC. In: Photosynthetic Research 23 (3), pp. 331-343.

USTIN, S., D. ROBERTS, J. GAMON, G. P. ASNER, G. P. GREEN & R. GREEN (2004): Using Imaging Spectroscopy to Study Ecosystem Properties and Processes. In: Bioscience 54 (6), pp. 523-534.

VERHOEF, W. & H. BACH (2003): Simulation of Hyperspectral and Directional Radiance Images Using Coupled Biophysical and Atmospheric Radiative Transfer Models. In: Remote Sensing of Environment 87 (1), pp. 32-41.

VERHOEF, W. & H. BACH (2007): Coupled Soil-Leaf-Canopy and Atmosphere Radiative Transfer Modelling to Simulate Hyperspectral Multi-angular Surface Reflectance and TOA Radiance Data. In: Remote Sensing of Environment 109 (2), pp. 166-182.

VERRELST, J., B. KÖTZ, M. KNEUBÜHLER & M. SCHAEPMAN (2006): Directional Sensitivity Analysis of Vegetation Indices from Multi-angular CHRIS/Proba Data. ISPRS midterm Symposium 2006 for remote sensing: from pixels to processes, 8-11 May, Enschede (NL), pp. 7-14.

VOGELMAN, J. E., B. N. ROCK & D. M. MOSS (1993): Red Edge Spectral Measurements from Sugar Maple Leaves. In: International Journal of Remote Sensing 14 (8), pp. 1563-1575.

VON CAEMMERER, S. (2000): Biochemical Models of Leaf Photosynthesis. Collingwood.

WEISS, M., F. BARET, R. MYNENI, A. PRAGNERE & Y. KNYAZIKHIN (2000): Investigation of a Model Inversion Technique to Estimate Canopy Biophysical Variables from Spectral and Directional Reflectance Data. In: Agronomie 20, pp. 3-22.

WEISS, M., D. TROUFLEAU, F. BARET, H. CHAUKI, L. PREVOT, A. OLIOSO, N. BRUGUIER & N. BRISSON (2001): Coupling Canopy Functioning and Radiative Transfer Models for Remote Sensing Data Assimilation. In: Agricultural and Forest Meteorology 108 (2), pp. 113-128.

WIDLOWSKI, J., B. PINTY, N. GOBRON, J. VERTRAETE, E. DINER & A. DAVIS (2004): Canopy Structure Parameters Derived from Multi-angular Remote Sensing Data for Terrestrial Carbon Studies. In: Climatic Change 67 (2-3), pp. 403-415.

YODER, B. & R. PETTRIGREW-CROSBY (1995): Predicting Nitrogen and Chlorophyll Content and Concentrations from Reflectance Spectra (400-2500nm) at Leaf and Canopy Scales. In: Remote Sensing of Environment 53 (3), pp. 191-211.

ZARCO-TEJADA, P., J. R. MILLER, G. H. MOHAMMED & T. L. NOLAND (2000): Chlorophyll Fluorescence Effects on Vegetation Apparent Reflectance. In: Remote Sensing of Environment 74 (3), pp. 596-608.

ZARCO-TEJADA, P., A. BERJONC & R. LOPEZ-LOZANO (2005): Assessing Vineyard Condition with Hyperspectral Indices: Leaf and Canopy Reflectance Simulation in a Row Structured Discontinuous Canopy. In: Remote Sensing of Environment 99 (3), pp. 271-287.

ZHAO, D., K. R. REDDY, V. G. KAKANI, J. J. READ, G. A. CARTER (2003): Corn (Zea mays L.) Growth, Leaf Pigment Concentration, Photosynthesis and Leaf Hyperspectral Reflectance Properties as Affected by Nitrogen Supply. In: Plant and Soil 257 (1), pp. 205-217.

ZMP (Zentrale Markt- und Preisberichtsstelle des Statistischen Bundesamtes) (2007): Agrarmärkte in Zahlen/Deutschland. Bonn.

Appendix

List of symbols, variables and constants

A	[µMol m^{-2} s^{-1}]	Net CO_2 assimilation rate
A_a	[%]	Absorption at 663.6 nm
A_b	[%]	Absorption at 646.6 nm
abs	[dimensionless]	Leaf absorptance
abs_{const}	[dimensionless]	Constant leaf absorptance (0.89 according to EVANS 1987)
abs_{RS}	[dimensionless]	Remotely sensed leaf absorptance
α_p	[µMol m^{-2} s^{-1}]	Empirical parameter (0.0913 according to CHEN et al. 1994)
$ANIF$	[dimensionless]	Anisotropy factor
BM_{dry}	[g m^{-2}]	Dry matter
BM_{wet}	[g m^{-2}]	Wet biomass (wet matter)
$brdf$	[sr^{-1}]	Bidirectional reflectance distribution function
brf	[dimensionless]	Bidirectional reflectance factor
C_i	[ppm]	Internal concentration of CO_2 in the intercellular air spaces
C_m	[µMol m^{-2} s^{-1}]	CO_2 concentration in the mesophyll
$chl\ a$	[µg g^{-1}] or [mg m^{-2}]	Chlorophyll a content
$chl\ b$	[µg g^{-1}] or [mg m^{-2}]	Chlorophyll b content
D	[%]	Absorption depth
D_c	[%]	Absorption depth at the centre of an absorption feature
D_n	[dimensionless]	Normalized absorption depth
DC	[digital number]	Dark current
DN	[digital number]	Grey value
DN_{ref}	[digital number]	Grey value measured on the reflectance panel
E_i	[W m^{-2} nm^{-1}]	Hemispherical irradiance
$Est.err$		Estimation error Est.err= $(\sigma^2 /N)^{0.5}$
FOV	[rad] or [°]	Field of View
H	[m]	Aircraft altitude above ground
i	[s^{-1}]	Frame rate
I_2	[µMol quanta^{-1} m^{-2} s^{-1}]	PAR absorbed by PSII
I_P	[µMol m^{-2} s^{-1}]	Incident PAR
J	[µMol quanta^{-1} m^{-2} s^{-1}]	Electron transport

J_{max}	[µMol quanta^{-1} m^{-2} s^{-1}]	Maximum electron transport
K_c	[µl l^{-1} O_2]	Michaelis constant for RUBISCO carboxylation
K_o	[ml l^{-1} CO_2]	Michaelis constant for RUBISCO oxygenation
K_p	[µMol m^{-2} s^{-1}]	Michaelis constant for PEPcase
L	[W m^{-2} sr^{-1} nm^{-1}]	Sensor radiance
N		Number of samples
O	[ml l^{-1}]	Internal concentration of O_2 in the intercellular air spaces
P	[dimensionless]	Probability of rejecting a null-hypothesis
PM	[N m^{-1}]	Number of plants along a sowing row
φ_i	[°]	Sun azimuth angle
Φ_r	[°]	View azimuth angle
θ	[dimensionless]	Curvature factor (θ = 0.7 according to EVANS (1987))
θ_i	[°]	Sun zenith angle
θ_r	[°]	View zenith angle
R	[%]	Spectral reflectance
R'	[%]	Continuum-removed reflectance
R_d	[µMol m^{-2} s^{-1}]	Day respiration
RD	[m]	Row distance
SW_{dry}	[g]	Sampling mass of dry biomass
SW_{wet}	[g]	Sampling mass of wet biomass
v	[m s^{-1}]	Velocity
V_C	[µMol m^{-2} s^{-1}]	Carboxylation rate of Rubisco
V_j	[µMol m^{-2} s^{-1}]	Carboxylation rate of RuBP
V_{pm}	[µMol m^{-2} s^{-1}]	Maximum carboxylation rate of PEPcase
V_{cmax}	[µMol m^{-2} s^{-1}]	Maximum rate of carboxylation
vol	[ml]	Final volume where chlorophyll is dissolved
w_i	[g]	Initial mass of the solved plant powder for chlorophyll analysis
σ		Standard deviation
σ^2		Variance
λ	[nm]	Wavelength

List of plant and soil variables used in PROMET

Plant variables

Leaf mass per leaf area	[kg m^{-2}]
Day of sowing	[DOY]
Day of harvest	[DOY]
Width of leaf	[m]
Carboxylation capacity at 25° C	[µMol m^{-2} s^{-1}]
Maximum rate of electron transport	[µMol quanta m^{-2} s^{-1}]
Michaelis constant for O_2	[dimensionless]
Michaelis constant for C	[dimensionless]
Respiration capacity at 25° C	[µMol quanta m^{-2} s^{-1}]
Fraction of day respiration	[dimensionless]
Light use efficiency	[µMol quanta m^{-2} s^{-1}]
Ball-Berry coefficient of stomatal conductance	[dimensionless]
Minimum leaf conductance through cuticle	[mMol m^{-2} s^{-1}]
Leaf-internal concentration of O_2	[ml l^{-1}]
Cardinal temperatures	[°C]
Vernalisation temperatures	[°C]
Maximum root depth	[cm]
Leaf mass per leaf area	[kg m^{-2}]
Day of sowing	[DOY]
Day of harvest	[DOY]
Width of leaf	[m]
Carboxylation capacity at 25° C	[µMol quanta m^{-2} s^{-1}]
Max. rate of electron transport at PSII at 25°C	[µMol quanta m^{-2} s^{-1}]
Temperature sum for emergence	[° C]

Soil variables

Number of layers	[dimensionless]
Soil temperature	[°C]
Ground water level	[m]
Permeability	[cm sec^{-1}]
Eff. pore volume	[%]
Pore size distr. index	[dimensionless]
Bubbling pressure head	[dimensionless]
Layer thickness	[cm]
Clay content	[m^3 m^{-3}]

Sand content	[$m^3\ m^{-3}$]
Organic matter	[$m^3\ m^{-3}$]
Retention water content	[%]
Cumulative pore volume	[%]
Initial Pf-value	[Pf]

Glossary

ALADIN	Coupled **A**nalysis of ch**l**orophyll and w**a**ter status of vegetation using hyperspectral, bi-**di**rectional remote se**n**sing
ANIF	**Ani**sotropy **f**actor
ATP	**A**denosine **T**ri**P**hosphate
AVIS	**A**irborne **V**isibel/**I**nfrared imaging **S**pectrometer
AVIRIS	**A**irborne **V**isible, **I**nfra**r**ed **I**maging **S**pectrometer
BBCH	Federal **B**iological Research Centre for Agriculture and Forestry, German Federal Office of Plant Varieties and German Agrochemical Association (**B**iologische Bundesanstalt für Land- und Forstwirtschaft, **B**undessorten amt und **Ch**emische Industrie)
bgr	**B**lue, **g**reen and **r**ed band
bmb+f	German federal ministry of education and research (**B**undes**m**inisterium für **B**ildung und **F**orschung)
brdf	**b**i-directional **r**eflectance **d**istribution **f**unction
bw	**b**ack**w**ard
C	**C**arbon
C3	Photosynthetic pathway with a 3-carbon primary compound
C4	Photosynthetic pathway with a 4-carbon primary compound
CAI	**C**hlorophyll **A**bsorption **I**ntegral
CHRIS	**C**ompact **H**igh **R**esolution **I**maging **S**pectrometer
CO_2	**C**arbon di**o**xide
cv	**c**ulti**v**ar
DEM	**D**igital **E**levation **M**odel
DFG	German Research Foundation (**D**eutsche **F**orschungs**g**emeinschaft)
dGPS	**d**ifferential **G**lobal **P**ositioning **S**ystem
DWD	German weather service (**D**eutscher **W**etter**d**ienst)
Est.err	**est**imation **err**or
fAPAR	**f**raction of **a**bsorbed **p**hotosynthetically **a**ctive **r**adiation
FOV	**F**ield **o**f **V**iew
Fw	**F**or**w**ard
FZA	**F**ly-by **z**enith **a**ngle
GAP	**G**lycer**a**ldehydes-3-**p**hosphate
GLOWA	**Glo**baler Wandel des **Wa**sserkreislaufs (Global change and the hydrological cycle)
GPS	**G**lobal **p**ositioning **s**ystem
GSD	**G**round **s**ampling **d**istance
HDF	**H**ierarchical **d**ata **f**ormat
HYMap	**HY**perspectral **Map**ping
INS	**I**nertia **n**avigation **s**ystem

LAI	**L**eaf **A**rea **I**ndex
LUE	**L**ight **u**se **e**fficiency
m a.s.l.	**M**eters **a**bove **s**ea **l**evel
MISR	**M**ultiangle **I**maging **S**pectro**R**adiometer
MODIS	**Mod**erate **I**maging **S**pectrometer
MZA	**M**inimum **z**enith **a**ngle
N	**N**itrogen
NADPH	**N**icotinamide-**a**denine **d**inucleotide **ph**osphate
NIR	**N**ear **i**nfra**r**ed spectral domain
n.s.	**n**ot **s**ignificant
O_2	Molecular **O**xygen
OAA	**O**bservation **a**zimuth **a**ngle
OZA	**O**bservation **z**enith **a**ngle
PAR	**P**hotosynthetically **a**ctive **r**adiation
PCR	**P**hotosynthetic **c**arbon **r**eduction
PEP	**P**hospho**e**nyl**p**yruvate
PEPcase	**P**hospho**e**nyl**p**yruvate **ca**rboxyla**se**
PGA	3-**p**hospho**g**lyceric **a**cid
POLDER-2	**POL**arization and **D**irectionality of the **E**arth's **R**eflectances
PROBA	**Pr**oject for **o**n-**b**oard **a**utonomy
PROMET	**P**rocesses of **r**adiati**o**n, **m**ass and **e**nergy **t**ransfer
RED	**Red** wavelength region
Rubisco	**R**ib**u**lose-1,5-**bis**phosphate **c**arboxylase/**o**xydase
RuBP	**R**ib**u**lose-1,5-**b**is**p**hosphate
stdev	**St**andard **dev**iation
SVAT	**S**oil-**v**egetation-**a**tmosphere **t**ransfer
UTC	**C**oordinated **u**niversal **t**ime
VIS	**Vis**ible spectral domain

Ältere Bände der
Schriften des Geographischen Instituts der Universität Kiel
(Band I, 1932 - Band 43, 1975)
sowie der
Kieler Geographischen Schriften
(Band 44, 1976 - Band 57, 1983)
sind teilweise noch auf Anfrage im Geographischen Institut der CAU erhältlich

Band 58

Bähr, Jürgen (Hrsg.): Kiel 1879 - 1979. Entwicklung von Stadt und Umland im Bild der Topographischen Karte 1:25 000. Zum 32. Deutschen Kartographentag vom 11. - 14. Mai 1983 in Kiel. 1983. III, 192 S., 21 Tab., 38 Abb. mit 2 Kartenblättern in Anlage. ISBN 3-923887-00-0. 14,30 €

Band 59

Gans, Paul: Raumzeitliche Eigenschaften und Verflechtungen innerstädtischer Wanderungen in Ludwigshafen/Rhein zwischen 1971 und 1978. Eine empirische Analyse mit Hilfe des Entropiekonzeptes und der Informationsstatistik. 1983. XII, 226 S., 45 Tab. und 41 Abb. ISBN 3-923887-01-9. 15,30 €

Band 60

*Paffen, Karlheinz und Kortum, Gerhard: Die Geographie des Meeres. Disziplingeschichtliche Entwicklung seit 1650 und heutiger methodischer Stand. 1984. XIV, 293 S., 25 Abb. ISBN 3-923887-02-7.

Band 61

*Bartels, Dietrich u. a.: Lebensraum Norddeutschland. 1984. IX, 139 S., 23 Tab. und 21 Karten. ISBN 3-923887-03-5.

Band 62

Klug, Heinz (Hrsg.): Küste und Meeresboden. Neue Ergebnisse geomorphologischer Feldforschungen. 1985. V, 214 S., 45 Fotos, 10 Tab.und 66 Abb.
ISBN 3-923887-04-3. 19,90 €

Band 63

Kortum, Gerhard: Zuckerrübenanbau und Entwicklung ländlicher Wirtschaftsräume in der Türkei. Ausbreitung und Auswirkung einer Industriepflanze unter besonderer Berücksichtigung des Bezirks Beypazari (Provinz Ankara). 1986. XVI, 392 S., 36 Tab., 47 Abb. und 8 Fotos im Anhang. ISBN 3-923887-05-1. 23,00 €

Band 64

Fränzle, Otto (Hrsg.): Geoökologische Umweltbewertung. Wissenschaftstheoretische und methodische Beiträge zur Analyse und Planung. 1986. VI,130 S., 26 Tab. und 30 Abb.
ISBN 3-923887-06-X. 12,30 €

Band 65

Stewig, Reinhard: Bursa, Nordwestanatolien. Auswirkungen der Industrialisierung auf die Bevölkerungs- und Sozialstruktur einer Industriegroßstadt im Orient. Teil 2. 1986. XVI, 222 S., 71 Tab., 7 Abb. und 20 Fotos. ISBN 3-923887-07-8
19,00 €

Band 66

Stewig, Reinhard (Hrsg.): Untersuchungen über die Kleinstadt in Schleswig-Holstein. 1987. VI, 370 S., 38 Tab., 11 Diagr. und 84 Karten
ISBN 3-923887-08-6. 24,50 €

Band 67

Achenbach, Hermann: Historische Wirtschaftskarte des östlichen Schleswig-Holstein um 1850. XII, 277 S., 38 Tab., 34 Abb., Textband und Kartenmappe.
ISBN 3-923887-09-4. 34,30 €

*= vergriffen

Band 68

Bähr, Jürgen (Hrsg.): Wohnen in lateinamerikanischen Städten - Housing in Latin American cities. 1988. IX, 299 S., 64 Tab., 71 Abb. und 21 Fotos.
ISBN 3-923887-10-8. 22,50 €

Band 69

Baudissin-Zinzendorf, Ute Gräfin von: Freizeitverkehr an der Lübecker Bucht. Eine gruppen- und regionsspezifische Analyse der Nachfrageseite. 1988. XII, 350 S., 50 Tab., 40 Abb. und 4 Abb. im Anhang. ISBN 3-923887-11-6. 16,40 €

Band 70

Härtling, Andrea: Regionalpolitische Maßnahmen in Schweden. Analyse und Bewertung ihrer Auswirkungen auf die strukturschwachen peripheren Landesteile. 1988. IV, 341 Seiten, 50 Tab., 8 Abb. und 16 Karten. ISBN 3-923887-12-4.
15,70 €

Band 71

Pez, Peter: Sonderkulturen im Umland von Hamburg. Eine standortanalytische Untersuchung. 1989. XII, 190 S., 27 Tab. und 35 Abb. ISBN 3-923887-13-2.
11,40 €

Band 72

Kruse, Elfriede: Die Holzveredelungsindustrie in Finnland. Struktur- und Standortmerkmale von 1850 bis zur Gegenwart. 1989. X, 123 S., 30 Tab., 26 Abb. und 9 Karten.
ISBN 3-923887-14-0. 12,60 €

Band 73

Bähr, Jürgen, Christoph Corves und Wolfram Noodt (Hrsg.): Die Bedrohung tropischer Wälder: Ursachen, Auswirkungen, Schutzkonzepte. 1989. IV, 149 S., 9 Tab. und 27 Abb. ISBN 3-923887-15-9 13,20 €

Band 74

Bruhn, Norbert: Substratgenese - Rumpfflächendynamik. Bodenbildung und Tiefenverwitterung in saprolitisch zersetzten granitischen Gneisen aus Südindien. 1990. IV, 191 S. 35 Tab., 31 Abb. und 28 Fotos.
ISBN 3-923887-16-7. 11,60 €

Band 75

Priebs, Axel: Dorfbezogene Politik und Planung in Dänemark unter sich wandelnden gesellschaftlichen Rahmenbedingungen. 1990. IX, 239 S., 5 Tab. und 28 Abb.
ISBN 3-923887-17-5. 17,30 €

Band 76

Stewig, Reinhard: Über das Verhältnis der Geographie zur Wirklichkeit und zu den Nachbarwissenschaften. Eine Einführung. 1990. IX, 131 S., 15 Abb.
IBSN 923887-18-3. 12,80 €

Band 77

Gans, Paul: Die Innenstädte von Buenos Aires und Montevideo. Dynamik der Nutzungsstruktur, Wohnbedingungen und informeller Sektor. 1990. XVIII, 252 S., & 64 Tab., 36 Abb. und 30 Karten in separatem Kartenband. ISBN 3-923887-19-1.
45,00 €

Band 78

Bähr, Jürgen & Paul Gans (eds): The Geographical Approach to Fertility. 1991. XII, 452 S., 84 Tab. und 167 Fig. ISBN 3-923887-20-5.
22,40 €

Band 79

Reiche, Ernst-Walter: Entwicklung, Validierung und Anwendung eines Modellsystems zur Beschreibung und flächenhaften Bilanzierung der Wasser- und Stickstoffdynamik in Böden. 1991. XIII, 150 S., 27 Tab. und 57 Abb.
ISBN 3-923887-21-3. 9,70 €

Band 80

Achenbach, Hermann (Hrsg.): Beiträge zur regionalen Geographie von Schleswig-Holstein. Festschrift Reinhard Stewig. 1991. X, 386 S., 54 Tab. und 73 Abb.
ISBN 3-923887-22-1. 19,10 €

Band 81

Stewig, Reinhard (Hrsg.): Endogener Tourismus. 1991. V, 193 S., 53 Tab. und 44 Abb.
ISBN 3-923887-23-X. 16,80 €

Band 82

Jürgens, Ulrich: Gemischtrassige Wohngebiete in südafrikanischen Städten. 1991. XVII, 299 S., 58 Tab. und 28 Abb. ISBN 3-923887-24-8. 13,80 €

Band 83

Eckert, Markus: Industrialisierung und Entindustrialisierung in Schleswig-Holstein. 1992. XVII, 350 S., 31 Tab. und 42 Abb
ISBN 3-923887-25-6. 12,70 €

Band 84

Neumeyer, Michael: Heimat. Zu Geschichte und Begriff eines Phänomens. 1992. V, 150 S. ISBN 3-923887-26-4. 9.00 €

Band 85

Kuhnt, Gerald und Zölitz-Möller, Reinhard (Hrsg): Beiträge zur Geoökologie aus Forschung, Praxis und Lehre. Otto Fränzle zum 60. Geburtstag. 1992. VIII, 376 S., 34 Tab. und 88 Abb. ISBN 3-923887-27-2. 19,00 €

Band 86

Reimers, Thomas: Bewirtschaftungsintensität und Extensivierung in der Landwirtschaft. Eine Untersuchung zum raum-, agrar- und betriebsstrukturellen Umfeld am Beispiel Schleswig-Holsteins. 1993. XII, 232 S., 44 Tab., 46 Abb. und 12 Klappkarten im Anhang.
ISBN 3-923887-28-0. 12,20 €

Band 87

Stewig, Reinhard (Hrsg.): Stadtteiluntersuchungen in Kiel, Baugeschichte, Sozialstruktur, Lebensqualität, Heimatgefühl. 1993. VIII, 337 S., 159 Tab., 10 Abb., 33 Karten und 77 Graphiken. ISBN 923887-29-9. 12.30 €

Band 88

Wichmann, Peter: Jungquartäre randtropische Verwitterung. Ein bodengeographischer Beitrag zur Landschaftsentwicklung von Südwest-Nepal. 1993. X, 125 S., 18Tab. und 17 Abb. ISBN 3-923887-30-2. 10.10 €

Band 89

Wehrhahn, Rainer: Konflikte zwischen Naturschutz und Entwicklung im Bereich des Atlantischen Regenwaldes im Bundesstaat São Paulo, Brasilien. Untersuchungen zur Wahrnehmung von Umweltproblemen und zur Umsetzung von Schutzkonzepten. 1994. XIV, 293 S., 72 Tab., 41 Abb. und 20 Fotos. ISBN 3-923887-31-0. 17,50 €

Band 90

Stewig, Reinhard (Hrsg.): Entstehung und Entwicklung der Industriegesellschaft auf den Britischen Inseln. 1995. XII, 367 S., 20 Tab., 54 Abb. und 5 Graphiken.
ISBN 3-923887-32-9. 16,60 €

Band 91

Bock, Steffen: Ein Ansatz zur polygonbasierten Klassifikation von Luft- und Satellitenbildern mittels künstlicher neuronaler Netze. 1995. XI, 152 S., 4 Tab. und 48 Abb.
ISBN 3-923887-33-7. 8,60 €

Band 92

Matuschewski, Anke: Stadtentwicklung durch Public-Private-Partnership in Schweden. Kooperationsansätze der achtziger und neunziger Jahre im Vergleich. 1996. XI, 246 S., 16 Tab., 34 Abb., und 20 Fotos.
ISBN 3-923887-34-5. 12,20 €

Band 93

Ulrich, Johannes und Kortum, Gerhard.: Otto Krümmel (1854-1912): Geograph und Wegbereiter der modernen Ozeanographie. 1997. VIII, 340 S. ISBN 3-923887-35-3. 24,00 €

Band 94

Schenck, Freya S.: Strukturveränderungen spanisch-amerikanischer Mittelstädte untersucht am Beispiel der Stadt Cuenca, Ecuador. 1997. XVIII, 270 S.
ISBN 3-923887-36-1. 13,20 €

Band 95

Pez, Peter: Verkehrsmittelwahl im Stadtbereich und ihre Beeinflussbarkeit. Eine verkehrsgeographische Analyse am Beispiel Kiel und Lüneburg. 1998. XVII, 396 S., 52 Tab. und 86 Abb.
ISBN 3-923887-37-X. 17,30 €

Band 96

Stewig, Reinhard: Entstehung der Industriegesellschaft in der Türkei. Teil 1: Entwicklung bis 1950, 1998. XV, 349 S., 35 Abb., 4 Graph., 5 Tab. und 4 Listen.
ISBN 3-923887-38-8. 15,40 €

Band 97

Higelke, Bodo (Hrsg.): Beiträge zur Küsten- und Meeresgeographie. Heinz Klug zum 65. Geburtstag gewidmet von Schülern, Freunden und Kollegen. 1998. XXII, 338 S., 29 Tab., 3 Fotos und 2 Klappkarten. ISBN 3-923887-39-6. 18,40 €

Band 98

Jürgens, Ulrich: Einzelhandel in den Neuen Bundesländern - die Konkurrenzsituation zwischen Innenstadt und "Grüner Wiese", dargestellt anhand der Entwicklungen in Leipzig, Rostock und Cottbus. 1998. XVI. 395 S., 83 Tab. und 52 Abb.
ISBN 3-923887-40-X. 16,30 €

Band 99

Stewig, Reinhard: Entstehung der Industriegesellschaft in der Türkei. Teil 2: Entwicklung 1950-1980. 1999. XI, 289 S., 36 Abb., 8 Graph., 12 Tab. und 2 Listen.
ISBN 3-923887-41-8. 13,80 €

Band 100

Eglitis, Andri: Grundversorgung mit Gütern und Dienstleistungen in ländlichen Räumen der neuen Bundesländer. Persistenz und Wandel der dezentralen Versorgungsstrukturen seit der deutschen Einheit. 1999. XXI, 422 S., 90 Tab. und 35 Abb.
ISBN 3-923887-42-6. 20,60 €

Band 101

Dünckmann, Florian: Naturschutz und kleinbäuerliche Landnutzung im Rahmen Nachhaltiger Entwicklung. Untersuchungen zu regionalen und lokalen Auswirkungen von umweltpolitischen Maßnahmen im Vale do Ribeira, Brasilien. 1999. XII, 294 S., 10 Tab., 9 Karten und 1 Klappkarte.ISBN 3-923887-43-4. 23,40 €

Band 102

Stewig, Reinhard: Entstehung der Industriegesellschaft in der Türkei. Teil 3: Entwicklung seit 1980. 2000. XX, 360 S., 65 Tab., 12 Abb. und 5 Graphiken
ISBN 3-923887-44-2. 17,10 €

Band 103

*Bähr, Jürgen & Widderich, Sönke: Vom Notstand zum Normalzustand - eine Bilanz des kubanischen Transformationsprozesses. La larga marcha desde el período especial habia la normalidad - un balance de la transformación cubana. 2000. XI, 222 S., 51 Tab. und 15 Abb. ISBN 3-923887-45-0. 11,40 €

*= vergriffen

Band 104

Bähr, Jürgen & Jürgens, Ulrich: Transformationsprozesse im Südlichen Afrika - Konsequenzen für Gesellschaft und Natur. Symposium in Kiel vom 29.10.-30.10.1999. 2000. 222 S., 40 Tab., 42 Abb. und 2 Fig.
ISBN 3-923887-46-9. 13,30 €

Band 105

Gnad, Martin: Desegregation und neue Segregation in Johannesburg nach dem Ende der Apartheid. 2002. 281 S., 28 Tab. und 55 Abb.
ISBN 3-923887-47-7. 14,80 €

Band 106

*Widderich, Sönke: Die sozialen Auswirkungen des kubanischen Transformationsprozesses. 2002. 210 S., 44 Tab. und 17 Abb. ISBN 3-923887-48-5. 12,55 €

Band 107

Stewig, Reinhard: Bursa, Nordwestanatolien: 30 Jahre danach. 2003. 163 S., 16 Tab., 20 Abb. und 20 Fotos.ISBN 3-923887-49-3. 13,00 €

Band 108

Stewig, Reinhard: Proposal for Including Bursa, the Cradle City of the Ottoman Empire, in the UNESCO Wolrd Heritage Inventory. 2004. X, 75 S., 21 Abb., 16 Farbfotos und 3 Pläne. ISBN 3-923887-50-7. 18,00 €

Band 109

Rathje, Frank: Umnutzungsvorgänge in der Gutslandschaft von Schleswig-Holstein und Mecklenburg-Vorpommern. Eine Bilanz unter der besonderen Berücksichtigung des Tourismus. 2004. VI, 330 S., 56 Abb. ISBN 3-923887-51-5. 18,20 €

Band 110

Matuschewski, Anke: Regionale Verankerung der Informationswirtschaft in Deutschland. Materielle und immaterielle Beziehungen von Unternehmen der Informationswirtschaft in Dresden-Ostsachsen, Hamburg und der TechnologieRegion Karlsruhe. 2004. II, 385 S., 71 Tab. und 30 Abb. ISBN 3-923887-52-3. 18,00 €

Band 111

*Gans, Paul, Axel Priebs und Rainer Wehrhahn (Hrsg.): Kulturgeographie der Stadt. 2006. VI, 646 S., 65 Tab. und 110 Abb.
ISBN 3-923887-53-1. 34,00 €

Band 112

Plöger, Jörg: Die nachträglich abgeschotteten Nachbarschaften in Lima (Peru). Eine Analyse sozialräumlicher Kontrollmaßnahmen im Kontext zunehmender Unsicherheiten. 2006. VI, 202 S., 1 Tab. und 22 Abb. ISBN 3-923887-54-X. 14,50 €

Band 113

Stewig, Reinhard: Proposal for Including the Bosphorus, a Singularly Integrated Natural, Cultural and Historical Sea- and Landscape, in the UNESCO World Heritage Inventory. 2006. VII, 102 S., 5 Abb. und 48 Farbfotos. ISBN 3-923887-55-8. 19,50 €

Band 114

Herzig, Alexander: Entwicklung eines GIS-basierten Entscheidungsunterstützungssystems als Werkzeug nachhaltiger Landnutzungsplanung. Konzeption und Aufbau des räumlichen Landnutzungsmanagementsystems LUMASS für die ökologische Optimierung von Landnutzungsprozessen und -mustern. 2007. VI, 146 S., 21 Tab. und 46 Abb.
ISBN 978-3-923887-56-9. 12,00 €

Band 115

Galleguillos Araya-Schübelin, Myriam Ximena: Möglichkeiten zum Abbau von Segregation in Armenvierteln. Die Frage nach der sozialen und ökonomischen Nachhaltigkeit urbaner Ballungsräume am Beispiel Santiago de Chile. 2007. VIII, 226 S., 6 Tab. und 19 Abb. ISBN 978-3-923887-57-6. 15,00 €

*= vergriffen

Band 116

Sandner Le Gall, Verena: Indigenes Management mariner Ressourcen in Zentralamerika: Der Wandel von Nutzungsmustern und Institutionen in den autonomen Regionen der Kuna (Panama) und Miskito (Nicaragua). 2007. VIII, 390 S., 14 Tab. und 44 Abb.
ISBN 978-3-923887-58-3. 18,00 €

Band 117

Wehrhahn, Rainer (Hrsg.): Risiko und Vulnerabilität in Lateinamerika. 2007. II, 314 S., 13 Tab. und 50 Abb.
ISBN 978-3-923887-59-0. 16,50 €

Band 118

Klein, Ulrike: Geomedienkompetenz. Untersuchung zur Akzeptanz und Anwendung von Geomedien im Geographieunterricht unter besonderer Berücksichtigung moderner Informations- und Kommunikationstechniken. 2008. XI, 244 S., 89 Tab. und 57 Abb.
ISBN 978-3-923887-60-6. 15,50 €

Band 119

Sterr, Horst, Christoph Corves und Götz von Rohr (Hrsg.): The ToLearn Project, Learning how to Foster Sustainable Tourism in the North Sea Region 2009. III, 168 S., 6 Tab. und 23 farbige Abb.
ISBN 978-3-923887-61-3. 15,00 €

Band 120

Sandfuchs, Katrin: Wohnen in der Stadt. Bewohnerstrukturen, Nachbarschaften und Motive der Wohnstandortwahl in innenstadtnahen Neubaugebieten Hannovers. 2009. X, 282 S., 30 Tab. und 44 Abb.
ISBN 978-3-923887-62-0. 16,20 €

Band 121

Oppelt, Natascha: Monitoring of the Biophysical Status of Vegetation Using Multi-angular, Hyperspectral Remote Sensing for the Optimization of a Physically-based SVAT Model. 2010. XXII, 130 S., 34 Tab. und 62 Abb. davon 24 farbig
ISBN 978-3-923887-63-7. 14,50 €

Christian-Albrechts-Universität zu Kiel
Mathematisch-Naturwissenschaftliche Fakultät
Kieler Geographische Schriften
Band 121 | Kiel 2010
ISBN 978-3-923887-63-7